STUDY OF PERFORMANCE OF AN ATMOSPHERIC BUBBLING FLUIDIZED BED COMBUSTOR USING RICE WASTE

A thesis submitted
in fulfillment of the requirements
for the award of the degree of

Doctor of Philosophy
in
Mechanical Engineering

By
Ravi Inder Singh
Reg. No. 9050551

Department of Mechanical Engineering
THAPAR UNIVERSITY, PATIALA-147004
PUNJAB
INDIA
March, 2010

CERTIFICATE

Certified that the thesis entitled, "**STUDY OF PERFORMANCE OF AN ATMOSPHERIC BUBBLING FLUIDIZED BED COMBUSTOR USING RICE WASTE**" which is being submitted by **MR. RAVI INDER SINGH** to Thapar University, Patiala in fulfillment for the award of degree of Doctor of philosophy in Mechanical Engineering is a record of bonafied research work carried out by him under our guidance and supervision. The matter presented in this thesis has not been submitted either partially or fully to any other University or Institution for the award of any other degree.

S.K.Mohapatra
Professor and Head
Department of Mechanical Engineering
Thapar University
Patiala

D.Gangacharyulu
Associate Professor and Head
Department of Chemical Engineering
Thapar University
Patiala

ACKNOWLEGEMENT

It is indeed a great pleasure and moment of immense satisfaction for me to express my profound gratitude towards my guides **Dr. S.K.Mohapatra** and **Dr. D. Gangacharyulu** whose enthusiasm in guiding was a source of inspiration to me. I am extremely thankful for extending able guidance in every possible way, the support needed for carrying the work in an efficient manner and making the subject more understandable to me. Their constant encouragement, excellent guidance and invaluable help from the outset to the successful completion of the thesis work was as immense source of encouragement.

I am thankful to Er. S.Bandopadhya, Ex. Chief Engineer, 10 MW Jalkheri power plant, Jalkheri and Mr. Rajinder Sofat, Manager, 3.5 MW cogeneration plant at Nahar Spinning Mills Limited for collection of data from both the plants. I am also thankful to Er. Sukhwinder Singh, Ex. Electrical Engineer, 3.5 MW cogeneration plant, Ludhiana for his support during collection of data from 3.5 MW cogeneration plant. Finally I am thankful to many unknown officers and workers of both plants who supported me during study. At last I am thankful to Er. Puneetpal Singh Cheema Laboratory in charge, Environmental Pollution Control Laboratory, Guru Nanak Dev Engineering College, Ludhiana for his guidance during the operation of various instruments.

Above all I feel short of words for expressing my gratitude towards my parents (Father S. Gurmail Singh (Headmaster), my mother Mrs. Kirpal Kaur), my wife Mrs. Parvinder Kaur and my daughter Rishamnoor Kaur for continuously giving me moral support and inspiration during the course of this work.

March, 2010

Thapar University Patiala

Ravi Singh 19/4/2010

RAVI INDER SINGH

ABSTRACT

Rice is cultivated in all the main regions of world. The worldwide annual rice production is 666 million tons for year 2008. Rice husk, rice straw and rice bran are three types of rice crop waste materials available today. Of these, rice husk and rice straw are the only types of rice waste which could be incinerated in fluidized bed combustors. The total rice waste generated is comprised of 20% rice husk, 70-80% rice straw and 2-3% rice bran. Rice straw is burned in open fields, ploughed in fields, used in compost, cattle house flooring and about 10-15% of total rice straw is available for direct combustion in commercial fluidized bed combustors in Punjab state. The available 10-15% rice straw for combustion in fluidized bed combustors is also dependent on region/area. Due to higher collection cost of rice straw it was not used in many of commercial fluidized bed combustors in the state. Rice husk being easily bought from rice mill owners is easily available for most of the commercial fluidized bed combustors. The study presented here is mainly focused on rice husk, which is abundantly available in this region.

The combustion of rice husk/rice straw in fluidized bed combustors is an attractive possibility of future for power generation, the solution of waste disposal problems and the reduction of greenhouse gases. As paddy plants consume carbon dioxide emissions during photosynthesis process, the overall carbon dioxide emissions during combustion of rice husk/rice straw can be offset, which is fundamental advantage of extracting energy from rice husk/rice straw through combustion and gasification process in the perspective of sustainability. Rice husk characterized by having high ash content, low bulk density and poor flow characteristics makes it difficult for energy conversion. Where as rice straw is having low ash content as compared to rice husk, but when available for combustion it creates feeding and agglomeration problems more predominantly as compared to rice husk. The fluidized bed combustor is ideally suited to burn such fuels since the uniform mixing condition ensures efficient combustion, even at temperature as low as 873 to 923 K. The work presented in this thesis is mainly divided into three main parts.

In the first part a mathematical model for exit gas composition and solid population balance for a 10 MW bubbling fluidized bed combustor at Jalkheri, Distt. Fatehgarh Sahib, Punjab, India based on rice husk has been developed. The model is based on three phase theory of fluidization and material balance for shrinking rice husk particles. The burning of rice husk is assumed to take place according to single film theory. The model has been used to predict the exit gas composition particularly oxygen, carbon dioxide and nitrogen. Then solid population model has been developed to calculate bed carbon load and carbon utilization efficiency. The model predictions are compared with the data collected from the power plant at Jalkheri which uses rice husk as a fuel input (at the time of study). All the results from the two models for rice husk are coming within permissible limits.

In the second part, problem of agglomeration in fluidized bed combustors (FBC) using rice husk and rice straw has been discussed. The problem of agglomeration with respect to rice husk/straw has also been discussed as during study rice straw is available only in combination with rice husk. The agglomeration problem of 10 MW power plant at Jalkheri, which is main reason for defluidization of bed has been discussed. Scanning electron microscope (SEM) of ash agglomerates has been done. Ash samples taken from the Jalkheri power plant and Ludhiana based power plant has been analyzed and discussed. The problem of agglomeration at 3.5 MW cogeneration plant at Ludhiana with rice husk has also been studied.

In the third part computational fluid dynamics (CFD) analysis of an atmospheric bubbling fluidized bed combustors based on rice husk has been discussed. For CFD analysis mainly the fluidized bed has been considered. Due to less computational space the two dimensional fluidized bed has been considered. The Eulerian multiphase model has been used for the fluidized bed. Fluidized Bed is assumed to be in isothermal conditions. Modeling of fluidized bed has been done in Fluent 6.2 commercial code. The CFD modeling has been done to visualize the phases present in fluidized bed with respect to rice husk. The fluidized bed has been modeled with and without bed super heater tubes.

CONTENTS

LIST OF FIGURES

LIST OF TABLES

NOMENCLATURE

A_b	Cross sectional area occupied by the bubbles, cm^2
A_{cw}	Cross sectional area occupied by cloud wake phase, cm^2
A_t	Cross sectional area of the bed, cm^2
AFBC	Atmospheric fluidized bed combustor
A.M.V	Actual measured value
C_{bn-3}	$(n-3)^{th}$ stage oxygen concentration in the bubble phase, g-mol /cm^3
C_{bn-2}	$(n-2)^{th}$ stage oxygen concentration in the bubble phase, g-mol /cm^3
C_{bn-3}	$(n-3)^{th}$ stage oxygen concentration in the bubble phase, g-mol /cm^3
C_{bn-2}	$(n-2)^{th}$ stage oxygen concentration in the bubble phase, g-mol /cm^3
C_{bn-1}	$(n-1)^{th}$ stage oxygen concentration in the bubble phase, g-mol /cm^3
C_{bn}	n^{th} stage oxygen concentration in the bubble phase, g-mol /cm^3
C_{cwn-3}	$(n-3)^{th}$ stage oxygen concentration in the cloud wake phase, g-mol /cm^3
C_{cwn-2}	$(n-2)^{th}$ stage oxygen concentration in the cloud wake phase, g-mol /cm^3
C_{cwn-1}	$(n-1)^{th}$ stage oxygen concentration in the cloud wake phase, g-mol /cm^3
C_{cwn}	n^{th} stage oxygen concentration in the cloud wake phase, g-mol /cm^3
C_{en-3}	$(n-3)^{th}$ stage emulsion phase oxygen concentration, g-mol /cm^3
C_{en-2}	$(n-2)^{th}$ stage emulsion phase oxygen concentration, g-mol /cm^3
C_{en-1}	$(n-1)^{th}$ stage emulsion phase oxygen concentration, g-mol /cm^3
C_{en}	n^{th} stage emulsion phase oxygen concentration, g-mol /cm^3
C_o	Inlet oxygen molar concentration, g-mol /cm^3
C_d	Drag coefficient
C_p	Oxygen concentration in the particulate phase, g-mol /cm^3
C_s	Carbon concentration in the bed, g-mol /cm^3
CFD	Computational fluid dynamics
CPPDK	Cogeneration power plant at Dhandari Kalan, Ludhiana
D_b	Diameter of bubble, cm
D_g	Diffusivity of gas, cm^2/s
d_p	Diameter of rice husk particles, cm
d_s	Sand particle diameter, cm
e	Coefficient of restitution
E_{xair}	Fraction of Excess air
EJ	Exa Joule

ESP	Electrostatic precipitator
f_{cw}	Fraction of cloud wake phase in the bed
FME	Actual air feed rate to the combustor, g-mol/sec
FMTH	Stoichiometric air feed rate to the combustor, g-mol/sec
F_0	Total carbon feed rate, g/s
F_1	Carry over rate, g/s
F_2	Fly ash (Air heater and ESP hopper), g/s
F_3	Total carbon in carry over rate, g/s
F_4	Actual carbon in fly ash (Air heater and ESP hopper), g/s
F_5	Carbon lost due to unburnt rice husk, g/s
g	Acceleration due to gravity, cm/s^2
g_o	Radial distribution function
G	Solid stress modulus
G_s	Solid mass flux, $g/cm^2/s$
GHG	Green house gases
Gt	Giga ton
H_{mf}	Height of bed at minimum fluidization, cm
JPP	Jalkheri power plant
K	Overall reaction rate constant, cm/s
K_s	Intrinsic chemical reaction rate constant, cm/s
K_g	Mass transfer coefficient, cm/s
$k_{shrk} = \frac{dd_p}{dt}$	Shrinkage rate of rice husk particles, g/s
$(K_{bc})_b$	Gas interchange co-efficient from bubble to cloud wake phase, s^{-1}
$(K_{ce})_b$	Gas interchange co-efficient from cloud wake to emulsion phase, s^{-1}
$K^*(d_p)$	Elutriation rate constant, $g/cm^2.s$
$K(d_p)$	Elutriation constant, s^{-1}
K_{sg}	Gas-solid momentum exchange term
N	Number of g mole of oxygen
N_D	Number of holes in distributor
NSML	Nahar spinning mill limited, Ludhiana, Punjab, India
M_c	Molecular mass of carbon
P_{av}	Average pressure in the combustor, atm

$P_b(d_p)$	Char size distribution in the bed, cm^{-1}
$P_1(d_p)$	Size distribution of overflow rate, cm^{-1}
P_f	Frictional contribution to solid pressure, dyn/cm^2
P_g	Gas phase pressure, dyn/cm^2
P_s	Solid phase pressure, dyn/cm^2
PSEB	Punjab state electricity board
R	Gas constant, atm-cm^3/g-mol-K
Re_s	Reynolds number, based on slip velocity
Sh	Sherwood number
T_b	Absolute bed temperature, K
u_b	Average absolute velocity of crowd of bubbles, cm/s
u_{br}	Single bubble velocity, cm/s
U_b	Velocity of gas through bubble phase, cm/s
U_{cw}	Velocity of gas through cloud wake phase, cm/s
U_{cwn-1}	Velocity of gas through $(n-1)^{th}$ stage of cloud wake phase, cm/s
U_{cwn}	Velocity of gas through n^{th} stage of cloud wake phase, cm/s
U_g	Gas velocity, cm/s
U_o	Superficial gas velocity, cm/s
U_{mf}	Minimum fluidization velocity/emulsion phase gas velocity, cm/s
$W_{rice\ husk}$	Feed rate of rice husk, g/s
XC	Carbon weight percentage
XH	Hydrogen weight percentage
XO	Oxygen weight percentage
XS	Sulfur weight percentage
XW	Moisture weight percentage
XVM	Weight fraction of volatile matter in the rice husk
XFC	Weight fraction of fixed carbon in the rice husk
Z	Bed height ,cm
Z_{n-1}	Bed height at $(n-1)^{th}$ stage, cm
Z_n	Bed height at n^{th} stage, cm

Greek symbols

ε_b	Volume fraction of bubbles in the bed

ε_{mf}	Voidage in the bed at minimum fluidization
ε_g	Gas phase volume fraction
ε_s	Solid phase volume fraction
ε_{mf}	Gas volume fraction at minimum fluidization
$\varepsilon_{s,\min}$	Minimum solid fraction
$\varepsilon_{s,\max}$	Maximum solid volume fraction
ρ_p	Density of rice husk particles, g/cm^3
ρ_g	Gas phase density, g/cm^3
ρ_s	Solid phase density, g/cm^3
v_g	Gas phase velocity vector, cm/s
v_s	Solid phase velocity vector, cm/s
β	Inter-phase drag coefficient
η	Specularity co-efficient
φ	Internal angle of friction
ξ_s	Solid phase frictional stress, dyn/cm^2
σ	Solid phase shear stress, dyn/cm^2
τ_g	Gas phase shear stress, dyn/cm^2
τ_s	Solid phase shear stress, dyn/cm^2
γ	Dissipation of granular energy, gcm^{-3}s^{-1}
κ	Solid thermal conductivity, g cm^{-1}s^{-1}
μ_g	Viscosity of gas, g/cm.s
μ_s	Solid phase shear viscosity, g/cm.s
μ_f	Frictional contribution to solid viscosity, g/cm.s
Θ	Granular temperature, cm^{2}s^{-2}

Subscript

b	Bubble
g	Gas phase
mf	Minimum fluidization
s	Solid phase
w	Wall

CHAPTER 1

INTRODUCTION

Energy consumption in the world in the form of petroleum-based fuels has increased manifold during the last 40 years or so. Fast depleting stock of fossil fuel and steep increase in their prices may lead to an energy crisis in the not-too-distant future. With declining reserves and fluctuating prices of fossil fuels, the search for an alternative renewable raw material to replace petroleum has intensified all over the world. The new concept of collected solar energy, converted into new forms and stored in plant, has bought about the introduction of new notions, such as energetical cultures, agro-energetical and oil bearing plantations, photo-biofuels, green energy etc. The use of biomass as a substitute for fossil fuel, rather than solely for carbon sequestrization, will enable biomass to play much wider roles in coping with greenhouse warming. With an increasing proportion of the world's population residing in developing countries, which usually lack fossil fuels and the means to import them, it is essential that greater effort be put into producing and using biomass efficiently as a widely available and flexible fuel source.

Annually, photosynthesis stores 5-8 times more energy in biomass than man currently consumes from all sources. Residues (biomass) are invaluable as an immediate and relatively cheap energy resource to provide the initial feedstock in the development of a large bio-energy industry, offering an environmentally acceptable way of disposing of unwanted and often polluting waste. There are large quantities of residues, associated with agricultural production and processing industries which can be used for energy production. There have been many attempts to estimate the energy potential of agricultural residues, but this is a very difficult task and only rough estimates are possible. Smil [2] has calculated that in the mid 1990's the amount of crop residues amounted to about 3.5 to 4 Gt annually, with an energy content representing

65 EJ [2]. Hall et al. [3] have estimated that just using the world's major crops (wheat, rice, maize, barley, and sugarcane), and a 25% residue recovery rate could generate 38 EJ and off set 350 to 460 Mt of Coal annually. There is no doubt that a large part of the residues are wasted or handled inappropriately, causing undesirable effects from an environmental, ecological and food production viewpoint. Andreae et al. [4] has estimated that over 2 Giga ton of agricultural residues are burned annually world-wide, while Smil [2] estimates are between 1.0 and 1.4 Giga ton, producing 1.1 to 1.7 Giga ton/annum of CO_2 Worldwide, the generation capacity of agricultural residues (straw, animal slurries, green agricultural waste) is estimated to be about 4500 MW. In Asia-Pacific region, these residues are abundant because wide ranges of crops are grown to produce 56% of the world population [5] These crops causes huge amount of agro residues in these regions. Some agro residues are not viable for energy production because of huge investment involved setup and cost involved in collection, transportation and storage.

Rice waste means remaining residues of rice crop. Rice waste is one such agro residues which are found in regions where the demand for energy exists. Rice waste is comprises of rice straw, rice husk and rice bran mainly. There are primarily two types of residues from rice cultivation that have potential in terms of energy-straw and husk. Although the technology of using rice husk is well established in many Asian countries, rice straw is, as of now, rarely used as a source of renewable energy. One of the principal reasons for the preferred use of husk is its easy procurement-that is, it is available at the rice mill. In the case of rice straw, however, its collection is laborious and its availability is limited to harvest time. The logistics of collection could be improved through baling, but the necessary equipment is expensive and buying it is uneconomical for most rice farmers. Rice straw is 70-80 percent of rice crop. Most of rice straw is burned in open fields, little percentage is available for fluidized bed combustors in this region.

Rice husk and rice bran are by products of milling. Rice bran is used for oil and not available for combustion.

Rice husk is abundantly available throughout this region. Disposal of rice husk is becoming more and more costly in these regions, which makes their usage for energy production additionally attractive. Energy from rice husk is renewable and due to a balance between CO_2 consumption and release commonly entitled "CO_2 free". Combustion naturally produces carbon dioxide (CO_2), and gasification of rice husk produces combustible CO which further converted to CO_2, but it produces only the same amount that has been accumulated from the atmosphere during the growth of a plant. Decomposition of any biomass after its lifecycle releases not only approximately the same amount of CO_2 that would develop during combustion; it also releases methane, which is a much more hazardous greenhouse gas than CO_2. Hence, combustion and gasification of rice husk/rice straw not only substitutes fossil fuel, but additionally reduces the emission of methane and other problematic gases during uncontrolled decomposition. Figure 1.1 explains the CO_2 balance of rice husk/rice straw combustion.

Rice husk accounts for 14-35% of the weight of the paddy produced [6-7] depending on paddy variety and on average it represents 20% of the paddy produced [6-7] on weight basis. The worldwide annual rice production for year 2008 was 666 million tons [1]. The annual production for year 2008 of rice husk was 133.2 million tons considering rice husk being 20% of total paddy production and annual production of rice straw was 466 million tons. The average annual energy potential of rice straw is 7.0147×10^{12} MJ and rice husk is 1.998×10^{12} MJ considering calorific value of rice straw as 15 MJ/kg. India alone produces [8] about 22 million tones of rice husk per year as by product from rice milling. Figure 1.2 shows the rice husk production in the 20 highest rice producing countries, 2002 [9]. The data for year 2008 is not going much to change.

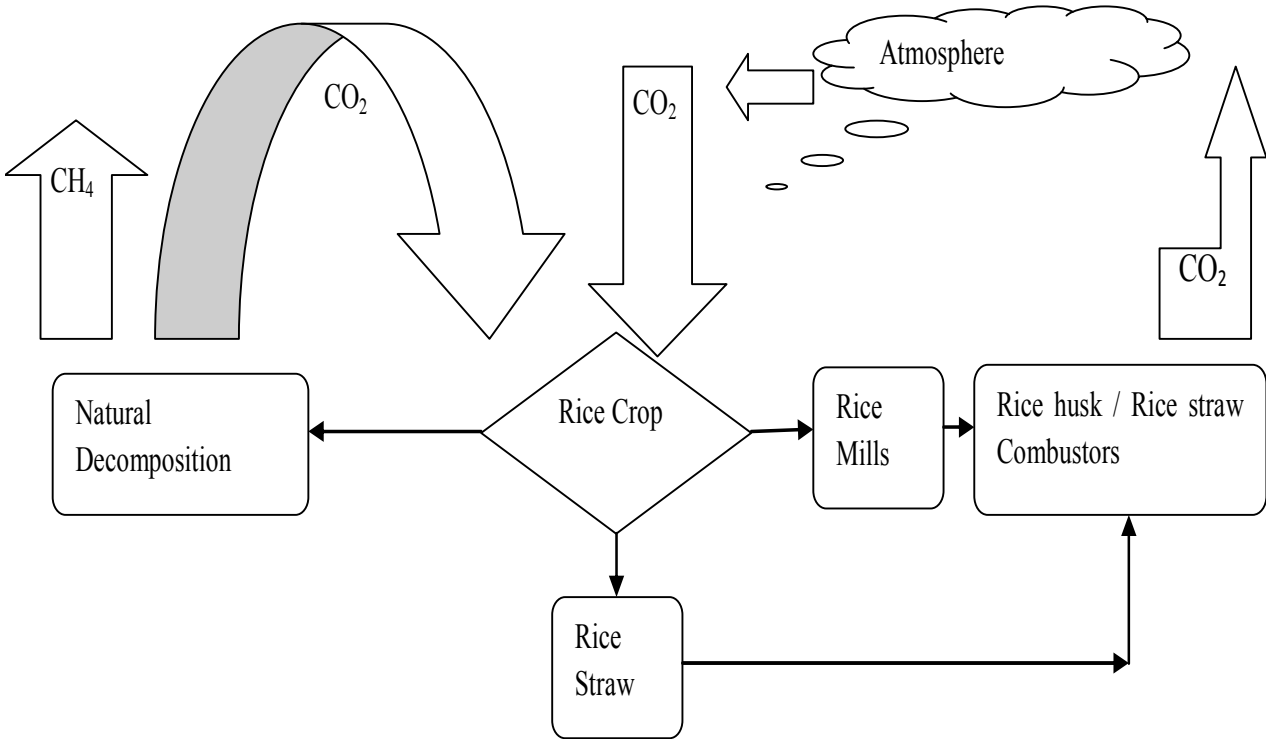

Figure 1.1: CO_2 balance of rice husk/rice straw combustion

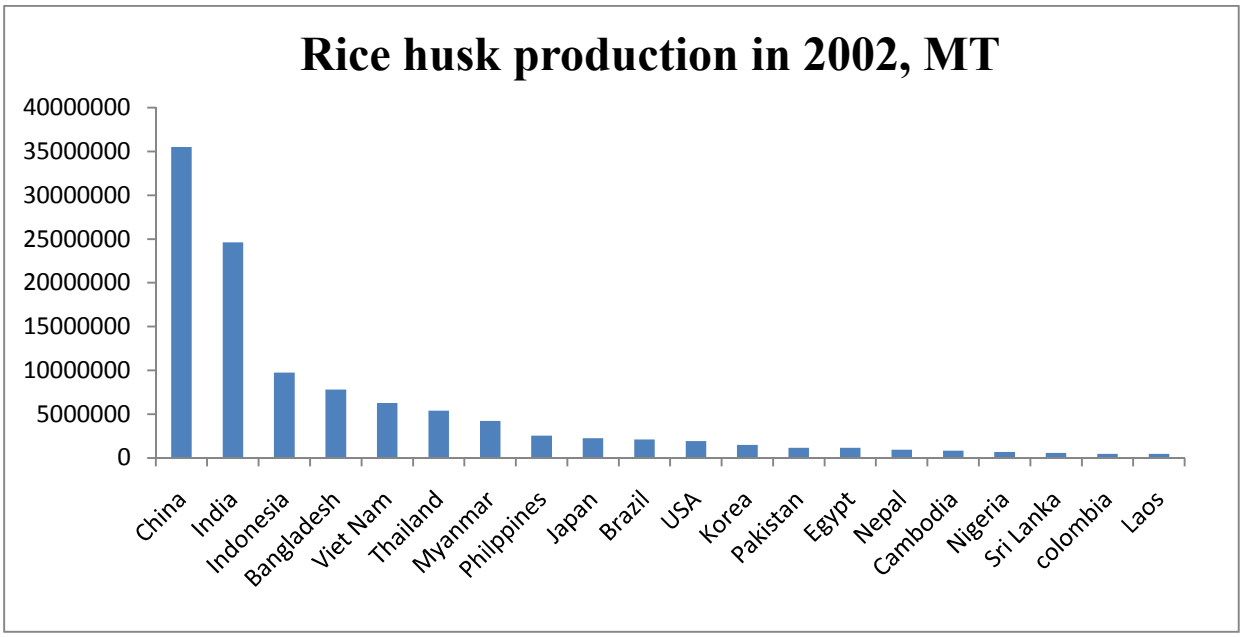

Figure 1.2: Rice husk production in the 20 highest rice producing countries, 2002 [9]

If this huge amount of rice husk/rice straw could be utilized at places or near to these places for energy production, then the need for disposing and producing energy can be done simultaneously.

Fluidized bed combustion process is one such technology, that it is producing energy efficiently with wide range of fuels, at low temperature and isothermal conditions. Due to these reasons a number of commercial fluidized bed power plants of 10-20 MW capacities based on rice husk/rice straw have been installed in the last two decades for power generations. Although a lot of literature is available on biomass gasification but limited study has been done on combustion of rice husk/rice straw in fluidized beds.

1.1 Biomass Scenario in Punjab

Punjab is an agricultural state with fertile land, plenty of water resources, livestock, and agricultural residues. Energy is one of the key factors for the development of national economics in India. Punjab is energy deficit state. Punjabis are India's largest energy consumers, with some 790 KWh per year per person, against an Indian average of 283 KWh per person [10]. Still, compared to Western standards, this is very modest (compared with for example France, where per capita consumption stands at 7584 KWh per annum). The major portions of the electricity generated in Punjab state is from rapid depleting fossil fuel coal. Usage of coal threatens the life of human being through various environmental impacts like air pollution, global warming and etc. Moreover huge amount of money is wasted in bringing coal to northern state like Punjab. Biomass is one kind of renewable energy resource, which is abundant in agricultural states like Punjab of India. The disposal of biomass is a major problem here because if it is burnt in open field it creates problems to environment. The biomass if dumped in land can also be harmful as it creates gas like methane. The total amount of unused agricultural biomass is about

13.73 Mt $year^{-1}$. The total power generation capacity from unused [11] biomass is approximately 900 MW. The collection cost in the field up to the carrier unit is US$3.90 t^{-1}. 900 MW of power from biomass could satisfy the energy needs of some 8 to 16 million Punjabis (low number if inefficient technologies are used; high number when biomass plants are used). If the biomass generated in Punjab could be incinerated in the state in fluidized bed combustors for power generation it could reduce shortage of electricity in state and reduce burden of harmful gases on environment. Therefore Punjab has attracted extensive research and development efforts since the last two decades. In the significant development which could enable the Punjab Government to overcome the acute shortage of electricity, the Punjab Energy Developing Agency (PEDA) has allocated six projects to the private companies to produce 66 MW of power from bio-mass.

The major driving force that led to the development of fluidized bed combustors is the need for more efficient technologies for the utilization of the low-grade fuel. In pulp and paper industry, bubbling fluidized bed is the preferred technology for the combustion of wood wastes and bark in smaller co-generation plants. Higher environmental awareness, larger plants and multi-fuel capabilities have favored the circulating fluidized bed boilers for the power and steam generation from biomass fuels.

1.2 Fluidized Bed Combustors

Fluidized bed combustors are widely used in the power plants for the production of power. Fluidized beds are also going to be widely used in the next generation power plants in aiding conversion of coal to clean gas. However, in spite of their ubiquitous application, understanding of the complex multi-phase flows involved is still limited. A fluidized bed combustor consists of a collection of inert particles suspended in an upward flowing gas stream at such a velocity that the particles are not carried out of the vessel but continue to circulate vigorously within the

vessel. Cavities usually called 'bubbles' move through the suspended mass, which help the vigorous circulation of the bed material. Since the bed offers resistance to flow, the drag forces, as given by pressure drop across the bed, are sufficient to support the weight of the bed. Fluidized bed combustors having advantage of smooth liquid like continuous flow of particles which allow controlled operation with ease of handling and makes it suitable for large-scale operations. It allows rapid mixing of solids that leads to nearly isothermal conditions throughout the bed. As a result of which the operation can be controlled easily and reliably. Heat and mass transfer rates between gas and particles are high when compared with other modes of contacting. Since the bed temperature is kept normally below 1000^{o}C, little atmospheric nitrogen is converted to NO_x. Any type of fuel can be used in the system.

In addition, the whole vessel of well mixed solids represents a large thermal flywheel that resists rapid temperature changes, responds slowly to abrupt changes in operating conditions and gives a large margin of safety in avoiding temperature runaways for exothermic reactions. The rate of heat transfer between a fluidized bed and immersed object is high; hence heat transfer within fluidized bed requires relatively small surface transfer area. Fluidized bed rice husk combustors appear to offer some distinct advantages due to their unique operating characteristics. The turbulence due to fluidization in the bed can break the rigid ash skeleton [12] to make the trapped carbon available for conversion. Rice husk ash can easily be removed from the fluidized bed by entrainment in the gas stream, from which it can be separated by particle separating systems such as cyclones. The bed temperature can be kept below the ash slagging temperature by properly controlling its operating parameters and maintaining uniform fluidization [13]. The global FBC capacity is going to grow steeply in future. Figure 1.3 and Figure 1.4 present recent information on fluidized devices and capacity of fluidized bed

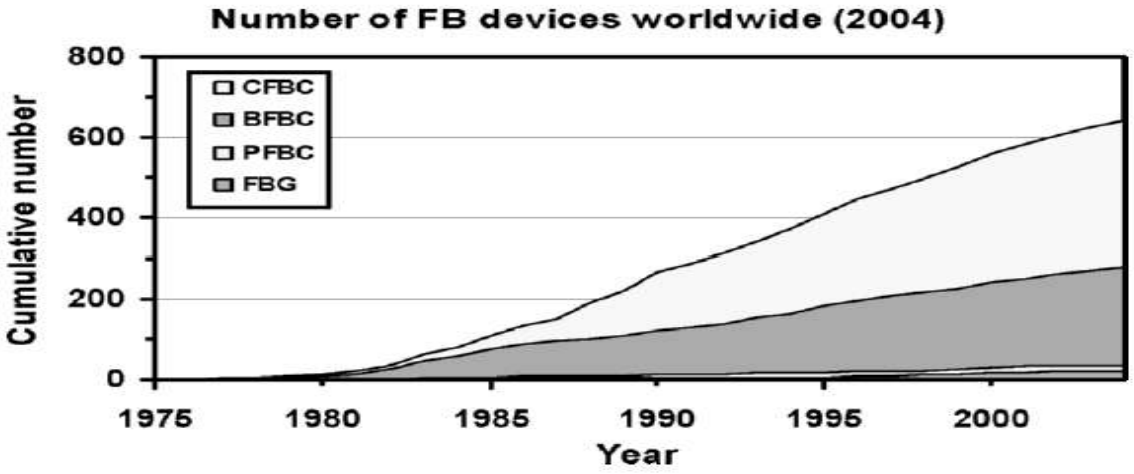

Figure 1.3: Cumulative number of fluidized bed devices worldwide [14]

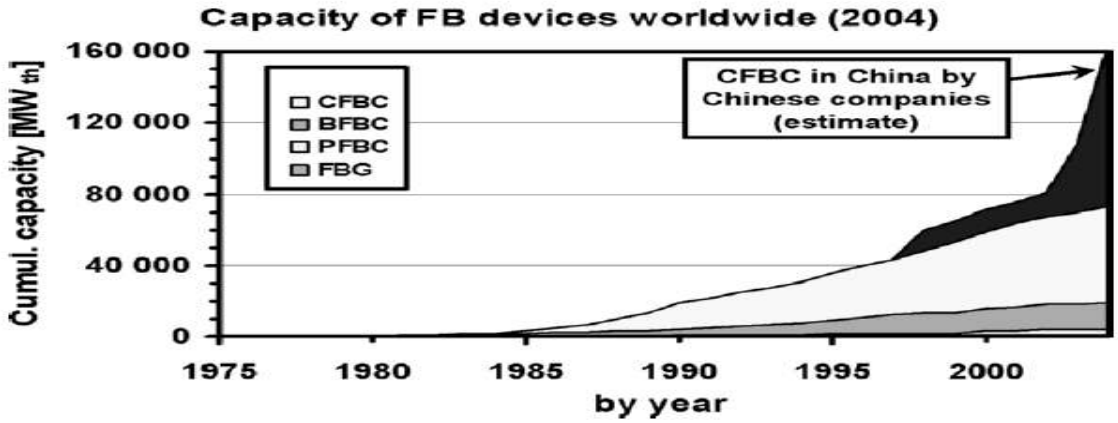

Figure 1.4: Capacity of fluidized bed devices worldwide [14]

units through out the world. Currently several hundred boilers are either at the planning stage or under construction throughout the world, when realized, will double global capacity in the near future.

1.3 Fluidized Bed Combustion of Biomass in Fluidized Bed

Beside from suspension firing of wood, the most efficient method of directly burning biomass is in a fluidized bed combustor (FBC). This is also the most versatile since the system can cope with a wide range of fuels and a range of moisture contents. The basis for a fluidized bed combustor system is a bed of an inert mineral such as sand or limestone through which air is

blown from below. The air is pumped through the bed in sufficient volume and at a high enough pressure to entrain the small particles of the bed material so that they behave much like a fluid. The combustion chamber of a fluidized bed plant is shaped so that above a certain height the air velocity drops below that necessary to entrain the particles. This helps retain the bulk of the entrained bed material towards the bottom of the chamber. Once the bed becomes hot, combustible material introduced into it will burn, generating heat as in a more conventional furnace. The proportion of combustible material such as biomass within the bed is normally only around 5%. There are different designs of fluidized bed combustor system which involve variations around this principle.

The most common for biomass combustion is the circulating fluidized bed which incorporates a cyclone filter to separate solid material from the hot flue gases which leave the exhaust of the furnace. The solids from the filter are re-circulated into the bed, hence the name. The fluidized bed has two distinct advantages for biomass combustion: First, it is the ability to burn a variety of different fuels without affecting performance. Second is the ability to introduce chemical reactants into the fluidized bed to remove possible pollutants. In FBC plants burning coal, for example, limestone can be added to capture sulphur and prevent its release to the atmosphere as sulphur dioxide. Biomass tends to contain less sulphur than coal so this strategy may not be necessary in a biomass plant. A fluidized bed boiler can burn wood with up to 55% moisture. The fluidized bed combustors are also used to burn chicken litter, the refuse from the intensive farming of poultry. Power stations have been built that are devoted specifically to this fuel source and these plants use fluidized bed combustors. The fluidized bed combustor technology is best suited for a range of small and medium scale operation for combined heat and

power. With technological advancements the fluidized bed combustor boilers give efficiency of as high as 80-82% and can be used for a wide variety of fuels.

1.4 Mechanism of Fluidized Bed Combustion Systems

When an evenly distributed air or gas is passed upward through a finely divided bed of solid particles such as sand supported on a fine mesh, the particles remain undisturbed at low velocities. As the air velocity is gradually increased, a stage is reached when the individual particles are suspended in the air stream and the bed is called “fluidized”. With further increase in air velocity, there is bubble formation, vigorous turbulence, rapid mixing and formation of dense defined bed surface. The bed of solid particles exhibits the properties of a boiling liquid and assumes the appearance of a fluid “bubbling fluidized bed”. At higher velocities, bubbles disappear, and particles are blown out of the bed. Therefore, some amounts of particles have to

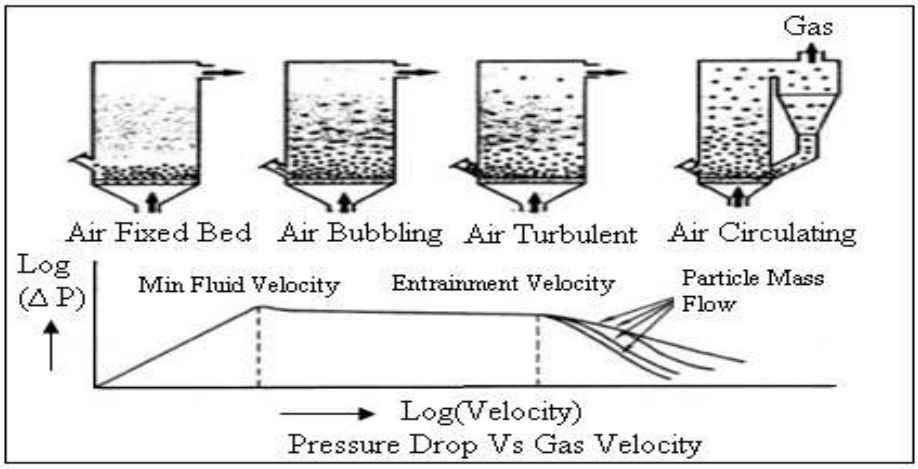

Figure 1.5: Principles of fluidization [184]

be re-circulated to maintain a stable system and is called as “circulating fluidized bed". This principle of fluidization is illustrated in Figure 1.5. As the velocity of a gas flowing through a bed of particles increases, a value is reached when the bed fluidizes and bubbles form as in a

boiling liquid. At higher velocities the bubbles disappear; and the solids are rapidly blown out of the bed and must be recycled to maintain a stable system. Fluidization depends largely on the particle size and the air velocity. The mean solids velocity increases at a slower rate than does the gas velocity. The difference between the mean solid velocity and mean gas velocity is called as slip velocity. Maximum slip velocity between the solids and the gas is desirable for good heat transfer and intimate contact.

If sand particles in fluidized state are heated to the ignition temperatures of fuel (rice husk, coal or bagasse), and fuel is injected continuously into the bed, the fuel will burn rapidly and the bed attains a uniform temperature. The fluidized bed combustion takes place at about 840°C to 950°C. Since this temperature is much below the ash fusion temperature, melting of ash and associated problems are avoided. The lower combustion temperature is achieved because of high coefficient of heat transfer due to rapid mixing in the fluidized bed and effective extraction of heat from the bed through in-bed heat transfer tubes and walls of the bed. The gas velocity is maintained between minimum fluidization velocity and particle entrainment velocity. This ensures a stable operation of the bed and avoids particle entrainment in the gas stream.

Any combustion process requires three “T”s - that is Time, Temperature and Turbulence. In fluidized bed combustor, turbulence is promoted by fluidization. Improved mixing generates evenly distributed heat at lower temperature. Residence time is many times higher than conventional grate firing. Thus a fluidized bed combustor system releases heat more efficiently at lower temperatures. Since limestone can also be used as particle bed (in case the fuel with sulphur content is used), control of SOx and NOx emissions in the combustion chamber is achieved without any additional control equipment. This is one of the major advantages over conventional boilers.

1.5 Types of Fluidized Bed Combustors

The following three types of fluidized bed combustors are in use.

1.5.1. Atmospheric Fluidized Bed Combustors (AFBC)

1.5.2 Circulating Fluidized Bed Combustors (CFBC)

1.5.3 Pressurized Fluidized Bed Combustors (PFBC)

1.5.1 Atmospheric fluidized bed combustors (AFBC)

AFBC is one of the most important types of FBC boilers as it can be used for variety of fuels; such as agricultural residues like rice husk or bagasse and even low quality coal. These types of boiler find use in industries where there is a possibility of having a combined heat and power generation application. In AFBC boilers the fuel is sized depending on the type of fuel (in case of coal, the coal is crushed to a size of 0.1–1 cm depending on the grade of coal) and the type of fuel feeding system and is fed into the combustion chamber. The atmospheric air, which acts as both the fluidization air and combustion air, is delivered at a pressure and flows through the bed after being preheated by the exhaust flue gases. The velocity of fluidizing air is in the range of 120 to 370 cm /sec. The rate at which air is blown through the bed determines the amount of fuel that can be reacted. Almost all AFBC/ bubbling bed boilers use in-bed evaporator tubes in the bed of limestone, sand and fuel for extracting the heat from the bed to maintain the bed temperature. The bed depth is usually 80 cm to 150 cm deep and the pressure drop averages about 1 inch of water per inch of bed depth. Very little material leaves the bubbling bed. Only about 2000 to 4000 g of solids is recycled per ton of fuel burned.

Typical fluidized bed combustors of this type are shown in Figures 1.6 and 1.7. The combustion gases pass over the super heater sections of the boiler, flow past the economizer, the dust collectors and the air pre-heaters before being exhausted to atmosphere. The special feature

of atmospheric fluidized bed combustion is the constraint imposed by the relatively narrow temperature range within which the bed must be operated. With coal, there is risk of clinker formation in the bed if the temperature exceeds 950°C and loss of combustion efficiency if the temperature falls below 800°C. For efficient sulphur retention, the temperature should be in the range of 800°C to 850°C.

1.5.1 General Arrangements of Atmospheric Fluidized Bed Combustor

Figure 1.6 and Figure 1.7 represent atmospheric fluidized bed combustor (AFBC) boilers.

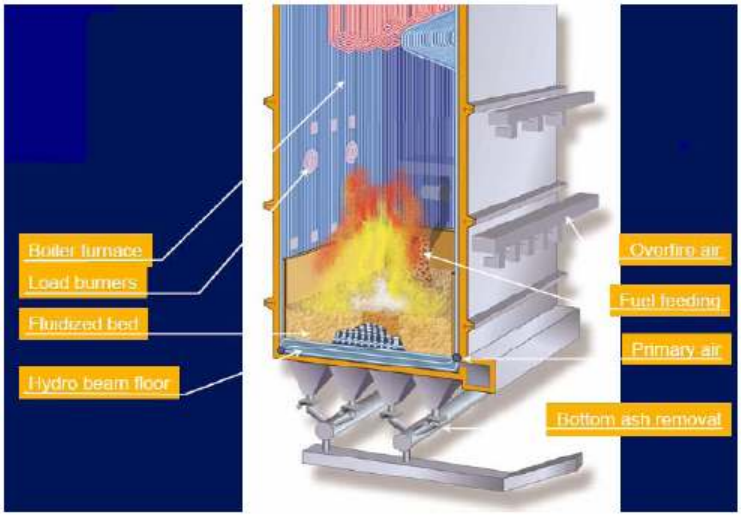

Figure 1.6: A view of atmospheric fluidized bed combustor [184]

Main components of a fluidized bed combustor are

(a) Fuel feeding system

(b) Air distributor

(c) Bed and in-bed heat transfer surface

(d) Ash handling system.

Many of these components are common to all types of FBC boilers.

a) Fuel feeding system

For feeding fuel and adsorbents like limestone or dolomite, usually two methods are followed: under bed pneumatic feeding and over-bed feeding.

Under bed pneumatic feeding

If the fuel is coal, it is crushed to 0.1–0.6 cm size and pneumatically transported from feed hopper to the combustor through a feed pipe piercing the distributor. Based on the capacity of the boiler, the number of feed points is increased, as it is necessary to distribute the fuel into the bed uniformly.

Over bed feeding

The crushed coal, 0.6–1 cm size is conveyed from coal bunker to a spreader by a screw conveyor. The spreader distributes the coal over the surface of the bed uniformly. This type of fuel feeding system accepts over size fuel also and eliminates transport lines, when compared to under-bed feeding system. Now-a-days for rice husk and other agricultural residues, over bed feeding system is quite prominent and economical. Some of the boilers are so designed that they have both types of feeding systems.

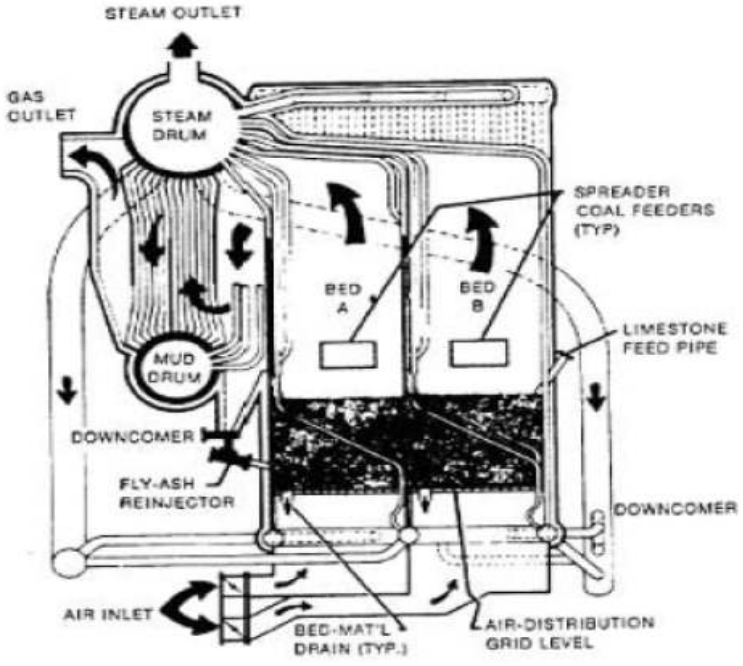

Figure 1.7: A detailed view of different components of AFBC [184]

b) Air distributor

The purpose of the distributor is to introduce the fluidizing air evenly through the bed cross section thereby keeping the solid particles in constant motion, and preventing the formation of de-fluidization zones within the bed. The distributor, which forms the furnace floor, is normally constructed from metal plate with a number of perforations in a definite geometric pattern. The perforations may be located in simple nozzles or nozzles with bubble caps, which serve to prevent solid particles from flowing back into the space below the distributor. The distributor plate is protected from high temperature of the furnace by refractory lining and a static layer of the bed material or water cooled tubes.

c) Bed and in-bed heat transfer surface

Bed

The bed material can be sand, ash, crushed refractory or limestone, with an average size of about 0.1 cm. Depending on the bed height these are of two types: shallow bed and deep bed. At the same fluidizing velocity, the two ends fluidize differently, thus affecting the heat transfer to an immersed heat transfer surfaces. A shallow bed offers a lower bed resistance and hence a lower pressure drop and lower fan power consumption. In the case of deep bed, the pressure drop is more and this increases the effective gas velocity and also the fan power.

In-bed heat transfer surface

In a fluidized in-bed heat transfer process, it is necessary to transfer heat between the bed material and an immersed surface, which could be that of a tube bundle, or a coil. The heat exchanger orientation can be horizontal, vertical or inclined. From a pressure drop point of view, a horizontal bundle in a shallow bed is more attractive than a vertical bundle in a deep bed. Also, the heat transfer in the bed depends on number of parameters like (i) bed pressure (ii) bed

temperature (iii) superficial gas velocity (iv) particle size (v) heat exchanger design and (vi) gas distributor plate design.

d) Ash handling system

Bottom ash removal

In the FBC boilers, the bottom ash constitutes roughly 30-40% of the total ash, the rest being the fly ash. The bed ash is removed by continuous over flow to maintain bed height and also by intermittent flow from the bottom to remove over size particles, avoid accumulation and consequent defluidization. While firing high ash coal such as washery rejects, the bed ash overflow drain quantity is considerable so special care has to be taken.

Fly ash removal

The amount of fly ash to be handled in FBC boiler is relatively very high, compared to conventional boilers. This is due to elutriation of particles at high velocities. Fly ash carried away by the flue gas is removed in number of stages; firstly in convection section, then from the bottom of air pre-heater/economizer and finally a major portion is removed in dust collectors. The types of dust collectors used are cyclone, bag filters, electrostatic precipitators (ESP's) or some combination of all of these. To increase the combustion efficiency, recycling of fly ash is practiced in some units.

1.5.2 Circulating Fluidized Bed Combustors (CFBC)

Circulating fluidized bed combustion (CFBC) technology has evolved from conventional bubbling bed combustion as a means to overcome some of the drawbacks associated with conventional bubbling bed combustion (see Figure 1.8). CFBC technology utilizes the fluidized bed principle in which crushed (0.6–1.2 cm size) fuel and limestone are injected into the furnace or combustor. The particles are suspended in a stream of upwardly flowing air (60-70% of the

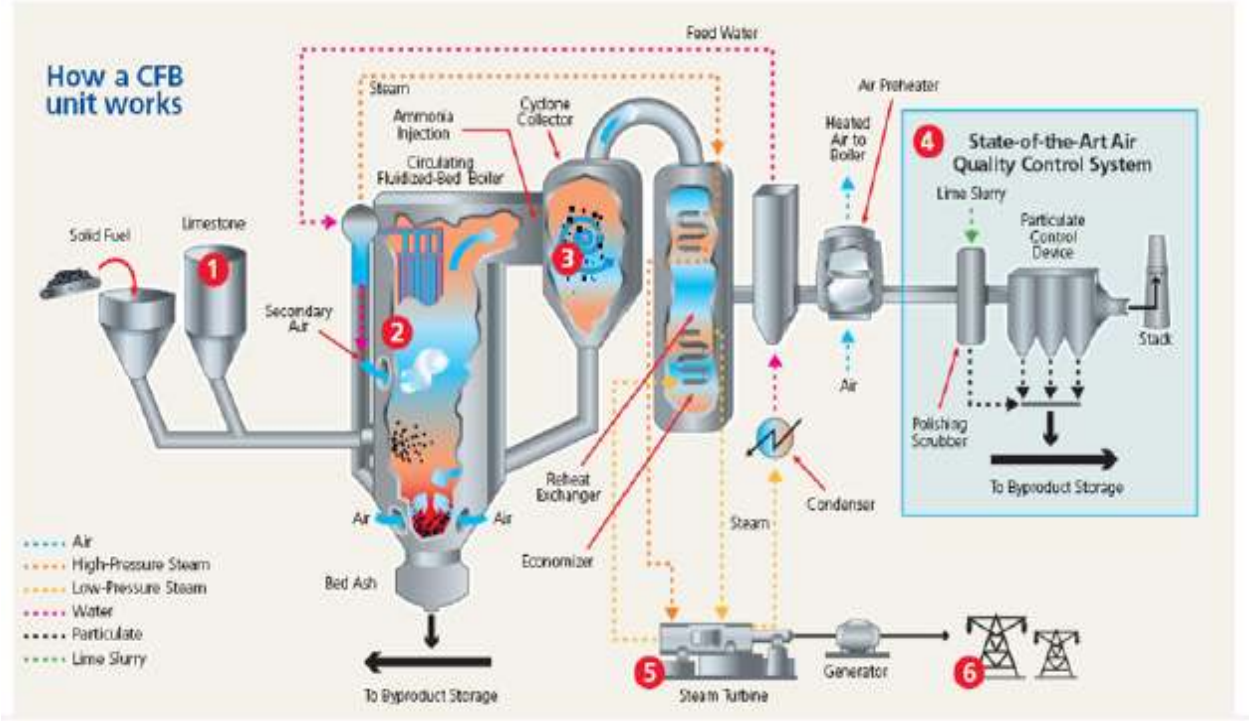

Figure 1.8: A circulating fluidized bed combustor [184]

total air), which enters the bottom of the furnace through air distribution nozzles. The fluidizing velocity in circulating beds ranges from 370 to 900 cm/s. The balance of combustion air is admitted above the bottom of the furnace as secondary air. The combustion takes place at 840-900 °C, and the fine particles (<450 microns) are elutriated out of the furnace with flue gas velocity of 400–600 cm/s.

The particles are then collected by the solids separators and circulated back into the furnace. Solid recycle is about 50000 to 100000 g per g of fuel burnt. There are no steam generation tubes immersed in the bed. The circulating bed is designed to move a lot more solids out of the furnace area and to achieve most of the heat transfer outside the combustion zone – convection section, water walls, and at the exit of the riser. Some circulating bed units even have external heat exchanges. The particles circulation provides efficient heat transfer to the furnace walls and longer residence time for carbon and limestone utilization. The controlling parameters

in the CFB combustion process are temperature, residence time and turbulence. For large units, the taller furnace characteristics of CFBC boiler offers better space utilization, greater fuel particle and adsorbent residence time for efficient combustion and SO_2 capture, and easier application of staged combustion techniques for NOx control than AFBC generators. CFBC boilers are said to achieve better calcium to sulphur utilization – 1.5 to 1 vs. 3.2 to 1 for the AFBC boilers, although the furnace temperatures are almost the same. CFBC requires huge mechanical cyclones to capture and recycle the large amount of bed material, which requires a tall boiler. A CFBC could be good choice if the following conditions are met. Capacity of boiler is large to medium sulphur emission and NOx control is important The boiler is required to fire low-grade fuel or fuel with highly fluctuating fuel quality. Some of the performance features of the CFBC system are as follows:

It has a high processing capacity because of the high gas velocity through the system. The temperature of about 870°C is reasonably constant throughout the process because of the high turbulence and circulation of solids. The low combustion temperature also results in minimal NOx formation. Sulphur present in the fuel is retained in the circulating solids in the form of calcium sulphate and removed in solid form.

The use of limestone or dolomite adsorbents allows a higher sulfur retention rate, and limestone requirements have been demonstrated to be substantially less than with bubbling bed combustor. The combustion air is supplied at higher velocity as required by bubbling bed combustors. It has high combustion efficiency. It has a better turndown ratio than bubbling bed systems. Erosion of the heat transfer surface in the combustion chamber is reduced, since the surface is parallel to the flow. In a bubbling bed system, the surface generally is perpendicular to

the flow. CFBC boilers are generally claimed to be more economical than AFBC boilers for industrial application requiring more than 20,833.3 -27777.8 g/s of steam.

1.5.3 Pressurized Fluidized Bed Combustors (PFBC)

Pressurized fluidized bed combustors are type of FBC technology that is meant for large-scale coal burning applications. In PFBC, the bed vessel is operated at pressure up to 15.8-16 atm.

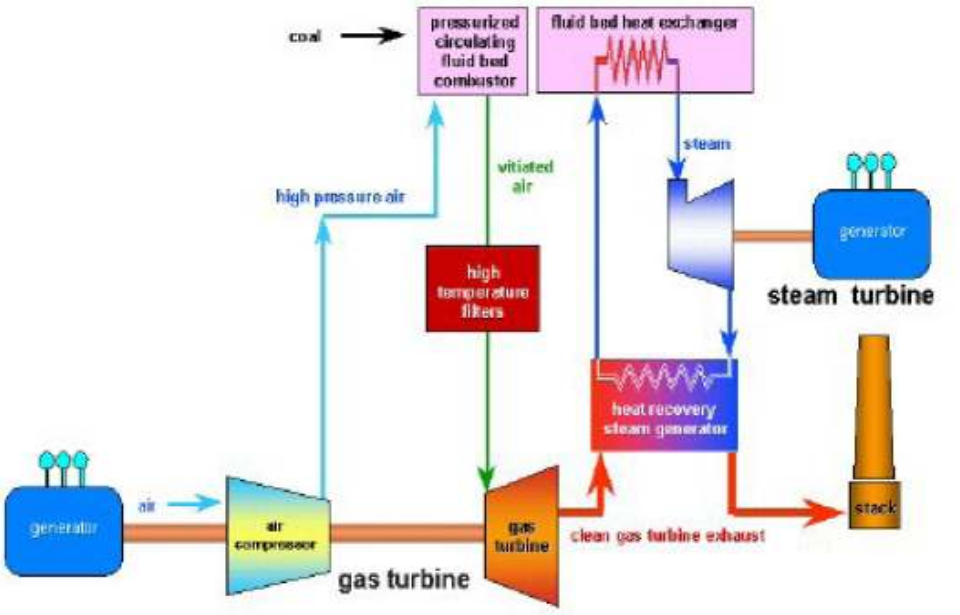

Figure 1.9: Pressurized bed combustion combined cycle [184]

The off-gas from the FBC drives the gas turbine. The steam turbine is driven by steam raised in tubes immersed in the fluidized bed. The condensate from the steam turbine is pre-heated using waste heat from gas turbine exhaust and is then taken as feed water for steam generation. The PFBC system can be used for cogeneration or combined cycle power generation. By combining the gas and steam turbines in this way, electricity is generated more efficiently than in conventional system. The overall conversion efficiency is higher by 5% to 8%. Figure 1.9 shows the pressurized bed combustion cycle.

1.6 Advantages of Fluidized Bed Combustors

- **High efficiency**: FBC boilers can burn fuel with a combustion efficiency of over 95% irrespective of ash content. FBC boilers can operate with overall efficiency of 84% *(±2%)*.
- **Reduction in boiler size**: High heat transfer rate over a small heat transfer area immersed in the bed results in overall size reduction for the boiler.
- **Fuel flexibility:** FBC boilers can be operated efficiently with a variety of fuels. Even fuels like flotation slimes, washer rejects, agro waste can be burnt efficiently. These can be fed either independently or in combination with coal into the same furnace.
- **Ability to burn low grade fuel:** FBC boilers would give the rated output even with an inferior quality fuel. The boilers can fire coals with ash content as high as 62% and having calorific value as low as 2500 kcal/kg. Even carbon content of only 1% by weight can sustain the fluidized bed combustion.
- **Ability to burn fines:** Coal containing fines below 6 mm can be burnt efficiently in FBC boiler, which is very difficult to achieve in conventional firing system.
- **Pollution control:** SO_2 formation can be greatly minimized by addition of limestone or dolomite for high sulphur coals (3% limestone is required for every 1% sulphur in the coal feed). Low combustion temperature eliminates NOx formation.
- **Low corrosion and erosion:** The corrosion and erosion effects are less due to lower combustion temperature, softness of ash and low particle velocity (around 100 cm/s).
- **Easier ash removal – No clinker formation:** Since the temperature of the furnace is in the range of 750 – 900°C in FBC boilers, even coal of low ash fusion temperature can be burnt without clinker formation. Ash removal is easier as the ash flows like liquid from the combustion chamber. Hence less manpower is required for ash handling.

- **Less excess air – Higher CO_2 in flue gas:** The CO_2 in the flue gases will be of the order of 14 – 15% at full load. Hence, the FBC boiler can operate at low excess air -only 20 - 25%.
- **Simple operation, quick start-up:** High turbulence of the bed facilitates quick start up and shut down. Full automation of start up and operation using reliable equipment is possible.
- **Fast response to load fluctuations:** Inherent high thermal storage characteristics can easily absorb fluctuation in fuel feed rates. Response to changing load is comparable to that of oil fired boilers.
- **No slagging in the furnace – No soot blowing:** In FBC boilers, volatilization of alkali components in ash does not take place and the ash is non sticky. This means that there is no slagging or soot blowing.
- **Provisions of automatic coal and ash handling system:** Automatic systems for coal and ash handling can be incorporated, making the plant easy to operate comparable to oil or gas fired installations.
- **Provision of automatic ignition system:** Control systems using micro-processors and automatic ignition equipment give excellent control with minimum supervision.
- **High reliability:** The absence of moving parts in the combustion zone results in a high degree of reliability and low maintenance costs.
- **Reduced maintenance:** Routine overhauls are infrequent and high efficiency is maintained for long periods.
- **Quick responses to changing demand:** FBC can respond to changing heat demands more easily than stoker fired systems. This makes it very suitable for applications such as thermal fluid heaters, which require rapid responses.

- **High efficiency of power generation:** By operating the fluidized bed at elevated pressures, it can be used to generate hot pressurized gases to power a gas turbine. This can be combined with a conventional steam turbine to improve the efficiency of electricity generation resulting in a potential fuel savings of at least 4%.

1.7 Classification of Biomass Fuels / Agri Residues

Biomass fuels cover a large diversity of biomass feed stocks that have a variety of compositions and therefore, it is appropriate to classify them into several categories. Generally, there are five main categories of biomass [15]

i. Wastes ii. Herbaceous iii. Aquatic iv. Woody v. Derivatives

Wastes for instance would include refused-derived fuel (RDF) and sewage sludge. Herbaceous on the other hand would include grass, straws and stalks. Aquatic would include kelp whereas woody would take both soft and hard wood into account. Paper would be categorized under derivatives [15]. Biomass consists of lingo cellulose, which collectively included three main components of biomass; cellulose, hemi cellulose and lignin. Cellulose is a crystalline polymer of glucose; hemi cellulose is a morphous polymer of 5 or 6 carbon sugars whereas lignin is a phenolic polymer having a random structure [16]. Generally, when compared with coal, biomass as a fuel has the following characteristics:

i. Higher volatile matter content [17]

ii. Lower heating values [18]

iii. Less carbon [17]

iv. More oxygen [17]

v. Higher moisture content [18]

vi. Biomass ash is more alkaline [18]

vii. Usually lower density [19]

viii. Wider size distribution even after pulverization [20]

1.8 Types of Rice Waste

Rice waste means remaining residues of rice crop. Rice waste is one such agro residues which are found in regions where the demand for energy exists. Rice waste is composing of rice straw, rice husk and rice bran mainly as shown in Figure 1.10. Rice crop waste composed of 70-80% rice straw, 20-30% rice husk and 1-2% rice bran. Most of rice straw is burned in open fields; little percentage is available for commercial fluidized bed combustors in this region. Rice husk and rice bran are by products of milling. Rice bran is used for oil and not available for combustion. Rice husk as it could easily bought from rice mill owners is available for commercial fluidized bed combustors.

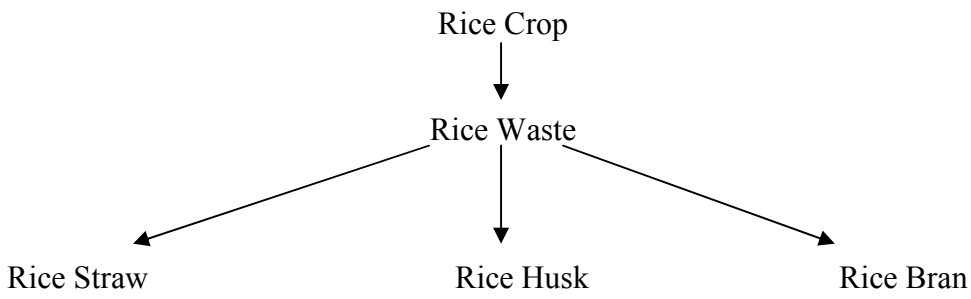

Figure 1.10: Types of rice waste

1.8.1 Characteristics of Rice Husk

Rice is a member of the grass family. There are more that 10,000 species of grasses distributed among 600 genera [21]. The rice kernel has four primary components: the hull or husk, the seedcoat or bran, the embryo or germ, and the endosperm. The main objective of milling rice is to remove the indigestible hull and additional portions of bran to yield whole unbroken endosperm [21]. Figure 1.11 shows the rice husk particles. The rice husk is cylindrical in shape. The size of rice husk particle varies from 0.4 to 1 cm.

The rice hull/husk contains approximately 20% opaline silica in combination with a large amount of the phenyl propanoid structural polymer called lignin. Such a high percentage of silica is very unusual within nature [22] and this intimate blend of silica and lignin makes the rice hull not only resistant to water penetration and fungal decomposition, but also resistant to the best efforts of man to dispose of it. Since hulls do not biodegrade or burn very easily, they are sometimes available free-of-charge [22]. The hull is a very tough and abrasive packaging material, consisting of two interlocking halves. It encapsulates the tiny space vacated by the milled grain, and in proximity to a myriad of other hulls, it forms a thermal barrier that compares well with that of excellent insulating materials [22].

The peculiar silica-cellulose 'drinking-straw bundle' structural arrangement of the husks results in an object that does not burn or even liberate heat in a manner

Figure 1.11: Rice husk particles

resembling that of any organic substance. These minute silica-crested tubular structures offer an inherent resistance to burning. Often they seal off and prevent the thorough, uniform burning essential to obtaining a desired end-product [22]. Rice husks are flame retarding and, at ordinary temperatures self extinguishing. A lighted match, tossed onto a pile of rice husks will generally burn out without producing a self-sustaining flame in the husks [22]. Distillation of husk decomposes the cellulose to carbon and steam volatiles residues and tar go with steam. When

heated to red heat in presence of air or oxygen, the carbon is burnt off to CO_2, leaving carbon-silica residue. To increase carbon recovery, a uniform and adequate heating of whole mass of husk-cinder, draught control and air distribution of size distribution are very critical. Increasing oxygen level in air improves carbon recovery.

The analysis of husk varies within a limited range depending upon the variety paddy, region and ageing. When the rice husk burning is intended for utilization of heat directly for steam generation, heating of heat transfer fluids etc., it is very convenient to burn it with excess air as compared to other methods. It is necessary to complete the combustion of husk in the furnace zone. There are a few difficulties associated combustion of rice husk:

- It is high silica-cellulose structure arrangement couple with nodular shape makes it the most difficult organic substance for combustion and handling. The minute silical crested tubular structures offer an inherent resistance to burning. They often seal off and prevent through and uniform burning.
- Size/ volume of ash make grate design and ash handling difficult and inefficient.
- Irregular supply and low bulk density (0.1- 0.2 g/cm^3) need large storage yard. Due to low density generally it gets drifted by wind. Inert solid materials and metal scrap mix with it. When rain soaked and decomposed, the pile gets a fire by spontaneous combustion.
- It has low inertia and high air resistance, making it difficult to throw pneumatically
- The husk and its ash both cause excessive wear to the handling machinery.

1.8.2 Characteristics of Rice Straw

Rice straw is low density fuel, having density approx. 0.09 g/cm^3. Rice straw is presently used and disposed of in the following ways: burned in fields/plowing into fields 61.5%, animal feed 11.6%, compost 10.1%, cattle house flooring 6.5%, covering material for fields 4%, straw

handicraft 1.3%, other 0.3%, combustion 4.6% [23]. Strictly speaking, only 4.6%, the portion now disposed of through fluidized bed combustion, can be used as energy source. However, other materials can easily substitute rice straw in its current uses. Figure 1.12 shows the pellets of rice straw in fields, available for fluidized bed combustion. Huge cost is involved in collection of rice straw. Moreover it has to be collected immediately after harvesting season or during harvesting season. Rice straw when available for combustion creates problems like feeding and agglomeration. Agglomeration problems are more predominant in case of rice straw when burned in fluidized bed combustors. About 80 % of rice straw available in region is burned in open fields. In some areas all of remaining rice residues burned in open fields.

Figure 1.12: Pellets of rice straw

1.8.3 Characteristics of Rice Bran

Bran is the hard outer layer of grain and consists of combined aleurone and pericarp. Along with germ, it is an integral part of whole grains, and is often produced as a by-product of milling in the production of refined grains. When bran is removed from grains, the latter lose a portion of their nutritional value. Bran is present in and may be milled from any cereal grain, including rice,

corn, wheat, maize, oats, barley, and millet. Bran should not be confused with chaff, which is coarser scaly material surrounding the grain, but not forming part of the grain itself. Bran is particularly rich in dietary fiber and omegas and contains significant quantities of starch, protein, vitamins, and dietary minerals.

Figure 1.13: Rice bran [185]

Rice bran is a by-product of the rice milling process and it contains various antioxidants that impart beneficial effects on human health. 100000 g of paddy rice will generate approx 5000 to 8000 g of bran. The moisture content of rice bran is 10 to 15 %. Rice bran is a mixture of substances, including protein, fat, ash, and crude fiber. In many cases, bran contains tiny fractions of rice hull, which increases the ash content of bran. The bulk density of rice bran is about 0.15-0.2 g/cm^3. The high oil content of bran makes it subject to rancidification, one of the reasons that is often separated from the grain before storage or further processing. The bran itself can be heat-treated to increase its longevity. Bran is often used to enrich breads (notably muffins) and breakfast cereals, especially for the benefit of those wishing to increase their intake of dietary fiber. Figure 1.13 shows the pile of rice bran in the rice mill.

1.9 Ultimate and Proximate Analysis

1.9.1 Rice Husk

The average properties of rice husk as reported by Pathak and Jain [24] were as follows. On the dry basis, the volatile matter was ~60%, the fixed carbon ~ 20% and the ash ~20%. The ultimate analysis (dry basis) was: C~38%; H~4%; O~38%; S~0.02%; N~0.4%; ash~20%. The gross calorific value was 14 MJ/kg. The ash [25] composition was SiO_2~95%; K_2O~2.0%; Na_2O~1.5%; CaO ≥1.5%; MgO ≤1.0. The elementary analysis of rice husk (on dry basis) were reported by Simonov et al. [26] C 43.5 %, H 5.5 %, O 35.2% N 0.05% S 0.02% Cl 0.015% Ash 15.7%.

1.9.2 Rice Straw

The average properties of rice straw as mentioned by [27] were as follows. The volatile matter was 63.13%, fixed carbon 18.1%, ash 9.87% and moisture was 8.9%. The ultimate analysis was carbon 42.04 %, Hydrogen 6.26%, Nitrogen 1.23%, Sulphur 0.64 % and Oxygen 39%. The elementary ash analysis reported as CaO 9.23%, K_2O 38.92%, Na_2O 2.16%, SiO_2 44.72%, Al_2O_3 1.13%, FeO 0.14%, TiO_2 0.03%, MnO 0.04%, MgO 1.96%, BaO 0.04% and P_2O_5 1.63%. The gross calorific value was 15 MJ/kg.

1.10 Fluidization Behavior of Rice Husk

The quality of fluidization of rice husk can be controlled by changing superficial velocity of air within permissible limit for a chosen particle size. It is [28] difficult to fluidize rice husk due to its cylindrical shape, non granular and flaky nature. The fluidization behavior of rice husk can be [28, 29, 30] improved when it is mixed with other solid particles.

Flanigan et al. [12] and Xu et al. [30] studied fluidized bed gasification of rice hulls. It was presented that fluidization of rice husk was difficult unless it was mixed sand/char/ash to

form multi-solid system. It was found that fluidization behavior of mixture of husk and its ash is better than sand and rice husk. Further it was concluded that minimum fluidization and terminal velocities of husk ash was about 16 and 80 cm/sec respectively. The minimum fluidization velocity of husk and sand mixture was approximately equal to the terminal velocity of sand.

Qiaoqun et al. [31] studied the fluidization behavior of rice husk-sand mixture in the gas bubbling fluidized bed experimentally and theoretically. The relevancy of the pressure drop profile of rice husk-sand mixture to the definition of its minimum fluidization velocity was discussed, and the minimum fluidization velocity of rice husk-sand binary mixture was determined. The distributions of mass fraction of rice husk particles along the bed height were measured, and the profiles of the mean particle diameter of mixture are determined. A multi-fluid gas-solid flow model was presented where equations are derived from the kinetic theory of granular flow. Separate transport equations were constructed for each of the particle classes, allowing for the interaction between particle classes, as well as the momentum and energy are exchanged between the respective classes and the carrier gas. The distributions of the mass fraction of rice husk particles and the mean particle diameter of binary mixture were predicted. The numerical results were analyzed and compared with experimental data.

Nguyen [32] studied that the rice husk and wood pellets had particular characteristics so that they could not be fluidized alone. In order to process rice husk and wood pellets for fluidization applications, another fluidization material must be added to support the fluidization of the bed. Inert materials such as quartz sand, calcite, dolomite, olivine, etc. could be used as such fluidization bed materials. However, the fluidization behavior of the mixture of two different materials would be dependent on the percentage of biomass in the mixture. Many experiments had been carried out to study the fluidization and mixing behavior of the mixtures of

biomass and quartz sand. Fluidization behavior had become more complex and the characteristic values of the mixture (e.g. U_{mf}) were not easy to determine. The standard deviation of pressure drop fluctuation was decreased when adding biomass to the sand bed depending on the percentage of biomass in the mixture. A good mixing was difficult to obtain when biomass and sand was initially in separated layers but becomes easier when biomass was continuously fed into the fluidized bed. Rice husk affected the fluidization behavior of the bed more than wood pellets due to its lower density and different shape. Experiments were carried out also on gasification of rice husk and wood pellets in a laboratory scale fluidized bed gasifier. Gas product compositions and tar content were measured at different temperatures and equivalent ratios. Temperatures inside reactor, gas compositions, and tar content in the producer gas were recorded or analyzed to understand the gasification process. While the gasification process occured quite stable with wood pellets, some problems had been recognized when gasifying rice husk. Due to its low bulk density, high ash content and specific characteristic of rice husk ash, the problem of rice husk ash removal had become significant. Furthermore, also the feeding of rice husk due to its low density and surface characteristics was not easy. This was a quite normal because there will be no existing gasifier that can be operated with every fuel.

Sen and Ghosh [28] studied the fluidization and combustion characteristics of rice husk. They studied the fluidization behavior of rice husk using a perspex column with 7.6 cm diameter and 90 cm high and a multiorifice distributor plate. They found that fluidization of ground/broken husk was smoother compared to the whole husk. They further found that minimum fluidization velocity and bed pressure drop for whole rice husk were greater than for ground husk. Fluidization of mixtures of char, ash and husk was shown channeling and poor movement of individual particles at low air velocities, but good mixing was observed at the

bubbling velocity with little classification among the different particles. Fluidization behavior of whole husk char was better than that of char but not as good as that of ash. It was also found that bubbling velocities of char and the mixture are same as that of husk.

1.11 Reaction involved in Combustion and Gasification of Rice Husk

The initial decomposition [33] of biomass fuel into combustible matter, water and ash can be expressed according the equations mentioned below. The biomass fuel containing carbon (C), hydrogen (H), oxygen (O), sulphur (S) and nitrogen (N), and water (W) and an ash (A) decomposes into combustible matter containing all these elements, water vapor and ash.

$$C_{xc}H_{xh}O_{xo}S_{xs}N_{xn}W_{xw}A_{xa} = C_{xc}H_{xh}O_{xo}S_{xs}N_{xn} + xw.W + xa.A \quad (1.1)$$

The biomass (dry and ash free) can also be represented as $CH_hO_oS_sN_n$ where the variables h, o, s and n are determined from the ultimate analysis of the biomass.

1.11.1 Pyrolysis (Devolatilization)

The pyrolysis reaction as reported by Manasray et al. [34] can be represented as follows:

$$CH_{\alpha h}\,O_{\beta h}(SiO_2)_{\delta h} \longrightarrow CH_{\alpha}O_{\beta}(SiO_2)_{\delta} + \text{volatiles} \quad (1.2)$$

rice husk char

where αh, βh, δh and (α, β, δ) are determined from the ultimate analyses of rice husk and char, respectively. The volatiles include CO, CO_2, H_2, H_2O, CH_4, low molecular weight hydrocarbons, char, and tars.

1.11.2 Combustion and Gasification

The devolatilized char first undergoes partial combustion by oxygen to produce CO and CO_2 as reported by Manasray et al. [34] is as follows:

$$CH_{\alpha}O_{\beta}(SiO_2)_{\delta} + \gamma O_2 \longrightarrow [2 - 2\gamma - \beta + \alpha/2]CO + [2\gamma + \beta - (\alpha/2)]CO_2 + (\alpha/2)H_2O + \text{ash} \quad (1.3)$$

and the rest undergoes several gasification reactions, some of which are shown below:

$$CH_\alpha O_\beta(SiO_2)_\delta + (1 - \beta)H_2O \longrightarrow CO + [1 - \beta + \alpha/2\ ]\ H_2 + ash \quad (1.4)$$

$$CH_\alpha O_\beta(SiO_2)_\delta + CO_2 \longrightarrow 2CO + \beta H_2O + [\alpha/2 - \beta\ ]H_2 + ash \quad (1.5)$$

$$CH_\alpha O_\beta(SiO_2)_\delta + [(4- \alpha +2\beta)/2]H_2 \longrightarrow CH_4 + H_2O + ash \quad (1.6)$$

$$H_2+1/2\ O_2 \longrightarrow H_2O \quad (1.7)$$

$$CO\ +1/\ 2O_2 \longrightarrow CO_2 \quad (1.8)$$

$$CO\ +\ H_2O \longrightarrow CO_2 + H_2 \quad (1.9)$$

$$CH_4\ +\ H_2O \longrightarrow CO + 3H_2 \quad (1.10)$$

1.12 Scope of Work

The work presented in this thesis with respect to study of performance of atmospheric bubbling fluidized bed combustors based on rice waste is not only limited to rice waste but could be correlated with other types of agriwaste or biomass.

Rice husk and rice straw are only waste materials from rice crop, which are incinerated in fluidized bed combustor in Punjab and adjoining areas. Due to higher collection cost, feeding problems and agglomeration problems the rice straw is not incinerated in most of commercial fluidized bed combustors in present form.

Rice husk can be easily bought from commercial rice mill owners. Due to this reason rice husk is the main fuel used in commercial atmospheric fluidized bed combustors based on rice husk/rice straw. So our focus of study is mainly the fluidized bed combustion of rice husk.

1.13 Organization of Thesis

The division of dissertation is into mainly eight parts. First part regarding the introduction on fluidized bed combustion of rice husk/rice straw, biomass scenario, types of fluidized bed

combustors, advantages of fluidized bed combustors, classification of biomass fuels, types of rice waste, fluidization behavior of rice husk were already explained in **Chapter 1.**

Chapter 2 is related to literature review and problem formulation. Extensive literature on two phase and three phase combustors basic approach, modeling of fluidized bed combustors, fluidized bed combustors based on rice husk, agglomeration in fluidized bed combustors and CFD analysis is reviewed. Later in this chapter objectives and problem formulation are explained.

Chapter 3 is related mainly to real plant data of rice husk power plant. Description of two rice husk plants from which data is collected is explained in this chapter. The results from fuel analysis and various reading/parameters noted from plant are explained in this chapter.

Chapter 4 is related to mathematical modeling of fluidized bed combustor of rice husk. It starts with physico chemical processes of fluidized bed combustors. Exit gas model and solid population models are formulated in this unit.

Chapter 5 is related with agglomeration mechanism of biomass based fluidized bed combustor units. The problem of defluidization of fluidized bed combustor with respect to rice husk alone and rice husk/rice straw combination is explained in this chapter. The data collected related to agglomeration is presented in this chapter. TGA of rice husk and rice straw done on Perkin Elmer-6 is explained. SEM and quantitative elementary analysis of various samples are presented here.

Chapter 6 is mainly related to CFD analysis of fluidized bed combustor based on rice husk. Two dimensional bed is considered here because of limited computational space. Rice husk diameter of 0.438 cm and superficial velocity of 120 cm/s is considered. Bed Temperature

is assumed to be isothermal and main purpose to validate three phases present in fluidized bed combustor based on rice husk.

Chapter 7 is related with results and discussion. This is also divided into three parts. In first part exit gas and solid population balance models were validated against plant data. Then the results of agglomeration mechanism were explained. The results of SEM, TGA of rice husk samples done explained in this chapter. Final part of this chapter contains the results pertaining to CFD analysis of fluidized bed combustor. The results related to solid volume fraction and velocity contour were explained in this.

Chapter 8 is related with conclusion and future scope of thesis. References and appendix is given at end which provides all the experimental and other details required in study.

CHAPTER 2

LITERATURE REVIEW AND PROBLEM FORMULATION

This chapter starts with basic approach to two and three phase fluidized bed combustor modeling. It is followed by extensive literature survey on modeling of fluidized bed combustors. Then literature survey on fluidized bed combustors based on rice husk and agglomeration of fluidized bed combustors based on biomass is done. Later in this chapter literature on CFD modeling is reviewed. The objective of this chapter is to review all the literature related to the subject extensively. Finally limitations of literature review are explored and problem is formulated.

2.1 Two and Three Phase Combustors: Basic Approach

Many types of two phase and three phase models have been developed to describe fluidized bed combustion operation. It is commonly assumed that the bed is composed of two distinct phases, viz. a dense phase (consisting of solid particles and interstitial gas) and a bubble phase containing almost no solids. The more sophisticated models also consider an additional phase, viz. a cloud-wake phase associated with bubble. Further variations appear in the characterization of gas flow within each phase, mode of exchange of gas among phases, bubble shape, and velocity etc. In modeling of any fluidized-bed combustor, a primary objective must be to represent accurately the key physical or hydrodynamic features of the system before inserting chemical kinetics and other chemical parameters. At the same time, it is important that model should be sufficiently straightforward and simple so that their application does not demand excessive computation. The word ‘phase’ (Geldart [35]) refers to a region that may include both gas and solid particles. The phases are distinguished from one another in terms of the volume fraction of solids, physical appearance, and their characteristics. In one group of models, the

dilute phase is either free of particles or assumed to contain widely dispersed solids. In these models, no distinction is made between cloud and other interstitial gas elements. In the second group of models, the cloud, gas and solids (with or without bubble wakes) are lumped with bubbles to give a combined bubble/cloud phase).

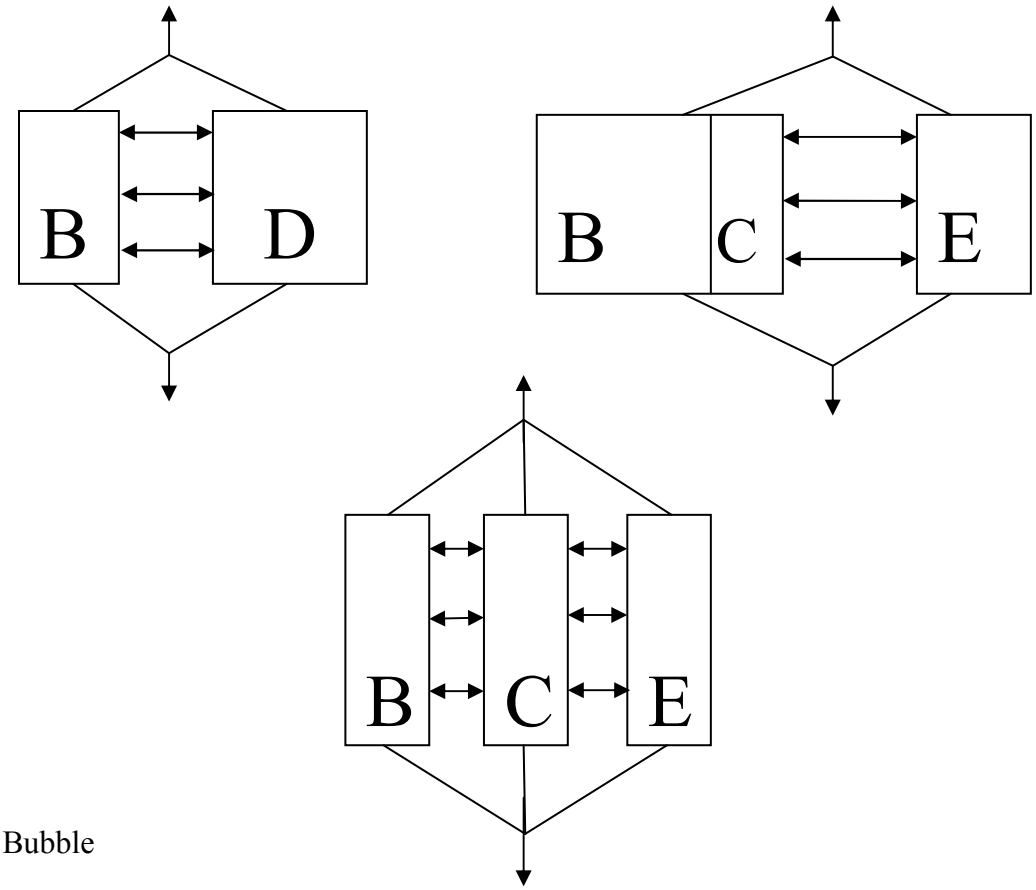

B = Bubble

C = Clouds

D = Dense phase

E = Emulsion

Figure 2.1: Schematic diagram showing different phases in fluidized bed, Geldart [35]

Gas within the cloud is then assumed to have the same composition as gas within the bubble surrounded by the cloud. In a third group, the cloud is treated separately from both

bubbles and remaining dense phase (often called the emulsion), so that there are three phases (Figure 2.1) chosen in fluidized bed combustor models. Depending upon the general physical nature of the phases the decision of the distribution of gas flow between the phases, and heterogeneous gas solid reactions is done in the following ways:

- The particles usually undergo significant physical changes (e.g., shrinkage, density and shape) during the course of combustion
- The kinetics of combustion may be complex (single film model or double film model) as suggested by many model builders. In addition to this, expressions for carbon burnout time, Sherwood number, and Nusselt number have been presented by many model builders to describe the combustion kinetics and heat transfer in a fluidized bed coal combustor.
- In fluidized bed operations, particle size distribution in the bed governs and contributes to many physical and chemical aspects of fluidization. Therefore the size distribution of solid particles is an important parameters for the accurate analysis of the processes occurring in a fluidized bed. So in order to account for the behavior of different size fractions during combustion solid population balance are often written incorporating the particle shrinkage, elutriation, and attrition etc. So a perfect model for a fluidized bed combustor should incorporate all of the following;
    - Gas solid reaction in all possible phases that is in emulsion, wakes, and clouds.
    - Exchange of gas and solids between all possible phases.
    - Flow of gas and solids within phases.
    - Variation of gas and solid flow due to combustion.
    - Change in particle composition and size distribution due to combustion.

In addition, carbon loss, bubble diameter, bubble velocity, temperature profile, and carbon utilization efficiency in fluidized bed combustors have been studied by many scientists and engineers. Some of their major findings are presented and discussed in literature survey. The importance of the burning rate (i.e., rate of oxygen transfer) of individual particles is that, it enables carbon load and carbon utilization efficiency to be predicted. The reactions which govern the combustion of are;

$$C + O_2 \longrightarrow CO_2 \quad (2.1.1)$$

$$2C + O_2 \longrightarrow 2CO \quad (2.1.2)$$

$$CO_2 + C \longrightarrow 2CO \quad (2.1.3)$$

$$2CO + O_2 \longrightarrow 2CO_2 \quad (2.1.4)$$

The first three are heterogeneous reactions and are generally assumed to take place either at the external or internal surface area of the char particles. The relative contribution of internal surface area varies from one type of coal to another type. The fourth one is a homogenous reaction and takes place in or outside the boundary layer of the char particles. Although the char is a porous substance and inner particle diffusion probably plays a role in the combustion process according to Smith et al. [36].

In this context, two basic mechanisms; single film and double film have been postulated for char combustion. The first postulate assumes the direct oxidation of the char particles by diffusion of oxygen through a stationary film to the surface of the carbon particles where it reacts to produce varying amounts of CO and CO_2 by reactions 2.1.1 and 2.1.2 respectively. The CO formed is then oxidized to CO_2 by a homogenous reaction 2.1.4, which takes place in the

boundary layer around the particle or in the remaining gaseous phase of the bed. When the combustion of CO occurs close to the particle, the reaction at the surface may effectively be described by reaction 2.1.1. Figure 2.2 shows the concentration profile of various

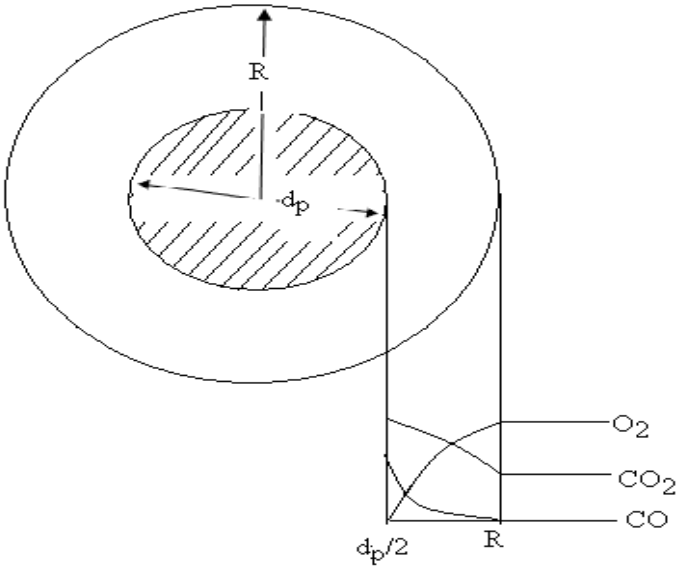

Figure 2.2 Single film theory

species as per single film model.

In the second postulate, oxygen diffusing towards burning particles is consumed before it reaches the particle by reaction 2.1.4 and carbon reacts at the surface with CO_2 only by reaction 2.1.3. The CO formed diffuses away the particle and burned in a thin flame front in the boundary layer with incoming oxygen. This reaction produces more CO_2 of which from the stochiometry, one half diffuses away and other half diffuses back to the surface to complete the cycle. Hence no oxygen will reach the external edge of the boundary layer. The schematic representation of the double film is shown in Figure 2.3.

The two theories of combustion have received support from number of researchers and the detail of the subject can be found in the works of Spalding [37], Field [38], Caram and

Amunson [39], Yates and Walker [40], Bukur and Amundson [41], Ross and Davidson [42], Turnbull et al. [43] and Park [44].

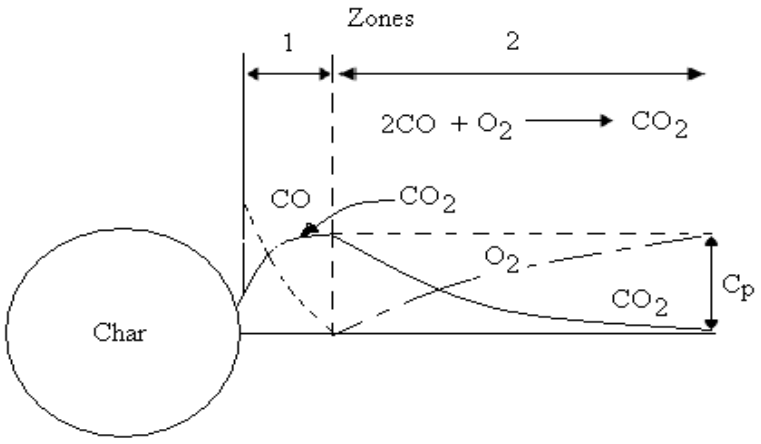

Figure 2.3 Double film theory

2.2 Fluidized Bed Combustion Models

In this paragraph overall fluidized bed combustor models are shortly reviewed. Fluidized bed models consider the division between the bubble phase and the particulate phase, also called emulsion or dense phase, the degree of mixing in the particulate phase and the transfer of gas between the two phases. The reason for developing a conceptual model for the bubbling bed is to estimate its main features, such as velocities of gas and solid, volume fractions and contacting regimes, from very little information about the solid particles in the bed. The first attempt to model fluidized bed combustors was presented by Yagi and Kunii [45], who did not consider, however, the presence of the bubble phase.

The significant breakthrough was made by Davidson [46] who proposed a straightforward, simple model for single rising bubbles, based on the following postulates: a gas bubble is solid-free and circular in shape; as a bubble rises, particles move aside. The emulsion

behaves like an incompressible fluid of bulk density through which the gas flows as an incompressible viscous fluid. Pressure in the bubble is assumed to be constant. One of the most appreciable results of this model is the pressure distribution near a 3-D bubble: the pressure in the lower part of the bubble is lower than that of the surrounding bed, whereas in the upper part it is higher. Hence, gas flows into the bubble from below and leaves at the top. Although the circular shape of the bubble is not a realistic hypothesis, the Davidson model fits the data quite well.

A significant attempt to understand the behavior of a bubbling bed as a whole was made by Toomey and Johnstone [47], the fathers of the two-phase theory of fluidization. Since experiments in bubbling beds indicate roughly that all gas in excess of that needed to fluidize the bed passes through the bed as bubbles and the emulsion phase remains close to minimum fluidizing conditions, they considered the bubbling bed to be composed of two phases: the bubbling phase and the emulsion phase. The emulsion flow rate is equal to the flow rate for incipient fluidization (U_{mf}) while the bubble phase carries the additional flow of fluidizing fluid (U_o-U_{mf}). Comparison between predicted and experimental data makes it clear that the two-phase theory overestimates the volume of gas passing through the bed as bubbles. Besides, evaluation of solids movement in the bed is not considered.

A more detailed description of the bubbling bed was proposed by Kunii and Levenspiel [48]. They introduced a new phase called ‘‘cloud’’ thus their contribution is also known as the three-phase theory (Figure 2.4). Consider the following flow patterns: if the emulsion gas rises faster than the bubble, it enters the bottom of the bubble and leaves at the top; this generates an annular ring of gas that circulates within the bubble. On the contrary, if the bubble rises faster than the emulsion, the gas leaving the top of the bubble is swept around and returns to the base of

the bubble. The region around the bubble covered by this circulating gas is the cloud: slow bubbles are cloudless whereas, in the case of fast bubbles, cloud cannot be neglected. In addition, this model is the first to show that solids are dragged up the bed behind bubbles and drift downwards in the emulsion. Although, the volume fraction of particles dispersed in rising bubbles might be less than 0.1%, these could enormously affect processes in which rapid kinetics

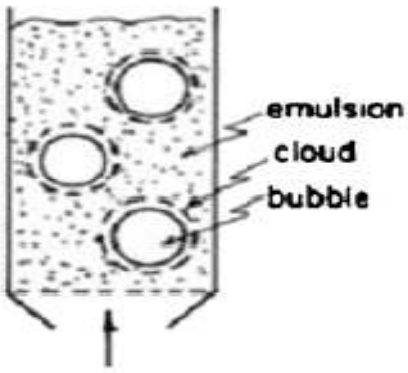

Figure 2.4 Representation of the three phases in a fluidized bed

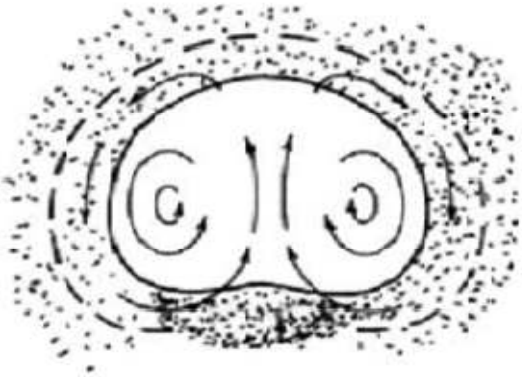

Figure 2.5 Gas flow pattern around and within the bubble according to Kunii and Levenspiel's

occurs. Unlike the previous theory, bubbles are not spherical but have a flattish, or even concave base (Figure 2.5). The region just below the bubble is the wake: this leaks the solid matter that a rising bubble drags up, assuring an interchange with the emulsion. This model hypothesizes that all the fluid passes through the bubble phase (the gas flow through the emulsion is negligible) and solid matter mixes perfectly with the gas in the emulsion phase.

A big impulse to fluidized bed combustion modeling was given in the seventies and eighties. Since then a great amount of models has been presented in literature as reviewed by La Nauze [49] and Adanez and Abanades [50]. Davidson and Harrison [46] explained that most models apply the two-phase theory of fluidization in order to characterize bubbling bed fluid

dynamics. A limited number of models assume the presence of three phases: bubbles, clouds (and wakes) phase and emulsion as reported by Chen and Saxena [51]; Sriramulu et al. [52].

The typical assumption for two-phase models is to consider gas in the bubble phase in plug flow while gas in the dense phase well mixed (Gordon et al. [53], Bukur and Amundson, [54]). Exceptions to this assumption are the models of Horio and Wen [55], Rajan et al. [56] and Rajan and Wen [57] where mixed flow in both phases is considered, and the models of Becker et al.[58], Chen and Saxena [51] and Arena et al. [59] where plug flow in both phases is considered. On the other hand authors proposing models for large scale operation suggested that no distinction has to be made between bubble phase and dense phase because bubbles are in the cloudless regime, so that global plug flow can be assumed (Park et al. [60] and Bellgardt et al. [61]). A similar assumption was made also for shallow bed combustors by Chakraborty and Howard [62]. Solids in the dense phase are usually assumed to be well mixed. Fan et al. [63] and Bellgardt et al. [61] considered finite radial dispersion of solids. A more complex circulation pattern of solids was developed by Sriramulu et al. [52].

Early models assumed kinetics of char combustion controlled only by external diffusion (Avedesian and Davidson [64]; Becker et al. [68]; Chen and Saxena [61], Fan et al. [63]; Bukur and Amundson [54]), while later models recognized that also surface reaction and intraparticle diffusion can be relevant to the overall char combustion kinetics. Some models took into account also resistance to gas diffusion through a coherent ash layer that forms around the char particle (Saxena and Rehmat [65]; Lemcoff [66]).

Zhang et al. [67] presented combustion model for a CFB boiler with consideration of post-combustion in the cyclone. In this study, post combustion in cyclone was modeled and a novel 1D combustion model of CFB boiler with consideration of post combustion in cyclone

was developed. This model was used to predict post combustion in CFB boilers with the capacity of 135 MW, and the predictions were consistent with measured data. The influences of coal rank and excess air ratio on post combustion were also studied by this model. It was found the influence of coal rank on post combustion is significant and post combustion is more intensive when anthracite is fired than that when bituminous and lignite is fired. With the increment of excess air ratio, temperature augment and heat release ratio in the cyclone also increase. They further concluded that in future, the 1D CFB combustion model with consideration of post combustion in the cyclone will be further improved.

Mohapatra et al. [68] developed a mathematical model for oxygen mass balance for a 10 MW fluidized bed coal combustion power plant operated at Jamadoba (TISCO, India) using coal washery rejects. Assuming three-phase theory of fluidization, the fluid bed is considered to consist of a number of equivalent stages in series. Within each stage, an exchange of gas takes place between the bubbles, cloud wake and emulsion phases. The model has been used to predict the consumption of oxygen in the fluidized bed combustor, the outlet gas composition, variation of average oxygen concentration along the bed height. Model prediction was compared with plant data and reasonable accuracy was obtained. They had reported a decrease in the average concentration of the oxygen, as the bed height is increased, as shown in the Figure 2.6 and this is true for different amount of excess air values. A variation of the oxygen concentrations in different phases along the bed height was also explained. The oxygen concentration in the bubble phase decreases gradually but, it is steep in the cloud-wake and the emulsion phase at the lower bed levels. The oxygen concentration in the bubble phase is highest, followed by the

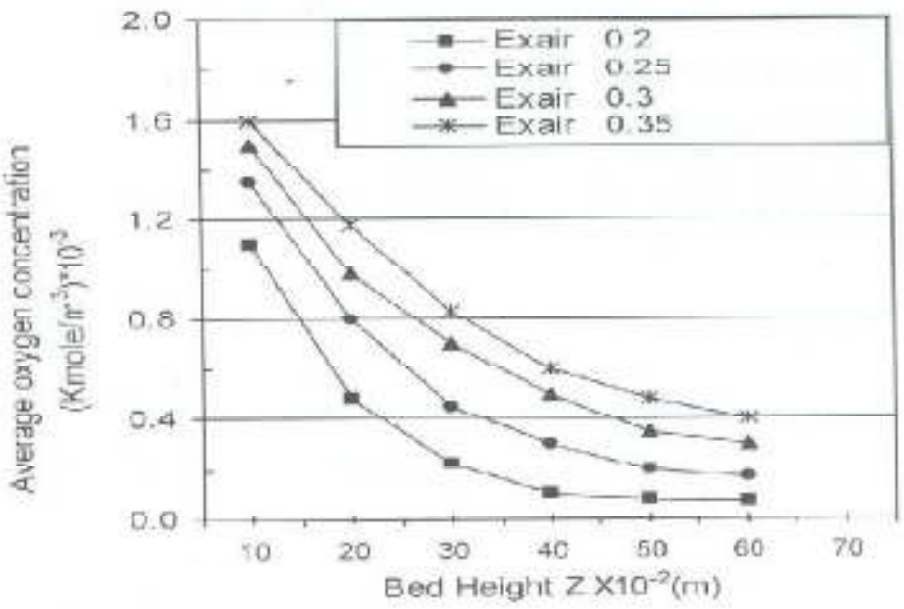

Figure 2.6 Variation of average oxygen concentration with bed height at different fraction of excess air

cloud-wake and the emulsion phases, because combustion occurs in the emulsion phase, as a result of which oxygen consumption in this phase is highest and hence the oxygen concentration lowest.

Due to distinct features of biomass, it is difficult to model fluidized bed combustor based on biomass. However a few models have been reported in literature for fluidized bed combustors based on biomass. The following literature is about modeling of fluidized bed combustors based on biomass.

Galgano et al. [69] presented a dynamic model of an atmospheric bubbling fluidized bed combustor using biomass. The model was used to predict the dynamic behavior of the combustor with some of the operating parameters. Towards end bifurfication analysis was done to study the influence of selected parameters on the number and quality of steady state solutions. Dynamic simulation showed that the bed temperature changes slowly when a step

wise change was imposed on the selected parameters. Either a new steady state or extinction eventually results, depending upon the step wise change. The relaxation time of the bed was determined by the heat capacity of the fluidized solids and by the fraction of the heat released recycled to the bed as thermal feed back.

Arena et al. [70] provided a framework for the quantitative assessment of the fate of fixed carbon in a fluidized bed combustor during the fluidized-bed combustion of a coal and two waste-derived fuels. The proposed series-parallel network of attrition-combustion-elutriation processes was based on the assumption that fixed carbon in the bed could be divided into a coarse phase and a fine phase made of respectively non-elutriable and elutriable particles of fixed size. Results showed that for the high-volatile fuels conversion of fixed carbon occurred to a large extent via the generation of carbon fines and the subsequent post combustion of these over their residence time in the combustor.

Irusta et al. [71] presented a three-phase model for high-volatile fuel fluidized bed combustion, incorporating attrition and fragmentation phenomena as well as secondary air injection above the bed. Devolatilization was assumed to occur partly in the freeboard and partly in the bed, the relative amount depending on a so called "internal devolatilization degree" adjustable parameter. Comparison with pilot plant experimental results of combustion of a lignocellulose waste allowed the authors to set the value of this parameter. Results showed that a significant amount (20-40%) of the volatiles burned in the freeboard.

Borodulya et al. [72] proposed a modified two-phase plume model for biofuel combustion in fluidized beds, taking in to consideration combustion of volatiles and char in both bed and freeboard but neglecting a particle attrition and fragmentation. The model predicts that up to 40% of the volatiles may burn in the freeboard.

Mansray et al. [34] [73] [74] presented two models (a single compartment and two compartments) capable of predicting the steady state performance of a dual distributor type fluidized bed rice husk gasifier under a wide range of operating conditions. They presented the performance of two thermodynamic models; one compartment and two compartment models developed for fluidized bed gasification of rice husk. The models were analyzed and compared in terms of their predictive capabilities of the product gas composition. They discussed the validity of the two compartment model developed for the fluidized bed gasification of biomass that was tested using experimental data obtained from a dual–distributor type fluidized bed gasifier.

Khan et al. [75] had developed a model of 1 MW atmospheric bubbling fluidized combustor burning waste wood fuel. The model was incorporated with solid and gas phases. The bed was assumed to consist of two phases, of which the emulsion phase takes both gas and solids into account, while the bubble phase consists only of gas. A wide size distribution of biomass feed, representative of the actual boiler feed, has been assumed. The model calculates the gas composition, velocities, and other important hydrodynamic parameters in both the emulsion and bubble phase. A particle size distribution model was included to calculate elutriation losses of fine char particles. This approach was novel in the sense that a population balance for fine particle class is derived, using the well-known mass balance principles, and a coupled discretized population balance equation, valid for the whole particle size range, is presented. The model took into account devolatilization, fragmentation, and attrition of the solid phase along with gaseous profiles. It was included with nine components for which differential equations had been derived and solved to calculate species concentration at any point along the bed height. The model was aimed to assess the effect of different parameters on boiler performance and gaseous emissions. A sensitivity analysis of the gaseous emission profiles with respect to different variables and

parameters defining different sub-models had been carried out. A homogeneous NOx model had been included with individual kinetic parameters for relevant species. It had been found that gas hydrodynamics play a significant role, and the system can be optimized using these parameters. Species concentration along the height of boiler was shown in Figure 2.7. The Oxygen concentration decreased along with bed height. CO_2 increased along with bed height. The effect

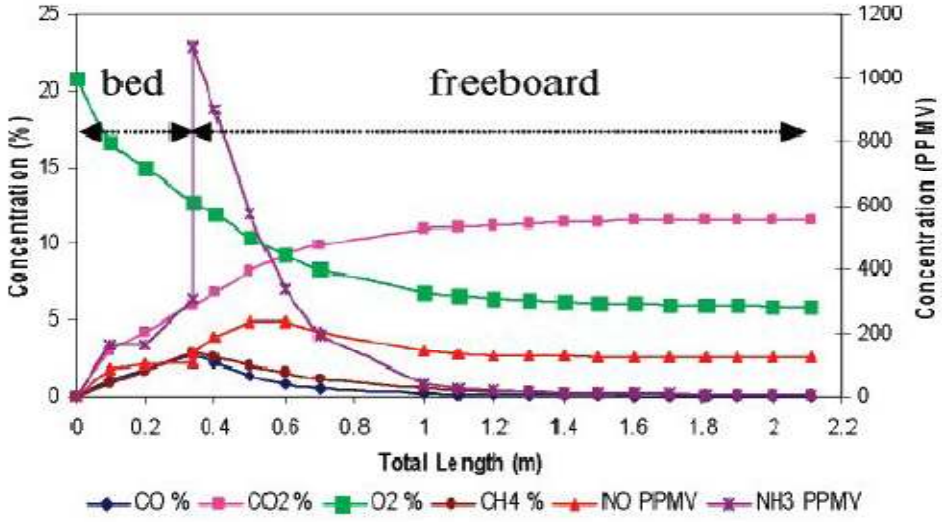

Figure 2.7 Predicted species concentration along the boiler height

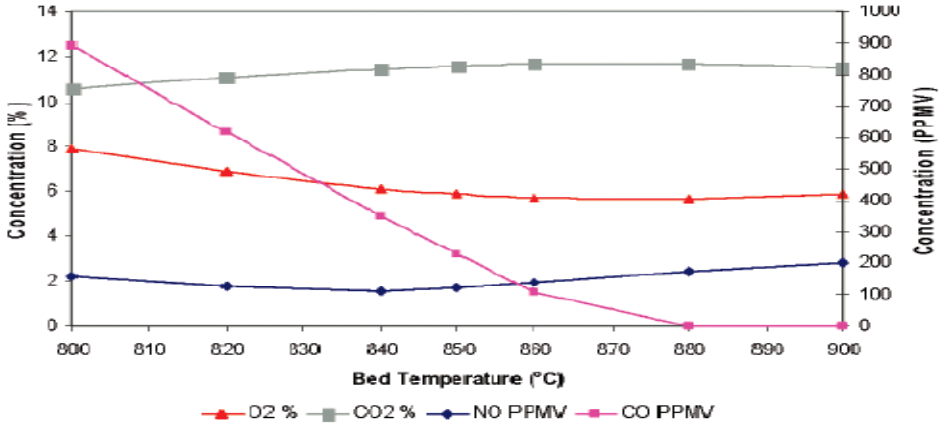

Figure 2.8 Effect of temperature on gaseous emissions

temperature on gaseous emissions was shown in Figure 2.8. The carbon monoxide decreased with bed temperature and NO increased with bed temperature. With increase in bed voidage as

shown in Figure 2.9 CO was decreased sharply after bed voidage of 0.45 and CO_2 was increased with bed voidage. Table 2.1 represents the brief review of previous fluidized bed combustion models.

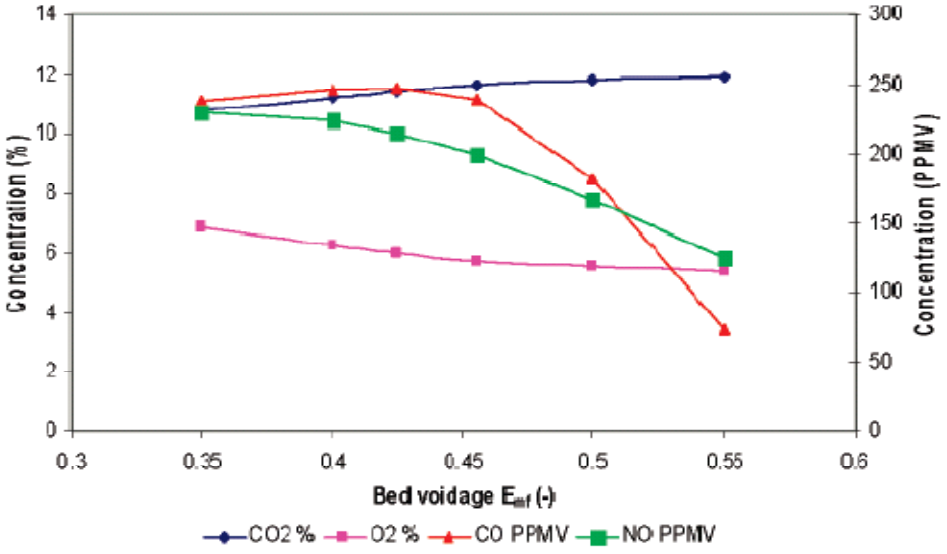

Figure 2.9 Effect of bed voidage on gaseous emissions

Table 2.1 Review of established fluidized bed combustion models

S no	References	Kinectics	Phases	Interphase Transfer	Gas Mixing	Solid Mixing	Heat Balance	Application and Comments
1	Yagi and Kunii [45]	CR, SC	1: SP	NS	St.	PM	No	Combustion of single coke particles, Population balance, monosize distribution, no validation with data
2	Davidson and Harrison [46]	SC, CR	2: B and E	Molecular Diffusion	PM	PM	Yes	Combustion in baffle bed, uniform bubble diameter, correlation for gas interchange coefficients present
3	Kunii and Levenspiel [48]	SC, CR	3: B, C and E	As in their catalytic model	St.	PM	No	General model, considered various limiting cases, no validation with plant data
4	Yoshida and Wen [76]	SC	2 :B and D	$11/d_{eq}$	C in S	C in S	No	General model comparison for equations roasting, bubbles grow with bed height
5	Avedesian and Davidson [77]	Diff.	2: B and D	Hovmand and Davidson [97]	PM	Batch	No	Coal Combustion double film model char combustion, Expressed for carbon burn out rate, no validation with plant flow parameters
6	Cambell and Davidson [78]	Diff	2: B and D	Molecular Diffusion	PM	Batch	No	Coal Combustion, double film model, Char combustion, Expression for char burnout rate, no validation with plant flow parameters
7	Becker, Beer and Gibbs [79]	Diff.	2: B and D	Penetration + leakage of circulating gases	PF	PM	Yes	Coal Devolatilization and combustion, isothermal bed, applicable to batch operation, elutriation neglected
8	Basu et al.[80]	SC	2: B and D	As Davidson and Harrison [60]	PM	PM, PB	No	Coal combustion, Single model, modified expression for char burning rates
9	Gibbs [81]	Diff.	2: B and D	As Davidson and Harrison [46]	PM	A, E, PB	No	Coal combustion, uniform and wide distribution, burning rate is distribution, burning rate is diffusion controlled, comparison with NCB
10	Gordon and Amudson [53]	CR, SC	2: B and D	B-I, as Kunii and Levenspliel	PM	PC	Yes	Carbon combustion, double film mechanism non isothermal bed, comparison with published data, effect of bubble size studied
11	Mori and Wen [82]	Ist O	2: B and D	$11/d_{eq}$	C in S	PM, E	No	General model, bubbles grow with bed height

Table 2.1 Continued

12	Horio and Wen [55]	2rxs	2: B and D	$11/d_{eq}$ followed by Hovmand and Davidson [97]	C in S	PM, E	No	Coal combustion, SO_2 limestone reaction, bubble grow with height
13	Chen and Saxena [51]	2rxs	3: B, C and E	As Kunii and Levenspiel [48]	PF	PB, PM	No	Coal combustion and sulphation of additives, bubble grow with height, monosize distribution, comparison with pilot plant data(PER, CPU)
14	Horio and Wen [55]	Ist O	2 : B and D	$11/d_{eq}$	C in S	PB, E	Yes	Coal combustion, bubbles grow with height, location of heat transfer tubes, Comparison with experimental data of Gibbs(1975)
15	Rajan Krishnan, and Wen [56]	4 rxs	2: B and D	$11/d_{eq}$	C in S	C in S	Yes	Coal combustion, devolatilization and sulphur removal, bubbles grow with height, comparison with experimental data
16	Baron and Hodges [83]	SC	2 : B and D	As per Davidson and Harrison [46]	PM	PM,E	No	Coal combustion, general comparison with published data
17	Fan et. al.[63]	CR	2: B and D	As per Avedesian and Davidson [77]	PM	Lateral	No	Coal combustion, bed carbon load 1% of total bed weight
18	Caram and Amundson [70]	CR	2: B and D	As per Kunii and Levespiel [48]	PM	PM	No	Char combustion, single particle size considered, Comparison with experimental data
19	Bukur and Amundson [54]	CR	2: B and D	As per Kunii and Levenspiel [48]	PM	PB,PM	No	Combustion of char, both single and double film models are considered, comparison with published data, SFM more appropriate.
20	Bear et al. [84]	SC, CR	2: B and D	As Kunii and Levenspiel [48]	PM	A, PB, PM, E	No	Combustion of coal, effect of mean particle size on carbon loss for bed

Table 2.1 Continued

21	Donsi et al. [85]	Ist O, SC	2: B and D	As per Kunii and Levenspiel [48]	PM	E,AP M	No	Combustion of coal, Expression for elutriation and shrinkage, Comparison with experimental data
22	Saxena and Rehmat [65]	Diff.	3: B,C and E	As per Avedesian and Davidson [64]	PM	Batch	No	Combustion of char, expression for burnout time, ash film resistance considered, results compared with Avedesian and Davidson(1973)
23	Ross and Davidson [86]	Diff.	2: B and D	As per Avedesian and Davidson [64]	PM	E, batch Sh=3.5	Yes	Combustion of char, expression for char burnout time, combustion governed by diffusion and chemical kinetics
24	Chang, Rong and Fan [89]	I^{st} O	2: B and D	As per Kunii and Levenspiel [48]	PM	Disper sion model	No	Shallow bed, general model applied to ZINC roasting, steady and unsteady solution
25	Miccio and Salatino [90]	CR	2: B and D	As per Kunii and Levenspiel [48]	PM	PM,PB	No	Coal combustion, discrete cut feed distribution, Comparison with experimental data
26	Sundback et al. [91]	SC	2: B and D	As per Kunii and Levenspiel [48]	PM	NS	No	Coal combustion, allowance for coal fragmentation and devolatilization, Single wide size distribution
27	El-halwagi and El-Rifai [92]	I^{st} O	3: B, C and E	As per Kunii and Levenspiel [48]	C in S	PM	No	Chemical reactor, constant bubble diameter, comparison with published data
28	De-souza Santos [93]	SC	2: B and D	As per Kunii and Levenspiel [48]	PM	PB,PM	Yes	Coal combustion, allowance for devolatilization, comparison with plant data
29	Basu and Halder [94]	CR	2: B and D	NS	PM	A, PM	Yes	Combustion of coarse carbon particles, expression for burn rates, comparison with experimental data
30	Westby et al. [95]	SC	3: B, C and E	Kunii and Levenspiel [48]	PM	PB, E	No	Combustion of coal monosize distribution(6 mm), effect of bed temperature excess and superficial gas carbon conversion, validation with experimental data

Table 2.1 Continued

31	Adanez et al. [50]	SC	2: B and D	As per Kunii and Levenspiel [48]	PM	PB	No	Combustion of liginite discrete size distribution, effective bed temperature and excess on carbon conversion efficiency, Validation with experimental data
32	Reddy and Prasad [96]	CR, SC	3: B,C and E	As per Kunii and Levenspiel [48]	PM	PB, E, A	No	Combustion of high ash coal, wide size distribution, Constant bubble diameter and elutriation rate, Comparison with plant data
33	Mohapatra et al. [68]	CR, SC	3: B, C and E	As per Kunii and Levenspiel [48]	PM	PB, E, A	No	Combustion of high ash coal, Constant bubble diameter and elutriation rate, Comparison with plant data
34	Mohapatra and Ravi Inder [181]	CR, SC	3: B, C and E	As per Kunii and Levenspiel [48]	PM	PM, E, A	No	Combustion of high ash coal, wide size distribution, Bubble diameter varying along bed height, Comparison with plant data
35	Khan et al. [75]	SC	2: B and D	As per Davidson and Harrison [46]	PM	PB	No	Combustion of burning waste wood fuel, wide size distribution, Comparison with plant data

CR- Continuous reaction Model, Diff.- Control by diffusion through ash layer, SC- Shrinking core model, O- Order

rxs- Reactions, B-Bubble phase, C- Cloud phase, D-Dense phase, E-Emulsion phase, I-Interstitial gas, J-Jet phase

P-Particles, C in S- Well mixed compartments in series, PF- Plug flow, PM- Perfect mixing, PB-Population balance

A-Attritions allowance E- Entrainment allowance, St. Stagnant, NS- Not Specified

2.3 Experimental Work on Combustion of Rice Husk/Rice Straw in Fluidized Bed

Combustion of biomass in fluidized beds is becoming more and more attractive as a result of the constantly increasing price of fossil fuels, the presence of high quantities of biomass to be disposed of and global warming issues. Fluidized bed technology usually is the best choice, or sometimes the only choice, to convert biomass to energy due to its fuel flexibility and the possibility to achieve an efficient and clean operation. Extensive experimental investigation has been carried out to date on the feasibility and performance of biomass combustion and gasification in fluidized beds. Even if a great amount of operating data has been collected so far, detailed comprehension of the basic mechanisms taking place during conversion in fluidized beds of biomass is still lacking. Usually biomass is treated just like fossil fuels in spite of the great differences and variability of chemical and physical properties.

Biomass usually have a much higher moisture and volatile content, a more porous and fragile structure, often anisotropic, a lower density and a much higher intrinsic reactivity. While basic phenomena in fluidized bed combustion of these fuels are the same as those for fossil fuels, differences arise because of the different chemical and physical properties of these fuels that determine the greater or smaller relevance of the various phenomena. Drying time is usually longer due to the higher moisture content of these fuels and results in small delay of the subsequent devolatilization, but in general has a limited influence on overall performance. The high volatile content of biomass leads to longer devolatilization times and larger quantities of volatiles evolved. As a consequence a distinctive feature of biomass in fluidized bed combustion is the larger heat release associated with homogeneous combustion of volatile matter. Figure 2.10 shows the line diagram of atmospheric fluidized bed combustor at any commercial site.

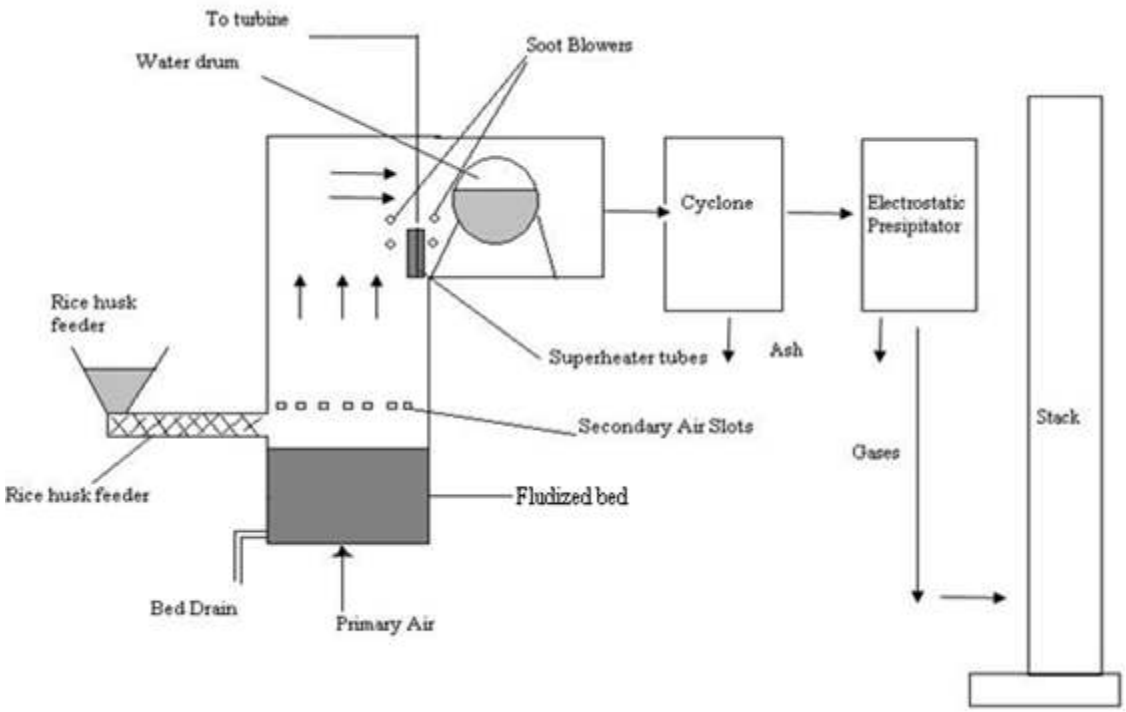

Figure 2.10 Fluidized bed rice husk combustor diagram

Fang et al. [98] introduced the experimental study on rice husk combination in a circulating fluidized bed. Circulating fluidized bed combustion had proven to be an effective way of converting biomass wastes into clean energy. Experiments on cold model elaborated that rice husk was difficult to fluidize and addition of silicon sand and coal improved the fluidization conditions. Effects of sand diameter, gas velocity and mass fraction on rice husk mixing were tested. The rice husk could mix well with 0.03–0.08 cm sand at gas velocity 80–200 cm/s. Experiments on 1 MW thermal test facility show that rice husk ignition temperature was only 340°C, much lower than coal. The gas velocity and air split had great effect on rice husk combustion. At proper operation condition, the rice husk combustion efficiency reached 97%, and the carbon content in fly ash was between 3% and 8%, whereas CO emissions was varied from 200 to 800 ppm, SO_2 from 50 to 100 ppm and NO_x from 150 to 220 ppm.

Natrajan et al. [99] in their paper provided an overview of previous works on combustion and gasification of rice husk in atmospheric bubbling fluidized bed reactor and summarized the state of the art knowledge. As the high ash content, low bulk density, poor flow characteristics and low ash melting point makes the other types of reactors either insufficient or unsuitable for rice husk conversion to energy; the fluidized bed seemed to be the promising choice. They explained that combustion intensity up to 0.014 g/s/cm^2 and combustion efficiency upto 80% was available in the literature. Their major conclusions were that results reported in the literature were limited and vary widely, emphasizing the need for further research to establish commercials implementations.

Thipwimon et al. [100] studied the use of fossil fuels which cause environmental and energy security problems. Renewable energy was being looked at as an alternative for Thailand. Biomass from agriculture, especially rice husk, was a very promising renewable energy source since it was indigenous and was considered to have environmental benefits. However, the environmental profile of the electricity production from biomass must be assessed to ensure reduced environmental damage. This article considered the environmental evaluation of a 10 MW pilot plant using rice husk as feedstock. The environmental impact from rice husk energy power plant was evaluated using the life cycle assessment (LCA) methodology. Energy, material and carbon balances had been determined for tracing the system flow. Most impact potentials from rice husk energy were lesser than fossil fuels plants; except the photo-oxidant formation potential from CO. The performance of rice husk power plants could be enhanced by improving the combustion efficiency.

Premchart et al. [101] did the experimental study on combustion of three distinct biomass fuel (sawdust, rice husk, and pre dried cane sugar baggase) in a conical bed using silica sand as

the inert bed material. There temperature, CO, NO and O_2 concentrations along the combustor height as well as in flue gas were measured. They found the effects of fuel properties and operating conditions (load and excess air) on these variables. Based on CO emission and unburned carbon in fly ash the combustion efficiency of the conical FBC was quantified for selected biomass fuels fired under different operating conditions. They found that the axial temperature profile in the conical fluidized bed combustor was fairly uniform for all the fuels and weakly affected by fuel analysis and operating conditions. CO formation rates, and consequently CO_{max}, for rice husk were much greater than those for sawdust and baggase for similar operating conditions. The rate of NOx reduction for rice husk was much greater than those for sawdust and baggase due to the significant role of heterogeneous reactions in the freeboard region. Maximum combustion efficiency for firing rice husk was obtained for excess air of about 60%. Increase in excess air up to 100% resulted in a deterioration of the combustion efficiency of rice husk to 81%.

Kaewklum et al. [102] did the study related to the experimental results on combustion of Thai rice husk in a conical fluidized-bed combustor (conical FBC) for different fuel qualities and operating conditions. They performed two groups of experimental tests using (1) high-ash rice husk and (2) medium-ash rice husk, the latter being burned at different fuel moistures (provided by water injection into the fuel). Temperatures and CO, NO and O_2 concentrations along the combustor height and in the flue (stack) gas were measured in the tests. The effects of fuel properties and excess air on the axial temperature, CO and NO profiles, as well as on the combustion efficiency and environmental performance of the conical FBC were discussed. The fuel ash showed quite strong effects on the combustion heat losses and efficiency, while the fuel moisture demonstrated substantial influences on the emission characteristics of the combustor.

They found that a conical fluidized bed combustor was successfully tested when firing rice husks with different ash and moisture contents at 22.88–23 g/s fuel feed rate and different excess air values. The moisture and ash contents in rice husk and excess air value were found to affect substantially the axial CO and NOx profiles and showed different influences on formation and reduction of these pollutants. The combustion efficiency of 91–96% could be achieved when firing medium-ash rice husk for a wide range (11–35.5%) of the fuel-moisture contents. The best performance of the conical fluidized bed combustion can be achieved at different (optimal) values of excess air: while high-quality rice husks (with low ash and moisture contents) can be burned at excess air of 40–60%, the burning of rice husks with high-ash and/or high-moisture contents requires higher values of excess air of the order of 80–100%. Then they found that by adding water to the "as-received" rice husk, the temperature profiles could be reduced up to 150°C. Also their findings were that water injection into the fuel, the NOx emissions from the combustor could be noticeably reduced; however, an increase in the fuel moisture resulted in deterioration of the combustion efficiency and increasing the CO emissions from the conical fluidized bed combustion. By increasing excess air the CO emission was reduced, which however led to the increased NOx emissions and diminished combustion efficiency.

Madhiyanon et al. [103] developed a novel cyclonic fluidized-bed combustor (ψ-FBC) with 100 kW design capacity and tested for burning rice husk. The purpose of the new design was to integrate cyclonic and fluidized-bed combustion into a unique combustor for more efficient combustion, while maintaining its compact nature. The performance of the ψ-FBC, with a design capacity of 100 kW, was analyzed in terms of combustion and thermal efficiency, volumetric combustion intensity, and pollutant emissions. For all conditions, insignificant effects of primary, secondary, and tertiary air velocity on combustion efficiency were observed.

Combustion efficiency of 98% was easily obtained, and a maximum volumetric intensity up to 0.95 MW/m^3 was achieved. Too-high fluidizing air velocity (>155 cm/s) decreased combustion efficiency. Temperature profiles within the lower combustion chamber indicated the existence of nearly isothermal bed conditions, operating at temperatures of around 900–1000^oC. The changes in the amount of primary, secondary, and tertiary air corresponding to excess air of 67–130% seemed to have an insignificant effect on combustion efficiency. Analysis of gas emissions within the combustor displayed a successful merging of the two distinct combustion technologies. Emissions of CO and NOx, based on 6% (volume) O_2, were determined to be in the range 50–400 and 350–425 ppm, respectively.

Bhattacharya et al. [104, 105] studied the aspects of fluidized bed combustion of paddy husk. Large carry over of sand particles from the bed at high air flow rate was observed. In normal operating range all ash was entrained in the stream of the flue gas. Bed height was influenced the combustion intensity. Increase in bed height was caused to increase the sand entrainment rate. Up to 0.014 $g/s/cm^2$ combustion intensity was achieved. Increase in bed height from 10 to 15 cm had caused combustion efficiency to increase with same mass flow rate. Combustion efficiency lies within 81% to 98% which further depend on air flow rate. Secondary air flow causes to increase combustion efficiency up to certain level after which no appreciable change observed.

Preto et al. [106] did the combustion trials of rice hulls in a pilot-scale fluidized bed. They observed higher temperature in the over bed region for all fluidization velocities due to volatiles burning in the freeboard. Combustion efficiency had shown no dependence on fluidization velocity and excess air and only minor dependence on temperature. Carbon monoxide (CO) emission was increased with increase in fluidization velocity and

temperature. Husk ash was very fine and easily elutriated out of bed. Even low fluidizing velocity was sufficient to blow all ash out of bed. Combustion efficiency of more than 97% with low emissions could be obtained over a wide range of fluidizing velocities. Carbon conversion efficiency of 96.9-98% could be attained. CO emissions varied from 200 to 5000 ppm, whereas SO_2 and NOx emission ranges were 50-150 ppm and 100-180 ppm (20-200 ng/J) respectively. Carbon content in the cyclone product was varied from 1 to 4%. Cyclone ash was contained 98% silica (SiO_2).

Bhattacharya and Wu [5] studied the fluidized-bed combustion of rice husk for disposal and energy recovery. They observed that heat loss due to unburnt carbon increased with excess air level and also with combustion intensity for same excess air level. Heat loss due to carbon monoxide in flue gas decreased with both the above factors. No particular operational problem was experienced in the lab or pilot combustor. Overbed feeding seemed to be more convenient. Combustion efficiency greater than 95% was achieved. Heat loss due to unburnt carbon in ash is 1-3% and CO loss was 3-10%. Proper splitting of total air into primary and secondary air and by providing enlarged freeboard resulted in higher combustion efficiency. Pozzolana cement obtained by mixing rice husk and portland cement (30:70) was found to have higher strength.

Ganesh et al. [107] did combustion and gasification studies of rice husk to understand the problem of incomplete carbon conversion. Rice husk when used in gasifiers and boilers yields carbonaceous residue. They performed themogravimetric experiments using carbon dioxide, nitrogen, air and steam atmospheres under different temperature conditions. SEM analysis of ash sample obtained under different reaction conditions and X-ray diffraction patterns of the residues was done. Combustion and gasification kinetics were also very sensitive to the rate of heating. At

temperature greater than 700^{o}C there was incomplete carbon conversion, while at lower temperature complete conversion occurs. In partial oxidation gasification combustion of any biomass, the process of pyrolysis, gasification, thermal cracking and combustion normally take place simultaneously. This leads to a complex situation, hot spots invariably develop and husk ash becomes subjected to temperature beyond 900^{o}C. At these temperatures the amorphous silica in ash results in chemical/physical bondage of carbon to the silica matrix. In order to achieve complete conversion of carbon, it was desirable to maintain a low temperature during pyrolysis and or partial combustion of husk, followed by steam gasification in either case.

Armestoa et al. [108] studied combustion behavior of rice husk in a bubbling fluidized bed. An experimental combustion work using the rice husk as fuel was performed in a 30 kW atmospheric bubbling fluidized bed pilot plant. The influence of different variables such as temperature, fluidization velocity on the combustion efficiency and carbon monoxide emissions was investigated. The characteristics of ash removed from the bed, cyclones and baghouse were studied. The combustion efficiencies in all test runs were higher than 97%. The carbon monoxide emissions obtained during the test runs were higher than 1000 ppm. The temperature profile in the furnace has a strong influence on both carbon monoxide emissions and combustion

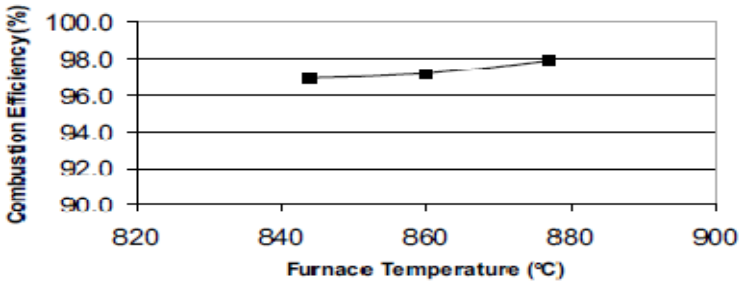

Figure 2.11 Effect of the furnace temperature on the combustion efficiency

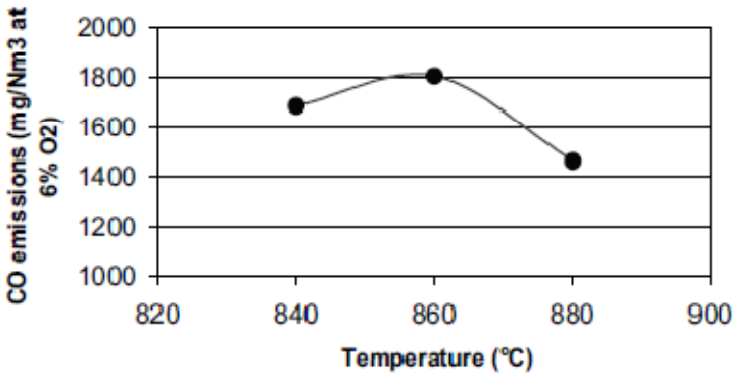

Figure 2.12 Effect of temperature on the CO emissions

efficiency. The main crystalline compounds in the ashes from the bed were quartz and hematite, but when the bed material was not changed between the test runs, the presence of potassium–calcium silicates was detected. The main crystalline compound of the ash from the cyclones was sylvite. The effect of furnace temperature on combustion efficiency was shown in Figure 2.11 and the effect of temperature on CO emissions was shown in Figure 2.12. Combustion efficiency was found to increase with furnace temperature and CO emissions increased up to 860^{o}C and then decreased. CO emissions were increased with increase in fluidization velocity as shown in Figure 2.13.

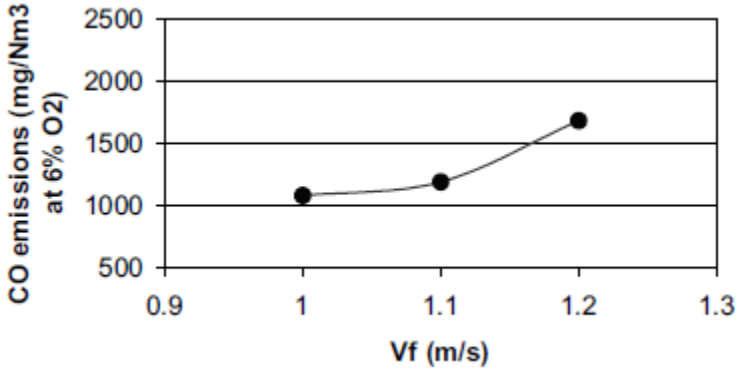

Figure 2.13 Effect of the fluidization velocity on the CO emissions

Swasdisevi et al. [109] studied the design, construction and testing a rice husk furnace for fluidized bed paddy dryer with capacity of 2777.8 g/s. The husk furnace was cylindrical in shape

with inner diameter of 137 cm, height of 275 cm, husk feed rate of 33.3-41.66 g/s and air flow rate before entering suction blower is of 1160 g/s. Air and rice husk were fed in combustion chamber in tangential direction with vortex rotation. Average temperature of air exit furnace (at height of ash 60 cm) and before entering suction blower (at height of ash 30, 45, 50 and 60 cm) are 504^{o}C and 293-297^{o}C respectively. Ambient air temperature was 32-34^{o}C. Thermal efficiencies of the rice husk furnace and the furnace system were approximately 59% and 58% (at height of ash 60 cm) respectively. Carbon conversion efficiency was 90% (at height of ash 60 cm). The research also elaborated the effect of gases (CO, CO_2, N_2 and NO_2) from combustion of husk in furnace on environment and ash.

Skrifvars et al. [110] studied slagging and fouling behavior of rice husk ash in fluidized bed combustion. Characteristic properties of the rice husk ash, as measured by a variety of laboratory tests and analyses and comparison of these characteristics with eucalyptus bark and rice straw was done. Rice husk ash had been shown to produce large, almost millimeter-sized ash particles with a characteristic shape. These particles consisted almost purely of silica, with just a few percent of potassium. The melting properties for this type of ash was characterized by a very high melting temperature and consequently no molten fly ash was expected under any fluidized-bed combustion conditions when husks were burned alone.

Skrifvars et al. [141] studied slagging and fouling behavior of rice husk or in combination with other fuels in fluidized bed combustion. Results were found for fireside fouling measurement when burning rice husk alone and together with eucalyptus bark in various rations. Influence of the fuel mixture ratio on the fouling tendency of the fly ash formed was done using more systematic measurements. It was based on short-term deposit samples taken with air-cooled deposit probes in the super heater region of a large-scale bubbling fluidized-bed boiler burning

rice husk and eucalyptus bark. Burning of rice husk alone did not result in any detectable fouling. The combustion of eucalyptus bark alone caused significant fouling. Fouling tendency of mixture of rice husk and bark showed a nonlinear dependence on the fuel mixture ratio. The rice husk ash acted as an erosive, cleaning agent in the fly ash mix.

Chunsangunsit et al. [111] did environmental assessment of electricity production from rice husk considering the case study of 9.8 MW fluidized bed combustor based on rice husk. The study indicated that rice husk was a viable feedstock for electricity production and it performed better than fossil fuels. Then comparison of pilot plant with other conventional power plants in Thailand was done. The percentages of gases reported from the stack of plant are CO_2:10.1%, O_2:7%, SO_2:15.9%, NO_x: 175.1, CO: 81.8, TSP (dust): 11.3 mg/Nm^3. At 434 K flue gas flow rate was 19×10^6 cm^3/s. They further concluded that the emission of CO_2 from combustion of rice husk was considered zero since it do not contribute to global warming. NO_X and SO_2 emissions were lower than conventional plants. Carbon monoxide emissions were slightly higher than conventional power plants. Combustion efficiency of the biomass based power plant need to be improved.

Simonov et al. [26] discussed combustion and processing of rice husk in the vibrofluidized bed of catalyst or inert material. Studies on solid products of the rice husk combustion had shown that their texture was determined mainly by silica, which was contained in rice husk as amorphous silica $SiO_2.nH_2O$. The adsorption ability of solid products of rice husk in respect to methylene blue (MB) was investigated. The replacement of inert particles in the vibrofluidized bed by the catalyst particles did not change the general scheme of rice husk combustion. The presence of the catalyst had provided a sufficiently high burn-off of the rice husk at the same temperature of the vibrofludized bed and rice husk particles. The process

mentioned appeared to be environmentally benign, since in the flue gas after such combustion there are no products of partial oxidation of organics like CO even at rather low temperature of 500^{o}C. The process had enabled to obtain in one stage i.e without additional stage of the coke activation, some solid products with a high specific surface and good adsorption properties.

Osaka [27] studied staged combustion of rice straw using an atmospheric bubbling fluidized bed combustor. The internal diameter and height of the combustor was 30 cm and a 330 cm height respectively. Secondary air was introduced in the freeboard at 150 cm above the primary air distributor. Rice straw was fed as cylindrical pellets of a 1.2 cm diameter and 1–1.5 cm lengths. The obtained results indicated that staged combustion was appeared an effective technique to reduce NOx emissions, in particular, at higher operating temperatures. Typically, at 850^{o}C bed temperature, NOx concentration reduces by about 50% when 30% of fed air is introduced as secondary air. Staged operation had slight, non-monotonic effect on SO_2 emission. Combustion efficiency improved with increasing secondary air ratio, it was reaching a maximum value that was mainly attributed to a reduction in fixed carbon loss. With further increase in secondary air ratio, combustion efficiency; however, decreased again since entrained fixed carbon and exhausted carbon monoxide tend to increase. The range of secondary air ratio, over which combustion efficiency improve, expands at higher operating temperatures.

Rajaram and Malliah [112] studied the fluidized bed combustion of rice straw. In this experimental study 30 × 30 × 30 cm^3 straw bales were introduced through an overbed chute into a 250000 cm^2 bubbling bed. The superficial velocities were kept between 150 and 300 cm/s and stable operation was reportedly maintained at 600°C bed temperature. Combustion efficiencies on the order of 95-98% were reported without ash recirculation. The fuel energy input to the system was 465 kW. Freeboard temperatures were 100 K greater than those in the bed. No

agglomeration was noticed after 50 h of operation. The success of this operation may be attributed to operating temperatures below the initial deformation temperature (a standard measure of the onset of ash softening as discussed later) of rice straw ash, and also to the high bulk density of the bales. Low temperature operation in the freeboard was required significant heat removal due to the volatility of the straw. The rate of heat removal from the bed or freeboard was not reported. The high bulk density of the bales allowed them to sink in the bed, increasing the residence time and apparently allowing more complete combustion.

2.4 Agglomeration in Fluidized Bed Combustors Based on Biomass

Olanders and Steenari [113] studied the ash characteristics of biomass. They found that ash characteristics of biomass were different from those of coals. Though the compositions vary with plant types and the growth conditions, biomass ashes are normally dominated by silicon, calcium and potassium and contain little aluminum.

Jenkins [114] studied the composition of ash deposits in biomass fueled boilers. They found that potassium was dispersed in biomass in ionic and organometallic forms, while silicon occurs primarily as hydrated silica grains. During combustion, potassium was likely to be volatilized with organic species. It may be released as potassium chloride if chlorine was present in the fuel. Without chlorine, hydroxides, oxides, sulphates or carbonates may be formed. Alkali and alkaline earth metal ions associate primarily with sulphate, carbonate and chloride ions during ash formation.

Skrifvars [115] studied to predict bed agglomeration tendencies for biomass fuels fired in FBC boilers. They applied various methods to characterize different types of biomass ashes. Then it was reported that the elemental compositions of the ashes should not be released to the

gas phase, but tend to remain in the ash matrix by recapture of the vapors by some mineral components in the ash under fluidized bed combustion conditions.

Ergudenler and Ghaly [116] studied the gasification experiments of wheat straw in a fluidized bed with silica sand as bed material. It was found that agglomerates were formed when temperature approached 800^{o}C and severe defluidization occurred as soon as the temperature exceeded 800-820^{o}C. They concluded that the high fraction of potassium in straw ash was the major contributor to this phenomenon.

Salour et al. [13] elaborated that bed agglomeration in a pilot scale atmospheric fluidized bed combustor was controlled by blending wood into rice straw in concentrations of 50% wood or more and stoichiometrically holding reaction temperature at or below 800°C. At higher straw concentrations, agglomeration of the bed occurred over run times inversely proportional to the straw concentration in the blend. Bed agglomeration was preceded by a characteristic decline in bed pressure drop most likely related to combustion air channeling through the bed. Blend ash composition was not substantially affected until straw concentration decreased to 50% or below because of the four-fold higher ash concentration in the straw compared to wood. Blend ash base-to-acid ratio also was not substantially affected above 50% straw concentration, remaining essentially constant at 0.3, compared to the wood ash base-to-acid ratio of 1.1. Initial deformation temperature, as measured by standard cone test of the blend ash, increased from a minimum of 880°C for a 75% straw blend to 1120°C for a 10% straw concentration in the blend.

Grubor et al. [117] reported agglomeration and defluidization problems in 150 kW continuously straw-fired FBC even though the temperature was maintained below 700^{o}C. Further it was suggested using alternative bed materials like ferric oxide to avoid formation of low melting temperature eutectic compounds of alkali-silicates.

Skrifvars et al. [115] and Nordin et al. [118] tested the agglomeration behaviors of different biomass ashes in a pilot scale fluidized bed combustor systematically with programmed temperature change without combustion. Further it was examined that the defluidization temperature, at which the sand bed containing biomass was defluidized was close to the initial sintering temperature of the ash determined by compression strength method.

Ryabov et al. reported [119] that traditional way to reduce the negative effects of bed agglomeration was lied in increasing the bed drain with the addition of fresh inert material. Further it was elaborated that chemical and physical characteristics of bed materials must be interpreted to a suitable form for the boiler operation.

Weiganag et al. [120] described that agglomeration and defluidization phenomenon in fluidized bed combustors based on wheat straw. They found that defluidization was caused by the high content of potassium in the straw ash. During combustion the potassium in straw was transformed from organic and inorganic forms to various salts and amorphous of K_2O-SiO_2. The compounds were clearly identified as the coating layer on the sand surfaces, which caused the formation of agglomerates and eventually defluidization.

Elisabet et al. [121] studied the mechanisms of bed agglomeration during fluidized-bed combustion of biomass fuels. The low-melting calcium-based silicates including minor amounts of for example potassium were formed with subsequent viscous-flow sintering and agglomeration. For high-alkali-containing biomass fuels, direct attack of the quartz bed particle by potassium compounds in a gas or aerosol phase formed a layer of low-melting potassium silicate. Thus, formation and subsequent viscous-flow sintering and agglomeration seemed to be the dominating agglomeration mechanism for these fuels.

Korbee et al. [122] reported an early agglomeration recognition system (EARS) for small scale bubbling-fluidized bed combustors. The small scale bubbling-fluidized-bed gasification and combustion tests with various fuels have shown that agglomeration can be recognized 30-60 min earlier with EARS than with conventional methods based on changes in pressure drop or temperature difference. EARS may help plant operators in preventing agglomeration-induced plant shut downs and minimizing bed material makeup and residue production.

Natrajan et al. [123] studied the agglomeration tendencies of some common agricultural residues in fluidized bed. The agricultural residues chosen for the study were rice husk, baggase, cane trash and olive flesh. The results showed that the initial agglomeration temperatures were less than the initial deformation temperature predicted by the ASTM standard ash fusion tests for all fuels considered. The initial agglomeration temperatures of rice husk and baggase were more than 1000^{o}C. The agglomeration of cane trash and olive flesh was encountered at relatively low temperatures and their initial agglomeration temperature in gasification was lower than those in combustion with both bed materials. The use of lime as bed material instead of quartz improved the agglomeration temperature of cane trash and olive flesh in combustion and decreased the same in gasification. The results indicated that rice husk and baggase could be used in the fluidized bed for energy generation since their agglomeration temperatures are sufficiently high.

Mansaray and Ghaly [124] investigated the agglomeration characteristics of alumina sand-rice husk ash mixtures at various levels of temperature (750, 850, 900, 950, and 1000°C) and ash content (0·0, 5·0, 10·0, 15·0, 20·0, and 25·0%) using light microscopy, scanning electron microscopy, and energy dispersive X-ray analysis techniques. The scanning electron microscopy and X-ray analysis were also used for the identification of the rice husk and elemental makeup of rice husk ash. There was no indication of melting at all the levels of temperature and ash content

studied. However, weak and friable agglomerates were observed at 950 and 1000°C. The structure of the particles was not altered, and bonding by surface diffusion may be a possible mechanism for the formation of the weak, friable agglomerates. Physical entrapment by minute whiskers at the surface of rice husk ash was also a factor. The use of alumina sand as an inert fluidizable material in fluidized bed systems will prevent the formation of these easily breakable structures because of particle friction caused by mixing and fluidization. Thus these friable structures were not expected to cause any problem during the normal operation of fluidized bed gasification systems that are normally operated at temperatures in the range of 700-800°C.

2.5 CFD Analysis of Fluidized Bed Combustor

Due to a combination of increased computer efficacy and advanced numerical techniques, the numerical simulation techniques such as CFD became a reality and offer an effective means of quantifying the physical and chemical process in the biomass fluidized bed reactors under various operating conditions within a virtual environment. The resulting accurate simulations can help to optimize the system design and operation and understand the dynamic process inside the reactors. CFD modeling techniques are becoming widespread in the biomass thermochemical conversion area. Researchers have been using CFD to simulate and analyze the performance of thermochemical conversion equipment such as fluidized beds, fixed beds, combustion furnaces, firing boilers, rotating cones and rotary kilns. CFD programs predict not only fluid flow behavior, but also heat and mass transfer, chemical reactions, phase changes, and mechanical movement. Compared to the experimental data, CFD model results are capable of predicting qualitative information and in many cases accurate quantitative information. CFD modeling has established itself as a powerful tool for the development of new ideas and technologies.

With the advent of increased computational capabilities computational fluid dynamics, CFD is emerging as a very promising new tool in modeling hydrodynamics. While it is now a standard tool for single-phase flows, it is at the development stage for multiphase systems, such as fluidized beds. Work is required to make CFD suitable for fluidized bed combustor modeling and scale-up. Two different approaches have been taken in early attempts to apply CFD modeling to gas–solid fluidized beds: a discrete method based on molecular dynamics (Lagrangian model); and a continuous approach based on continuum mechanics treating the two phases as interpenetrating continua (multi fluid or Eulerian–Eulerian model). These two approaches have been compared by Gera et al. [125]. In the Lagrangian model of two-phase flow; the Newtonian equations of motion for each individual particle are solved with inclusion of the effects of particle collisions and forces acting on the particles by the gas. Particle–particle collisions are modeled by the hard sphere (Gera et al., [125]) or soft sphere approach (Kobayashi et al., [126]). The distinct element method, DEM, is one of the trajectory models, which can calculate the particle velocity and the corresponding particle trajectory to examine interactions, such as those due to multi body collisions (Kaneko et al., [127]). Trajectory models are applied to multiphase flows for dilute systems where a continuum model for the particle is not appropriate. Though models based on a DEM allow the effects of various particle properties on the motion of fluid to be studied, it is computationally intensive. Due to computational limitations, the Eulerian–Lagrangian model is normally limited to a relatively small numbers of particles. Therefore, the multi fluid model is the preferred choice for simulating macroscopic hydrodynamics.

Pain et al. [128] studied the bubbling and slugging fluidized bed using the two-fluid granular temperature model. In this scheme, collections of particles were modeled using

continuous medium mechanics. The solid particles were generally considered to be identical having a representative diameter and density. The general idea in formulating the multi fluid model was to treat each phase as an interpenetrating continuum, and therefore to construct integral balances of continuity, momentum and energy for both phases, with appropriate boundary conditions and jump conditions for phase interfaces. Since the resultant continuum approximation for the solid phase had no equation of state and lacks variables such as viscosity and normal stress, certain averaging techniques and assumptions were required to obtain a momentum balance for the solids phase.

Sharma and Mohan [129] studied the influence of tube-bank on the hydrodynamics of a freely bubbling fluidized bed reported in the literature using CFD. In this study results obtained from CFD of a two dimensional gas-solid fluidized beds with horizontal tube-bank are compared with the published experimental data. A 2-D bed, 100 cm high and 20 cm wide with tubes of diameter 2.6 cm was taken for the calculations. Two different tube arrangements of staggered and inline pitch with center-to-center distance of 5 cm were considered. Air was used as the fluidizing medium and ballotini glass (diameter: 23 cm and density: 2.723 g/cm^3) was the fluidized material. Air velocities used were 15 cm/s and 18.7 cm/s. The Eulerian-Eulerian two-fluid CFD model was employed for modeling the momentum equations for both the gas and the solid phase with kinetic theory modification for the solid phase to account for the inter-particle interactions.

Taghipour et al. [130] studied the experimental and computational study of gas–solid fluidized bed hydrodynamics. The hydrodynamics of a two-dimensional gas–solid fluidized bed reactor were studied experimentally and computationally. Computational fluid dynamics (CFD) simulation results from a commercial CFD software package, Fluent, were compared to those

obtained by experiments conducted in a fluidized bed containing spherical glass beads of 0.025–0.03 cm in diameter. A multi fluid Eulerian model incorporating the kinetic theory for solid particles was applied in order to simulate the gas–solid flow. Momentum exchange coefficients were calculated using the Syamlal–O'Brien, Gidaspow, and Wen–Yu drag functions. The solid-phase kinetic energy fluctuation was characterized by varying the restitution coefficient values from 0.9 to 0.99. The modeling predictions compared reasonably well with experimental bed expansion ratio measurements and qualitative gas–solid flow patterns. Pressure drops predicted by the simulations were in relatively close agreement with experimental measurements at superficial gas velocities higher than the minimum fluidization velocity, U_{mf}. Furthermore, the predicted instantaneous and time-average local voidage profiles showed similarities with the experimental results. Further experimental and modeling efforts are required in a comparable time and space resolutions for the validation of CFD models for fluidized bed reactors.

Behjat et al. [131] simulated gas–solid fluidized bed reactor using CFD techniques in order to investigate hydrodynamic and heat transfer phenomena. His study revealed that Eulerian-Eulerian model is suitable for modeling of industrial fluidized bed reactors. The model had continuity equations as well as momentum equations for both phases and the equations for granular temperature of solid particles. A suitable numerical method that employed finite volume method had been applied to discritize the equations. In order to validate the model, predicted time-average bed expansion ratio and cross- sectional voidage profiles were compared with corresponding values of experimental data. This comparison showed that the model could predict hydrodynamic behavior of gas solid fluidized bed reasonably well. Simulation results also indicated that small bubbles were produced at the bottom of the bed. These bubbles collided with each other as they moved upwards forming larger bubbles. Model predictions of bubble size and

gas–solid flow pattern using both Syamlal–O'brien and Gidaspow drag models were similar. When the bed containing two different solid phases was simulated, the results showed particles with smaller diameters had lower volume fraction at the bottom of the bed and higher volume fraction at the top of the reactor. In addition, it was revealed that bed expansion was larger when a bimodal particle mixture was applied compared with the case of mono-dispersed particles. Gas and solid phase temperature distributions in the reactor were also computed, considering the hydrodynamic of the fluidized bed and the heat generated by the solid particles. The results showed that gas temperature increases as it moves upward in the reactor due to the heat of polymerization reaction leading to the higher temperatures at the top of the bed.

Chiesa et al. [132] and Ranade [133] reported that computational fluid dynamic (CFD) is an important tool for design and optimization of chemical processes. There were several gas–solid CFD models reported by the researchers that differ mainly in closure law used in those models. These models were similar when predicting flow pattern since it is not sensitive to solid phase stress and radial distribution function. Most of CFD researchers employ a simple granular energy equation to calculate granular temperature, since this simplification would lead to insignificant errors while decreases computational effort for about 20%.

Dixon et al. [134] explained that CFD is essential tool for development of advanced technology for biomass combustion. They shared the experience with CFD in the sugar industry through Sugar Research Institute (SRI) with full range of applications from fundamental code development, through the generation and commercialization of new ideas and technologies, to the resolution of practical plant problems. They summarized that the numerous applications where SRI had achieved successful results utilizing CFD. They demonstrated that the full benefits of CFD in the delivery of commercial outcomes, for new technologies and the solution

of operating plant problems were achieved through the close interaction between the code development and validation via full scale plant simulation.

Ravelli et al. [135] presented the description, applications and numerical modeling of bubbling fluidized bed combustion in waste-to-energy plants. The extend the computational fluid dynamics (CFD) modeling, which has recently proved to be an effective means of analysis and optimization of energy-conversion processes, even to fluidized bed combustion of refuse-derived fuel (RDF). The increase in computer power over recent years had made this goal attainable. This paper was divided into three main parts. In the first one, after a brief introduction to the fluidized bed hydrodynamics, the phenomena taking place during fluidized bed combustion of solid fuels were explained, with particular interest in drying, devolatilization and char oxidation. Differences in combustion between conventional and alternative fuels were highlighted so as to fully characterize the RDF behavior in the bed. In the second part, a review of the state of the art of combustion modeling was presented: not only one-dimensional but also multidimensional models, applied to the fluidized bed and conventional combustors, were analyzed in order to emphasize what had already been done and what remains to be done. From the investigation it emerges that multi-dimensional models of fluidized bed furnaces were still lacking in literature: up to now, several bed hydrodynamics models had been achieved but none of them takes chemical reactions into account. In the last section, a numerical model of a bubbling FBC fed by RDF was presented. The combustor was divided into two regions: the bed and the freeboard. The calculation of mass and energy fluxes entering from the bed into the freeboard provides the boundary conditions for the subsequent CFD analysis. The freeboard model, implemented by means of the commercial code FLUENT 6.1, was mainly concerned with employing the two mixture-fraction-pdf approach to track both the gases coming from the bed and the solid fuel

particles that do not burn in the bed but above it. The excess air was injected through four series of nozzles; furthermore, the heat transfer between the flue gases and the internals was taken into account. The freeboard operation was simulated consistent with two conditions representing the combustor minimum and maximum load. The comparison between the predicted and the experimental data were in agreement: the reliability of the model results proved that CFD modeling is a powerful method to give insight into the behavior of a full-scale FBC fed by a non-conventional fuel. The minimum load condition was found to reduce combustion efficiency and heat transfer from the flue gas to the boiler tubes.

Stastny et al. [136] had performed a 3-D combustion modeling for a 200 MW dedicated biomass-fired boiler in a power plant in Fyris, Sweden, in which the pulverized fuel was made up of wood residuals and peat. The software used to model the combustion process in the boiler was FLUENT. In this work, the turbulence model chosen was RNG k-ε and the mixture fraction/Probability Density Function (PDF) approach was applied in modeling the reaction between the fuel and oxidizer. However, the standard k-ε model was used for the preliminary solution before proceeding with RNG k- ε model for the final calculations. In this study, biomass combustion was modeled in a similar approach as coal combustion.

Walsh [137] had modeled the combustion of volatiles released from burning biomass particles via the species transport model in FLUENT. In this method, the combustion reactions rates were defined by the stoichiometry, kinetics and turbulent reaction rates. The turbulence model chosen was the standard k-ε model whereas the rates of reactions in the model were controlled by the kinetic finite rate/eddy dissipation mechanism. The eddy dissipation mechanism stated that the reaction rate was defined by turbulence and concentrations of both reactants and products. The radiation model used was the P1 radiation model.

Kaer [138] presented numerical modeling of a 33MW Straw-fired grate boiler. The CFD prediction was carried out using Ansys-CFX commercial code. In this steady state governing equations were solved using the SIMPLE algorithm and the effect of turbulence on the mean flow field was accounted for using the RNG k-ε model. Radiative heat transfer was modeled using the discrete transfer model. Maximum local value of heat flux was approximately 200,000 W/m^2. High heat fluxes were mainly found in the regions of fast reaction rates close to the air injections nozzles. These regions were also characterized by high heat release rates and gas temperatures. In particular there were large regions of high heat fluxes around the secondary nozzles and further up along the front and side walls. His main results were that the combustion of biomass in grate-based boilers was often associated with high emission levels and relatively high amounts of unburnt carbon in the fly ash, the overall heat transfer predictions were in relatively good agreement with process data from the boiler except at the secondary super heater, where the predicted heat transfer rate exceeded the data by more than 100%, the relatively poor mixing in the furnace between the bulk flow and the secondary air jets were partly responsible for the high concentration of CO and un burnt carbon in the fly ash typical for grate-fired boilers.

Ma et al. [139] formulated CFD model that simulates combustion of biomass in existing pf coal fired furnaces and model results for the combustion of a typical wood in a 1 MW industrial test facility had been presented. The model formed had been based on coal combustion submodels using an Eulerian–Lagrangian frame of reference. Biomass specific constants that define the submodels had been investigated and employed in the simulation. In particular, potassium release during biomass combustion and the formation of NOx had been simulated. Numerical predictions were compared with some experimental measurements that had been taken and reasonably good agreement was been achieved. A KOH concentration of 7 ppm was

predicted in the exit plane of the furnace and at the exit of the furnace a NO concentration of 280 ppm had been predicted using the NH_3 mechanism only. When using the NCH mechanism alone, the calculated NO was 90 ppm. However, using a combination of the two, on a 1:3 basis (this means 1 NO from NH_3 and 3 NO from HCN), yields a predicted concentration of 137 ppm NO which was similar to the 140 ppm found experimentally. This was in consistent with the protein content of 70–90% of the total nitrogen content.

Backreedy et al. [140] applied the CFD modeling study to examine the co-firing of pulverized coal and biomass with particular regard to the burnout of the larger diameter biomass particles. They used P_1 radiation model and RNG k-ε turbulence model. Computations were based on a research combustion facility that replicates an industrial coal-fired power station. Pinewood blended with a bituminous UK coal and effects of the wood particle size and shape on the burnout of the combined wood and coal char were investigated. A similarity between the coal and biomass sub models was assumed, although they involve slightly different mechanisms and different kinetic data. There main results were that combustion of small (0.02 cm) wood particles was rapid but the rate of combustion of larger particles was dependent on their composition, size and shape. Further they concluded that the addition of small amount of biomass to a coal flame, the reaction environment in the combustor is determined by the combustion of the coal rather than by the biomass kinetics. Particle shape and size are important because biomass does not melt and irregular shape is maintained during combustion. The reactions of the major components of wood, hemi cellouse and lignin, are interconnected at high temperature, and wood reacts at one composite rate.

2.6 Limitations from Literature

Literature survey revealed that understanding of the complex multi-phase flows involved is still

very limited. In particular, existing computer simulations are not sufficiently accurate/fast to serve as a primary approach to the design, optimization, and control of industrial-scale fluidized bed combustors based on biomass. To be particular many models exist for fluidized bed combustor based on coal, but no model is available which represent fluidized bed combustor based on rice husk.

Even though few models has been discussed in literature for fluidized bed gasifiers based on rice husk, but the approach for this model is entirely different from basic modeling approach of fluidized bed combustors. Availability of more sophisticated computer models is expected to result in greatly increased performance and reduced costs associated with fluidized bed implementation and operation. Such improved performance would positively affect chemical/energy industry competitiveness and increase energy efficiency. Based on literature survey the following points are revealed

- Although rice husk has been identified as a source for energy production, only limited experience exists from rice husk firing in larger-scale combustors. Mostly the experience from small scale or the experimental fluidized bed combustors were reported.
- Computer simulations and modeling techniques are used for optimization of many processes. However limited data have been available.
- Rice husk is mainly used as energy fuel. Even though quantity of rice straw is more, but due the higher cost of collection and feeding problems, it is not much used in commercial fluidized bed combustors in the Punjab State.
- Defluidization problems of other biomass for fluidized bed combustors has been discussed for large plants, but none such experience mentioned for large scale power

plants based on fluidized bed combustors based on rice husk and rice straw. Even though it was done for experimental units.

- Rice straw poses high agglomeration problems as compare to any other fuel or when used with rice husk. None such experience with respect to only rice straw based plant is mentioned.
- Computational Fluid Dynamics (CFD) is important tool for design and optimization of chemical processes. The power of CFD based commercial software/tool has not been yet utilized for design and optimization of fluidized bed combustors based on rice husk. No such experience has been mentioned in literature in which CFD of fluidized bed combustors based on rice husk is described.
- The study done previously focused on mainly the aspects of gas-solid interactions, none such paper is found which is considering the aspects of three phases of fluidization.
- Previous studies were not much focused on biomass.

2.7 Problem Formulation

Due to huge amount of rice waste generated every year and due to direct incineration of rice waste in open fields, which leads to environmental problems, the Punjab government took step to harness energy from it. With this aim, in the last decade, a large number of rice-husk/biomass based power plants have been developed in Punjab, the agricultural state of India. The project activity of rice husk/rice straw power plant leads to green house gases on-site emissions in the form of CO_2 from combustion of biomass that will be consumed by plant species, representing a cyclic process of carbon sequestration. Since the rice husk contains only negligible quantities of other elements like nitrogen, sulphur etc. release of other green house gases are considered as negligible.

A very limited study on fluidized bed rice husk and rice straw combustors is done in past but due to the complicated nature of fluidized bed behavior; study for a specific system may not represent properly other systems that differ in design and operating features. Besides most of the study is correlated with the experimental results obtained from laboratory scale fluidized bed combustor units. In this work a three phase mathematical model for exit gas composition and solid population balance for shrinking particles in an atmospheric bubbling fluidized bed combustor using rice-husk has been developed including some features neglected or simplified in the previous studies. Biomass being neutral fuel, no emissions is considered so our exit gas model is quite useful which results in CO_2, O_2 and N_2 mainly. In commercial installations, the occurrence of agglomeration is still one of the main reasons for unscheduled outrages. It damages the image of fluidized bed combustor installations by reducing reliability of electricity production from rice husk/rice straw and in addition, it negatively influences the investments in future fluidized-bed combustion projects. Our finding will also help to explain the reasons of defluidization of fluidized bed at rice husk/rice straw power plants. CFD analysis of fluidized bed combustors based on rice husk has been discussed to visualize the three phases present in bed. Bed is assumed to be isothermal. The Eulerian multiphase model has used for fluidized bed. Modeling of bed has been modeled in Fluent 6.2 commercial code.

The study done here will help the engineer in optimizing the operating conditions of commercial plants. This study will help an engineer to predict hydrodynamic parameters, exit gas composition, carbon utilization efficiency, bed carbon load, and causes of agglomeration leading to defluidization of the bed of commercial operated rice husk fluidized bed power plants. The study also explains the reasons for agglomeration when rice straw is used in commercial fluidized bed combustors.

2.8 Objectives of Research

The objectives of the research work done here are:

1. To develop a mathematical model for an atmospheric bubbling fluidized bed combustor using rice-husk that will incorporate the following:

- Physico-chemical parameters in the bed i.e., minimum fluidizing velocity, bubble properties, operating velocity, bed carbon load etc.
- Oxygen mass balance to find out exit gas composition.
- Solid population balance to find out carbon utilization efficiency.

2. To investigate the causes of agglomeration with respect to rice husk and rice straw.

3. CFD analysis of fluidized bed to visualize the fluid flow pattern and solid volume fraction contours assuming bed to be in isothermal condition.

CHAPTER 3
PLANTS DETAILS AND DATA COLLECTION

In this chapter plant details, collection of samples and its analysis of 10 MW Jalkheri power plant and 3.5 MW cogeneration power plant has been discussed. Data was collected and analyzed in various laboratories. It was clear from literature that much of the work is done in experimental FBC units. During the study period rice straw was used only at Jalkheri power plant (JPP) that too in combination with rice husk for less than one month. Rice straw is not used at 3.5 MW co-generation power plant at Dhandari Kalan, Ludhiana (CCPDK) during study period. The data collected w.r.t rice husk from Jalkheri power plant used to validate the exit gas model, solid population balance model. The collected data is also explained w.r.t rice husk and rice straw to study the problem of agglomeration at plant sites in Chapter 5. The data of Jalkheri power plant is used to validate both models. Numerous difficulties like extreme air pollution, excessive noise and too much heat near the furnace was faced during measurements. The experience faced at JPP and CPPDK is also provided in this chapter. Some of the necessary measured data required for model is provided in chapter 7.

3.1 Description of 10 MW Power Plant at Jalkheri

Punjab state electricity board took first step to exploit non conventional sources of energy, when a 10 MW plant was set in village Jalkheri (Distt. Fatehgarh Sahib, Punjab) in 1992. This was a demonstration unit wholly designed and manufactured by Bharat Heavy Electrical Limited (BHEL), India. This is basically a mini thermal plant, which uses biomass as a fuel instead of coal for releasing heat energy. The heat so liberated goes into water, which is converted into superheated steam. The superheated steam is used to run steam turbine, which is coupled with generator to produce electricity. Requirement of water is taken from near by canal. The

generation voltage of power is 11 kV, which is, stepped upto 66 kV for linking it to PSEB transmission network. Initially the plant was shut down due to some drawbacks and non-availability of fuel but after some time it was recomissioned. Presently a private entrepreneur is running it on leasehold basis and plant now runs satisfactorily. Figure 3.2 shows the actual picture of atmospheric bubbling fluidized boiler at Jalkheri power plant. Figure 3.1 shows how the feeding of fuel through the conveyor belt to the fluidized bed combustor is done at Jalkheri power plant. Plant is fully automatic which uses conveyor for feeding fuel.

All the main controls of plant and other performance parameters can be handled from single computer placed inside control room. Fuel is fed to the conveyor belt using rollers. Fuel through conveyor belt is passed to boiler for incineration. Any type of biomass (rice /wheat husk, rice straw, saw dust, cotton waste, baggase, tree chips, and cow dung cakes etc. can be used. At the time of study fuel used is rice husk. In order to ensure adequate raw material for the plant a consortium of type as shown in Figure 3.3 has been formed.

Figure 3.1 Fuel input to combustor through conveyor belt at JPP

Figure 3.2 Bubbling fluidized bed combustor at JPP

Pile of rice husk lying under the shed of Jalkheri power plant is shown in Figure 3.4. Figure 3.5 shows the rice husk before the conveyor belt to atmospheric bubbling fluidized bed combustor.

Figure 3.6 shows the actual detailed line diagram of bubbling fluidized bed combustor at Jalkheri power plant. Figure 3.7 shows the process flow diagram of 10 MW Jalkheri power plant.

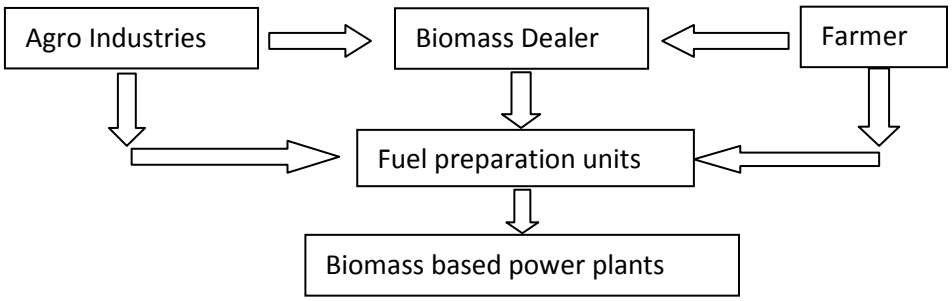

Figure 3.3 Consortium for collection of biomass

Figure 3.4 Pile of rice husk at Jalkheri power plant

Figure 3.5 Arrangement shows the rice husk after the conveyor belt to atmospheric bubbling fluidized bed combustor at Jalkheri power plant

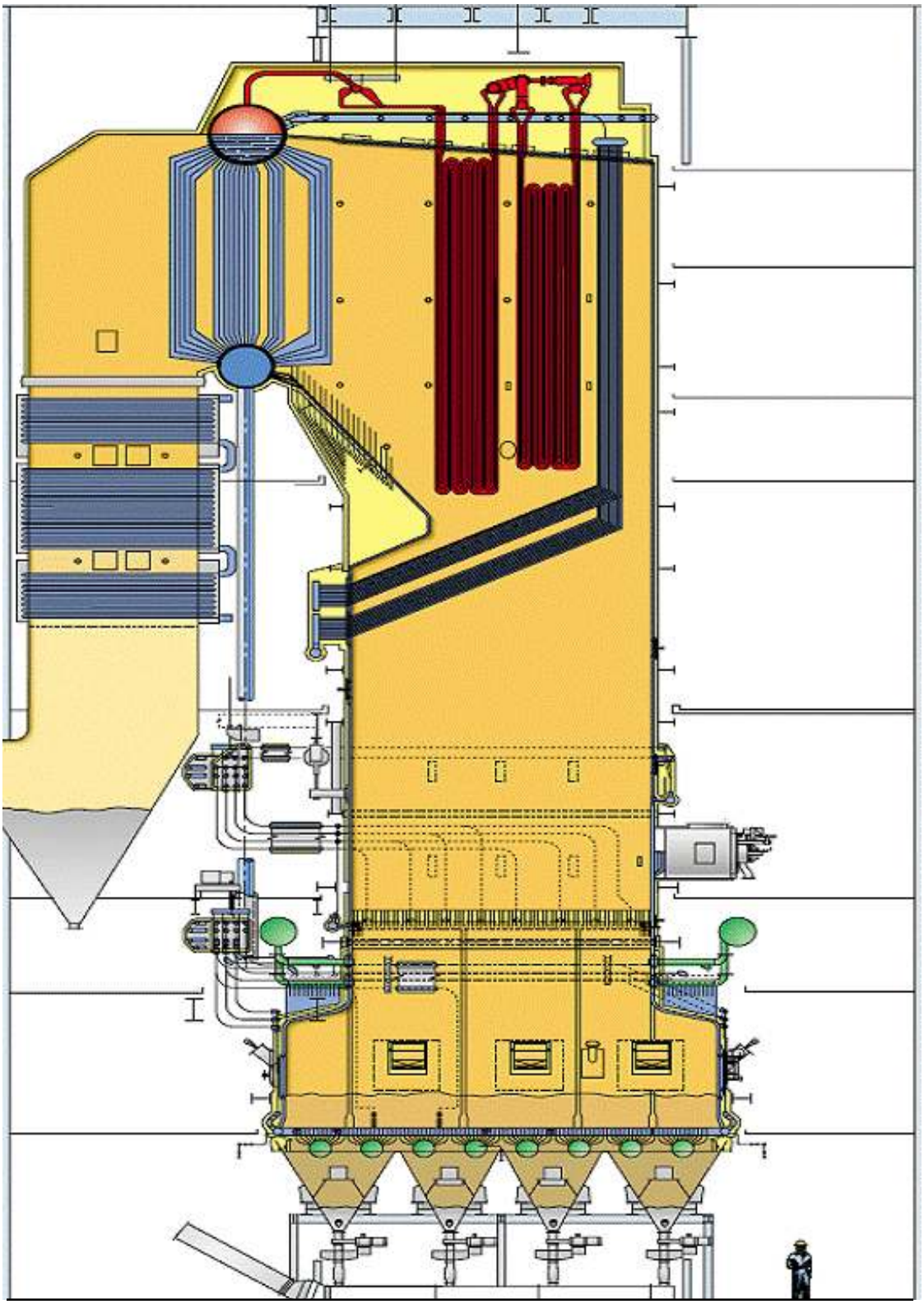

Figure 3.6 Actual detailed diagram of bubbling fluidized bed combustor at JPP

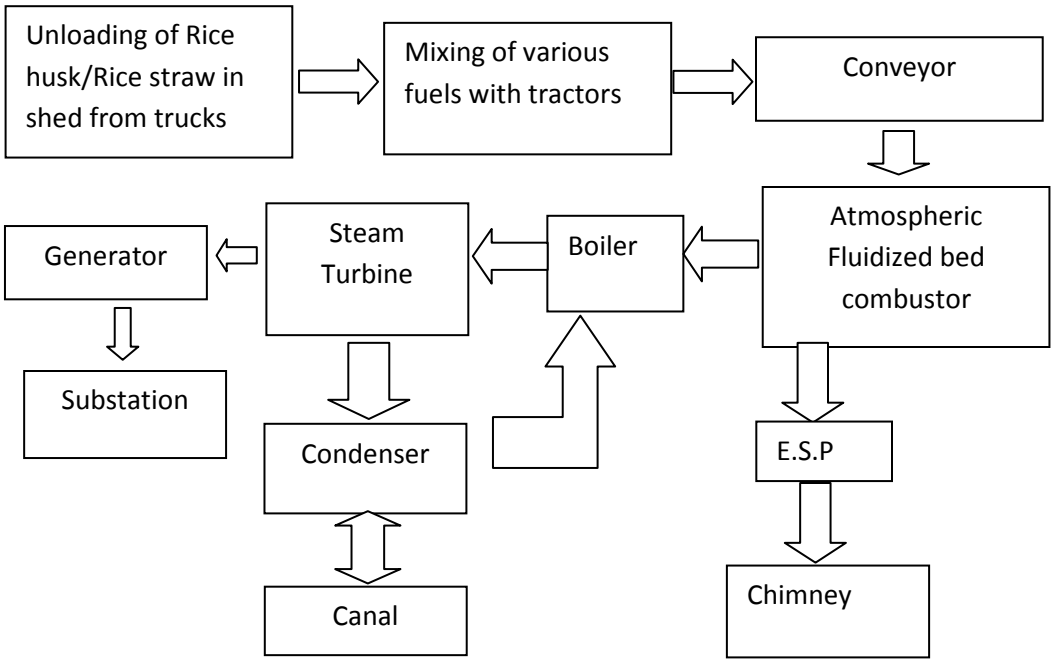

Figure 3.7 Process flow of 10 MW Jalkheri power plant

3.1.1 Experience at 10 MW Jalkheri Power Plant

The rice husk burns with a dull flame in the freeboard rising up to the roof/convection super heater probably due to insufficient mixing of air and combustibles. The rice husk/rice straw also burns with dull flame in freeboard. Due to the burning of volatiles in the freeboard, higher proportion of the heat is released in the freeboard zone. The resultant higher temperature softens the ash due to its high alkali content and the ash deposits on the convection super heater tubes on the flue gas path. The ash deposition rate is such that in less than 12 hours of operation, the space between the convection super heater tubes are bridged with ash and flue gas could not pass through it. The ash deposition rate is quite higher when rice husk is used in combination with rice starw. However, the ash deposition is observed to be related to the surface temperature as there were no deposits on the furnace walls; roof and hanger tubes which carry water/steam mixture.

The rate of ash deposition on the convection super heater tubes increases on increasing the firing rate. As the soot blower was located after the convection super heater, the cleaning of the

ash deposits at super heater inlets was insufficient. The ash deposit (larger mass) falls back on the furnace and disturbs the fluidization. The fly ash when allowed to accumulate in the hoppers is observed to sinter and affect the flow ability of ash from the hoppers. The various plant parameters have been shown in Table 3.1.

Table 3.1 Physico chemical parameters of 10 MW Jalkheri power plant

Type of fuel	Any type of biomass depending upon availability
Type of fuel used (at time of study)	Rice husk and rice straw
Feed rate of fuel	3200 g /s
Feed rate of water	11110 g/s
Air flow rate	20×10^6 cm^3/s
Rate of steam generation	10830 g/s
Main steam temperature	400^oC
Area of fluidized bed	391000 cm^2
Type of distributor	Nozzle type tuyre
Total no. of holes in distributor	22500
Specific fuel consumption	1300 g of fuel /unit generation
Bed Voidage	0.48
Bed height at minimum fluidization	48 cm
Combustion efficiency	82%
Boiler capacity	50 T/hr equivalent to 13888.88 g/sec
Average bed temperature(w.r.t rice husk)	800^oC
Average bed temperature(w.r.t rice husk/rice straw)	700^oC
Rice husk density	120 kg/m^3 equivalent to 0.12 g/cm^3
Rice straw pellet density	80 kg/m^3 equivalent to 0.8 g/cm^3

3.1.2 Proximate and Ultimate Analysis of Rice Husk, Rice Straw

The proximate and ultimate analysis of rice husk and rice straw used at 10 MW power plant at Jalkheri have been done. The proximate analysis has done in the chemistry laboratory at Guru Nanak Dev Engineering College, Ludhiana. Numbers of samples are being tested at different time intervals. The result of one sample of rice husk is given in Table 3.2. Table 3.4 shows the proximate and ultimate analysis of rice straw sample.

Table 3.2 Proximate and ultimate analysis of rice husk sample for JPP

Proximate Analysis (Rice Husk)		Ultimate Analysis (Rice Husk)	
Volatile	58.03	C	38.9
Fixed Carbon	16.65	H	5.1
Ash	17.82	S	0.12
Moisture	7.5	O	37.9
		N	2.17

Table 3.3 Proximate and ultimate analysis of rice straw sample for JPP

Proximate Analysis (Rice straw)		Ultimate Analysis (Rice straw)	
Volatile	63.12	C	41.04
Fixed Carbon	18.2	H	6.26
Ash	10.1	S	0.64
Moisture	8.58	O	38
		N	1.22

3.1.3 Proximate Analysis of Fly Ash

Table 3.4 shows the proximate analysis of fly ash collected from electrostatic precipitator and air heater, when rice husk is used. Table 3.5 shows the proximate analysis of fly ash collected from electrostatic precipitator when rice husk and rice straw is used.

Table 3.4 Proximate analysis of fly ash collected from air preheater and ESP hopper for JPP when rice husk is used

Ash	91.5%
Volatile matter	---
Fixed Carbon	8.5%
Moisture	---

Table 3.5 Proximate analysis of fly ash collected from air preheater and ESP hopper for JPP when rice husk-rice straw combination is used

Ash	90 %
Volatile matter	---
Fixed Carbon	10 %
Moisture	---

3.1.4 Measured Value of Carbon Utilization Efficiency

Table 3.6 show the measure value of carbon utilization efficiency at JPP. The measured value of carbon utilization efficiency comes out to be 92.64% as mentioned in Table 3.6.

Table 3.6 Measured value of carbon utilization efficiency for JPP

Fuel feed rate g/s	3200
%carbon Inlet (From Proximate Analysis)	16.65%
F_o Feed rate of carbon (g/s)	532.8
Fly ash (air heater + ESP Hopper) g/s	444.4
% of Carbon in fly ash	8.5 %
F_4 Carbon rate from fly ash (g/s)	37.78
Bed ash (g/s)	97.22
%Carbon in bed ash	Nil
Unburnt rice husk (g/s)	8.33
F_5 % Carbon along rice husk (g/s)	1.39
Carbon Utilization Efficiency $= \frac{F_o - (F_4+F_5)}{F_o} \times 100$	92.64%

3.1.5 Environmental Assessment of Jalkheri Power Plant

In the present scenario of power generation, the need for using non conventional fuels other than fossil fuels cannot be overemphasized on two counts. Firstly, this helps not only to maximize the potential of non-fossil fuels including bio mass fuels but also places a check on the rate of exploitation and consequent depletion of fossil sources. Secondly there is an incidental benefit of minimizing the all round environmental degradation and stress associated with mining, processing and Transportation of conventional fuel. From this perspective, the 10 MW bio mass based Jalkheri power plant can be considered as one of the most environmental friendly options available. The operation of 10 MW Jalkheri power plants produces air emissions, fly ash (ash from Air heater and ESP Hopper), waste water and solid wastes such as boiler ash. The data measured from JPP w.r.t rice husk is given in Table 3.7. The emissions data when a mixture of rice husk and rice straw is used at the JPP is not available. The design philosophy of this project activity is driven by the concept of providing the energy with no impact on the environment. The environmental aspects of the project activity are discussed below. The pollutants generated from the power plant include:

Table 3.7 Measured values w.r.t rice husk at JPP

Parameter	Value
O_2	6.9% by volume
CO_2	12.1% by volume
SO_2	15.4 ppm
N_2	78.1% by volume
NO_x(as NO_2)	176.2 ppm
CO	80.7 ppm
TSP(dust)	121 mg/Nm^3
Fly Ash(Air heater and ESP Hopper)	1600 kg/h equivalent to 444.44 g/s
Bed Ash	350 kg/h equivalent to 97.22 g/s
Un burnt Rice Husk Along with Bed Ash	30kg/h equivalent to 8.33 g/s

3.1.5.1 Dust and Particulate Matters

The pollution control norms stipulate a maximum dust concentration of 150 mg/Nm^3. The power plant has an Electrostatic Precipitator, which separates the dust from the flue gas and dust concentration is the flue gas leaving the ESP is kept below 150 mg/Nm^3. The dust concentration level in the chimney is periodically monitored. Corrective steps are taken, if the concentration is not as per the acceptable limits.

3.1.5.2 Sulphurdioxide and Nitrogen dioxide

The main fuel in the power plant is biomass, which does not have significant amount of sulphur in it. Hence, the sulphur dioxide produced is within permissible limits. However, the stack height is as per the local pollution control board stipulations. The nitrogen dioxides are produced in firing is also with in permissible limits.

3.1.5.3 Fly Ash and Bottom Ash

The ash is collected from the bottom of furnace (bed ash) and the ash collected in the air heater hoppers and ESP hoppers is taken through an underground pipe as slurry and deposited on an empty land. In order to ensure that there is no leachate, the land is properly lined and necessary prevention measures are taken.

3.1.5.4 Control Methods for Water Pollution

(a) *Effluents from Water Treatment Plant*

Water drained from the water treatment plant is pumped to a neutralization pit so that the water let out is neutral. The neutralization pit has effluent resistant cement lining.

(b) *Boiler Blow Down*

In order to maintain the solid concentration in the boiler feed water, two types of blow down are employed in the boiler. One type is continuous blow down and the other intermittent blow down. The blow down water is at a temperature of approximately 100^{o}C. This water is taken to the neutralizing pit, where it will get cooled naturally.

(c) *Sewage from the Power Plant Buildings*

The sewage from the various power plant buildings is taken to a common septic tank through trenches. The sewage from the septic tank is disposed off manually.

3.1.5.5 Control Methods for Noise Pollution

The major source of noise pollution in the power plant is from the following:

- Rotating equipments like ID, FD and SA fans
- Feed pumps
- Boiler and super heater safety valves
- Start up vent
- Steam turbine

The start up vent, safety valve outlets and the DG sets are provided with silencers to reduce the noise level to the acceptable limits. The powerhouse building has been constructed suitably to keep the noise level within the acceptable limits.

3.1.5.6 Unburnt Rice Husk in Bed Ash

Figure 3.8 shows the unburnt rice husk along with bed ash. It comes along with bed ash when the bed ash is drained out. It accounts for carbon loss at Jalkheri power plant. Approximately value of unburnt rice husk is 8.33 g/s.

Figure 3.8 Unburnt rice husk along with bed ash

3.2 Description of 3.5 MW Power Plant at Nahar Spinning Mill Limited, Dhandari Kalan, Ludhiana (CPPDK)

The cogeneration project by Nahar Spinning Mills Ltd. (NSML) at Ludhiana (India) envisages utilization of rice husk available in the region for the generation of power and steam. The project is being implemented adjacent to the current NSML manufacturing facility in Dhandari Kalan, Ludhiana, in the state of Punjab, India. Nahar Spinning Mills Ltd. (NSML) is currently in the process of manufacturing cotton yarn, synthetic yarn and hosiery knitwear. The objective of the project is to reduce anthropogenic green house gases emissions by displacing fossil fuel based electricity generation with environmentally sustainable resource such as rice husk and these indirectly help in reducing the power deficit in the state of Punjab and also contribute towards natural resources conservation such as coal.

The cogeneration project comprised of a 3.5 MW condensing cum extraction turbine that replaced three existing low-pressure boilers with a new boiler of 30 tonnes per hour (TPH) steam generation capacity at 67 atmospheric pressure. While the net thermal energy output of project activity is less than 25 MW, the steam generation from the cogeneration activity has been

excluded from the project boundary, as it is not included under the CDM (Clean Development Mechanism) project activity. Before the starting of project the requirements for power were met from the Punjab state electricity board (PSEB) grid and requirements of steam were met by the three low pressure atmospheric fluidized bed combustion (AFBC) boilers. The technology used in the project activity is indigenously available in India. While the project emissions are nil, baseline emissions are calculated to be 0.85 kg CO_2 per kWh. The project is expected to result in emission reductions of 22,267 tonnes of CO_2 every year, during the ten year crediting period envisaged.

The fuel used in the plant is generally rice husk. But it depends on availability of rice husk. If rice husk not available then coal can also be used in this plant.

Figure 3.9 Atmospheric bubbling fluidized bed combustor at cogeneration plant at CPPDK

Figure 3.10 Feeding of rice husk to the atmospheric fluidized bed combustor through the conveyor belt at CPPDK

Figure 3.11 Pile of rice husk at CPPDK

Figure 3.12 Feeding of rice husk through pile on to the conveyor belt at CPPDK

Table 3.8 Data noted w.r.t rice husk at CPPDK

Parameter	Value
O_2	5-7% by volume
CO_2	9-13% by volume
SO_2	Not noted
N_2	76-79% by volume
TSP(dust)	42 mg/Nm^3
Fly ash(Air heater and ESP hopper)	550-600 kg/h equivalent to 152.7-166.67 g/s
Bed ash	100-150 kg/h equivalent to 27.7-41.6 g/s
Unburnt rice husk along with bed ash	10-12 kg/h equivalent to 2.7-3.3 g/s

Table 3.9 Physico-chemical parameters of CPPDK

Type of fuel can be used in plant	Any type of biomass depending upon availability
Type of fuel used(At time of study)	Rice husk
Feed rate of fuel	7820 kg/hr equivalent to 2172.2 g/s
Feed rate of water	30 T/hr equivalent to 8333.3 g/s
Air flow rate	7×10^6 cm^3/sec
Rate of steam generation	27 ton/hr equivalent to 7500 g/s
Main steam temperature	468^oC
Area of fluidized bed	17.914 m^2 equivalent to 179140 cm^2
Type of distributor	Nozzle type tuyre
Total no. of holes	Detail not found
Specific fuel consumption	1300 g of fuel /unit generation
Bed voidage	0.48
Bed height at minimum fluidization	40 cm
Combustion efficiency	82%
Boiler capacity	30 T/hr equivalent to 8333.3 g/s
Average bed temperature	800^oC
Rice husk density	120 kg/m^3 equivalent to 0.12 g/cm^3

3.2.1 Experience at 3.5 MW Power Plant at Nahar Spinning Mill Limited, Dhandari Kalan, Ludhiana (CPPDK)

After rice husk unloaded from trucks, it continued to lie under sheds. The rice husk is passed to conveyor belt with the help of tractors. Then workers with the help of tools are feeding rice husk from pile onto the conveyor belt as shown in Figure 3.12.

Figure 3.9 shows the atmospheric bubbling fluidized bed combustor at cogeneration plant at Nahar Spinning mills limited at Ludhiana. Figure 3.10 shows the rice husk input to the atmospheric fluidized bed combustor through the conveyor belt. Figure 3.11 shows the pile of rice husk at plant site.

Rice husk burns with dull flame and producing high heat in freeboard. The cleaning of super heater tubes is insufficient at plant. The problems like agglomeration exits at the plant site. The occurrence of agglomeration is generally three-four times in a month during study period. This was avoided generally with refreshment of sand after regular intervals. At this plant, the shortage of rice husk could be met by the coal.

The operation of 3.5 MW cogeneration power plant produces air emissions, fly ash (ash from air heater and ESP Hopper), waste water and solid wastes such as boiler ash. Table 3.8 shows the values of emission data and other values noted from plant. The physico-chemical parameters of CPPDK are given in Table 3.9. Only the values of CO_2, O_2 and N_2 are measured plant site. Punjab pollution control board norms apply for this plant also. The pollution control norms stipulate a maximum dust concentration of 150 mg/Nm^3. The power plant has an Electrostatic Precipitator, which separates the dust from the flue gas and dust concentration is the flue gas leaving the ESP is kept below 150 mg/Nm^3.The electrostatic precipitator is more efficient as compared to Jalkheri power plant and gas leaving this is generally below 50-60 mg/Nm^3. Plant was checked periodically for of harmful gases, it was always found that all permissible limits set by local pollution control are generally fulfilled.

3.2.2 Proximate and Ultimate Analysis of Rice Husk at CPPDK

The proximate and ultimate analysis of rice husk used at 3.5 MW power plant (CPPDK) has also been done. The proximate analysis is done in the chemistry laboratory at Guru Nanak Dev Engineering College, Ludhiana. Ultimate analysis is done at Panjab University, Chandigarh. The results are almost same as with rice husk collected from plant at Jalkheri. The result of one sample of rice husk is given in Table 3.10.

Table 3.10 Proximate and ultimate analysis of rice husk sample for CPPDK

Proximate Analysis (Rice Husk)		Ultimate Analysis (Rice Husk)	
Volatile	58.21	C	39.9
Fixed Carbon	17.13	H	5.2
Ash	16.2	S	0.11
Moisture	8.46	O	36.9
		N	2.2

3.2.3 Proximate Analysis Fly Ash at CPPDK

Table 3.11 shows the proximate analysis of fly ash collected from electrostatic precipitator and air heater.

Table 3.11 Proximate analysis of fly ash collected from air preheater and ESP hopper for CPPDK w.r.t rice husk

Ash	92.5%
Volatile matter	---
Fixed Carbon	7.5%
Moisture	---

CHAPTER 4

MODELING OF FLUIDIZED BED COMBUSTORS

In this chapter the significance of mathematical modeling, physico chemical properties of fluidized bed combustor, exit gas model and solid population balance of fluidized bed combustor based on rice husk are explained. Due to the complicated nature of fluidized bed combustion, a model developed to describe a specific system may not represent well other system differing in design and operating features. Availability of more sophisticated computer models is expected to result in greatly increased performance and reduced costs associated with fluidized bed implementation and operation. Such improved performance would positively affect chemical/energy industry competitiveness and increase energy efficiency.

4.1 Significance of Mathematical Modeling

The term ‘mathematical model’—usually abbreviated to ‘model’—will be used for any complete and consistent set of mathematical equations which is thought to correspond to some other entity, its prototype. The prototype may be a physical, biological, social, psychological or conceptual entity, perhaps even another mathematical model. Being derived from ‘modus’(a measure) the word ‘model’ implies a change of scale in its representation and only later in its history did it acquire the meaning of a type of design.

Developing various mathematical models will help us in understanding the various aspects of fluidization and its related phenomenon. Mathematical models have solved the problems in a systematic way and provide the actual picture of the whole process. The mathematical modeling helps in deciding the optimum values of the operating parameters, which results in an efficient operation of the fluidized bed systems. It helps in easy analysis of the system and its related parameters. Through mathematical modeling the best results can be

achieved. Figure 4.1 shows the flow chart for mathematically modeling of fluidized bed combustor based on rice husk.

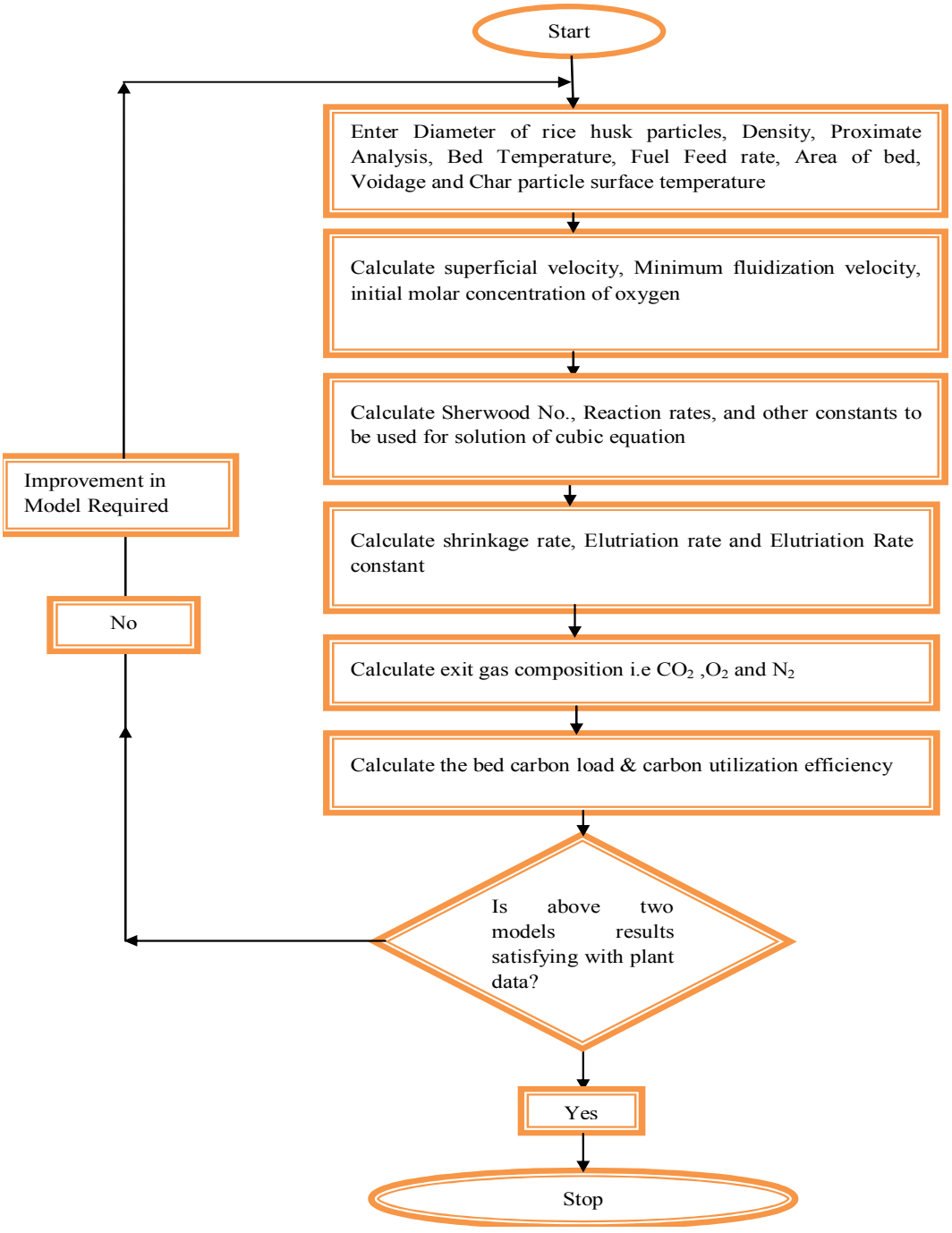

Figure 4.1 Flow chart for mathematical modeling of fluidized bed combustor based on rice husk

4.2 Model Assumptions

The aim of this work is to develop a mathematical model for exit gas composition of fluidized bed combustor suitable for biomass particularly rice husk. Above model is similar to the model developed by Kunii and Levenspiel but here attempt is to apply the three phase model to rice husk particles. It is based on three phase theory of fluidization and single film theory of carbon combustion. It is based on the assumption that essentially $C + O_2 = CO_2$ reaction is taking place in the combustor. It is assumed that the fluidized bed consists of a number of stages and height of each stage is equivalent to average bubble diameter. Each stage consists of bubble, cloud, and emulsion phase. Bubbles are solid free and gas in bubbles is in plug flow, bubbles and cloud-wake rise at the same absolute velocity. In each stage the emulsion and cloud-wake phases are in back mix condition. The voidage in both these stages is same i.e. at incipient condition. We have

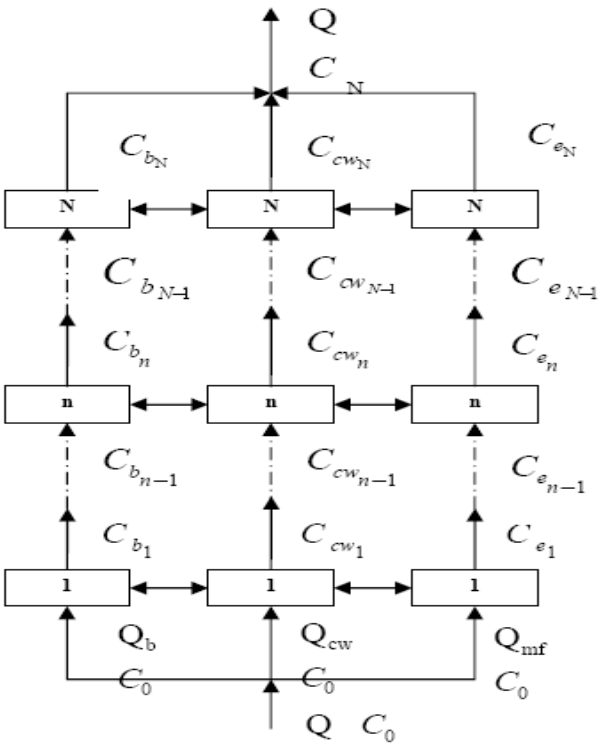

Figure 4.2 Multistage three phase model

also assumed that combustion does not involve a change in number of moles and char and volatile burn at the same rate throughout the bed. Figure 4.2 shows the multistage approach adopted by us in the given work. A mathematical model to describe the performance of fludized bed combustors based on rice husk is presented below. The main features are;

- Physico chemical processes occurring in a fluidized bed combustor based on rice husk
- Oxygen mass balance for exit gas composition.
- Solid population balance

4.3 Physico-Chemical Processes in a Fluidized Bed Combustor

4.3.1 Superficial Velocity

The stoichiometric air feed rate is determined from fuel (rice husk) composition and fuel (rice husk) feed rate from simple stoichiometrical relationship as follows;

$$F_{\mathrm{MTH}} = W_{\mathrm{fuel}}\left(1.0 - XW\right)\frac{\left[\frac{XC}{12.0} + \frac{XH}{4.0} + \frac{XS}{32.0} - \frac{XO}{32.0}\right]}{0.21} \tag{4.3.1}$$

Where W_{fuel} is the fuel feed rate into the combustor (g/s), and *XC, XH, XS, XO,* and *XW* are the ultimate carbon, hydrogen, sulphur, oxygen and moisture content of the Biomass respectively. The actual molar feed rate of fluidizing air is calculated as;

Where E_{xair} fractional excess air

$$F_{\mathrm{ME}} = F_{\mathrm{MTH}}(1.0 + E_{\mathrm{xair}}) \quad \text{g-mole/s} \tag{4.3.2}$$

Now the superficial velocity is calculated as;

$$U_0 = \frac{F_{\mathrm{ME}}\, R_{\mathrm{g}}\, T_{\mathrm{b}}}{P_{\mathrm{av}}\, A_{\mathrm{t}}} \ \text{cm/s} \tag{4.3.3}$$

4.3.2 Minimum Fluidization Velocity

Many correlations are available in the literature to define minimum fluidization velocity, the application of which varies to a great extent depending upon the particle size in the bed. Geldart [142] has pointed out that for particle size $\rangle 100\ \mu m$, the Wen and Yu [143] correlation gives the best result. However, none of the correlation is valid if agglomeration and sintering is taking place in the fluid bed. The Wen and Yu [143] correlation was used to calculate the minimum fluidization velocity in the present model because the particles are greater than 100 μm.

$$U_{mf} = \left(\frac{\mu_g}{d_p \,.\, \rho_g}\right)\left[\left\{(33.7)^2 + \frac{0.0408\, d_{pav}\, \rho_g\, (\rho_p - \rho_g)\, g}{\mu_g{}^2}\right\}^{0.3} - 33.7\right] \text{ cm/s} \qquad (4.3.4)$$

4.3.3 Viscosity of Fluidizing Gas

The viscosity of fluidizing air is estimated from Chapman-Enskog equation using the values of collision integral and Lennard-Jones parameters at the prevailing bed temperature. These important parameters can be found in the work of Bird et al. [144]. The final viscosity expression, which is a function of bed temperature only, is presented below;

$$\mu_g = 1.4\,(10^{-5})\,(T_b)^{1/2} \text{ g/cm.s} \qquad (4.3.5)$$

4.3.4 Average Equivalent Bubble Diameter

A number of correlations are found in the literature for the estimation of bubble diameter in a fluidized bed. One of the widely used correlation was proposed by Stubington et al. [145]. They presented the following equation for bubble diameter.

$$D_b = 0.43(U_o - U_{mf})^{0.4}\,(Z + 4(A_o)^{0.5})^{0.8}\ \ g^{-0.2} \qquad (4.3.6)$$

This equation is used as this most suitable for our case.

4.3.5 Bubble Velocity

The rise velocity of an isolated single rising bubble (u_{br}) is estimated by Davidson and Harrison [46] formula

$$u_{br} = 0.711\sqrt{g\,D_b} \tag{4.3.7}$$

Davidson and Harrison [46] have also derived the absolute rise velocity of a crowd of bubbles in fluid bed as;

$$u_b = U_0 - U_{mf} + u_{br} \tag{4.3.8}$$

4.3.6 Ratio of Cloud Wake Volume to Bubble Volume

Rowe and Patridge [146] have studied the behavior of bubbles in a fluid bed by X-ray method and have found that the size of wake averages one quarter of the total sphere volume and tends to increase as the particle size decreases. In the present case, (f_c) has been taken as an adjustable parameter, the value of which is adjusted between 0.01 and 0.15. For estimating the size of cloud(ratio of cloud volume to bubble volume , f_c), the Davidson and Harison [46] correlation is used;

$$f_{cw} = 0.25 + \frac{3\,U_{mf}}{(\varepsilon_{mf}\,U_{br} - U_{mf})} \tag{4.3.9}$$

The ratio of volume of cloud-wake phase to the volume of bubble, f_{cw} is obtained as follows

$$f_{cw} = f_c + f_w \tag{4.3.10}$$

Since the volumetric flow rate of fluidizing gas Q_f is distributed among the three phases, thus we can have;

$$Q_f = Q_{mf} + Q_{cw} + Q_b \tag{4.3.11}$$

Dividing equation (4.3.11) by the cross-sectional area of the bed, we can get the superficial velocity of fluidizing gas;

$$U_o = U_{mf} + U_{cw} + U_b \tag{4.3.12}$$

Here U_b is the superficial gas velocity of the bubble phase and it is different from the average absolute rise velocity of a crowd of bubbles.

U_{cw} is the velocity of cloud-wake phase

The cross-sectional area of the bed occupied by bubble is;

$$A_b = \varepsilon_b A_t \tag{4.3.13}$$

Where ε_b is the volume fraction of bubble in the bed or the fraction of the bed consisting of bubbles. The cross-sectional area of bed occupied by cloud-wake phase is given below;

$$A_{cw} = f_{cw}.\varepsilon_b.A_t \tag{4.3.14}$$

Now according to model assumptions, the void fraction in the cloud-wake phase is assumed to be ε_{mf}. Hence the cross-sectional area of bed available for gas flow in the cloud-wake phase is expressed by;

$$A_{cw_g} = f_{cw}.\varepsilon_b.\varepsilon_{mf} A_t \tag{4.3.15}$$

The bubble and its associated cloud and wake is assumed to rise at the same absolute rise velocity of crowd of bubbles, u_b. So the volumetric flow rate of gas flowing through the cloud-wake phase is expressed as;

$$Q_{cw} = u_b A_{cw_g} = U_{cw} A_t \tag{4.3.16}$$

Substituting the value of A_{cw_g} from equation (4.3.15) into equation (4.3.16), we get

$$u_b = \frac{U_{cw}}{(f_{cw}.\varepsilon_b.\varepsilon_{mf})} \tag{4.3.17}$$

The volumetric flow rate of gas through the bubble phase;

$$Q_b = u_b A_b = U_b A_t \tag{4.3.18}$$

Now substituting the value of A_b from equation (4.3.13) into (4.3.18), we get

$$\varepsilon_b = \frac{U_b}{u_b} \tag{4.3.19}$$

Equating equations (4.3.17) and (4.3.19), we have

$$U_{cw} = f_{cw}.\varepsilon_{mf}.U_b \tag{4.3.20}$$

After substituting equation (4.3.20) into equation (4.3.12), we get

$$U_b = \frac{U_0 - U_{mf}}{\left(1 + f_{cw}\,\varepsilon_{mf}\right)} \tag{3.3.21}$$

Equations (4.3.21) and (4.3.19) led to the calculation of ε_b with the known parameters of the bed.

From equation (4.3.21) and (4.3.20) the cloud-wake phase velocity may be calculated as;

$$U_{cw} = \frac{U_0 - U_{mf}}{\left(1 + f_{cw}\,\varepsilon_{mf}\right)} f_{cw}\,\varepsilon_{mf} \tag{4.3.22}$$

The bed expansion above the height at minimum fluidization is assumed to be entirely due to the presence of bubbles and hence it is related to expanded bed height;

$$H_{LF} = \frac{H_{mf}}{(1 - \varepsilon_b)} \tag{4.3.23}$$

4.3.7 Bed Weight

The total bed weight is calculated by the following relation;

$$W_b = H_{mf}\ A_t(1.0\ -\ \varepsilon_b) \tag{4.3.24}$$

4.3.8 Gas Interchange Coefficients

It is of particular importance because it is one of determining factors in predicting the performance of fluidized bed combustors. The overall coefficient of gas interchange between bubble and emulsion phase, therefore, has been investigated by several authors. Davidson and Harrison [46] have assumed that there were both convective and diffusional flows contributing to the gas interchange and the correlation is given by;

$$(K_{bc})_b = 4.5\left(\frac{U_{mf}}{D_b}\right) + 5.85\left(\frac{D_g^{1/2} g^{1/4}}{D_b^{5/4}}\right) \tag{4.3.25}$$

In the above equation the second term represents the mass transfer which is given by analogy with the liquid-film controlled diffusion process from a rising bubble. Kunii and Levenspiel [147] have then proposed a new relation for estimating the interchange coefficients. They have assumed that there are two transfer steps, the transfer between the bubble and cloud phase and that between the cloud and emulsion phases. They have further assumed that the coefficient for the former step is given by Davidson and Harrison [46] equation and the coefficient for the latter step is given by Higbie's penetration model. Their correlation is as follows:

$$1/K_{be} = 1/K_{bc} + 1/K_{ce} \tag{4.3.26}$$

$$K_{bc} = 4.5\left(\frac{U_{mf}}{D_b}\right) + 5.85\left(\frac{D_g^{1/2} g^{1/4}}{D_b^{5/4}}\right) \tag{4.3.27}$$

$$K_{ce} = 6.78\left(\frac{\varepsilon_{mf} D_g u_b}{D_b^{3}}\right)^{1/2} \tag{4.3.28}$$

4.3.9 Volatile Evolution and its Combustion

The mechanism of volatile evolution and its subsequent combustion is complex as quoted by La Nauze [148] and a great deal of confusion still exists in the literature. Despite extensive research, a reliable rate expression for devolatilization is not available till date. Zhange [149] has made devolatilization measurements with large bituminous coal particles and as per his estimation, the time for volatile evolution ranges from 20 seconds for a 5 mm diameter particle to 800 seconds for a 50 mm diameter coal. Bellgardt andWerther [150] have claimed from their mixing experiment that the coal particles are able to move more than one meter in the horizontal direction away from the feed region in less than 10 seconds.

Paul et al. [151] have determined the devolatilization behavior of coals representing a wide range of rank at particles sizes up to the maximum which may be used in bubbling fluidized bed combustors. From experiments performed for nine different coals of different sizes they found that for smaller particle size the devolatilization time ranges between 22~56 seconds whilst for more than 0.5 cm size, the devolatilization time ranges from 66~132 seconds. They have also pointed out that in the case of feeds below 0.5 cm size, a synergistic relationship exists between char and volatile combustion such that the increased temperature due to volatile combustion increases the rate of combustion of char particles. Therefore, it is likely that major portion of the volatiles will be released more or less uniformly within the bed. Taking into consideration of all these factors, we make the assumption for the proposed model calculation that volatiles are uniformly distributed in the bed so that volatile matter released and burned

proportional to the char combustion rate as a first approximation. It is due to the fact that the time required for devolatilization and solid mixing are of the same order of magnitude. Second assumption is that oxygen is large enough in the emulsion phase as well as cloud-wake phase to burn the volatile to completion. Since the rice husk are of non swelling type, the diameter of rice husk and char produced are same. Therefore the density of char related with density of rice husk is as follows;

$$\rho_{char} = \rho_p (1.0 - XW - XVM) \tag{4.3.29}$$

4.3.10 Char Particle Surface Temperature

Combustion of char involves the transfer of oxygen from the bulk of bed to the surface of the char, and chemical reaction on the surface and inside pores of the char. One interesting aspect of char combustion in fluidized bed combustor is the temperature difference between burning char particles and the bulk of the bed. In fluidized bed combustor, less than 1% of bed material is char and the rest is inert material such as sand, ash or limestone particles. During combustion, the temperature of the char particles is higher that that of the surrounding and the combustion rate, in turn depends on the temperature of the char particles. The temperature rise of the char particles depends on their size, the oxygen concentration, and the char reactivity.

Park [152] has shown that large particles at high temperature undergo mass-transfer controlled combustion, while small particles at low temperature exhibit kinetically controlled combustion, because mass transfer decreases with particles at low temperature exhibit kinetically controlled combustion, because mass transfer decreases with particle size and the chemical

reaction rate increases with temperature. By viewing a hot fluidized bed combustor, one can easily recognize bright particles visible against a dull background. Many investigators have observed this, and some of them reported temperature difference between burning char and surrounding particles have measured up to 200 K. Avedesian and Devidson [77] have observed that the temperature difference between char particle and its surrounding decrease with char particle size. However, the temperature history during burnout of single char particle, as reported by Chakraborty and Howard [62], shows a relatively constant temperature rise, except at the end of combustion when the temperature rise diminishes rapidly.

Bear at al. [84] have also observed that in the prevailing temperature range in fluidized bed i.e. 1000~1200 K, the char surface overshoot varies from 30 K for low oxygen concentration to 500 K for high oxygen concentration for 0.1 cm particle. The higher temperature overshoot occurs near the bed distributor where oxygen concentration approaches that of inlet air. Although there are still uncertainties on the reaction order in char combustion and the location of CO oxidation to CO_2, we have assumed char combustion is first order with respect to oxygen and that CO_2, is the reaction product. Moreover, we have assumed those char particles are spherical and that they shrink in size with combustion. The char particle surface temperature is assumed in our case is 200 K greater than bed temperature.

4.3.11 Reaction Rate Constant

Chemical reaction rate in fluidized bed combustion plays an important role in the formulation of oxygen mass balance model. In this context two basic mechanisms have been postulated for char combustion e.g single film model and double film model. According to single film theory

oxygen reaches carbon surface and reacts to form varying amounts of CO and CO_2. The CO formed is then oxidized to CO_2 by incoming oxygen. Whereas the double film model postulates that oxygen never reaches carbon particle surface, only CO_2 reacts with carbon to produce CO and which in turn is oxidized by incoming oxygen. The 10 MW fluidized bed rice husk combustor at Jalkheri normally operates at 1073 K when only rice husk is used. Park [152] has shown from extensive experiments that the temperature difference between burning char particles and bulk of the bed can be maximum up to 200 K. However, Campbell and Davidson [78] have pointed out that the combustion mechanism on which the double film theory is based requires particle temperature in excess of 1373 K as result of which the endothermic carbon dioxide reduction at the particle surface cannot be sustained due to the low particle temperature. Therefore in the present case the single film theory of char combustion for shrinking particles has been considered where carbon reacts with oxygen to produce CO_2.

The model assumptions for char combustion are summarized below;

- Char and volatile matter burn at the same rate
- Release of volatile matter from rice husk is instantaneous
- Reaction between carbon and oxygen takes place only on the outer surface of the particle i.e inner pores are inaccessible

The rate of mass transfer is defined as the flow material normal to a unit surface as;

$$Q_{transfer} = \frac{1}{S}.\frac{dN}{dt} \text{ g.mol oxygen/cm}^2\text{-s} \tag{4.3.30}$$

Hence the reaction step must similarly be defined as;

$$Q_{reaction} = \frac{1}{S}.\frac{dN}{dt} \text{g.mol oxygen/cm}^2\text{-s} \tag{4.3.31}$$

Oxygen diffuses through a film of thickness (ΔX) on to a plane surface of carbon particles where it reacts with carbon to yield gaseous product CO_2 which diffuses back through the film into the main gas stream. The intrinsic rate of chemical reaction will be proportional to oxygen concentration at the carbon surface C_s'. Considering the carbon oxygen reaction to be of first order;

$$\frac{1}{S}.\frac{dN}{dt} = K_s C_s' \tag{4.3.32}$$

Now at steady state the intrinsic rate must be equal to the rate at which oxygen is supplied to the surface via gas film. Hence

$$K_g(C_p - C_s') = K_s C_s' \tag{4.3.33}$$

i.e mass transported =surface reaction rate

The surface oxygen concentration C_s' is derived from equation (4.3.33) as follows;

$$C_s' = K_g.C_p/(K_g + K_s) \tag{4.3.34}$$

Substituting equation 4.3.34 in equation 4.3.32 we get

$$\frac{1}{S}.\frac{dN}{dt} = \frac{C_p}{(1/K_s + 1/K_g)} \tag{4.3.35}$$

The chemical reaction rate constant K at any instant which is controlled by surface reaction and gas diffusion coefficients and is obtained from the above equation as;

$$\frac{1}{K} = \frac{1}{K_s} + \frac{1}{K_g} \tag{4.3.36}$$

Here K_s is the surface reaction rate constant for rice husk particles.

We have used the correlation suggested by given by Parker and Hotel [153] to calculate the surface reaction rate constant;

$$K_s = 4.32 \times 10^{11} T_p^{-0.5} . \exp(-44000 / RT_p) \tag{4.3.37}$$

The mass transfer coefficient K_g is expressed by dimensionless Sherwood number (Sh) as;

$$K_g = \frac{Sh.D_g}{d_p} \tag{4.3.38}$$

Many correlations are available for estimating the Sherwood number but in our work La nauze et al. [154] correlation has been adopted which was developed on the assumption of frequent renewal of gas at particle surface. It is assumed that the particle environment changes as a result of which steady state concentration boundary layer is never achieved and the correlation is given as;

$$Sh = 2\varepsilon_{mf} + \left[\frac{4.0 d_p \left(U_{mf} / \varepsilon_{mf} + U_b \right)}{\pi D_g} \right]^{0.5} \text{ for } \frac{d_p}{d_{pbed}} > 4.0 \tag{4.3.39}$$

$$Sh = 2\varepsilon_{mf} + \left[\frac{4.0 d_p U_{mf}}{\pi D_g} \right]^{0.5} \quad \text{for} \quad \frac{d_p}{d_{pbed}} \leq 4.0 \tag{4.3.40}$$

In calculation $d_p / d_{pbed} = 4.0$ has been assumed as transition point.

4.4 Formulation of Model for Exit Gas Composition Based on Rice Husk

A model has been developed by the relations provided in the literature to analyze the exit gas composition. The oxygen present in the bubble cannot take part in combustion. The bubble phase oxygen is transported across the bubble cloud interface into the more carbon rich cloud-wake phase, where the combustion reaction takes place. Unreacted oxygen in the cloud-wake is further transported to the very carbon rich emulsion phase. Most of the oxygen is consumed in the emulsion phase. The net result of these events is that the observed combustion rate depends upon the transfer coefficients and chemical reaction rate constant.

Oxygen balance around stage 'n' for bubble phase

|Oxygen in by convection |– |Oxygen out by convection | – |Oxygen transfer to cloud-wake| = 0

It is represented symbolically as;

$$U_b C_{b_{n-1}} - U_b C_{b_n} - (K_{bc})_b \varepsilon_b \int_{Z_{n-1}}^{Z_n} (C_b - C_{cw_n}) dZ \tag{4.4.1}$$

Oxygen balance around stage 'n' for bubble-cloud wake phase

|Oxygen in by convection | + |Oxygen coming from bubble phase by transfer | – | Oxygen going out from cloud–wake to emulsion by transfer | – |Oxygen out from cloud-wake by convection | – | Oxygen consumed in cloud-wake phase| = 0

Symbolically, it can be represented as;

$$U_{cw} C_{cw_{n-1}} + (K_{bc})_b \varepsilon_b \int_{Z_{n-1}}^{Z_n} (C_b - C_{cw_n}) dZ + K_{ce} C_{e_n} - (U_{cw} + K_{cw} + K_{ce}) C_{cw_n} = 0 \tag{4.4.2}$$

Where

$$K_{ce} = (K_{ce})_b \varepsilon_b \Delta Z \tag{4.4.3}$$

$$K_{cw} = (K)(f_{cw})(\varepsilon_b)(\Delta Z) \tag{4.4.4}$$

$$dZ = Z_n - Z_{n-1} = D_b \tag{4.4.5}$$

Oxygen balance around stage 'n' for emulsion phase

|Oxygen in by convection| – |Oxygen out by convection | + |Oxygen transfer from cloud-wake phase| = |Oxygen consumed by Combustion reaction |

Symbolically, it can be represented as:

$$U_{mf} C_{e_{n-1}} + (K_{ce})(C_{cw_n}) - (U_{mf} + K_e + K_{ce}) C_{e_n} = 0 \tag{4.4.6}$$

Where

$$K_e = K[1 - \varepsilon_b (1 + f_{cw})] dZ \tag{4.4.7}$$

$$K_{ce} = (K_{ce})\varepsilon_b dZ \tag{4.4.8}$$

Now the oxygen balance over a height (dZ) in the bubble phase is written as:

$$U_b C_b - U_b(C_b + dC_b) - (K_{bc})_b \varepsilon_b (C_b - C_{cw_n})dZ = 0 \tag{4.4.9}$$

Above equation can be re-written as

$$-U_b dC_b = (K_{bc})_b \varepsilon_b (C_b - C_{cw_n})dZ$$

$$\frac{dC_b}{(C_b - C_{cw_n})} = -\frac{(K_{bc})_b \varepsilon_b dZ}{U_b}$$

Integrating we get

$$\int_{C_{b_{n-1}}}^{C_b} \frac{dC_b}{(C_b - C_{cw_n})} = -\frac{(K_{bc})_b \varepsilon_b}{U_b} \int_{Z_{n-1}}^{Z_n} dZ$$

Which can be written as

$$-U_b \left|\log(C_b - C_{cw})\right|_{C_{b_{n-1}}}^{C_b} = (K_{bc})_b \varepsilon_b (Z_n - Z_{n-1})$$

Expanding the limits, we get

$$-U_b \left|\log(C_{b_n} - C_{cw_n})\right| - \left|\log(C_{b_{n-1}} - C_{cw_n})\right| = (K_{bc})_b \varepsilon_b (Z_n - Z_{n-1})$$

Above equation can be written as

$$\log\left[\frac{C_{b_n} - C_{cw_n}}{C_{b_{n-1}} - C_{cw_n}}\right] = \frac{-(K_{bc})_b \varepsilon_b (Z_n - Z_{n-1})}{U_b}$$

Which implies

$$\frac{C_{b_n} - C_{cw_n}}{C_{b_{n-1}} - C_{cw_n}} = \exp\left[\frac{-(K_{bc})_b \varepsilon_b (Z_n - Z_{n-1})}{U_b}\right]$$

$$C_b - C_{cw_n} = (C_{b_{n-1}} - C_{cw_n}) \exp[\{-(K_{bc})_b \varepsilon_b (Z - Z_{n-1})\}/U_b] \tag{4.4.10}$$

At the bottom of the bed (n=0), the concentration of oxygen fed to each phase is the same as that of the incoming feed oxygen. Hence, the boundary conditions for solving the above equations are:

$$\text{At n=0, } C_{b_n} = C_{cw_n} = C_{e_n} = C_0 \tag{4.4.11}$$

Equations 4.4.1 - 4.4.10, together with the boundary conditions in equation 4.4.11, make up a complete mathematical description of the system.

Multiplying eq. (4.4.10) by $(K_{bc})_b \varepsilon_b$ and integrating along the length of stage **n**, we get

$$(K_{bc})_b \varepsilon_b \int_{Z_{n-1}}^{Z_n} (C_b - C_{cw_n}) dZ = \frac{U_b}{R} (C_{b_{n-1}} - C_{cw_n}) \tag{4.4.12}$$

Where $R_1 = \dfrac{1}{1 - \exp[-(K_{bc})_b \varepsilon_b dZ / U_b]}$ (4.4.13)

From equation (4.4.1)

$$U_b C_{b_{n-1}} - U_b C_{b_n} = (K_{bc})_b \varepsilon_b \int_{Z_{n-1}}^{Z_n} (C_b - C_{cw_n}) dZ$$

Since

$$(K_{bc})_b \varepsilon_b \int_{Z_{n-1}}^{Z_n} (C_b - C_{cw_n}) dZ = \frac{U_b}{R_1} (C_{b_{n-1}} - C_{cw_n})$$

So we get

$$U_b C_{b_{n-1}} - U_b C_{b_n} = \frac{U_b}{R_1} (C_{b_{n-1}} - C_{cw_n})$$

Which is further solved which leads to

$$C_{cw_n} = R_1 C_{b_n} - (R_1 - 1) C_{b_{n-1}} \tag{4.4.14}$$

Hence, one may write

$$C_{cw_{n-1}} = R_1 C_{b_{n-1}} - (R_1 - 1) C_{b_{n-2}} \tag{4.4.15}$$

Equation (4.4.1) may be rewritten as

$$(K_{bc})_b \varepsilon_b \int_{Z_{n-1}}^{Z_n} (C_b - C_{cw_n}) dZ = U_b (C_{b_{n-1}} - C_{b_n})$$

Substituting equations 4.4.13, 4.4.14 and 4.4.15 into eq. (4.4.2) and simplifying, we have

$$C_{e_n} = a_1 C_{b_n} + b_1 C_{b_{n-1}} + c_1 C_{b_{n-2}} \tag{4.4.16}$$

Where

$$a_1 = [(U_{cw} + k_{cw} + K_{ce}) R_1 + U_b] / K_{ce} \tag{4.4.17}$$

$$b_1 = [U_{cw} R_1 + (U_{cw} + k_{cw} + K_{ce})(R_1 - 1) + U_b] / K_{ce} \tag{4.4.18}$$

$$c_1 = (R_1 - 1) U_{cw} / K_{ce} \tag{4.4.19}$$

In a similar manner to equation (4.4.16), one may write

$$C_{e_{n-1}} = a_1 C_{b_{n-1}} + b_1 C_{b_{n-2}} + c_1 C_{b_{n-3}} \tag{4.4.20}$$

Equations (4.4.14), (4.4.16) and (4.4.20) may be substituted into eq. (4.4.6) to give

$$C_{b_n} + b C_{b_{n-1}} + c C_{b_{n-2}} + d C_{b_{n-3}} = 0 \tag{4.4.21}$$

With

$$a = -(U_{mf} + k_e + K_{ce}) a_1 + K_{ce} R_1 \tag{4.4.22}$$

$$b = [U_{mf} a_1 - (U_{mf} + k_e + K_{ce}) b_1 - K_{ce} (R_1 - 1)] / a \tag{4.4.23}$$

$$c = [U_{mf} b_1 - (U_{mf} + k_e + K_{ce}) c_1] / a \tag{4.4.24}$$

$$d = U_{mf} c_1 / a \tag{4.4.25}$$

Equation (4.4.21) is a third order homogenous linear finite-difference equation with constant coefficients. The solution of this equation is obtained by trying a solution of the form

$$C_{b_n} = f G^n \tag{4.4.26}$$

Where f is an arbitrary constant and G is a constant whose value is to be determined without recourse to the boundary conditions. When this solution is substituted into eq. (4.4.12), it leads to

$$f G^{n-3} (G^3 + b G^2 + c G + d) = 0 \tag{4.4.27}$$

Since f =0 and G=0 are trivial cases, eq. (4.4.27) may be written as

$$G^3 + bG^2 + cG + d = 0 \tag{4.4.28}$$

Equation (4.4.28) is a cubic algebraic equation which may be solved as follows:

Let

$$p = 1/3(3c - b^2) \tag{4.4.29}$$

$$q = 1/27(27d - 9bc + 2b^3) \tag{4.4.30}$$

$$T = p^3/27 + q^2/4 \tag{4.4.31}$$

$$\phi = \cos^{-1}\left(-\frac{q^2/4}{p^3/27}\right) \tag{4.4.32}$$

For T < 0, eq. (4.4.28) has three unequal roots given by

$$G_m = \mp 2\left\{(-p/3)^{1/2}\cos\left[\phi/3 + 120(m-1)\right]\right\} - b/3 \qquad \text{(m=1, 2, 3)} \tag{4.4.33}$$

Where the upper sign applies if q>0, and the lower if q<0. Thus, the general solution of equation (4.4.21) is

$$C_{b_n} = f_1 G_1^n + f_2 G_2^n + f_3 G_3^n \tag{4.4.34}$$

$$C_{b_{n-1}} = f_1 G_1^{n-1} + f_2 G_2^{n-1} + f_3 G_3^{n-1} \tag{4.4.35}$$

$$C_{b_{n-2}} = f_1 G_1^{n-2} + f_2 G_2^{n-2} + f_3 G_3^{n-2} \tag{4.4.36}$$

Substitution of equations (4.4.34) and (4.4.35) into equation (4.4.14) leads to

$$C_{cw_n} = g_1 f_1 G_1^n + g_2 f_2 G_2^n + g_3 f_3 G_3^n \tag{4.4.37}$$

Where

$$g_m = R_1 - (R_1 - 1)/G_m \qquad \text{(m=1, 2, 3)} \tag{4.4.38}$$

Substituting equations (4.3.34) - (4.3.36) into equation (4.3.16), we have

$$C_{e_n} = r_1 f_1 G_1^n + r_2 f_2 G_2^n + r_3 f_3 G_3^n \tag{4.4.39}$$

Where $r_m = a_1 + b_1 / G_m + c_1 / G_m^2$ (m=1, 2, 3) (4.4.40)

Inserting the boundary conditions given by equation (4.4.11) into equations (4.4.34), (4.4.37) and (4.4.39), respectively, one may write

$$C_o = f_1 + f_2 + f_3 \tag{4.4.41}$$

and $C_o = g_1 f_1 + g_2 f_2 + g_3 f_3$ (4.4.42

$$C_o = r_1 f_1 + r_2 f_2 + r_3 f_3 \tag{4.4.43}$$

Solving equations (4.4.41) - (4.4.43) simultaneously for $f_1 - f_3$, we obtain

$$f_1 = \left[(r_2 - r_3) + g_2(r_3 - 1) + g_3(1 - r_2)\right] C_o / D \tag{4.4.44}$$

Where

$$D = g_1(r_2 - r_3) + g_2(r_3 - r_1) + g_3(r_1 - r_2) \tag{4.4.45}$$

$$f_2 = \left[g_1(1 - r_3) + (r_3 - r_1) + g_3(r_1 - 1)\right] C_o / D \tag{4.4.46}$$

$$f_3 = \left[g_1(r_2 - 1) + g_2(1 - r_1) + (r_1 - r_2)\right] C_o / D \tag{4.4.47}$$

The average gas composition leaving the n^{th} stage, i.e at the top of the bed is determined as follows:

Oxygen

$$C_{avg} = (U_b C_{b_n} + U_{cw} C_{cw_n} + U_{mf} C_{e_n}) / U_0 \tag{4.4.48}$$

Carbon dioxide

$$CO_2 = C_0 - C_{avg} \tag{4.4.49}$$

Nitrogen:

$$N_2 = (0.79 / 22,400)(273 / T_b) + [XN(1 - XW)] / 28.U_0.A_t \tag{4.4.50}$$

The developed model would be validated with plant data. All the parameters determined from the above discussed equations, would be fed into exit gas equations, to calculate exit gas composition of 10 MW Jalkheri power plant is summarized in Table 4.1.

Table 4.1 Hydrodynamic parameters for Jalkheri power plant

Parameter	Theoretical or empirical correlation	Reference
1. Minimum fluidization velocity (cm/s)	$U_{mf} = (\frac{\mu}{d_p \rho_g})\left[\{(33.7)^2 + \frac{0.0408 d_p \rho_g (\rho_s - \rho_g) g}{\mu_g^{\ 2}}\}^{0.5} - 33.7 \right]$	Wen and Yu[155]
2. Gas viscosity (g/cm-s)	$\mu = 1.4(10^{-5})(T_b)^{1/2}$	Bird et al.[144]
3. Gas density(g/cm^3)	$\rho_g = 353.2(10)^{-3} / T_b$	Bird et al.[144]
4. Average bubble diameter (cm)	$D_b = 0.54(U_0 - U_{mf})^{0.4}\left[Z + 4\sqrt{\frac{A_t}{N_D}} \right].g^{-0.2}$	Stubington et al.[145]
5. Single bubble velocity (cm/s)	$u_{br} = 0.711\sqrt{g D_b}$	Davidson and Harrison [46]
6. Average absolute velocity of crowd of bubbles (cm/s)	$u_b = U_0 - U_{mf} + u_{br}$	Davidson and Harrison [46]
7. Ratio of cloud-wake volume to bubble volume	$f_{cw} = 0.25 + (3U_{mf} / \varepsilon_{mf} u_{br} - U_{mf})$	Davidon and Harrison [46]
8. Bubble to cloud wake gas interchange coefficient (s^{-1})	$(K_{bc})_b = 4.5\left(\frac{U_{mf}}{D_b} \right) + 5.85\left(\frac{D_g^{\ 1/2} g^{1/4}}{D_b^{\ 5/4}} \right)$	Kunii and Levenspiel [48]
9. Cloud-wake to emulsion phase gas interchange coefficient (s^{-1})	$(K_{ce})_b = 6.78\left(\frac{\varepsilon_{mf} D_g u_b}{D_b^{\ 3}} \right)^{1/2}$	Kunii and Levenspiel [48]

10. Superficial gas velocity through the bed (cm/s)	$U_0 = \frac{FME.R.T_b}{P_{av} A_t}$ $where\ FME = FMTH\,(1 + Exair)$ $FMTH = W_{RiceHusk}(1 - XW)\left[\frac{XC/12 + XH/4 + XS/32 - XO/32}{0.21}\right]$	Reddy et al. [156]
11. Oxygen molar concentration at the inlet g-mol/cm^3	$C_0 = \frac{0.21}{22400} \times \frac{273}{T_b}$	Reddy et al. [156]
12. Gas velocity through bubble phase (cm/s)	$U_b = \frac{U_0 - U_{mf}}{\left(1 + f_{cw}\,\varepsilon_{mf}\right)}$	El-Halwagi and El-Rifai [92]
13. Gas velocity through cloudwake phase (cm/s)	$U_{cw} = \frac{U_0 - U_{mf}}{\left(1 + f_{cw}\,\varepsilon_{mf}\right)} f_{cw}\,\varepsilon_{mf}$	El-Halwagi and El-Rifai [92]
14. Cross sectional area of bed occupied by bubble (cm^2)	$A_b = \varepsilon_b A_t$	El-Halwagi and El-Rifai [92]
15. Diffusivity of Gas D_g (cm^2/s)	$5.14(T_b)^{1.5}/100000$	Bird et al. [144]

4.5 Model for Solid Population Balance, Bed Carbon Load and Carbon Utilization Efficiency

4.5.1 Model for Solid Population Balance Based on Rice Husk

Model for solid population balance has been formed on the basis of Kunii and Levenspiel model for linear shrinkage, single-size feed and no elutriation. Model is used to calculate the bed carbon load. The overflow rate is considered to be zero in the model. At steady state conditions and

constant density of char, for back mix flow, the size distribution of the overflow stream is same as bed particles i.e

$$P_b(d_p) = P_1(d_p) \quad \text{and} \quad F_o = F_3 + F_5 \tag{4.5.1}$$

For details refer [157].

4.5.2 Elutriation Rate

Elutriation refers to the selective removal of fines by entrainment from a bed consisting of a mixture of particle sizes. Elutriation rate constant $K^*(d_p)$ and elutriation constant $K(d_p)$ are two important features in fluidized bed combustors. $K^*(d_p)$ varies with size of solids, a large value corresponds to a rapid removal rate and $K^*(d_p) = 0$ means that the particular size of solid is not removed at all by entrainment, whereas $K(d_p)$ varies proportionately with bed cross-section and inversely with bed height, but $K^*(d_p)$ is unaffected by these changes as long as quality of fluidization remains same. Since the generation of fines in the bed may be due to chemical, mechanical and hydrodynamic breakdown of the solids, it becomes difficult to predict the actual concentration of any particular size fraction in the bed.

Many correlations are available in the literature for the prediction of elutriation rate constant $K^*(d_p)$ viz. Yagi and Aochi[158], Zenz and Weil[159], Wen and Hashinger[160], and Geldart et al. [161] etc. Geldart et al. [161] have shown that high accuracy should not be expected from any of these correlation and agreement between experimental and prediction is unlikely to be better than ±100%. For low density solids such as coal char, cracking catalyst etc. and well mixed beds at velocities upto 120 cm/s, Zenz and Weil [159] correlation probably gives the most consistent values of $K^*(d_p)$. The Zenz and Weil [159] correlation has been used in our model to predict the elutriation rate of solids from the fluidized bed which is given below.

$$\frac{K^*(d_p)}{\mu_g.U_o} = [1.26\times10^7\left(\frac{U_o^2}{gd_p\rho_p^2}\right)^{1.88} \qquad \text{when} \quad \frac{U_o^2}{gd_p\rho_p^2} < 3\times10^2 \ \text{cm}^6/\text{g}^2 \tag{4.5.2}$$

$$\frac{K^*(d_p)}{\mu_g.U_o} = [4.31\times10^4\left(\frac{U_o^2}{gd_p\rho_p^2}\right)^{1.18} \qquad \text{when} \quad \frac{U_o^2}{gd_p\rho_p^2} > 3\times10^2 \ \text{cm}^6/\text{g}^2 \tag{4.5.3}$$

The elutriation constant K (d_p) is calculated from the elutriation rate constant $K^*(d_p)$ as follows;

$$K(d_p) = \frac{K^*(d_p)}{H_{mf}(1-\varepsilon_{mf}).\rho_p} \tag{4.5.4}$$

4.5.3 Particle Shrinkage Rate

Shrinking core model of Fluidized bed combustor has been used here. As soon as the rice husk enters into the FBC, it decomposes into volatiles and combustible matter. The assumptions of the model may not match reality precisely. For example, reaction may occur along a diffuse front rather than along a sharp interface between ash and fresh solid, thus giving behavior intermediate between the shrinking core and the continuous models. This problem has been considered by Wen and Ishida [162]. Also for fast reaction the rate of heat release may be high enough to cause significant temperature gradients within the particles or between particle and the bulk fluid. This problem is treated in detail by Wen and Wang [163].

Despite these complications Wen and Ishida [162] on the basis of studies of numerous systems, conclude that the shrinking core model is the best simple representation for the majority of reacting gas solid systems.

$$\left(\frac{dd_p}{dt}\right)_{\text{overall}} = \left(\frac{dd_p}{dt}\right)_{\text{attrition}} + \left(\frac{dd_p}{dt}\right)_{\text{combustion}} \tag{4.5.5}$$

The shrinkage rate by attrition for rice husk in fluidized bed combustor is neglected in our model, because rice husk is low density fuel. For particle shrinkage rate approach of Turnbull et al. [43] is used.

According to Turnbull et al. [43];

$$(\frac{dd_p}{dt})_{combustion} = \frac{2M_c}{\rho_c}\left(\frac{1}{K_s} + \frac{d_p}{Sh.D_g}\right)^{-1}.C_p \tag{4.5.6}$$

K_s the surface reaction rate for the combustion of pure carbon is given by Parker and Hottel [153].

Hence the final expression for particle shrinkage rate is given below; Here we assumed $C_p = C_o$.

$$k_{shrk} = \frac{dd_p}{dt} = \frac{2M_c}{\rho_c}\left(\frac{1}{K_s} + \frac{d_p}{Sh.D_g}\right)^{-1}.C_p \tag{4.5.7}$$

4.5.4 Bed Carbon Load

The size of rice husk particles which are fed to rice husk combustor is constant, so we chose Kunii and Levenspiel [157] approach i.e special case of linear shrinkage, single size feed and no elutriation to derive solid population balance for 10 MW rice husk combustor. In the extreme case when the particles shrink to zero and no solids leave the reactor, for more details refer [157].

Therefore bed carbon load

$$W_c = F_o d_p / 8k_{shrk} \tag{4.5.8}$$

In actual plant elutriation rate is not zero, this approach is only used to determine bed carbon load in 10 MW fluidized bed combustor at Jalkheri power plant.

4.5.5 Carbon Utilization Efficiency

The carryover rate i.e total particles/fines generated from the bed will be

Carry over rate = F_1=Elutriation rate constant × Total area of bed (g/s)

$F_1 = K^*(d_p) \times$ Area of Bed (g/s) (4.5.9)

Carbon carry over rate from the boiler (F_3)

$F_3 = F_1 \times$ (%age of carbon in fly ash (air heater and ESP)) (4.5.10)

Carbon utilization efficiency = $\frac{F_o - F_3}{F_o} \times 100$ (4.5.11)

CHAPTER 5
AGGLOMERATION

The defluidization of bed is a commonly occurred problem in biomass based power plants. It is frustrating for operators as agglomerates formed in such plants. Some times the operation has to be stopped leading to economic loss. The agglomerates are very soft in nature and can be broken by pressing it with hand. However some times these agglomerates are very hard to break with large force. The two plants which were focused for agglomeration study were, 10 MW Jalkheri power plant (JPP) at Jalkheri, Patiala and 3.5 MW cogeneration power plant at Dhandari Kalan, Ludhiana (CPPDK). At both the power plants the defluidization was common problem as observed from Figures 5.4 and Figure 5.5, when temperature greater than 750^{o}C, rice husk is used alone and rice husk-rice straw mixture is used. The problem of agglomeration is even more severe when rice straw is used alone. During study rice husk is major fuel used, so reliable data with respect to rice straw is not available. When rice straw is used with rice husk, the problem of agglomeration is severe. In this case plant has to operate at very low bed temperature of 650^{o}C. Rice husk is not available throughout the year, so any type of biomass which is conceivable is used at plant.

The main purpose of this work is to determine the causes of agglomeration while incinerating rice husk alone, rice husk-rice straw combination in the fluidized bed combustor and provide solutions for agglomeration problem with respect to rice husk, rice husk-rice straw combination**.** Figure 5.1 shows the flow chart methodology involved in this work.

5.1 Mechanism of Agglomeration

Two types of mechanisms of agglomeration formation [164,165] are shown in the Figure 5.2 and Figure 5.3. Figure 5.2 which is commonly observed in commercially operated fluidized-bed combustors using woody-type of fuels, results from “coating-induced” agglomeration. Here, a uniform coating is formed on the surface of the bed material grains. At certain critical

conditions, neck formation may occur between coatings of individual grains, which initiate

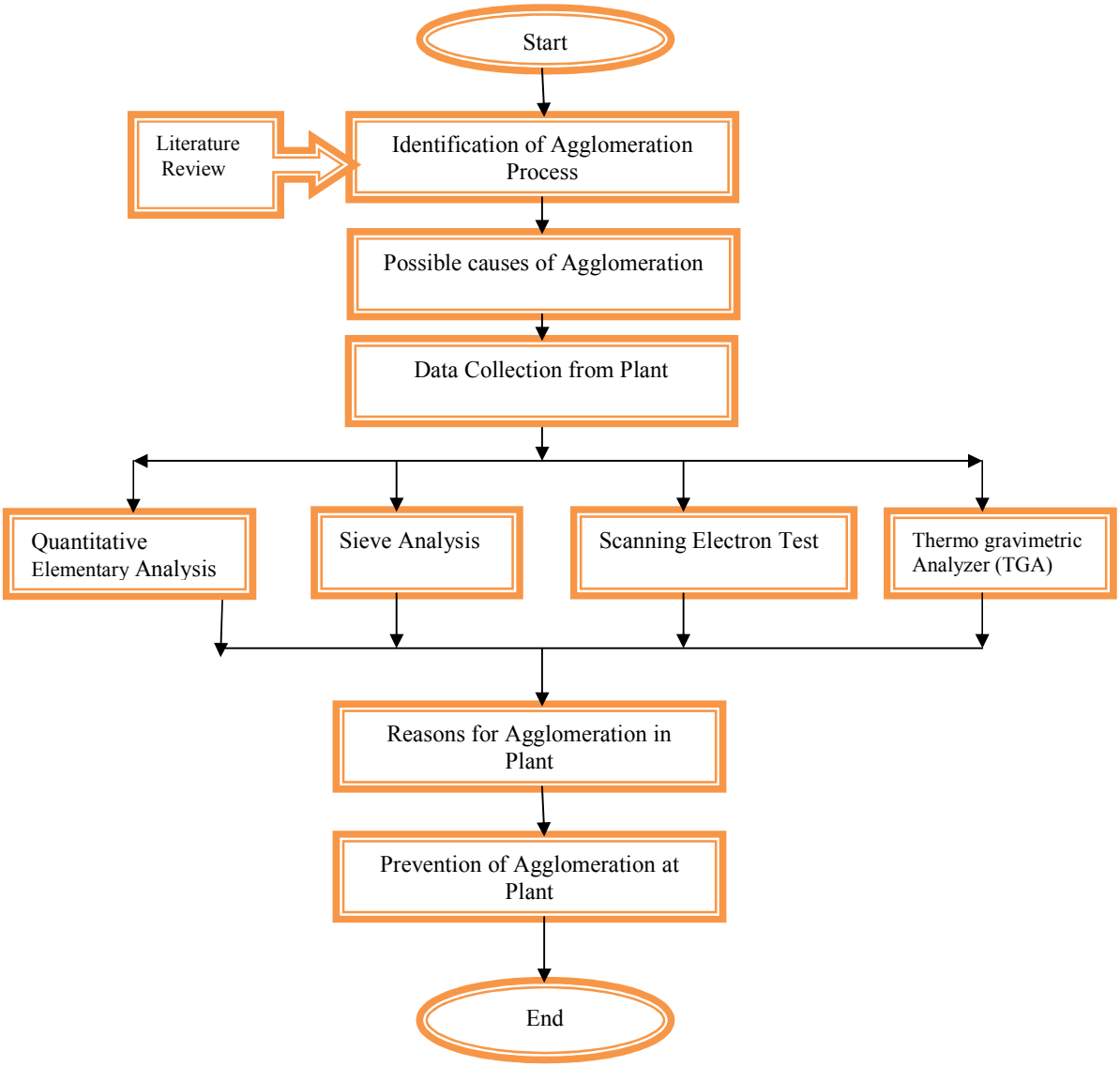

Figure 5.1 Flowchart methodology for study of agglomeration

the agglomeration. Other extreme type of agglomeration mechanism is shown in Figure 5.3, results from "melt induced" agglomeration. In this case, the bed materials are glued together by a melt phase, which roughly matches the chemical composition of the ash and is produced at normal operating temperature. Particle-to-particle bonding or sintering starts when a neck

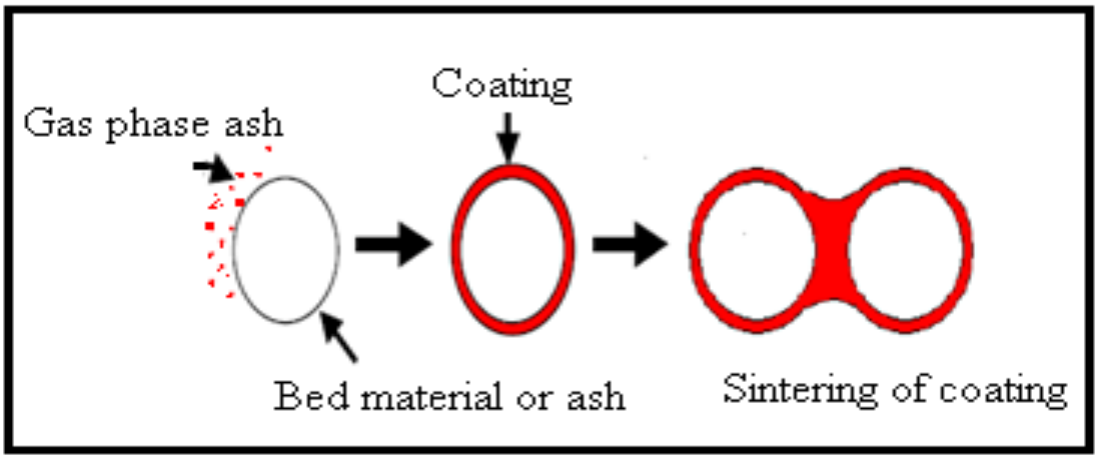

Figure 5.2 Agglomeration of bed material after coating formation from gas phase [164,165]

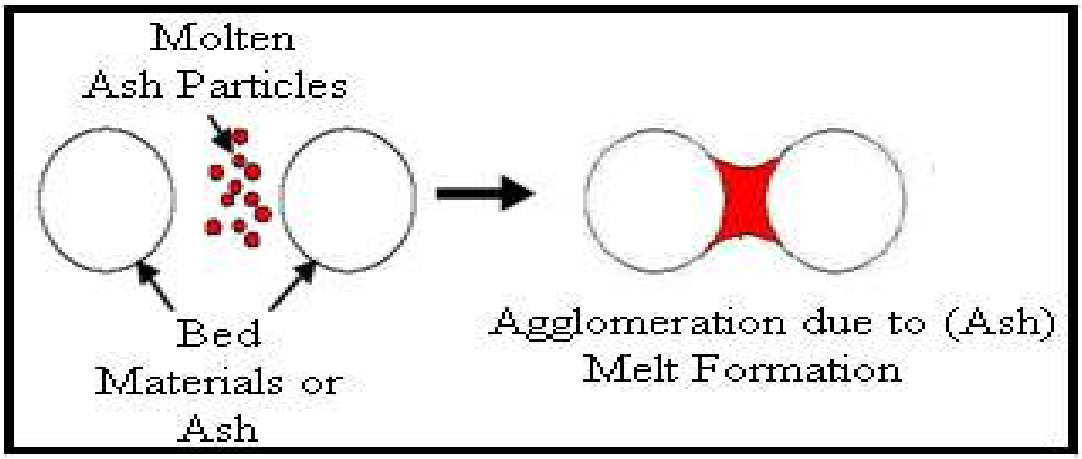

Figure 5.3 Agglomeration of bed materials after melt formation of ash components [164,165]

is formed between particles, resulting in an initially porous network. The neck regions grow until individual particles can no longer be identified. Finally, a dense mass forms. The driving force for this process is reduction of the surface energy of the particles. Sintering in the presence of a reactive non-viscous liquid phase consisting of molten alkali salts, where the solid phase is partly soluble in the liquid at the sintering temperature. The amount of liquid controls the neck formation. Cooling below the solidus temperature gives crystallization of the bonding agent and densification of the agglomerate. This mechanism is predominant for fuels with ashes high in low-melting eutectics causing sintering and agglomeration at

temperatures even at low temperatures. When a silicate ash is heated above the solidus temperature highly viscous liquid phase formed. Due to its high viscosity, the liquid remains viscous on rapid cooling below the solidus temperature forming a glassy phase. The absorption of alkalis on silicate fly ash particles gives rise to formation of low melting silicate on the surface of the particles. When the temperature in an ash-deposit rises, due to reduced heat transfer flowing of this viscous layer forms a neck between adjacent particles. On cooling this neck, it freezes to a glassy phase.

Agglomeration problems in fluidized beds are associated with a high content of organically bound (volatile) alkali metals in the fuel. In biomass, alkali metals (esp. potassium) concentrate in regions of most vigorous growth. The agglomerate sample collected from Jalkheri power plant is shown in Figure 5.4.

Figure 5.4 Ash agglomerate sample at JPP

The unburnt rice husk along with agglomerate sample has also been visualized in Figure 5.4. The number of agglomerates formed in the fluidized bed combustor is seen at the bottom of

Figure 5.5 Ash agglomerates at the bottom of furnace of fluidized bed combustor at JPP

Figure 5.6 Labourers cleaning sand at JPP

Figure 5.7 Agglomerate at bottom of furnace of JPP

Figure 5.8 Hard agglomerate when (rice husk-rice straw is used) at JPP

Figure 5.9 Cleaned sand for reusing at JPP

furnace of Jalkheri power plant is shown in Figure 5.5, when the bed ash has been drained out from the bottom of furnace. Figure 5.6 shows the labourers cleaning sand after regular internals to decrease agglomeration shut down at Jalkheri Power Plant. Figure 5.7 and 5.8 hard agglomerates, which require great force to break them. These types are formed when 30% rice straw and 70% rice husk is used. Figure 5.9 shows the cleaned sand which is ready for reuse. The sand surface still shows inorganic content, which causes shining to sand even after cleaning.

5.2 Thermogravimetric Analysis of Rice Husk and Rice Straw

Thermogravimetric analysis (TGA) is one of the major thermal analysis techniques used to study the thermal behavior of carbonaceous materials. The rate of weight loss of the sample as a function of temperature and time is measured to predict thermal behavior of the material. TGA provides semi quantitative understanding of thermal degradation processes occurring during thermo chemical conversion under various atmospheres.

A number of investigators (Skrifvars et al. [164], Bryers [165], Olanders and Steenari [166], Misra et al. [167], Livingstone [168]) had done DTA/TGA to characterize the melting and volatilization behavior of biomass ashes, or to study sorbents for alkali capture and reactions between bed material and alkali salts (Padban et al. [169]). Ahmaruzzaman and Sharma [170] did the kinetic study on cocracking of petroleum vacuum residue with thermoplastics and biomass. Kinetic study was carried out in a Perkin-Elmer thermogravimetric analyzer (TGA) for the purpose of comparing the process of the mixture with those of the individual components. Experiments were conducted at a heating rate of 40 K/min, in the temperature range of 30-900°C. The overall activation energies obtained were 25 kJ/mole for petroleum vacuum residue, 99 kJ/mole for polypropylene, 21 kJ/mole for coal, and 35 kJ/mole for the mixture of all these materials. Gadgil and Gupta [171] applied (TGA)

technique to pulverized coal to study the heterogeneous combustion kinetics. Later they did the mathematical modeling to verify their experimental results.

TGA is based on measuring heat effects in the sample (endothermic or exothermic processes) and simultaneous measurement of the weight loss. It can be a useful tool for determining initial melting temperatures and to estimate the volatilization of elements.

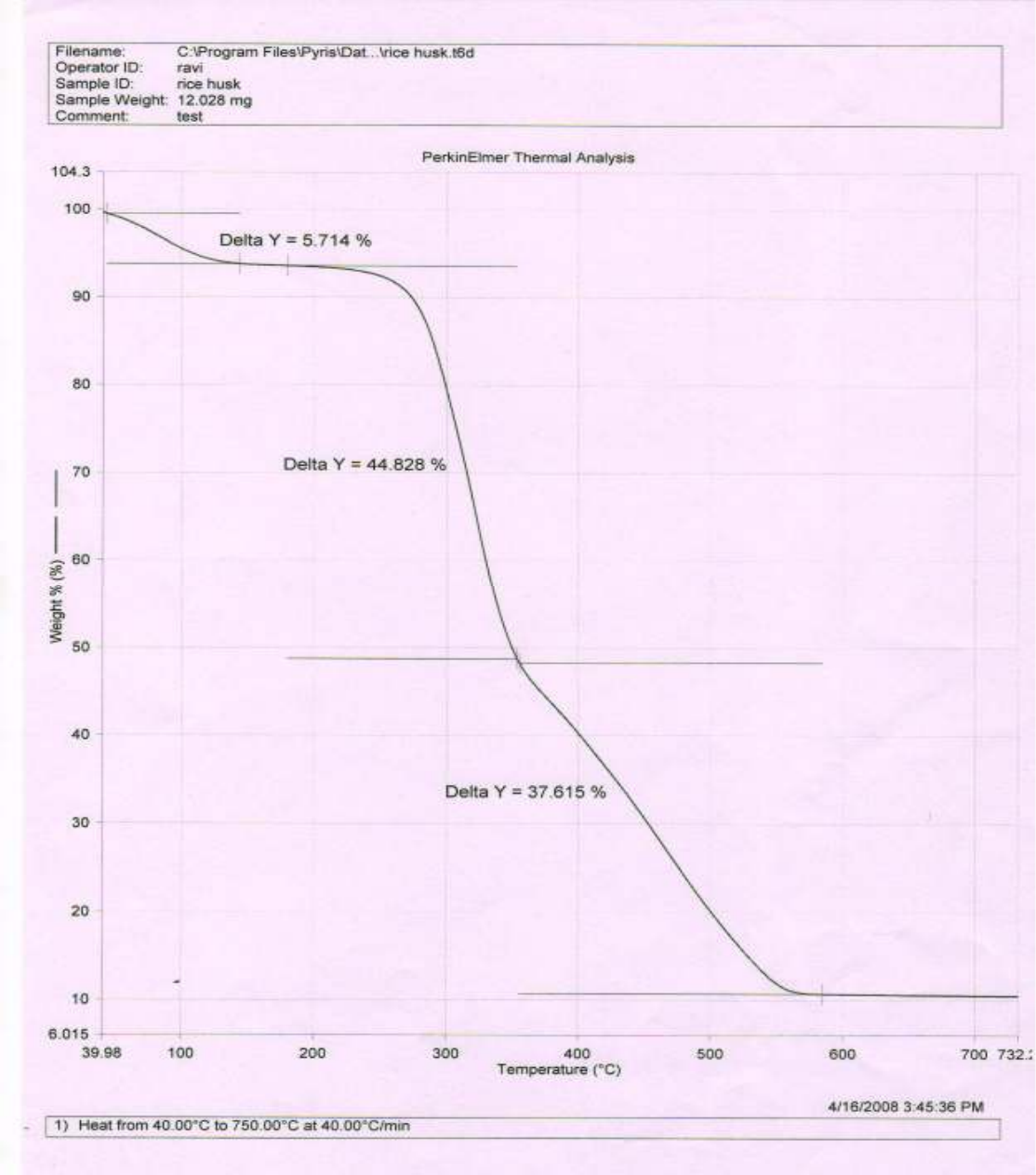

Figure 5.10 Thermogram of rice husk collected from Jalkheri power plant (JPP)

However, interpretation of the results without knowledge of the mineralogical composition of the ash is very difficult due to the many processes that can occur simultaneously in ash and the disturbing effects from absorption of gases and oxidation during storage, combustion of residual carbon, artifacts from low temperature ash etc. Thermogravimetric analysis of rice husk is done to correlate with agglomeration.

Thermogravimetrical analysis of rice husk and rice straw has been done at Mechanical Engineering Department, Thapar University using Perkin Elmer TGA. First of all 12.028 g of powdered rice husk sample was done thermogravimetrical analysis using 100% nitrogen gas. The results from thermogravimetric analysis are given in Figure 5.10. Increasing the temperature from ambient to about 100^{o}C resulted in weight losses of 3.9- 4.8 due to loss of water present in the samples and external water bounded by surface tension. The initial decomposition of the rice husk samples started at the temperatures of 220^{o}C (approx.), whereas the final temperatures for the first reaction zone were 340^{o}C (approx.). Very rapid decomposition of the rice husks took place slightly above the initial decomposition temperature at 220^{o}C (approx.), due to the rapid evolution of the volatile products. The average degradation rates observed in this zone were 45%. The end of the first reaction zone was accepted as the beginning of the second reaction zone. The total degradation and average degradation rates were lower in the second reaction zone as compared to those of the first reaction zone. The total degradation rate in second reaction zone was 38% (approx.) as shown in Figure 5.10.

Powdered form of rice straw weighing 8.279 g was undergone thermogravimetric analysis using 100% nitrogen gas. The result obtained from thermogravimetric analysis of rice straw is given in Figure 5.11. Increasing the temperature from ambient to about 100^{o}C resulted in weight losses of 4-5% due to loss of water present in the samples and external water bounded by surface tension. The initial decomposition of the rice straw started at the

temperatures of 240^{o}C (approx.), whereas the final temperature for the first reaction zone was 340^{o}C (approx.).

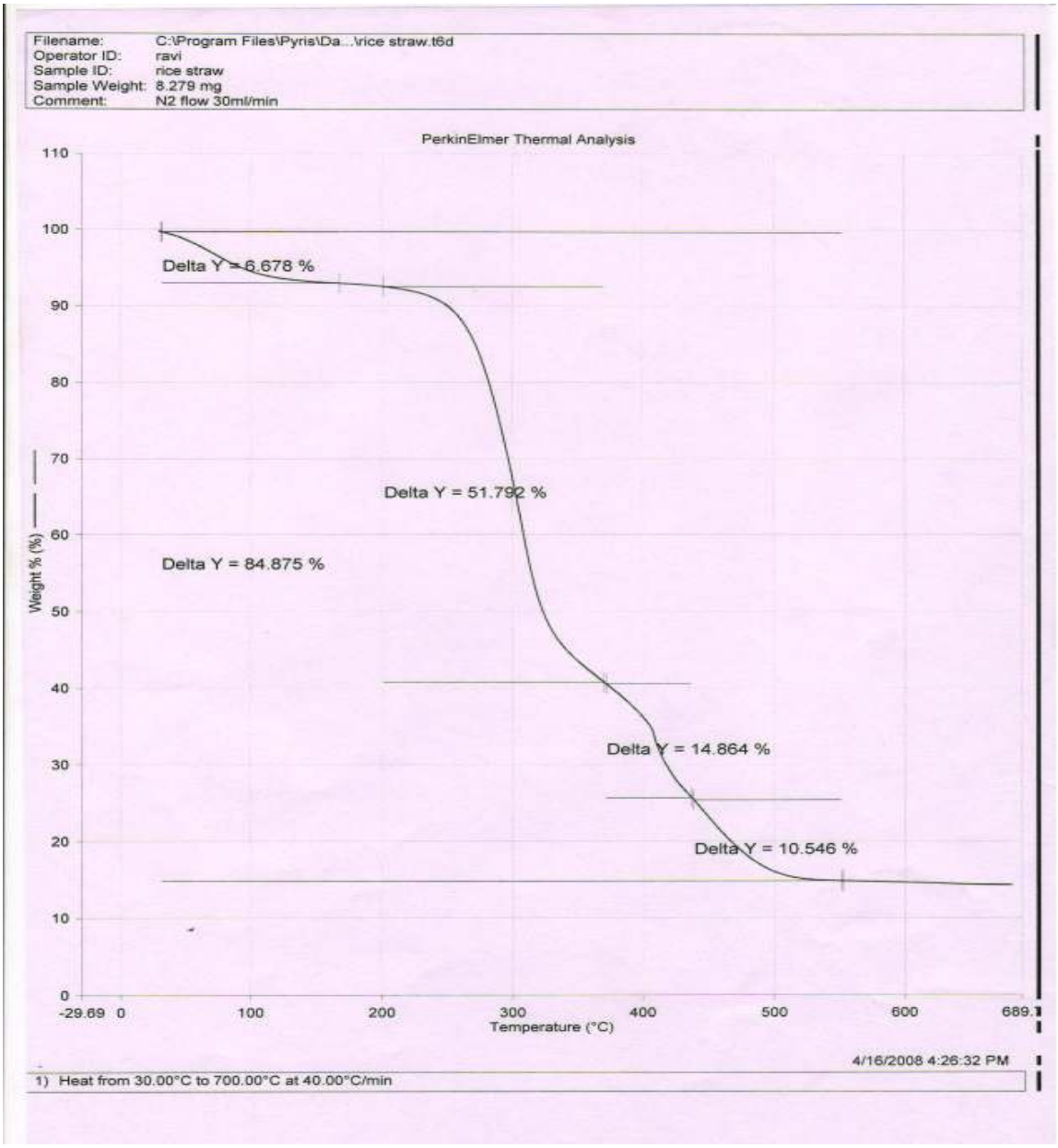

Figure 5.11 Thermogram of rice straw collected from Jalkheri Power Plant (JPP)

Very rapid decomposition of the rice straw took place slightly above the initial decomposition temperature at 240^{o}C (approx.), due to the rapid evolution of the volatile products. The average degradation rates observed in this zone were 45%. The end of the first reaction zone was accepted as the beginning of the second reaction zone. The total

degradation and average degradation rates were lower in the second reaction zone as compared to those of the first reaction zone. The total degradation rate in second reaction zone was 14% (approx.) as shown in Figure 5.11. The total degradation rate in third reaction zone is about 10 %. Approximately 95% of volatile matter is evolved up to 500^{o}C.

From the TGA it can be concluded that only inorganic compounds for which melting temperature lower than 600^{o}C in case of rice husk and 550^{o}C in case of rice straw results in agglomeration process. So the compound of potassium which is having temperature lower than 600-700^{o}C is converted into vapors which subsequently deposited on sand results in agglomeration of sand. Not much change in weight loss is recorded after 600^{o}C in case of rice husk and 550^{o}C in case on rice straw.

5.3 Analysis of Samples at Jalkheri Power Plant w.r.t Rice Husk

The plant was monitored for one month and samples were collected. These samples were subjected to sieve analysis tests, quantitative analysis and scanning electron microscopic tests at different scientific laboratories. Generally, sand of a specified grain size is used as bed material at plant. It is a common knowledge that some biomass ash components cause the bed particle size to increase. This was found at fluidized bed boiler of Jalkheri power plant.

Table 5.1 illustrates the size composition of the initial sand, bed sand removed from the boiler after one-week and 1 month operation, when rice husk is alone used at Jalkheri plant. The average size of the sand over the bed surface was about 0.8 mm (0.08 cm). After the one-week operation, the bed sand size was about as that of the initial sand. However, large sand fractions (over 2 mm (0.2 cm) 1.22% of total weight) appeared. The ash discharged after 1 month operation mostly consists of agglomerated particles of the average size of 1.1 mm (0.11 cm). In this case, the share of large fractions above 2 mm (0.2 cm) in size had become at 25.66%. Thus, during long operation, agglomeration increased as the time

span is increased. The bed drain flow rate was observed 350 kg/hr (97.2 g/s) to 400 kg/hr (111.1 g/s) in this period of operation.

The semi-quantitative elementary analysis of the bed ash taken from bottom of furnace at Jalkheri power plant when rice husk is used alone was done and the results obtained are given in Table 5.2. Table 5.3 shows the quantitative elementary analysis of agglomerate that was broken with hard force. The scanning electron microscopic test has been done on the agglomerates samples collected from power plant at Jalkheri. SEM test has

Table 5.1 Particle size distribution of sand at Jalkheri Power Plant w.r.t rice husk

Screen size(μm)	Initial sand (Over-size %)	Bed ash (one-week operation) (Over-size %)	Bed ash (1month operation) (Over-size %)
2000	0.02	1.22	25.66
1800	9.00	10.22	30.00
1600	42.23	60.71	56.17
1000	64.44	70.95	90.53
800	99.64	98.12	98.92
630	99.88	99.31	99.12
400	99.99	99.69	99.22

Table 5.2 Quantitative element analysis of bed ash at Jalkheri power plant w.r.t rice husk

	SiO_2	Al_2O_3	Fe_2O_3	CaO	MgO	SO_3	Na_2O	K_2O	Mn_2O_3	P_2O_5	TiO_2	Total
Original sand	X ↔	100 - X ↔										100
Bed Ash (One Week Operation)	92.00	2.2	2.75	0.45	0.19	0.06	0.26	2.0	0.20	0.40	0.12	100.57
Bed Ash (One Month Operation)	86.00	3.5	3.5	0.80	0.80	0.08	1.00	3.4	0.80	0.60	0.14	100.62

Table 5.3 Agglomerate sample analysis at Jalkheri power plant w.r.t rice husk

	SiO_2	Al_2O_3	Fe_2O_3	CaO	MgO	SO_3	Na_2O	K_2O	Mn_2O_3	P_2O_5	TiO_2	Total
Bed Ash (One Month Operation)	87.00	3.5	1.5	0.60	0.50	0.07	0.80	5.4	0.70	0.50	0.12	100.69

Figure 5.12 SEM of agglomerate sample

Figure 5.13 SEM of two coalesced sand particles

Figure 5.14 Sand particles showing rice husk ash-derived coating

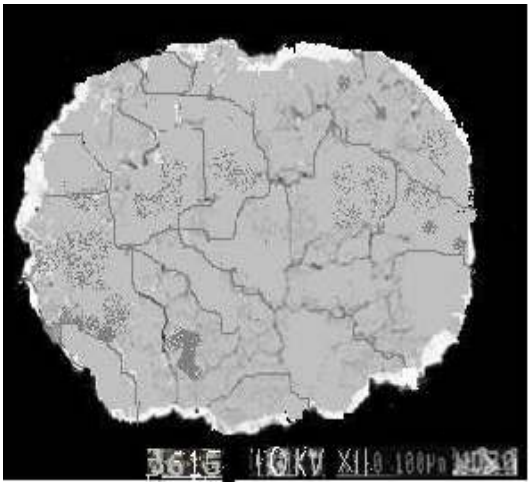

Figure 5.15 Sand particle showing internal cracks after long use

Figure 5.16 Particles with ash derived coating

been done at regional sophisticated instrumentation center (RSIC), Panjab University Chandigarh on JSM 6100 (JEOL) microscope. Figure 5.4 and Figure 5.5 show the actual agglomerates at bottom of furnace. SEM of the agglomerate sample collected from Jalkheri power plant can be seen in Figure 5.12. The sand the particles are coalesced together tightly as clearly visualized from Figure 5.12. Cluster of particles is crushed and SEM test is done again. The coalescing of two particles together is seen in Figure 5.13. Bonding between different particles may of the size of sand particles if sand is used repeatedly. Figure 5.14 and Figure 5.16 show the closed SEM of single particle with ash derived coating. Coating consists of inorganic elements found in rice husk ash. When sand particle was used repeatedly and continuously for one month it developed with cracks on its surface. Particle with cracks is shown in Figure 5.15.

5.4 Analysis of Sample at CPPDK

Table 5.4 shows the particle size distribution of sand used at cogeneration power plant, Dhandari Kalan, Ludhiana after one week and one month. Table 5.5 shows the quantitative element analysis of bed ash at CPPDK when fuel used is rice husk. During study period any other form of rice waste like rice straw is not used at CPPDK.

Table 5.4 Particle size distribution of sand at CPPDK w.r.t -rice husk

Screen size µm	Initial sand over-size %	Bed sand (one-week operation) over-size %	Bed sand (1 month operation) over-size %
1600	0.02	1.22	25.66
1000	9.00	10.22	80.00
630	72.23	92.20	95.17
400	94.44	90.95	98.03
200	99.64	98.12	98.92
90	99.88	99.51	99.12
63	99.99	99.69	99.22
<50	100.00	100.00	100.00

Table 5.5 Quantitative element analysis of bed ash at CPPDK w.r.t rice husk

	Original sand	Bed Ash (One week operation)	Bed Ash (One month old)
Elements			
SiO_2	X	92.00	80.00
Al_2O_3	100 – X	2.2	1.0
Fe_2O_3		1.75	6.5
CaO		0.45	5.5
MgO		0.19	0.40
SO_3		0.06	0.3
Na_2O		0.26	0.30
K_2O		3.0	5.2
Mn_2O_3		0.20	0.40
P_2O_5		0.40	0.6
TiO_2		0.12	0.12
Total	100	100.63	100.32

5.5 Analysis of Samples at JPP w.r.t Rice Husk-Rice Straw Combination

The particle size distribution of sand used at Jalkheri power plant after one week and one month when rice straw is used in combination with rice husk is given in Table 5.6. The quantitative element analysis of bed ash of Jalkheri power plant when fuel used is 70% rice husk and 30 % rice straw is given in Table 5.7.

Table 5.6 Particle size distribution of sand at Jalkheri power plant w.r.t rice straw-rice husk combination

Screen size (μm)	Initial sand (Over-size %)	Bed ash (one-week operation) Over-size %	Bed ash (1month operation) Over-size %
2000	0.02	6.44	8.66
1800	9.00	30.12	34.34
1600	42.23	70.44	74.36
1000	64.44	80.22	95.53
800	99.64	98.12	98.92
630	99.88	99.31	99.12
400	99.99	99.69	99.22

Table 5.7 Quantitative element analysis of bed ash of Jalkheri power plant w.r.t rice husk(70%)-rice straw(30%) combination

	SiO_2	Al_2O_3	Fe_2O_3	CaO	MgO	SO_3	Na_2O	K_2O	Mn_2O_3	P_2O_5	TiO_2	Total
Original sand	X	100 - X										100
Bed Ash (One Week Operation) (rice husk(70%)-rice straw (30%)	82	4.2	0.14	3.4	0.19	0.06	0.26	9.0	0.20	0.40	0.12	99.97
Fuel is was mixed with cotton waste in between, No suitable data found												

5.6 Analysis of Bed Temperature at Jalkheri Power Plant

Jalkheri power plant was monitored for one month when rice husk and rice straw combinations is was used. It was monitored in another month when rice husk alone is used. During last three years rice straw is never used alone. Rice straw is available for fluidized bed combustion immediately after harvesting season, or during harvesting season of rice crop.

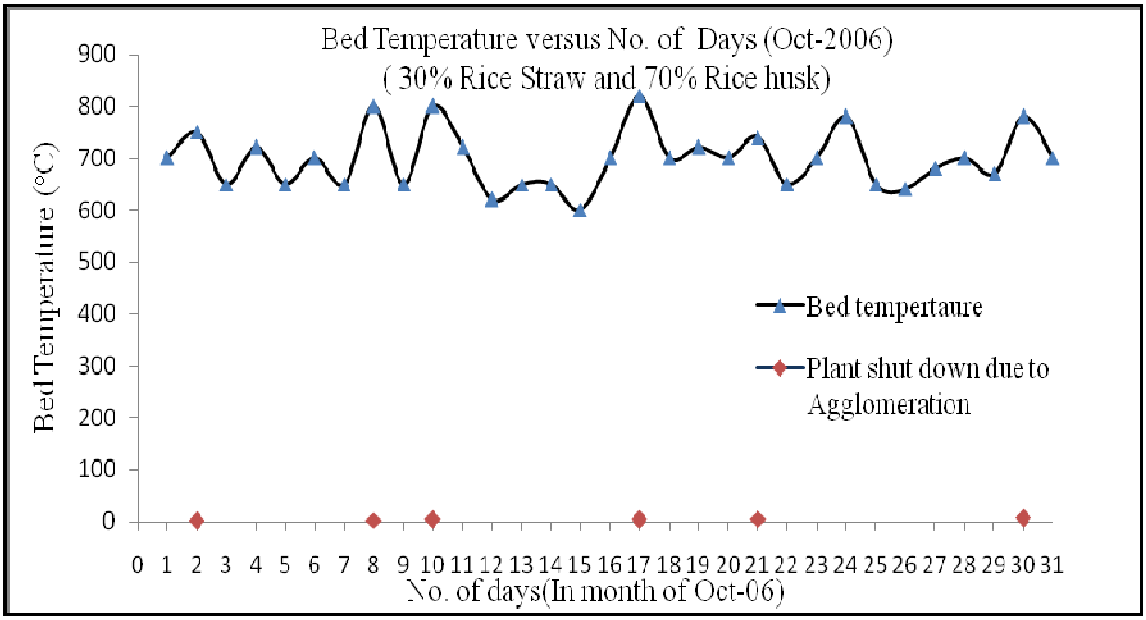

Figure 5.17 Bed Temperature versus No. of days at JPP (When rice husk/rice straw is used)

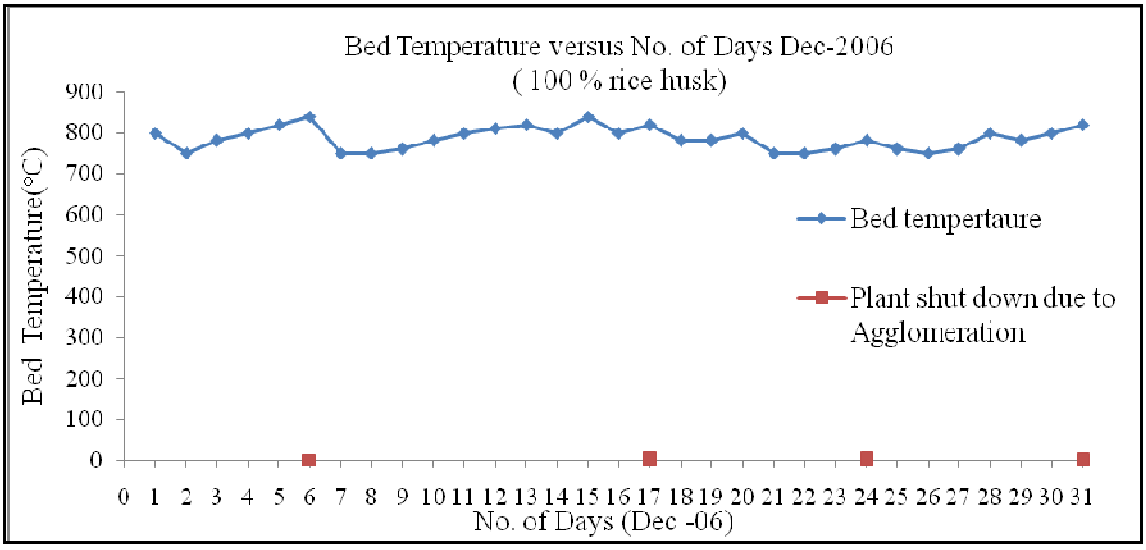

Figure 5.18 Bed Temperature versus No. of days at JPP (When rice husk is used alone)

The availability of rice husk is dependent on rice mill owners, so it can be available at any time from September to April. Figure 5.17 is the graph between bed temperature and number of days in the month of October 2006 when combination fuel is used. It also shows the data of defludization of fluidized bed due to agglomeration. Figure 5.18 is the graph between bed temperature and number of days in the month of Dec, 2006 when rice husk is used alone.

5.7 Prevention of Agglomeration

Following measures may be used to prevent or delay agglomeration related problems for plant.

5.7.1 Using Additives

The following additives may be used to reduce or delay bed-agglomeration and defluidization in combustion and gasification are

(a) Periclase (MgO), (b) Calcite (CaO), (c) Dolomite ($CaCO_3.MgCO_3$),

(d) Limestone ($CaCO_3$) (e) Clay minerals (Aluminosilicates), like Kaolin.

It was [172] reported that limestone addition in fluidized combustion of biomass blends gives rise to deposits consisting largely of calcium sulphates. The deposit initiating step is unclear and may be related to fuel in organics. It was [173] noticed that addition of

fine-grained limestone to a fluidized bed of silica sand at 850^{o}C caused defluidization after only 10 minutes.

5.7.2 Growing and Harvesting

The elements considered to be (partly) responsible for agglomeration are: K, Na, Cl, P and Si. Chlorine is not essential for growth. The chlorine content of biomass therefore is mainly the result of soil condition (location near the sea) and fertilizers used. Most fertilizers contain chlorine because these (KCl) generally are cheaper than sulphates. Alkali's (mainly K) is essential for growth and therefore is concentrated in fast growing parts. This explains the high concentration in annual crops but also the relative high amounts in young braches, leaves and needles from trees. One way to reduce the share of naive biomass is to postpone the harvest or leave those materials in the wood as natural fertilizers.

5.7.3 Fuel Pre-Treatment

In practice stones, pieces of iron and other tramp materials will find their way into the feedstock. Such heavy components may accumulate in the bottom of the reactor/bed and obstruct the normal flow conditions, which can limit the local mass and heat transport and lead to severe agglomeration. A too large fraction of coarse fuel particles will negatively impact the quality of fluidization. Especially under slow reaction conditions coarse char particles may accumulate to a concentration that negatively influences and eventually destabilize the fluidization. Such destabilization easily leads to hot spots that promote local sintering due to the obstructed heat transport and within a short time a large part of the whole bed may be involved in this irreversible process. Paradoxically, this risk is especially present in fluidized bed systems operated at low temperature, where the reactivity is low. Mechanical breaking and crushing may be a solution. Soil (mainly silica) attached to the fuel may be separated from the fuel by washing, sieving. The attached sand can be removed from the soil more easily if the fuel is dry, which be relevant when sieving is the pretreatment. However

the mentioned precaution is probably not worthwhile if not limiting or completely avoiding the addition of silica along with a potential addition of supplementing bed material. This means that the benefit from removing silica contamination is also doubtful when the inherent fuel ash contains a high concentration of silica. Alkalis and chlorine can be washed out using hot water as a fuel pre-treatment.

5.7.4 Bed Material

From the literature it is clear that silica sand is not a suitable bed material in FBC due to formation of low melting eutectics on the surfaces of bed particles by the reaction of silica with alkalis. Alumina does not react with the ash and is reported as the most suitable bed material in combustion of high alkalis biomass.

5.7.5 Periodical Refreshment of Bed Material

Regular sampling and analysis of the bed material during operation and refreshing the bed inventory before the critical alkali concentration or critical agglomeration level is reached may be necessary measure when firing of high alkali fuel alone.

5.7.6 Fluidization Conditions

Atakul and Ekinci [174] explained that the effect of fluidization conditions, particle size, bed material and lignite type on agglomeration and defluidization in FBC. They found that the agglomeration temperature could be lowered by:

(1) Larger fuel particles: Agglomeration temperature increased by 60-70^{o}C when the fuel particle size was increased from 1.4 to 4.5 mm.

(2) Smaller bed particles: Agglomeration temperature increased by 50-70^{o}C when the fuel particle size was increased from 0.85 to 1.4 mm.

(3) Higher fluidization velocity.

(4) The use of limestone and dolomite instead of quartz as bed material. This was ascribed to the lower density and thus lower minimum fluidization velocity.

The static bed height did not have an effect; due to the concurring effects of poorer fluidization and higher bed material to ash ratio. High fluidization velocities always lower the tendency for agglomeration and deposition problems because of the already mentioned competition between particle adhesion and friction forces. In some occasions it is seen that agglomerates already formed can be disintegrated by temporarily increasing the gas velocity. Increasing the gas velocity may also work in a negative direction. This is when the agglomerates are stronger and settlement on the base of the bed is already pronounced. Strong and slowly settling agglomerates are more typically formed in the lower temperature range. Increasing the gas velocity in the primary zone may then give a worse situation by reducing the buoyancy forces acting on the agglomerates from the bed even if the plant has to be stopped. It should be that a sudden increase of airflow could also result in an increase of temperature, which might worsen the situation.

As observed from Table 5.1 (Particle size distribution) the size of sand particles increases with the advent of time. Minimum fluidization velocity increases with increase in size of particles. It is clear from literature that at higher fluidization velocity tendency to defludize increases at same fluidization velocity. The tendency of agglomeration process increases with advent of time, if fresh bed particles are not replaced with fresh sand particles.

5.7.7 Blending

Blending or co-firing of biomass with coal is also a good remedy for agglomeration and fluidization problem. The mechanism primarily considered responsible for the positive influence of co-firing with coal is that a major part of alkaline from straw are bound into high melting aluminum silicates found in the coal. Furthermore a lower content of alkaline and chlorine in coal gives a diluting effect that may also be obtained by co-firing other less problematic types of biomass such as wood. Combination of fuels having high alkali and high

chlorine concentrations should be avoided. Also the combination of fuels rich in potassium chloride (e. g. straw) and sulphur (some coals) should be avoided.

5.7.8 Temperature Control

Agglomeration in most cases as studied by Vander Drift and Oslen [175] is caused by melted ash or ash derived components condensed at particle surfaces and acting as to glue particles together. It is therefore obvious to try to avoid agglomeration by keeping a sufficiently low temperature. Local temperature peaks should be avoided by

- Improving the distribution of fuel and oxygen.
- Moderating the temperature near gas nozzles e.g. by adding steam to gasifiers or by re circulating flue gas to combustor
- Better mixing e.g. by providing a more aggressive state of fluidization in critical areas.
- Inducing in bed "golf streaming" through critical in-bed areas.
- Allowing a higher particle flux through critical in-bed areas
- Addition of properly distributed heat absorption surfaces, e.g. providing "wing panel" walls in the free board of a bubbling fluidized bed.

Simply lowering the process temperature generally results in unacceptable carbon losses due to low reaction rates. Also percentage of CO in exit gas composition is increased with decrease in temperature inside furnace. For improved distribution of combustion air improved grid, nozzle design and staged oxidation may be a solution. Due to unacceptability of change in design improved grid and nozzle design ruled out. Staged oxidation i.e one more opening of air slots in combustor is under consideration and probably will be acceptable.

- From the above suggested methods periodical refreshment, mixing sand with alumina and temperature control are presently used at both plants to avoid agglomeration. Other suggested measures are presently under consideration at both plants.

CHAPTER 6

CFD ANALYSIS

In this chapter CFD modeling of fluidized bed boiler based on rice husk has been formulated. The governing equations and momentum equations which constitute the hydrodynamic system is explained. Geometry of bed which is under consideration is explained. Boundary and initial conditions required for simulation studies are explained in this chapter. CFD analysis has been done to strengthen three phases present in fluidized bed which was considered in exit gas model. Bed temperature as found from plant is considered to be constant.

6.1 CFD Analysis of Fluidized Bed Boiler Based on Rice Husk

CFD analysis of fluidized bed has been done using Eulerain-multiphase model approach. The combustion has not been considered due to limited computational approach. From the plant we got information regarding the size of rice husk and operating velocity used in plant. The average size of rice husk particles fed to combustors is 0.438 cm and operating velocity is 120 cm/s. The CFD analysis has been done at rice husk diameter of 0.438 cm and velocity 120 cm/s. Due to limited computational space fluidized bed considered here is two dimensional, which could be considered as a part of three dimensional bed. Following assumptions has been assumed.

1. The CFD model used in this work is based on the extended two-fluid model (TFM), which employs granular kinetic theory for the particulate phase.

2. Particles are considered smooth, spherical, inelastic and undergoing binary collisions. The fundamental equations of mass, momentum, and energy conservation are solved for each phase.

3. Density of rice husk in fluidized bed combustor combined with sand is assumed to be 1.2 g/cm^3.

4. Size of rice husk and sand considered here is of 0.438 cm.

6. Due to limited computational space the bed is assumed to be two dimensional.

7. The dimensions of the bed are assumed to be 100×28 cm^2.

8. Appropriate constitutive equations are specified in order to describe the physical and rheological properties of each phase and to close the conservation equations.

9. The granular temperature is estimated by solving a fluctuating kinetic energy equation for the particles. The solid viscosity and the pressure can then be computed as a function of the granular temperature at any time and position.

10. Three phase mathematical modeling is assumed to be present.

11. Bed is assumed to be in isothermal conditions.

In the following subsection, the governing and conservative equations and the inter-phase momentum exchange model are described.

6.1.1 Governing Equations

$$\frac{\partial}{\partial t}\left(\varepsilon_g \rho_g\right) + \nabla.\left(\varepsilon_g \rho_g \vec{v_g}\right) = 0 \qquad 6.1.1$$

$$\frac{\partial}{\partial t}\left(\varepsilon_s \rho_s\right) + \nabla.\left(\varepsilon_s \rho_s \vec{v_s}\right) = 0 \qquad 6.1.2$$

$$\varepsilon_g + \varepsilon_s = 1 \qquad 6.1.3$$

6.1.2 Momentum Equations

$$\frac{\partial}{\partial t}\left(\varepsilon_g \rho_g \vec{v_g}\right) + \nabla.\left(\varepsilon_g \rho_g \vec{v_g}\vec{v_g}\right) = -\varepsilon_g \nabla P_g + \nabla T_g + \varepsilon_g \rho_g g + \beta(\vec{v_s} - \vec{v_g}) \qquad 6.1.4$$

$$\frac{\partial}{\partial t}\left(\varepsilon_s \rho_s \vec{v_s}\right) + \nabla.\left(\varepsilon_s \rho_s \vec{v_s}\vec{v_s}\right) = -\varepsilon_s \nabla P_s + \nabla T_s + \varepsilon_s \rho_s g - \beta(\vec{v_s} - \vec{v_g}) \qquad 6.1.5$$

6.1.3 Fluctuating Energy Equation for Solid

Equivalent to the thermodynamic temperature for gases, the granular temperature can be introduced as a measure for the fluctuating kinetic energy of the particles. The granular temperature is defined as

$$\Theta = \frac{1}{3}\overrightarrow{v'_s}^2 \qquad 6.1.6$$

Where $\overrightarrow{v'_s}$ is the solids fluctuating velocity. The equation of conservation of the solids fluctuating energy is given as

$$\frac{3}{2}\left[\frac{\partial}{\partial t}\left(\varepsilon_s \rho_s \Theta\right) + \nabla.\left(\varepsilon_s \rho_s \overrightarrow{v_s}.\Theta\right)\right] = T_s : \nabla\overrightarrow{v_s} + \nabla.\kappa\nabla\Theta - \gamma \qquad 6.1.7$$

Where

$T_s : \nabla\overrightarrow{v_s}$: is the generation of the fluctuating energy due work done by shear stress in the particle phase

$\nabla.\kappa\nabla\Theta$: is the conduction of the fluctuating energy

γ : is the rate of dissipation of the fluctuating energy due to inelastic collision.

6.1.4 Constitutive Equations

The solid phase and the gas phase were considered incompressible. The gas phase was modeled as an incompressible Newtonian fluid. The laminar model is used for the gas phase as high solid concentration in the dense fluidized bed may damp out gas phase fluctuations. The gas phase tensor can thus be represented as

$$T_g = 2\varepsilon_g \mu_g \tau_g \qquad 6.1.8$$

$$\tau_g = \frac{1}{2}\left[\nabla\overrightarrow{v_g} + (\nabla\overrightarrow{v_g})^T\right] - \frac{1}{3}(\nabla\overrightarrow{v_g})I \qquad 6.1.9$$

The solid stress tensor, T_s can be expressed in terms of the solid pressure, P_s, bulk viscosity ξ_s, and shear viscosities, μ_s , a

$$T_s = (-P_s + \xi_s \nabla . \vec{v_s})I + 2\mu_s \tau_s \quad 6.1.10$$

$$\tau_s = \frac{1}{2}\left[\nabla . \vec{v_s} + \left(\nabla . \vec{v_s}\right)^T\right] - \frac{1}{3}(\nabla . \vec{v_s})I \quad 6.1.11$$

These solid properties can be determined as a function of granular temperature according to the following relations:

$$P_s = \varepsilon_s \rho_s \Theta\left[1 + 2(1+e) g_o \varepsilon_s\right] \quad 6.1.12$$

$$\xi_s = \frac{4}{3}\varepsilon_s{}^2 \rho_s d_s (1+e) g_o \left(\frac{\Theta}{\pi}\right)^{1/2} \quad 6.1.13$$

$$\mu_s = \frac{\mu_s, dil}{(1+e)g_o}\left[1 + \frac{4}{5}(1+e) g_o \varepsilon_s\right]^2 + \frac{4}{5}\varepsilon_s{}^2 \rho_s d_s (1+e) g_o \left(\frac{\Theta}{\pi}\right)^{1/2} \quad 6.1.14$$

$$\mu_s, dil = \frac{5\sqrt{\pi}}{96}\rho_s d_s \Theta^{1/2} \quad 6.1.15$$

where $\mu_{s,\,dil}$ is the dilute viscosity and g_o is the radial distribution function expressing the statistics of the spatial arrangement of particles. In this study the following expressing were used:

$$g_o = \left[1 - \left(\frac{\varepsilon_s}{\varepsilon_{s,\max}}\right)^{1/3}\right]^{-1} \quad 6.1.16$$

The granular conductivity, κ and the collisional rate of energy dissipation per unit volume, γ, are adopted as:

$$\kappa = \frac{2\kappa_{dil}}{(1+e)g_o}\left[1 + \frac{6}{5}(1+e) g_o \varepsilon_s\right]^2 + 2\varepsilon_s{}^2 \rho_s d_s \left(\frac{\Theta}{\pi}\right)^{1/2} \quad 6.1.17$$

$$\kappa_{dil} = \frac{75\sqrt{\pi}}{384}\rho_s d_s \Theta^{1/2} \qquad 6.1.18$$

$$\gamma = 3(1-e^2)\varepsilon_s \rho_s g_o \Theta \left[\frac{4}{d_s}\left(\frac{\Theta}{\pi}\right)^{1/2} - \nabla.\vec{v_s} \right] \qquad 6.1.19$$

6.1.5 Frictional Stress

At high solid volume fraction, such as that encountered in dense fluidized beds sustained contacts between particles occur. The resulting frictional stress must be taken into consideration for the description of the solid-phase stress. Zhang and Rauenzahn [176] concluded that at very high solid volume fraction particle collisions are no longer instantaneous, as is assumed in kinetic theory. Several approaches have been presented in the literature to model the frictional stress. The models are however very empirical. The frictional stress is written in a Newtonian form:

$$\sigma = P_f I + \mu_f \left[\nabla\vec{v} + (\nabla\vec{v})^T \right] \qquad 6.1.20$$

The frictional stress is added to the stress predicted by kinetic theory for $\varepsilon_s > \varepsilon_{s,\min}$:

$$P_s^* = P_s + P_f \qquad 6.1.21$$

$$\mu^*_s = \mu_s + \mu_f \qquad 6.1.22$$

In the present work, the frictional viscosity model proposed by Schaeffer [177] is used to describe the frictional stress:

$$P_f = A(\varepsilon_s - \varepsilon_{s,\min})^n \qquad 6.1.23$$

$$\mu_f = \frac{P_f.\sin\varphi}{\varepsilon_s\sqrt{\frac{1}{6}\left(\frac{\partial u_s}{\partial x} - \frac{\partial v_s}{\partial y}\right)^2 + \left(\frac{\partial v_s}{\partial y}\right)^2 + \left(\frac{\partial u_s}{\partial x}\right)^2} + \frac{1}{4}\left(\frac{\partial u_s}{\partial y} + \frac{\partial v_s}{\partial x}\right)^2} \qquad 6.1.24$$

Where φ is internal angle of friction. Values of A=10^{25}, n=10, $\varepsilon_{s,\min}$=0.59, and φ=25^{o} are typically employed.

Instead of solving the complete balance of the solids fluctuating energy, equation, 6.1.7 an algebraic expression was proposed was by Syamlal et al. [178]. This approach assumes that the granular energy is dissipated locally, neglecting the convection and diffusion, and retaining only the generation and the dissipation terms in the equation 6.1.7 resulting in:

$$(-P_s^* I + \tau_s) : \nabla \vec{v}_s - \gamma = 0 \qquad 6.1.25$$

This approach is valid only under the assumption that volume fraction of the solids phase stays high and the velocity of the solids phase stays relatively low. In this regime most granular energy is dissipated locally.

6.1.6 Inter-Phase Momentum Exchange

We need to specify the gas-solid drag coefficient for different solid concentrations. In this work the drag model suggested by gidaspow [179] was used

For $\varepsilon \geq 0.8$

$$\beta = \frac{3}{4} C_d \frac{\varepsilon_s \rho_s \left| \vec{v}_g - \vec{v}_s \right|}{d_s} \varepsilon_g^{-2.65} \qquad 6.1.26$$

Where the drag coefficient C_d is given by

$$C_d = \frac{24}{\mathrm{Re}_s}(1 + 0.15\,\mathrm{Re}_s^{0.687}) \text{ for } \mathrm{Re}_s \leq 1000 \qquad 6.1.27$$

$$C_d = 0.44; \text{ for } \mathrm{Re}_s \geq 1000 \qquad 6.1.28$$

$$\mathrm{Re}_s = \frac{\varepsilon_g \rho_g d_s \left| \vec{v}_g - \vec{v}_s \right|}{\mu_g} \qquad 6.1.29$$

For ε<0.8

$$\beta = 150\frac{\varepsilon_s^2 \mu_g}{\varepsilon_g^2 d_s^2} + 1.75\frac{\rho_g \varepsilon_s \left|\vec{v_g} - \vec{v_s}\right|}{d_s \varepsilon_g} \qquad 6.1.30$$

6.2 Computational Approach

The governing conservation equation to be solved, equation 6.1.1-6.1.2 were given in the previous sub-section. Their solution for the unknown scalars ε_g, ε_s, u_g, v_g, u_s and v_s by CFD essentially gives the full flow details in the flow domain. The basic CFD methodology consists of declining a suitable grid, discretizing the above differential equations on the grid to yield a set of algebraic equations whose solution gives the flow field variables and then post-processing to make the large amount of solution data intelligible. This methodology is described in somewhat more detail in the following. The actual implementation, however, was done using the well known commercial code Fluent 6.2 and not by writing fresh one.

6.2.1 Grid Generation

To start with, a grid is generated for the flow domain. The grid divides the domain into a finite number of sub-domains (i.e. control volumes) and specifies the discrete locations (nodes) at which the flow variables are to be calculated. A grid can be:

Structured(regular) Grid*:* Regular or Structured grids consists of families of grid lines with the property that members of a single family do not cross each other and cross each member of other families only once. This is simple grid and is logically equivalent to a Cartesian grid.

Unstructured Grid: This is a more flexible type of grid suitable for complex flow geometries with difficulty boundary shapes. The elements, areas or volumes, may have any shape. In 2-D, triangular or quadrilateral elements are used while in 3-D tetrahedral or hexahedral elements are used. Whatever may be the kind of mesh/grid, it has to follow certain norms, so that the

obtained solution is physically realistic. The quality of the mesh plays a significant role in the accuracy and stability of the numerical computation. The attributes associated with mesh quality are node point distribution, smoothness and skewness. The degree to which the salient features of the flow(such as shear layers, separated regions, shock waves, boundary layers and mixing zones) are resolved depends on density and distribution of the nodes in the mesh.

In many cases, poor resolution in critical regions can dramatically alter the flow characteristics. For example, the prediction of separation due to an adverse pressure gradient depends heavily on the resolution of the boundary layer upstream of the point of separation. In general, no flow passage should be represented by fewer than 5 cells; most cases will require many more cells to adequately resolve the passage. In regions of large gradients, as in shear layers or mixing zones, the grid should be fine enough to minimize the change in the flow variables from cell to cell. Rapid changes in cell volumes between adjacent cells translate into larger truncation error, which is the difference between partial derivatives in the governing equations and their discrete approximations. The shape of the cell (including its skewness and aspect ratio) also has a significant impact on the accuracy of the numerical solution. Skewness can be defined as the difference between the cell's shape and the shape of an equilateral cell of equivalent volume. Highly skewed cells can decrease accuracy and destabilize the solution. For example, optimal quadrilateral meshes will have vertex angles close to 90 degress, while triangular meshes should preferably have angles of close to 60 degrees and have all angles less than 9- degrees.

Aspect ratio is a measure of the stretching of the cell. For highly anisotropic flows, extreme aspect ratio may yield inaccurate results with fewer cells. However, a general rule of thumb is to avoid aspect ratio in excess 5:1 in the most sensitive part of the flow region. The

effect of resolution, smoothness and cell shape on the accuracy and stability of the solution process is strongly dependent on flow field being simulated. For example, much skewed cells can be tolerated in benign flow regions, but can be vary damaging in regions with strong flow gradients. Since the locations of strong flow gradients generally cannot be determined a prior, one should strive to achieve a high-quality mesh over the entire flow domain. The entire modeling of the geometry is done in GAMBIT using various combinations of vertices, edge and face. The geometry is then meshed either by dividing each edge or face into given number of mesh points or specifying the interval between the mesh points. Both uniform and non-uniform meshing can be done as per the requirement. The boundary zones are specified for e.g VELOCITY_INLET, WALLS and PREESURE_OUTLET. The grid is then checked so that the aspect ratio criterion is satisfied after which the entire geometry is exported to the solver, which is the FLUENT itself.

6.2.2 Discretization of Conservation Equations

Discretization refers to the process of converting partial differential equations into algebraic equations, which can be solved simultaneously to obtain a solution for the flow variables. In this work, the finite volume method of discretization has been used. This method uses the integral form of the conservation equations as its starting point. The solution domain, which is subdivided into a finite number of control volumes during the grid generation, is taken and the conservation equations applied to each volume. At the centroid of each control volume lies the computational node at which the variable values are to be calculated. The finite volume method can accommodate any type of grid and hence suitable for complex geometries. Discretization of the governing equation can be illustrated by considering the steady-state conservation equation

can be illustrated by considering the steady-state conservation equation in integral form for transport of a scalar quantity φ

$$\oint \rho\phi\vec{v}.\overrightarrow{dA} = \oint \Gamma_\phi \nabla\phi.\overrightarrow{dA} + \int_v S_\phi dV \qquad 6.2.1$$

Where A is the surface area vector, Γ_ϕ is the diffusion coefficient for $\phi, \nabla\phi$ is the gradient of ϕ and S_ϕ is the source of ϕ per unit volume. Equation (6.2.1) is applied to each control volume, or cell in the computation domain. Discretization of equation (6.2.1) on a given cell yields

$$\sum_f^{Nfaces} \psi_f \phi_f A_f = \sum_f^{Nfaces} \Gamma_\phi (\nabla\phi)_n A_f + S_\phi V \qquad 6.2.2$$

Where *Nfaces* is the number of faces enclosing cell, ϕ_f value of ϕ convected through face f, ψ_f is the mass flux through the face, A_f is the area of face, $(\nabla\phi)_n$ is the magnitude of $\nabla\phi$ normal to face f and V is the cell volume.

Discrete values of the scalar ϕ are stored at all the nodes. However, the face values ϕ_f are required for the convection terms in equations (6.2.2) and must be interpolated from the node values. This is accomplished using an interpolation scheme. Various interpolation schemes can be used such as;

- The central differencing scheme(CDS)
- The upwind scheme
- The power –law scheme
- The QUICK (Quadratic Interpolation for Convective Kinematics

CDS employs linear interpolation. The upwind scheme is a stepwise approximation and is unconditionally stable and required if convection is much stronger than diffusion. Depending

upon the accuracy required various upwind schemes, such as first order scheme second order scheme can be used. In Fluent, all the above interpolation schemes are available. For the present work, the first-order up winding scheme is used.

6.2.3 Linearised Form of Discrete Equation

Discrete transport equation (6.2.2) contains the unknown scalar variable ϕ at the node as the unknown values in the surrounding neighbor cells. This equation will, in general, be non-linear with respect to these variables. A linearised form of equation (6.2.2) can be written as

$$a_p \phi_P = \sum_{nb} a_{nb} \phi_{nb} + b \qquad 6.2.3$$

Where the subscript 'nb' refers to 'neighbor cells', and a_p and a_{nb} are the linearised coefficients for ϕ and ϕ_{nb}.

Similar equations can be written for each cell in the grid. This results in a set of algebraic equations with a separate coefficient matrix. For scalar equations, this linear system may be solved using a point implicit (Gauss-Seidel) linear equation solver in conjunction with an Algebraic Multigrid (AMG) method.

6.2.4 Pressure Calculations

From the conservation equations it will be noticed that pressure is also a dependent variable, but without an explicit equation for the gas phase pressure. Thus an auxiliary equation for obtaining the gas pressure is extracted from the continuity equation and the pressure field is obtained from the well known SIMPLE algorithm (Patankar [180]). Pressure-velocity coupling is achieved by deriving by deriving an equation for pressure from the discrete continuity equation. The SIMPLE algorithm uses a relationship between velocity and pressure correction to obtain the pressure field

$$a_p p'_p = \sum_{nb} a_{nb} p'_{nb} + b \qquad 6.2.4$$

Where b is the net flow rate into the cell; b goes to zero as the correct solution is approached.

6.2.5 Solution Method in FLUENT

For eulerian multiphase calculations, FLUENT uses the phase coupled SIMPLE (PC-SIMPLE) algorithm for the pressure velocity coupling. PC-SIMPLE is an extension of the SIMPLE algorithm to multiphase flows. The velocities, coupled by phases, are solved in a segregated fashion. The block algebraic multigrid scheme used by the coupled solver is used to solve a vector equation formed by the velocity components of all phases simultaneously. Then, a pressure correction is built based on total volume continuity rather than mass continuity. Pressure and velocities are then corrected so as to satisfy the continuity constraint.

6.2.6 Pressure-Correction Equation

For incompressible multiphase flow, the pressure-correction equation takes place the form

$$\sum_{k=1}^{n} \left\{ \frac{\partial}{\partial t} \varepsilon_k + \nabla . \varepsilon_k \vec{\nu}_k{}' + \nabla . \varepsilon_k \vec{\nu}^*_k \right\} = 0 \qquad 6.2.5$$

Where ν'_k is the velocity correction for the k[th] phase and $\nu^*{}_k$ is the value of ν_k at the current iteration. The velocity corrections are themselves expressed as functions of the pressure corrections.

6.2.7 Volume Fraction Calculation

The volume fractions are obtained from the phase equations. In discretized form, the equation of the k[th] volume fraction is:

$$a_{P,k} \varepsilon_k \sum_{nb} \left(a_{nb,k} \varepsilon_{nb,k} \right) + b_k = 0 \qquad 6.2.6$$

In order to satisfy the condition that all the volume fractions sums to one, In FLUENT, the solution of the model equations set up by specifying the type of solver to be used, segregated or coupled, the domain of the solution-2D or 2-D axi-symmetric and whether transient or steady state. The models used for the calculation is specified next, such as, laminar or turbulent, and single phase or multiphase.

The materials to be used for the calculations are then set if the flow is multiphase by selecting the required model. Next the operating conditions are set. The boundary values are set at the respective boundary zones, under-relaxation parameters are specified and interpolation schemes are selected. The computational domain is then initialized and the convergence criteria are set. Solution is started by specifying the total number of iterations required if the flow is steady state, while if the flow is unsteady state, then the time step size along with the number of iterations per time step is also set.

6.2.8 Post-Processing of Computed Results

FLUENT has an inbuilt post-processor where the results obtained from the solution of the equations can be presented in terms of contour plots, vector plots etc. either for the entire flow domain or for a specified location as required. The results can also be presented in terms of XY-plot, histograms. It is also possible to take the surface integral or the volume integral of a specific variable.

6.3 Simulation Studies

The geometries considered for the simulation are shown in Figure 6.1. The 3D geometry for the fluidized bed combustor was not chosen because of limited computational space. The two dimensional bed was considered as part of 3D bed with all the parameters same as original. Only two dimensional bed with and without bed superheater tubes has been considered. The

dimensions of 2-D bed are 100 × 28 cm^2. The diameter of bed super heater tubes for 2D bed is taken as 1.5 cm. The reason for choosing above dimension for the geometry is that above geometry is found in literature. The continuity, momentum and granular kinetic theory equations along with the constitutive equations mentioned earlier were solved using the commercial finite volume CFD package FLUENT 6.2 from FLUENT Inc., Lebanon, U.S.A. Simulations were carried out in a 2-D cartesian space. The first order upwind scheme was used to discretize the momentum and continuity equations. The first order upwind scheme is selected here because in most of archival work was done in it, so it was selected. The time step used in the simulations is 0.001. This was found to be sufficiently small to give a stable, converged solution. A non-uniform triangular unstructured grid was used for the computational purpose. A portion of the grid is shown in Figure 6.2 and Figure 6.3. The grid spacing was chosen automatically by Fluent software.

The grid density around the bed super heater tubes region was kept higher as the velocity gradient are expected to be higher in this region than compared to other regions of the bed. Also grid density in lower bed is higher as compared to top of bed. The grid density in freeboard is lower as compare to bed. Overall about 8494 computational cells were used in the calculations for fluidized bed with bed superheater tubes. For fluidized bed without bed super heater tubes 1392 computational cells were used. Also above both are dependent upon the simulation case. All the simulations were continued for 2 to 4 seconds of fluidization time.

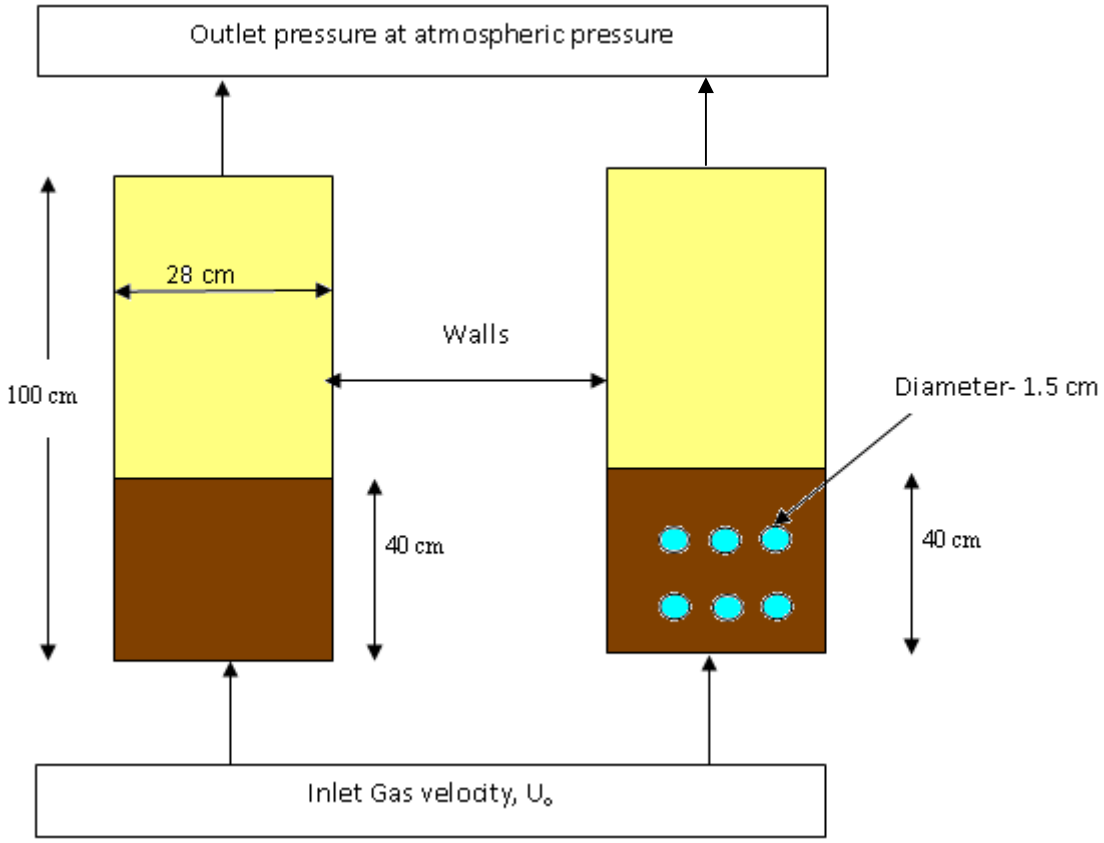

Figure 6.1 Geometries of fluidized bed with and without bed super heater tubes

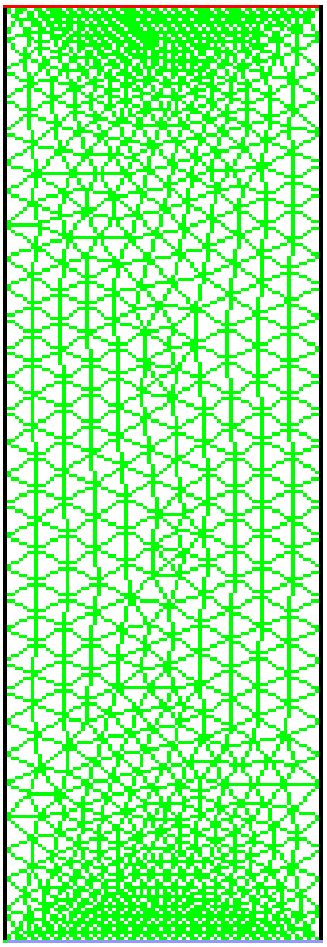

Figure 6.2

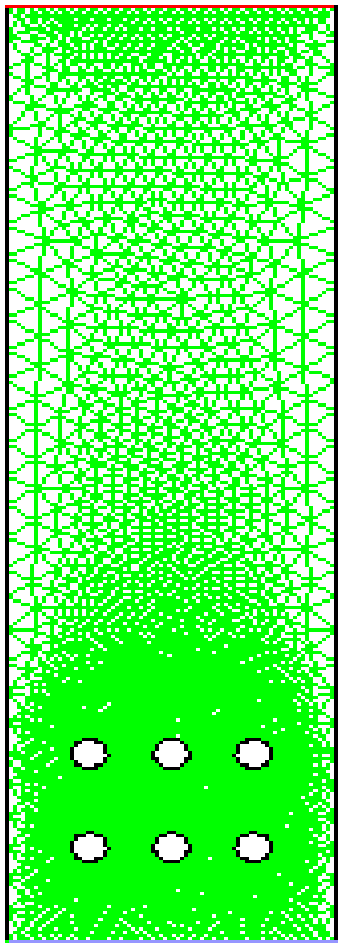

Figure 6.3

Figure 6.2 Computational grid of fluidized bed without bed super heater tubes

Figure 6.3 Computational grid of fluidized bed with bed super heater tubes

6.3.1 Boundary and Initial Conditions

No slip wall boundary condition was used for the gas phase and full slip condition was used for the solid phase. The boundary condition at the top of the fluidized bed is the pressure boundary. The pressure in the mesh cells at the top of the fluidized bed was fixed at atmospheric pressure. It is important that the freeboard of the fluidized bed is high enough, so that fully developed flow can be physically expected. At the bottom of the fluidized bed, the inlet air velocity was specified. The inlet was made impenetrable for the solids phase; the solids downward velocity was set to zero in the bottom cells.

For the initial condition, the bed was assumed to be in a minimum fluidized state with solid volume fraction of 0.59. The height of the bed was taken as 40 cm. The gas flow in the bed was set to minimum fluidization velocity at t=0. In the freeboard a zero solids were considered even though in fluidized bed combustor solid in freeboard cannot be zero.

6.3.2 Description of Typical Simulation

Using the vertices-edge face combination in GAMBIT, a two dimensional geometry was set up having the same dimensions as reported in the experimental set-up of Fariborz et al. [130]. The tubes, modeled as circles, were created as separate faces and placed at specified locations. These circles were then subtracted from main body which then created required body. As the bed does not have any symmetry, an unstructured triangular grid was set up. Figure 6.3 shows a part of the computational grid including the bed superheater tubes. Figure 6.2 shows the without bed superheater tubes. The grid quality was also checked. The superheater tube boundaries as well the left and right edges of the bed were specified as walls, the bottom edge was specified as velocity inlet, while the top edge was specified as the pressure outlet. In the bed without tubes the bottom edge was specified as velocity inlet. Left and right edges of bed were specified as

walls and top edge was specified as pressure outlet. The entire geometry was then exported to FLUENT.

The gas-solid models, the boundary values, the time step, number of iterations, discretization scheme, under relaxation factors and the numerical scheme used to solve the discretized algebraic equations were specified in FLUENT 6.2. The values used for a typical simulation are summarized in Table 6.1. Initialization of the fluidized bed is very important step. In all simulations the bed was assumed to be at the minimum fluidization condition initially. This is specified by patching a solid volume fraction of 0.59 (i.e porosity, ε_{mf} of 0.41). The bed height of 40 cm from the inlet was taken as the minimum fluidization height. The solid velocity was set to zero and the granular temperature was set to 10^{-1} cm^2/s^2. The gas velocity inside the bed was set to U_{mf}/ ε_{mf}. From the top of the bed surface to the exit the gas velocity was set at minimum fluidization velocity. Gas was fed uniformly from the lower side of fluidized bed. Red color indicates the solid phase in the bed, white circles represent the tubes and their arrangement and blue-green patches within the bed indicate the bubbles.

The simulation was carried out for 2-4 seconds of fluidization time in fluidization bed with and without bed super heater tubes. The case and data files were stored at intervals of different time intervals. Data files obtained upto 4 seconds were used for post-processing and analysis. In all about many frames at different fluidization times between 0 to 4 seconds were taken for analysis.

Table 6.1 Various parameters required for CFD modeling of fluidized bed

Geometry	Two Dimensional
Height of Fluidized Bed	100 cm
Width of Riser	28 cm
Flow Type	Laminar
Gas-Solid model	Eulerian-Eulerian , with Kinetic Theory
Garnular Viscosity model	Constant
Drag Model	Syamlal-obrien [178]
Frictional Viscosity model	Schaeffer [177]
Wall boundary condition for the solid phase	Full slip
Wall boundary condition for gas phase	No slip
Time	2-4 s
Discretization scheme	First order upwind
Maximum number of iterations per time step	80
Convergence criteria	0.001
Pressure velocity coupling	Phase coupled SIMPLE
Geometry	Two Dimensional
Maximum solid packing	0.63
Main Inlet gas velocity	120 cm/s
Initial Condition	Bed at minimum fluidization
Bed porosity at minimum fluidization	0.41
Bed Height at minimum fluidization	40 cm
Outlet condition	Atmospheric pressure
Particle-Particle restitution coefficient	0.9
Particle-wall restitution coefficient	0.95
Particle Density(rice husk combined with sand)	1.2 g/cm^3
Rice husk diameter	0.438 cm
Gas Density	0.00121 g/cm^3
Gas Viscosity	1.81×10^{-4} g/cm.s
Diameter of bed super heater tubes	1.5 cm

CHAPTER 7

RESULTS AND DISCUSSIONS

The input data required for the exit gas model was taken from a 10 MW FBC plant at Jalkheri (Jalkheri Power Pvt. Limited, Fatehgarh Sahib, Punjab, India). The plant uses the rice husk as feed stock (at the time of study). The input to model is rice husk and it is not suitable for rice straw as rice straw is fed to combustor in the form of bales. The average diameter of rice husk particles at JPP is found to be 0.438 cm. The proximate and ultimate analyses of rice husk have been done and results are given in Table 7.1. The results of above analysis, along with the other physico-chemical parameters taken from plant have been the input parameters to the model explained in Chapter 3. The physico-chemical parameters are noted from 10 MW plant and are given in the chapter 3 in Table 3.1. The input values to the model and output results are given in appendix. The model has been used to predict the consumption of oxygen in the combustor, which makes it possible to predict the outlet gas composition and variation of average oxygen concentration along with the height of the bed.

As mentioned earlier the fraction of cloud wake has been used as an adjustable parameter for a value of f_{cw}= 0.3. The predicted exit gas composition along with plant data are given in Table 7.2. From the Table 7.2 it is clear that the model predictions are in agreement with plant data. Thereby model is validated. Table 7.3 shows the actual measured data from plant at different values of fraction of excess air. The value of char particle surface temperature assumed in the model is 1323 K. Figure 7.1 shows the percentage of carbon dioxide and oxygen in flue gas with fraction of excess air. Figure 7.2 and Figure 7.3 show the variation of fractional conversion of oxygen and bubble diameter with fraction of excess air. As shown in Figure 7.1, the CO_2 percentage in flue gas decreases as the fraction of excess air increases. This is due to the

fact that the amount of combustibles available in the bed remains same. But at the same time, the percentage of oxygen in the exit gas increases, leading to excessive loss of sensible heat in the

Table 7.1 Proximate and ultimate analysis of rice husk sample

Proximate analysis (Rice husk)		Ultimate analysis (Rice husk)	
Volatile	58.03	C	38.9
Fixed Carbon	16.65	H	5.1
Ash	17.82	S	0.12
Moisture	7.5	O	37.9
		N	2.17

Table 7.2 Comparison of model predictions with real plant data at f_{cw}= 0.3

Components percentage by volume in exit gas	(Real) (%)	Simulated (%)
O_2	6-9	7.12
CO_2	10-14	13.87
N_2	76-79	79.41

flue gas. However, if the fractional conversion of the oxygen is considered, it decreases as the fraction of excess air increases as shown in Figure 7.2. Figure 7.3 also shows the gradual increase of the bubble diameter with fraction of excess air. This is due to the fact that the

superficial gas velocity increases as the fraction of excess air increases, leading to the gradual increase of bubble diameter.

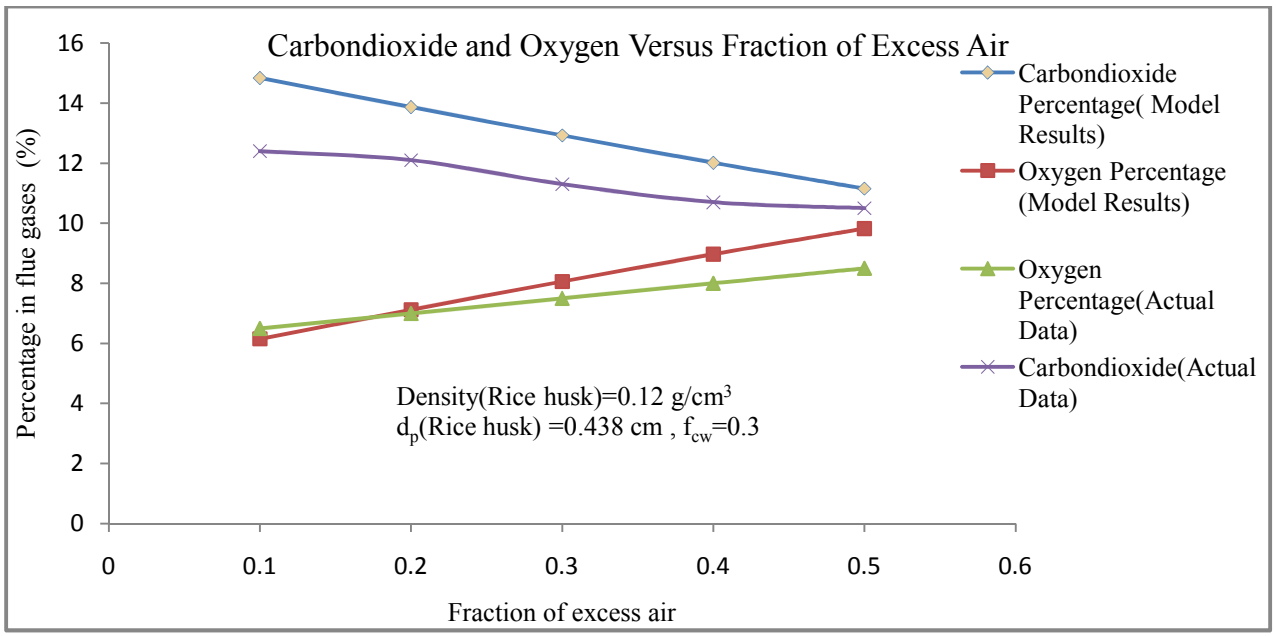

Figure 7.1 Variation of gases in flue gases versus fraction of excess air

The increase in the bubble diameter causes a decrease in the gas interchange coefficients, consequently the oxygen conversion decreases. Figure 7.4 shows the variation of expanded bed height with the fraction of excess air. The expanded bed height increases with increase in fraction of excess air. It is due to increase in diameter of bubble diameter which causes the increase in expanded bed height. Figure 7.5 shows the variation of superficial velocity versus fraction of excess air. It is because that superficial velocity is dependent on actual molar feed rate of air. Actual molar feed rate is dependent directly on fraction of excess air. So an increase in fraction of excess air causes superficial velocity to increase in fluidized bed combustor based on rice husk. Figure 7.6 shows the variation between minimum fluidization velocity and fraction of excess air. Minimum fluidization velocity is dependent on viscosity of fluidizing gas. Viscosity of fluidizing gas is affected with variation in temperature. With increase in fraction of excess air

Table 7.3 Measured values from Jalkheri power plant at different fraction of excess air

Fraction of Excess Air	Top of Bed Left Side of Furnace T_1 (^oC)	Top of Bed Right Side of Furnace T_2 (^oC)	Top of Bed Front Side of Furnace T_3 (^oC)	Top of Bed Back Side of Furnace T_4 (^oC)	Average Bed Temperature (^oC) $(T_1+T_2+T_3+T_4)/4$	CO_2 (%)	O_2 (%)	CO ppm	NO_x ppm	Fly Ash (g/s) (Air heater and ESP hopper)
0.1	780	780	800	784	786	12.4	6.5	92.2	150	436.1
0.2	795	810	795	800	800	12.1	6.9	80.1	152	444.4
0.3	810	805	818	811	811	11.3	7.5	75.5	155	452.8
0.4	820	825	810	817	818	10.7	8	71.1	155	472.2
0.5	820	825	815	820	820	10.5	8.5	61.1	157	480.6

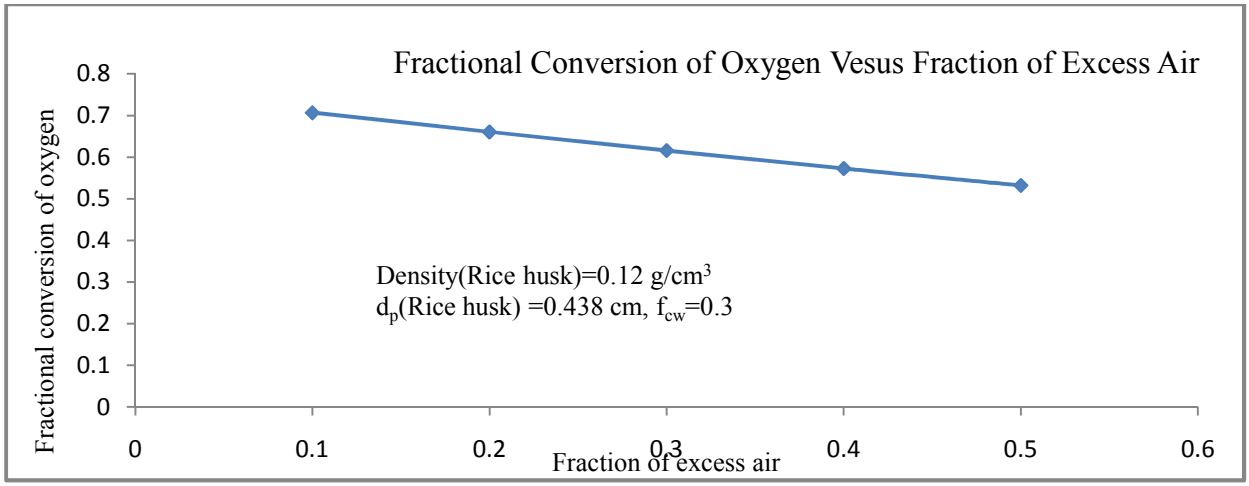

Figure 7.2 Variation of fractional conversion of oxygen versus fraction of excess air

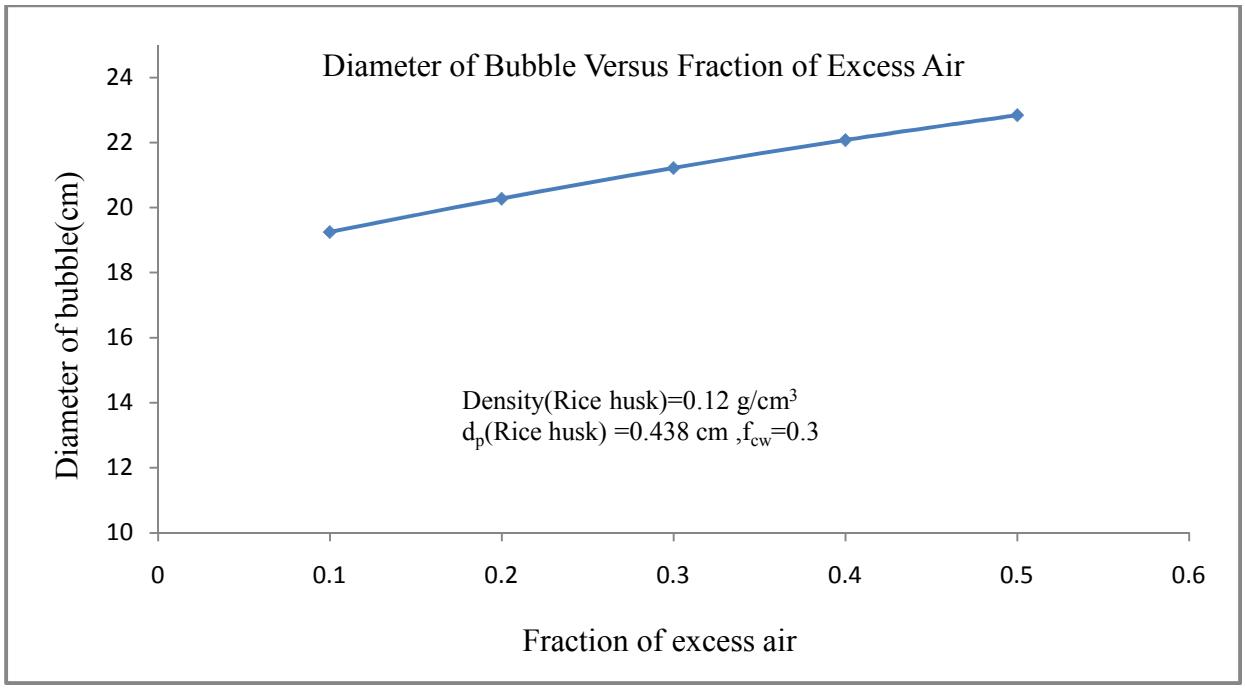

Figure 7.3 Variation of diameter of bubble versus fraction of excess air

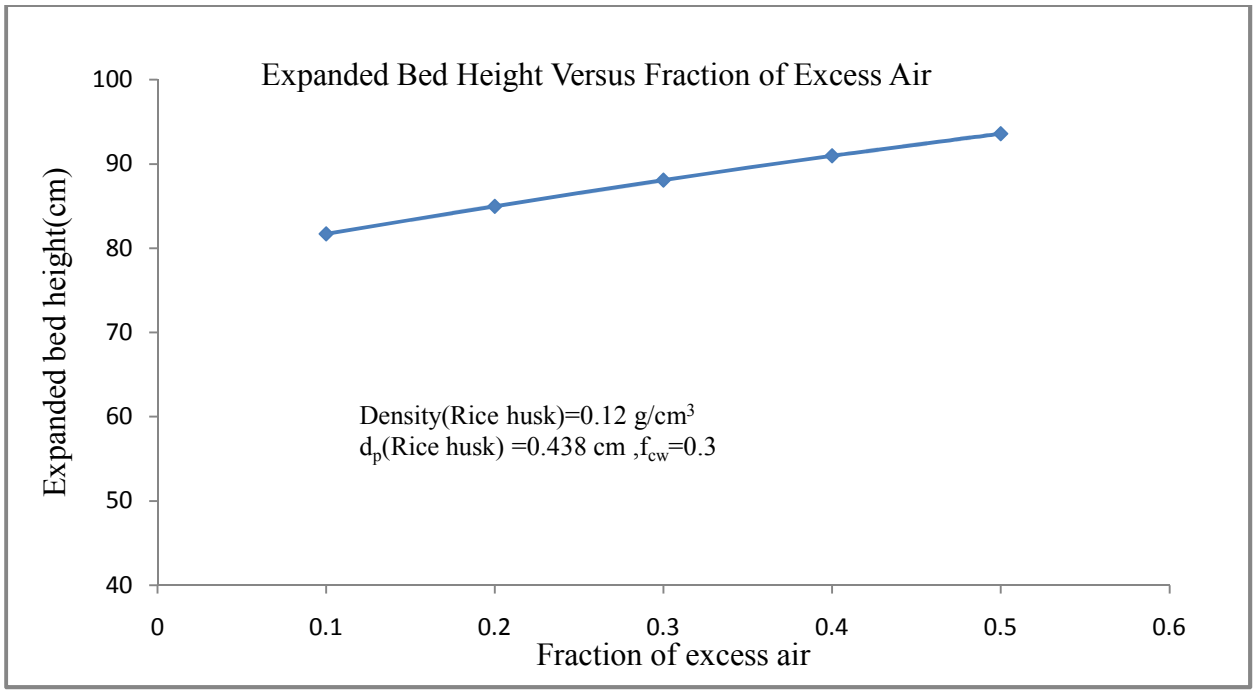

Figure 7.4 Variation of expanded bed height versus fraction of excess air

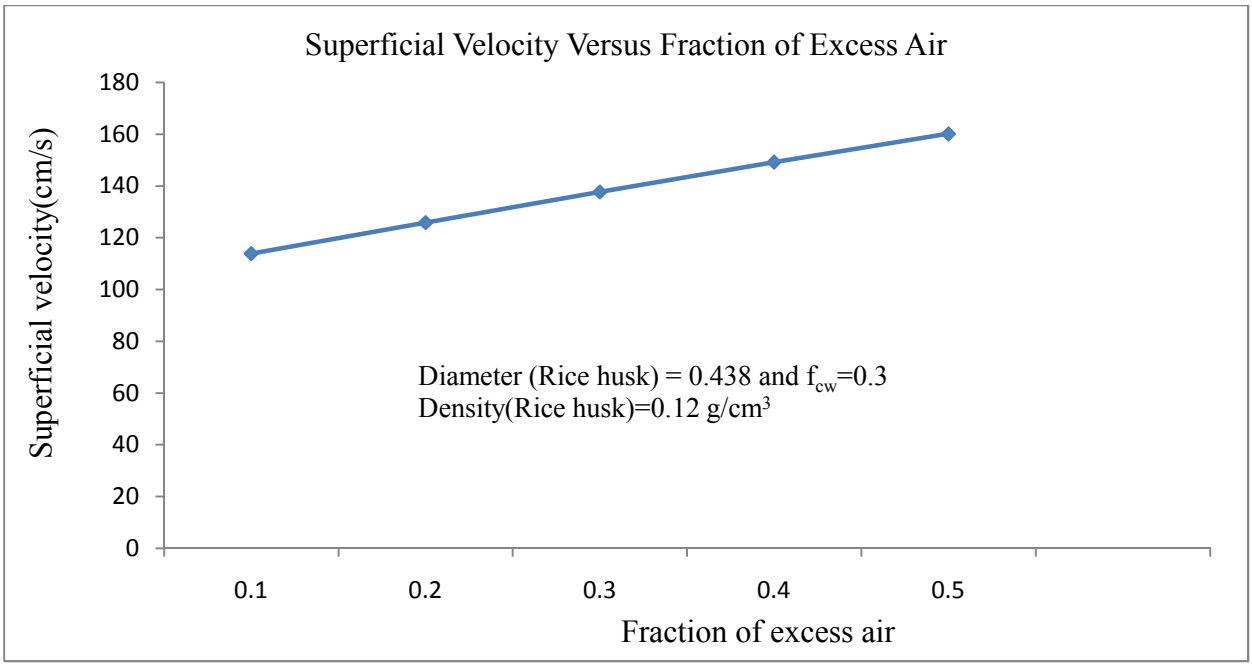

Figure 7.5 Superficial velocity versus fraction of excess air

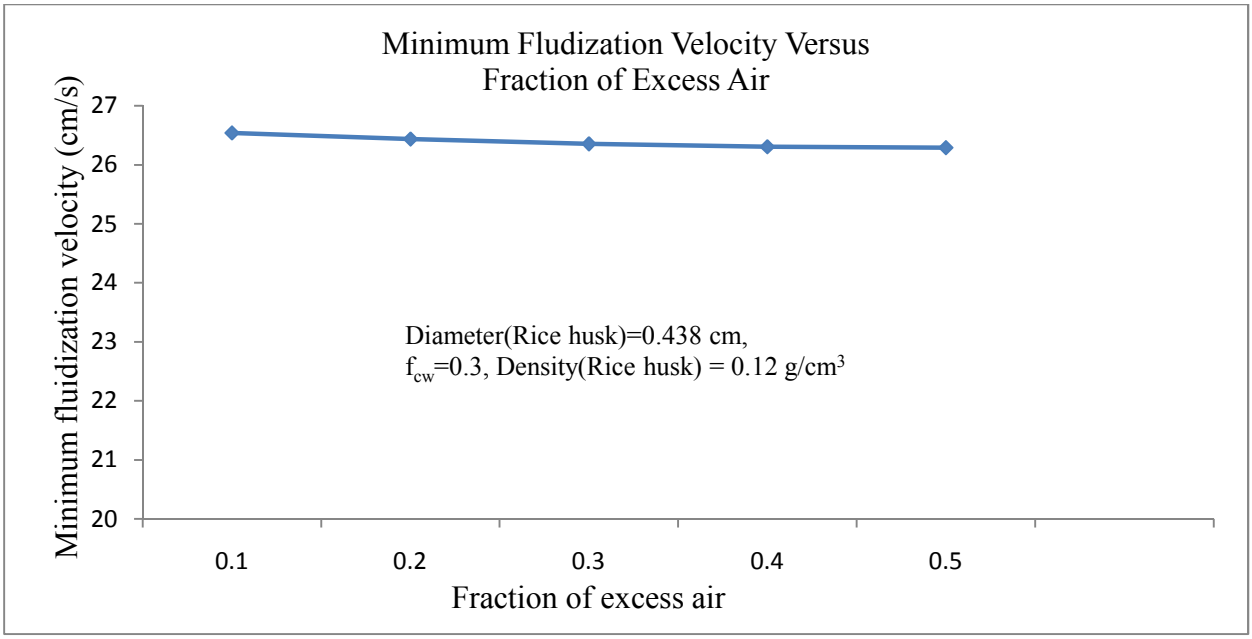

Figure 7.6 Variation of minimum fluidization velocity versus fraction of excess air

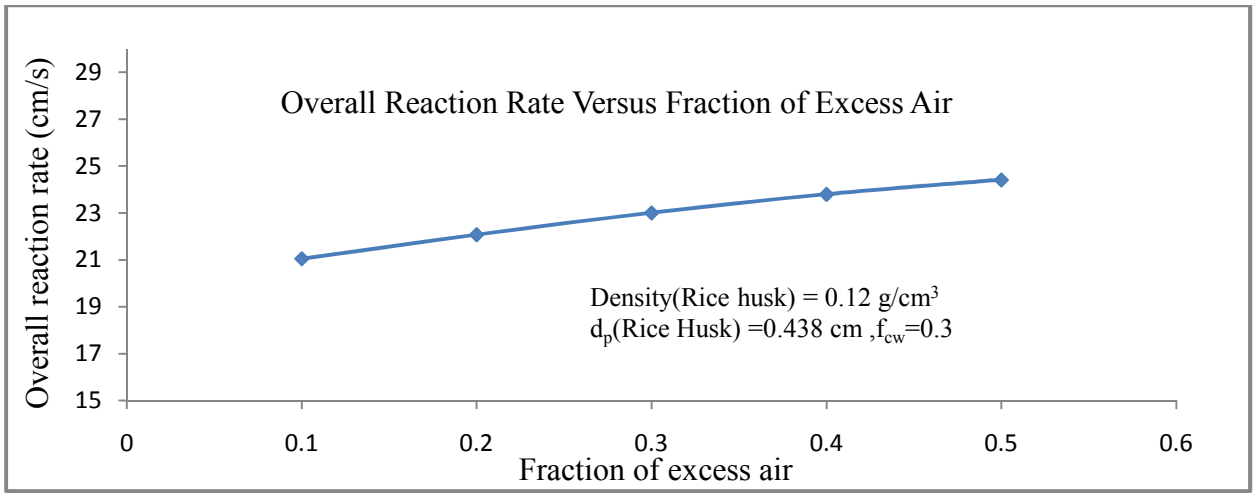

Figure 7.7 Overall reaction rate versus fraction of excess air

there is variation in temperature of fluidized bed which causes slight variation in viscosity of fluidizing gas. As minimum fluidization velocity is inversely proportional to viscosity of fluidizing gas so it decreases slightly with increase in fraction of excess air. Figure 7.7 shows the overall reaction rate with fraction of excess air. It increases with increase in fraction of excess air. It is probably due to increase in bed temperature that causes the overall reaction rate to increase with fraction of excess air. The fuel input to the plant has different percentage of moisture. Maximum permissible limit accepted at plant is 12.5%.

In normal days, the rice husk particles with 7-10% moisture content, is fed to fluidized bed combustor at Jalkheri power plant. In the rainy days the percentage of moisture in the fuel is quite high, which is unsatisfactory. The effect of moisture on oxygen concentration and carbon dioxide emitted from fluidized bed combustor is shown in Figure 7.8. The percentage of carbon dioxide increases with increase in moisture content and percentage of oxygen decreases with increase in moisture content of rice husk particles. Fuel with different moisture content is checked and model predictions are within satisfying limit. Figure 7.8 also shows the actual plant data noted at different moisture percentage of rice husk particles. The variation of actual plant

data is in accordance with the model values. It was described by Ganesh et al. [44] that in order to achieve complete conversion of carbon it is desirable to maintain a low temperature during pyrolysis and or partial combustion of rice husk, followed by steam gasification in either case. The increase in moisture content in fuel causes bed temperature to decrease at plant. Bed temperature decreases because more heat is needed to convert moisture from fuel into the vapors form. Since the phase change of liquid takes place. Therefore the latent heat required to change the phase is more which causes bed temperature to decrease. It is probably due to lower bed temperature the complete carbon conversion occurs and causing to increase carbon dioxide as mentioned in Figure 7.8. Table 7.4 gives us the actual measured data noted from the plant at different percentage of moisture content in fuel. Table 7.4 also shows the value of carbon monoxide and (NO_x) NO_2 with increase in moisture in fuel.

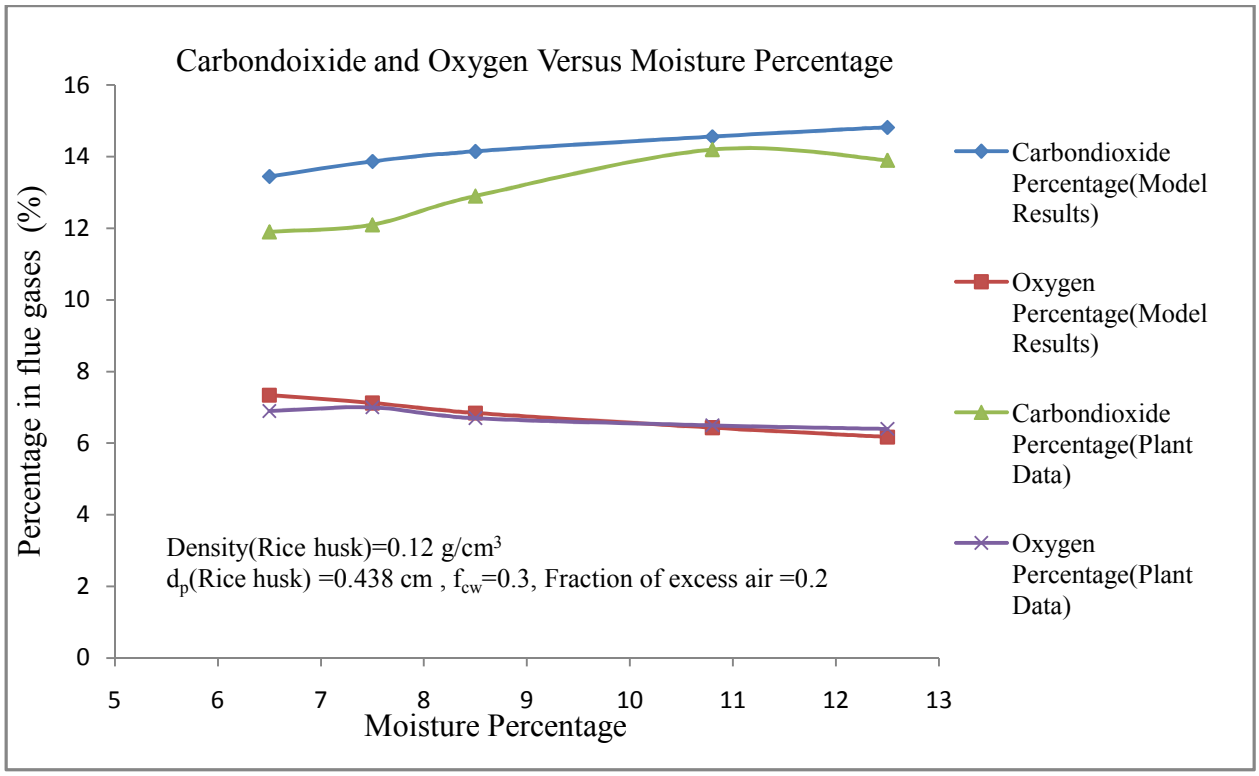

Figure 7.8 Variation of percentage of gases in flue gas with moisture

Figure 7.9 shows the variation between superficial velocity and moisture in fuel increases. The latent heat carried away by flue gases increases. This will cause the bed temperature to decrease. Since superficial velocity is dependent on molar feed rate of air which is further dependent on bed temperature. So the superficial velocity decreases with increase in moisture percentage in fuel.

Figure 7.10 shows the variation of minimum fluidization velocity versus moisture percentage in fuel. As percentage of moisture increases the bed temperature decreases. Since minimum fluidization velocity is inversely dependent on viscosity of fluidizing gas which is dependent on temperature. So decrease in bed temperature causes minimum fluidization velocity to increase slightly. The effect of moisture content on expanded bed height and bubble diameter

Table 7.4 Measured data from plant at different moisture percentage in fuel

Fraction of Excess Air	Moisture Percentage In Fuel (From Proximate Analysis)	Top of Bed Left Side of Furnace T_1(^{o}C)	Top of Bed Right Side of Furnace T_2(^{o}C)	Top of Bed Front Side of Furnace T_3(^{o}C)	Top of Bed Back Side of Furnace T_4(^{o}C)	Average Bed Temperature (^{o}C) $(T_1+T_2+T_3+T_4)/4$	CO_2 A.M.V %	O_2 A.M.V %	CO A.M.V ppm	NO_X A.M.V (ppm)	Fly Ash(Air heater and ESP) A.M.V (g/s)
0.2	6.5	815	805	807	813	810^{o}C	11.9	6.8	70.2	155	452.8
0.2	7.5	795	810	795	800	800^{o}C	12.1	6.9	80.1	152	444.4
0.2	8.5	775	780	785	780	780^{o}C	12.9	6.8	90.3	150	438.9
0.2	10.8	755	760	765	760	760^{o}C	14.2	6.6	100.2	145	433.3
0.2	12.5	745	755	752	748	750^{o}C	14.9	6.5	180.2	145	430.6

is shown in Figure 7.11 and 7.12 respectively. It can be observed from the Figure 7.11 the expanded bed height decreases with increase in moisture content. This is due to fact that as moisture content in fuel increases bubble diameter decreases which further decreases expanded bed height. Figure 7.13 shows the variation of overall chemical reaction rate with increase in percentage of moisture in fuel. Overall chemical reaction rate in combustion process decreases

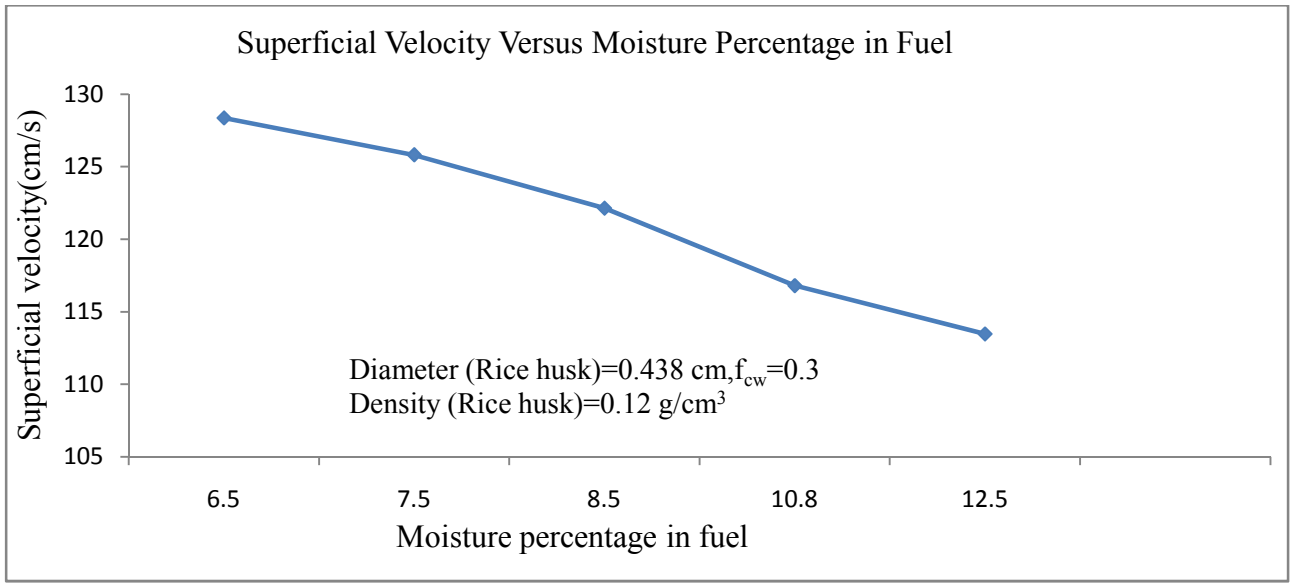

Figure 7.9 Variation of superficial velocity versus moisture percentage in fuel

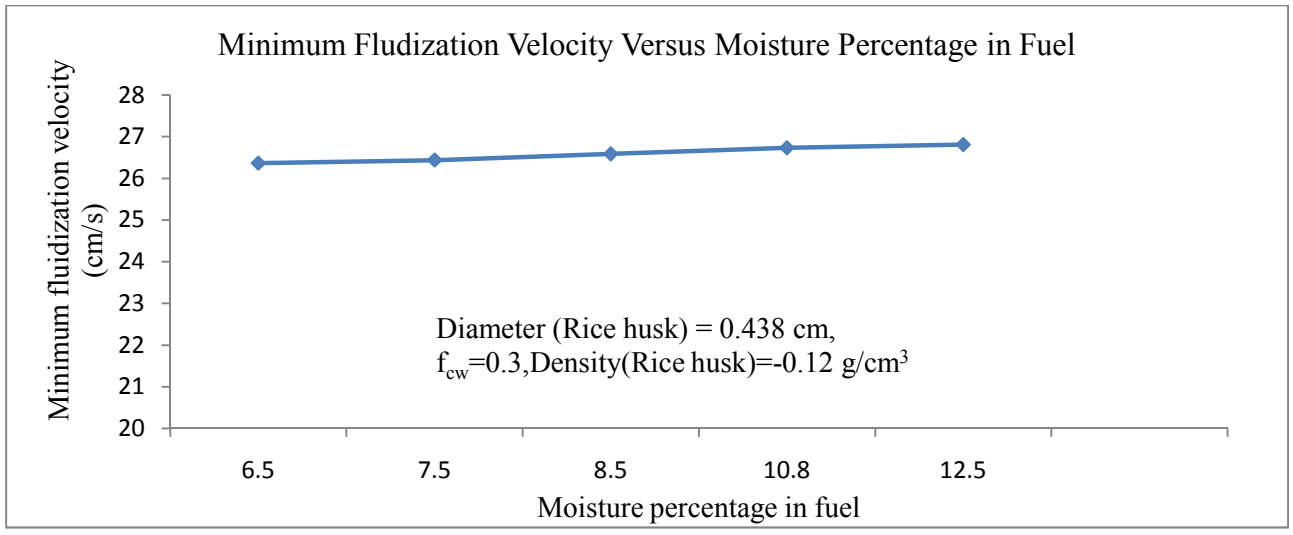

Figure 7.10 Variation of minimum fluidization velocity versus moisture percentage in fuel

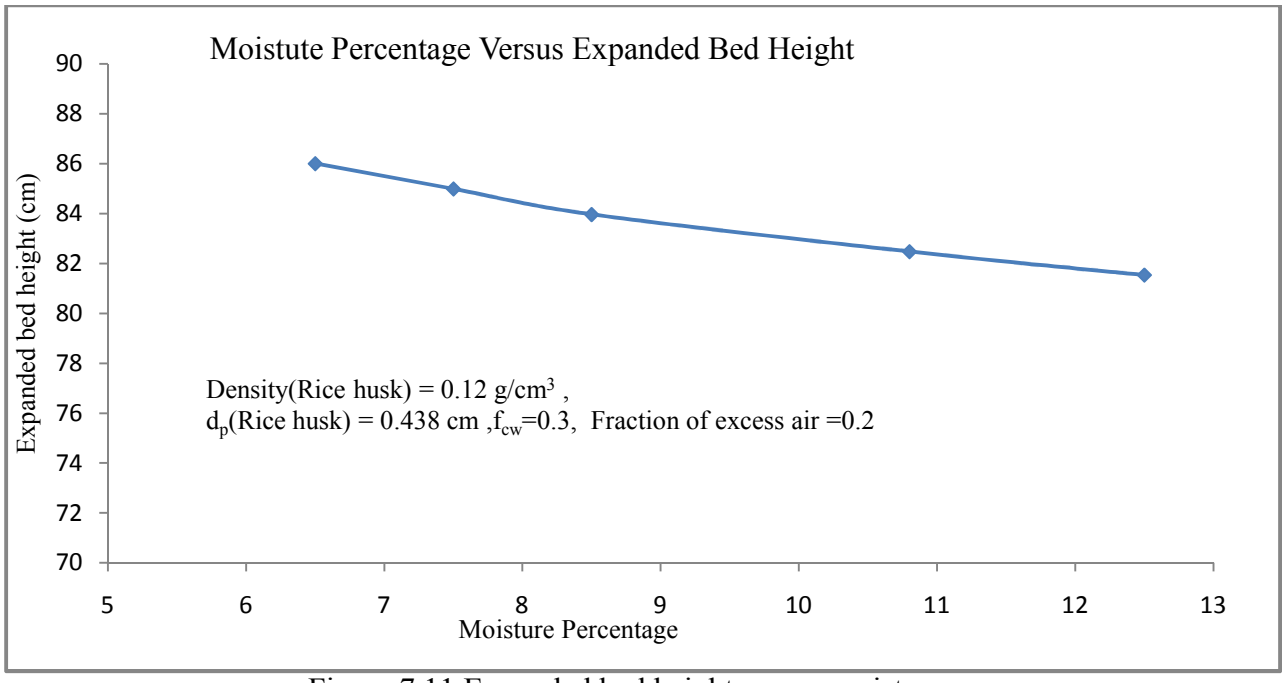

Figure 7.11 Expanded bed height versus moisture

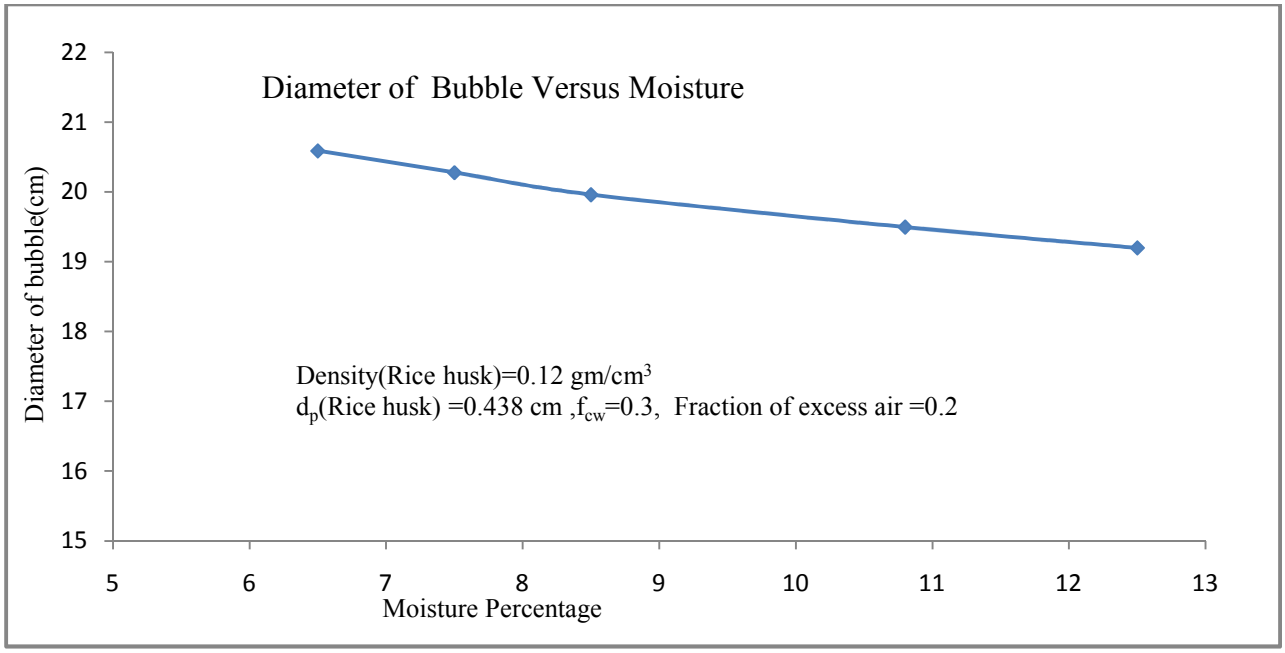

Figure 7.12 Diameter of bubble versus moisture

with increase in percentage moisture in fuel. It is probably due to dipping in bed temperature with increase in moisture content in the fuel. Bed temperature directly affects the reaction rates

in fluidized bed. Oxygen and carbon dioxide concentration decreases with bed height as shown in Figure 7.15 Oxygen increases with bed height and percentage of carbon dioxide increases with bed height. Figure 7.14 shows that conversion of oxygen is increased as the value of f_{cw} is increased. The three phase model is appropriate more at the f_{cw} =0.30 i.e when f_c is 0.25 and f_w=0.05. This is probably due to large size of rice husk particles.

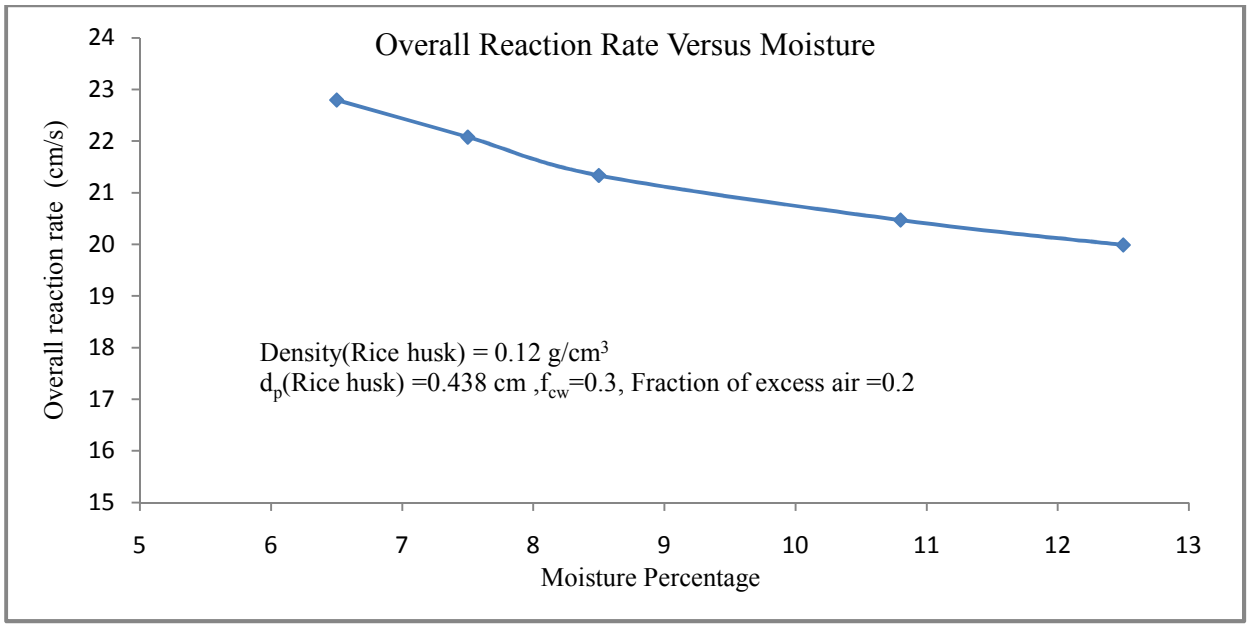

Figure 7.13 Variation of reaction rate constant with moisture percentage

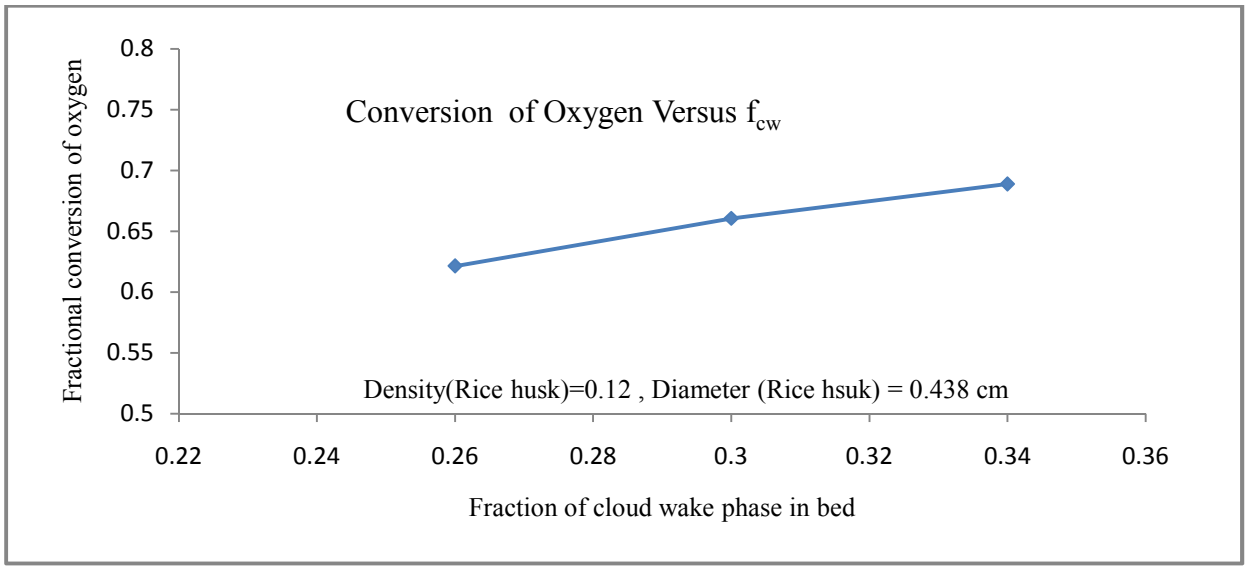

Figure 7.14 Conversion of oxygen versus f_{cw}

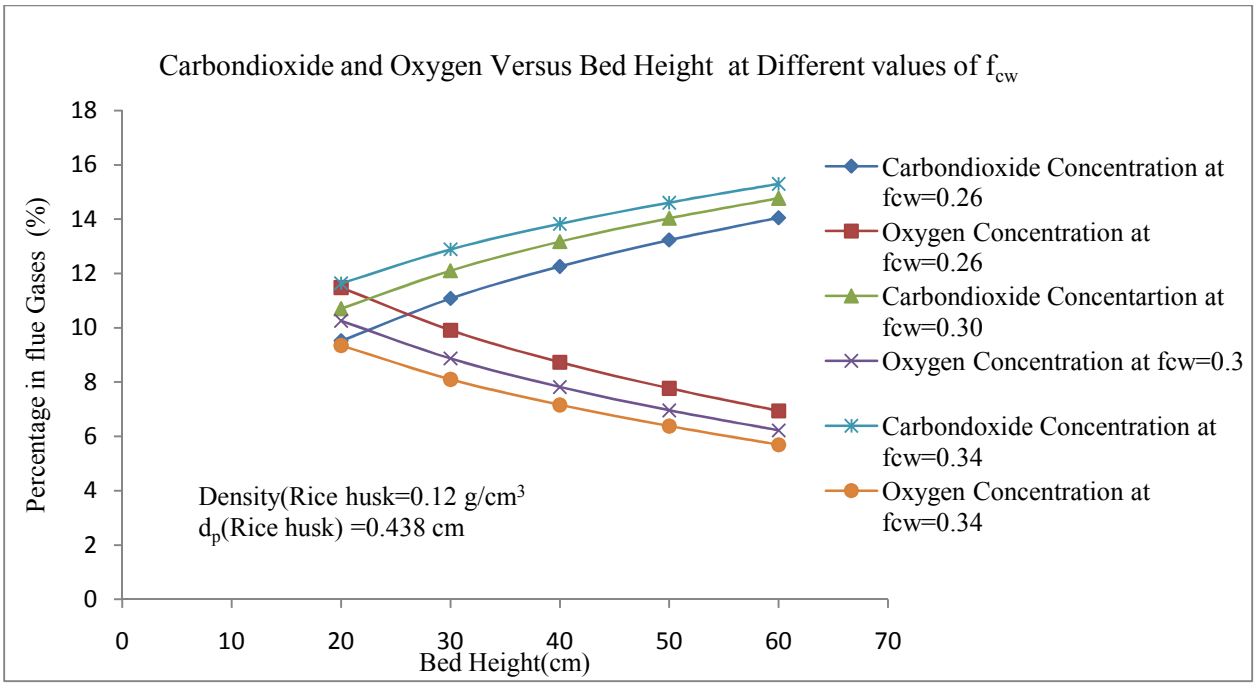

Figure 7.15 Concentration of CO_2 and O_2 along bed height at different f_{cw}

Figure 7.15 shows that as f_{cw} increases from 0.26 to 0.34 the percentage change in carbon dioxide is increased and corresponding percentage of oxygen in flue gas decreased with bed height. The model predictions are more appropriate when we choose f_{cw} = 0.30. The variation of f_{cw} indicates the presence of a separate cloud wake phase even in small scale rice husk plant. From Figure 7.15 we also got information that the size of rice husk particles is also affecting the percentage of carbon dioxide and oxygen in the commercial fluidized bed combustors.

The solid population balance formed is used to predict elutriation rate, carbon utilization efficiency, bed carbon load, carry over rate and shrinkage rate. The carbon utilization efficiency predicted by the model is 98.37% at 0.2 fraction of excess air. The actual carbon utilization efficiency is 92.64% as calculated in Table 3.6. The variation of above model is within 6% which is probably due to the simplified assumptions and neglection of attrition rate for our model. Table 7.3 and Table 7.4 shows the measured values of various parameters used in model

and other parameters which are used to calculate actual carbon utilization efficiency at plant. Figure 7.16 and 7.17 shows the variation of elutriation rate constant and carryover rate with fraction of excess air. Elutriation rate constant and carry over rate is increased with increase in fraction of excess air. It

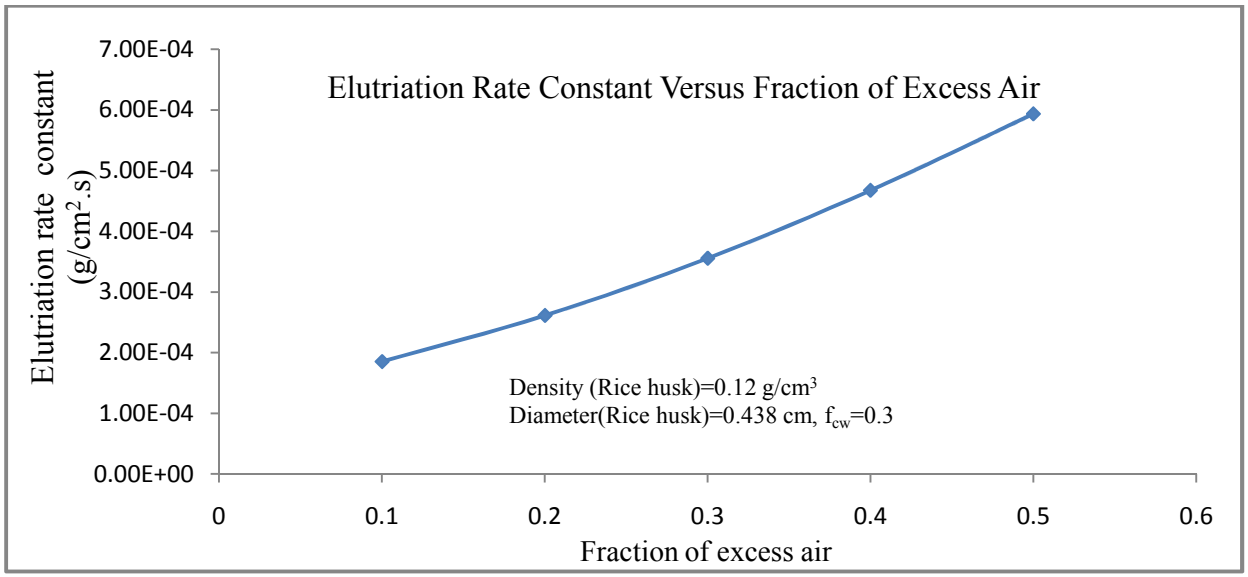

Figure 7.16 Elutriation rate constant versus fraction of excess air

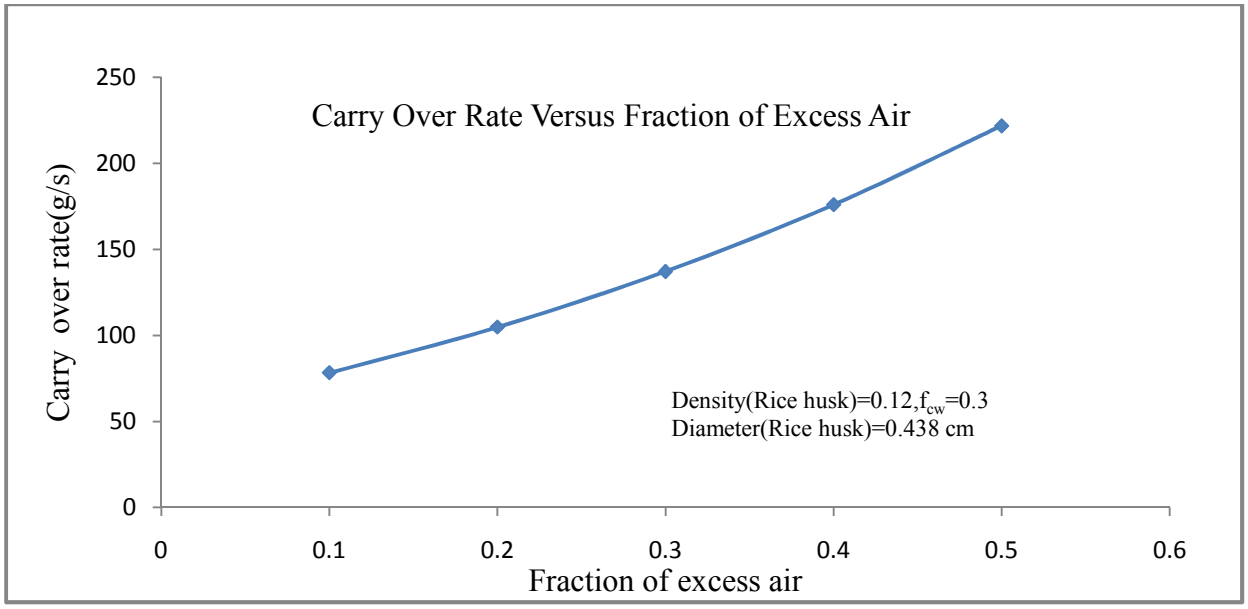

Figure 7.17 Carry over rate versus fraction of excess air

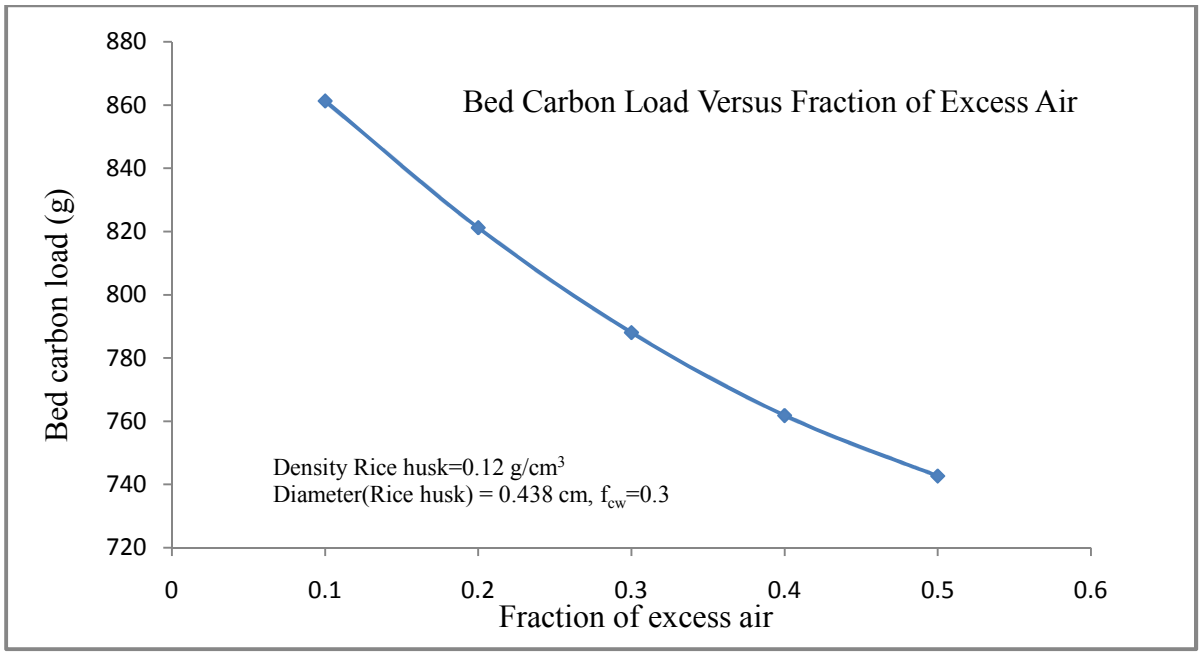

Figure 7.18 Bed carbon load versus fraction of excess air

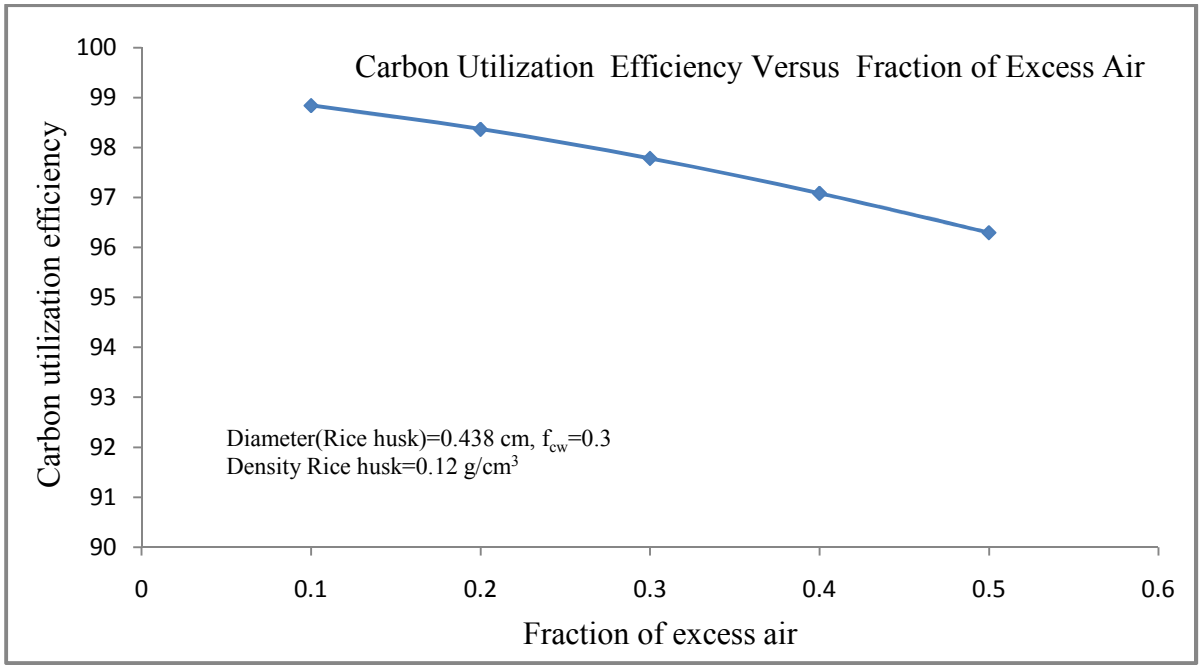

Figure 7.19 Carbon utilization efficiency versus fraction of excess air

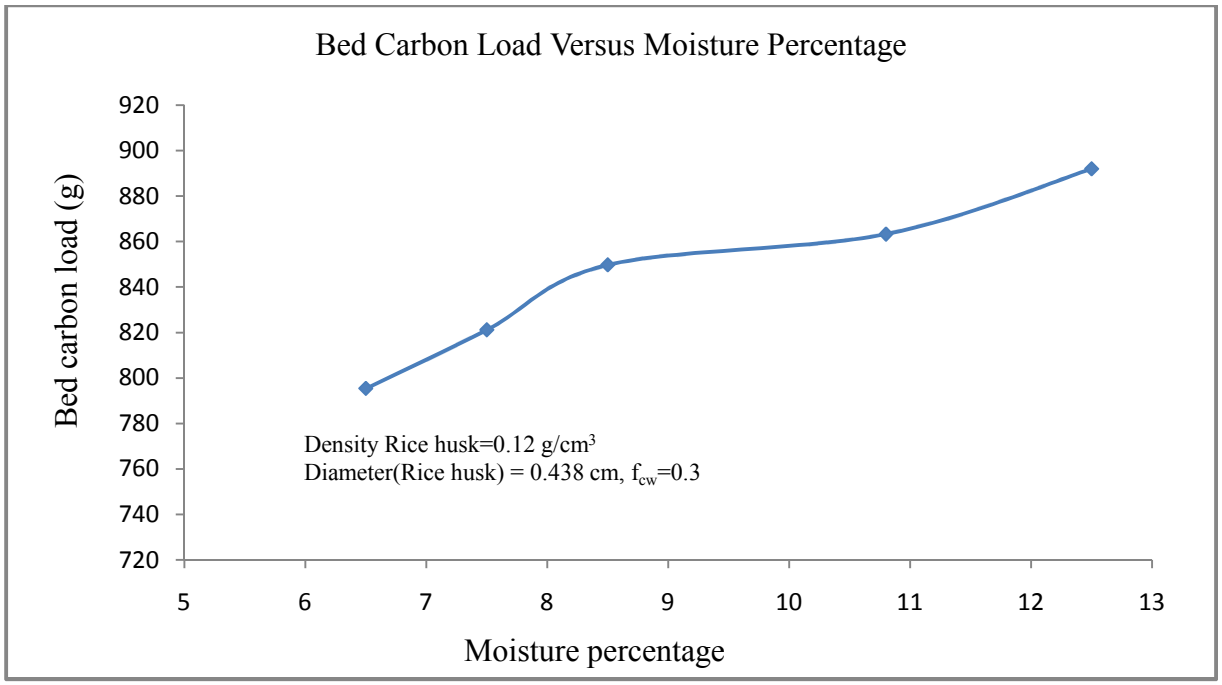

Figure 7.20 Bed carbon load versus moisture percentage in fuel

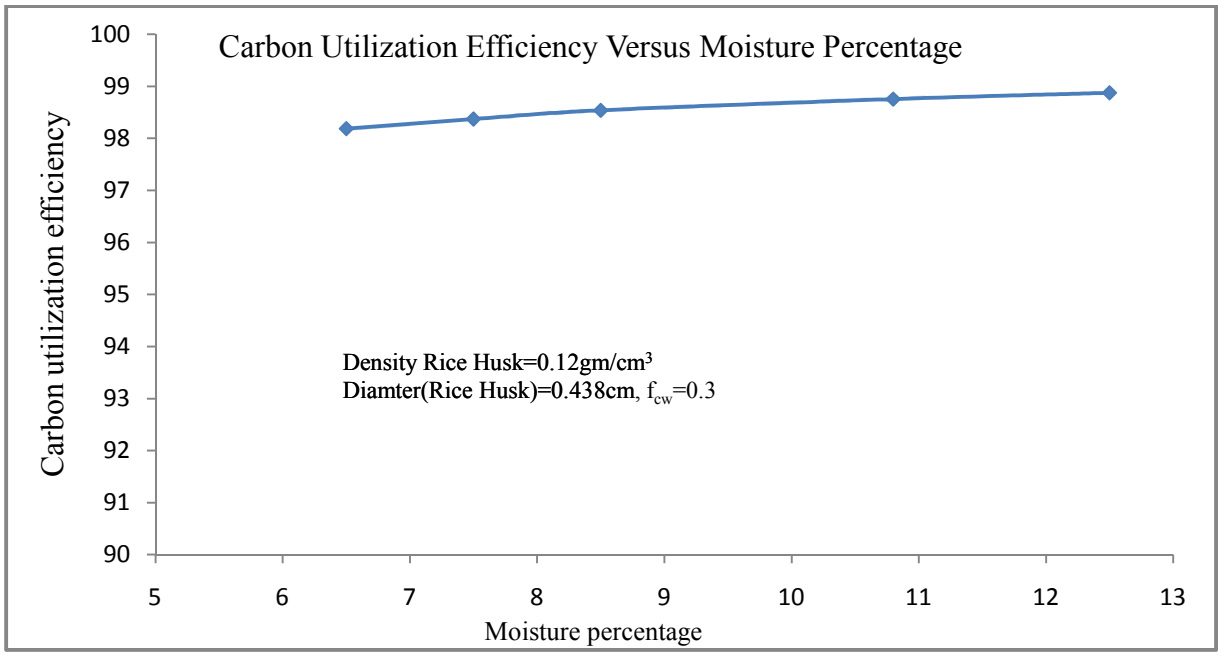

Figure 7.21 Carbon utilization versus moisture percentage in fuel

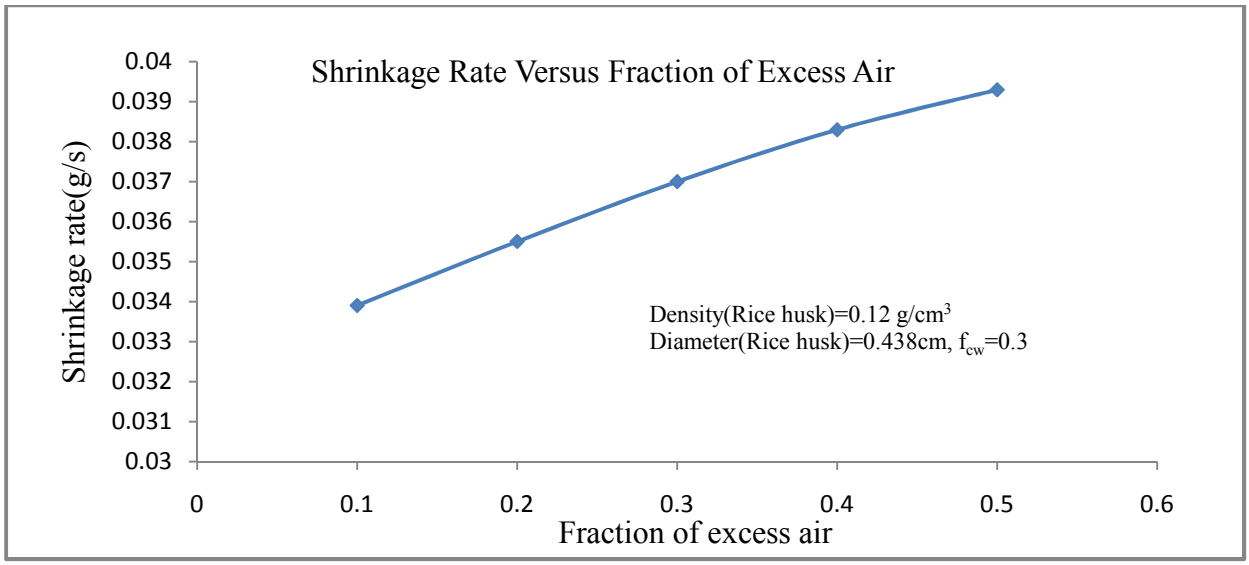

Figure 7.22 Shrinkage rate versus fraction of excess air

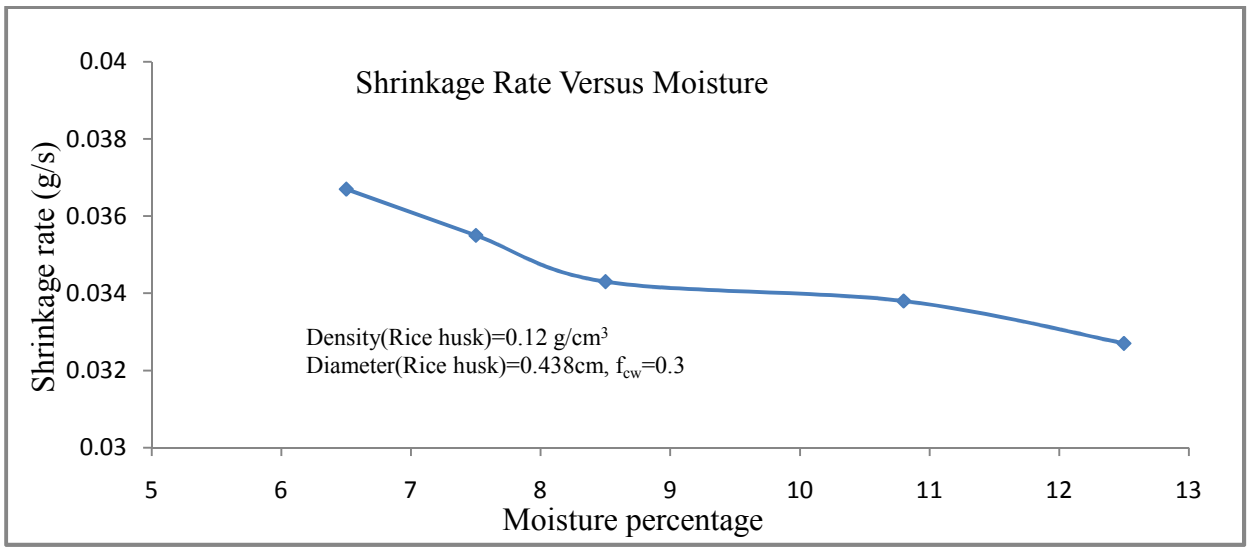

Figure 7.23 Shrinkage rate versus moisture percentage in fuel

is because due to fraction of excess air the temperature increases which increases the overall reaction rates. As the fraction of excess air increases the bed temperature increases because more oxygen is available to burn the combustibles present in bed. The combustibles present in the fluidized bed burn in an efficient manner in the bed with more available air. As fraction of excess air the increases, the fines generated due to combustion of fly ash increases. The increase is

probably due to higher overall reaction rates. Figure 7.18 shows the bed carbon load versus fraction of excess air. Bed carbon load decreases with increase in fraction of excess air. As the fraction of excess air increases the superficial velocity also increases which will decrease the loading of carbon in the bed. Figure 7.19 shows the carbon utilization efficiency versus fraction of excess air. Carbon utilization efficiency decreases as the fraction of excess air is increased. Figure 7.20 and 7.21 shows the bed carbon load and carbon utilization versus moisture percentage in fuel.

As the percentage of moisture in fuel increases the bed carbon load increases which is probably due to lower bed temperature and lower overall reaction rates as shown in Figure 7.20. It will increase the residence time of rice husk particles longer in the bed. Carbon utilization efficiency also increases with higher moisture percentage in fuel as shown in Figure 7.21. As reported by Ganesh et al. [44] that to achieve complete conversion of carbon it is desired to maintain low temperature during pyrolysis. Due to increased moisture and subsequently decreased temperature is also the reason why the carbon utilization efficiency is increased with increased percentage of moisture content in fuel as shown in Figure 7.21. Figure 7.22 shows the shrinkage rate of rice husk particles with the fraction of excess air. Shrinkage rate increases with increase in percentage of excess air which is due to higher bed temperature. Figure 7.23 shows the shrinkage rate versus moisture percentage in fuel. Shrinkage rate decreases with moisture percentage in fuel which is due to dipping in bed temperature as moisture content in fuel is increased.

Agglomeration

To investigate the reasons of agglomeration in fluidized bed combustion of rice husk and rice straw the analysis of sand was done. Based on data given in Table 5.2 from the analysis of ash it

may be concluded that the bed agglomerate material considerably differs from the initial sand and fuel ash in composition. The composition of original sand is variable which depends on operation, mainly comprises of silica and remaining alumina shown in Table 5.2. From Table 5.2 it is clear that after one week percentage of SiO_2 in ash is decreased to 92 % and after one month percentage of SiO_2 is further decreased to 86% at Jalkheri power plant when rice husk is used. The percentage of SiO_2 in ash as found in 3.5 MW cogeneration power plant after one week time is decreased to 92% and after month percentage is further decreased to 80% as shown in Table 5.3. When rice straw is used in combination with rice husk at Jalkheri power plant, the percentage of SiO_2 in ash is 82 % after one week as cleared from Table 5.7.

It is clear from Table 5.2 and Table 5.5 at both plants JPP and CPPDK when rice husk is used; the elements like Potassium, Magnesium, Sodium etc. present in the rice husk ash after one month are quite high to the rice husk ash after one week. When rice straw is used in combination with rice husk at JPP, the presence of potassium is higher than when rice husk is used. The analysis of ash of fluidized bed combustor when rice husk and rice straw mixture is used is shown Table 5.7. It may be higher if the sand was not refreshed periodically. As the plant continues to operate the agglomerates are continuously formed. These are generally removed along with bed material drain. Percentage of ferrous oxide is higher after one month is probably due to entries of debris or small pieces of iron gone to combustor along with rice husk. The only possibility to reduce the defluidization in Jalkheri power plant and cogeneration power plant is either to lower the bed temperature which will lower the reaction rates and consequentially the combustion is incomplete and percentage of carbon monoxide is increased in exit gas which is unsatisfactory because of norms set by pollution board. So lowering the bed temperature is not possible at Jalkheri power plant and cogeneration power plant when rice husk is used. When the

plant normally operates at 800^{o}C w.r.t rice husk it may the case at some position in bed or near the distributor plate the temperature is higher or even close to 1000^{o}C which causes mainly the agglomeration of sand particles at plant. Replacement of sand particles with small fresh sand daily/hourly basis and cleaning of used sand is normally done at Jalkheri power plant to decrease the defluidization. The same procedure i.e refreshment of sand is adopted at 3.5 MW cogeneration power plant.

It is known that the rate of formation of agglomerates is influenced by Ca and Na content of ash, bed temperature and fluidizing velocity. No one can exclude the formation of eutectics at a softening temperature in the ternary system SiO_2-CaO-FeO. It is noted [182] that at a temperature below 750^{o}C, the agglomeration processes are decelerated. The increased fluidizing velocity also decreases the rate of agglomeration. As reported in literature [182] sand as bed material contributes the most for agglomeration. The interaction of the ash components with the quartz sand causes the formation of readily softening eutectics. According to [117] and [119], the most probable reactions in the bed are given below.

$$2SiO_2 + Na_2CO_3 \rightarrow Na_2O.2SiO_2 + CO_2 \tag{7.3.1}$$

$$4SiO_2 + K_2CO_3 \rightarrow K_2O.4SiO_2 + CO_2 \tag{7.3.2}$$

In this case, the softening temperature of the reaction products (7.3.1) and (7.3.2) is 874^{o}C and 764^{o}C respectively. This is significantly lower as compared to individual components. The readily fusible eutectics have even lower softening temperatures. The governing equations for different softening temperatures are given below:

$$Na_2O.2SiO_2 - SiO_2 \rightarrow T_S = 790^{o}C(Na_2O - 26\%, SiO_2 - 74\%) \tag{7.3.3}$$

$$K_2O.2SiO_2 - K_2O.4SiO_2 \rightarrow T_S = 760^o C(K_2O - 33\%, SiO_2 - 67\%) \quad (7.3.4)$$

The data of [124] give the evidence that the ash ferric compounds also reacts with alkalines:

$$Fe_2O_3 + Na_2CO_3 \rightarrow Na_2Fe_2O_4 + CO_2 \quad (7.3.5)$$

$$Fe_2O_3 + K_2CO_3 \rightarrow K_2Fe_2O_4 + CO_2 \quad (7.3.6)$$

However, the softening temperature of the reaction (7.3.5) products reaches 1135^{o}C. Nevertheless, in the presence of large amount of ash Fe_2O_3, the alkalines will primarily react with Fe_2O_3, forming no readily softening eutectics. The coal ash features rather higher molar

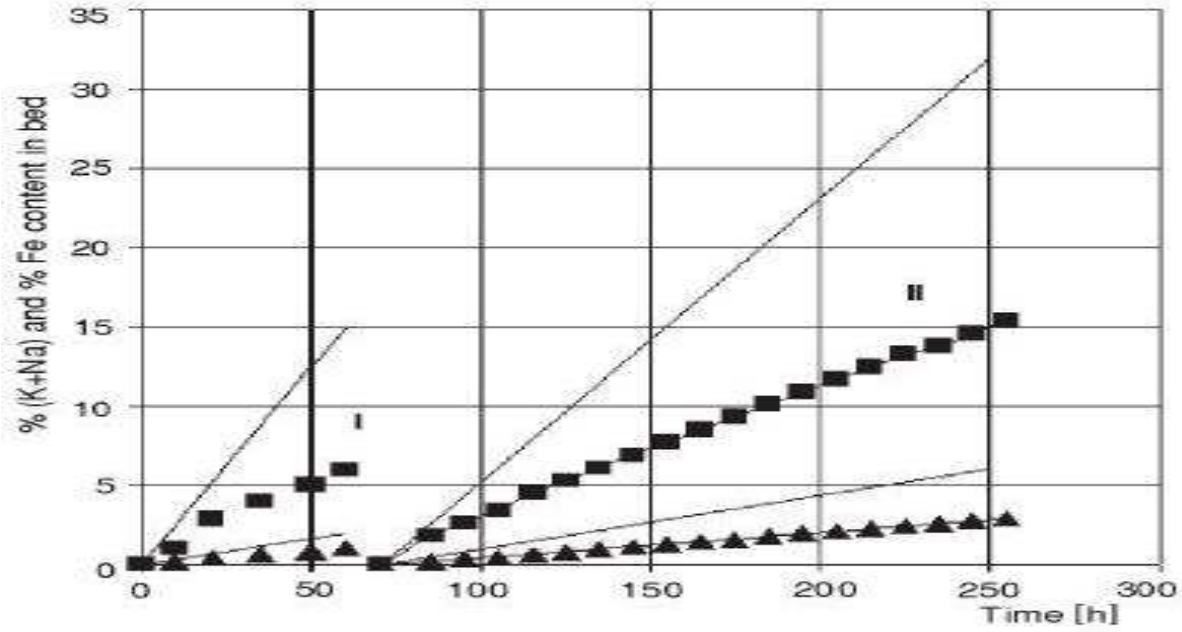

Figure 7.24 Buildup of Alkalines in bed due to combustion of corn corb [117]

■ measured(K + Na) –mass balance line

▲ measure(Fe)-mass balance line

ferric to alkalines ratio as compared to biomass ash. It is of importance to know the share of K, Na, and Fe compounds remaining in the bed. The data of [117] give the experimental results

obtained on 150 kW test facility when corn cob with high K_2O content was fired. The sand of the average granulation size of 0.76 cm (35 cm bed height) was used as bed material. Two runs were conducted, first at bed temperature of 820^oC with excess air 0.72 and fluidizing velocity of 158 cm/s. In the second run, the respective figures were 750^oC with excess air 0.87 and fluidization velocity 132 cm/s. Figure 7.24 illustrates the time variations of Na+K and Fe compounds in the bed along with the predictive mass balance data. It was found that approximate 6 % and 16 % (runs I (Approx. 60 h) and II (Approx. 260 h)) of Na and K compounds contained in the ash, remained in the bed. The comparative data for Fe compounds were approximate 2 and 4% respectively.

The data on the bed material at plant is in good agreement with those of [117]. Reduction of the bed temperature to 700^oC in Jalkheri plant increases the period of agglomeration. The same thing was occurred at 3.5 MW cogeneration plant. However, this approach results in impermissible CO emission rise. The traditional way to reduce the negative effects of bed agglomeration lies in increasing the bed drain with the addition of the fresh inert material. There are cases [119] where the 81-231 g/s of sand was added at some industrial boilers. Here, the bottom ash was regenerated by screening and recirculation on the required fractions in the bed. Practically, it is important to evaluate the necessary flow rate of sand to prevent agglomeration. In addition calcium gives problems in the special case of co-combustion of a high-sulphur fuel with a fuel rich in organically bound calcium. Calcium is also an important bulk component in ash deposits, especially when adding limestone to the bed, but in mostly not responsible for the initiation of deposits. The percentage of calcium increased when the agglomerates analyzed at different time period. It could be probably due to addition of limestone ($CaCO_3$) to decrease

defluidization. As sulphur content in rice husk is less, the probability of formation of agglomerate is less.

As evident from literature potassium is the most important element in rice husk and rice straw, which are responsible for ash related problems. In oxidizing conditions the thermodynamic stability of potassium compounds with increasing temperature as follows: sulphates ($<1000^{o}C$) < silicates < chlorides. In reducing temperature conditions sulphates do not form and silicates and chlorides are the stable compounds. These compounds all have low melting points and can form even at lower-melting eutectics. A high amount of volatile potassium in biomass combustion is therefore associated with slagging in the furnace due to fluxing of silicates. Fouling and corrosion in convective passes are due to condensation on the heat transfer surfaces as chlorides, sulphates, hydroxides or oxides and subsequent sulfation to sticky and corrosive sulphates.

Agglomeration in fluidized beds is due to formation of low-melting compounds or eutectics by heating with silica, sulphur and chlorine. It is mainly responsible for agglomeration problem. It is evident from ash analysis as shown in Table 5.2; the percentage of potassium in sand has increased from 2.0 to 3.4 with one month of operation at JPP. The percentage of potassium is increased up to 9 after one week when rice husk-rice straw combination is used at JPP as shown in Table 5.6. The percentage of potassium is increased 3.0 to 5.2 after one month at CPPDK as shown in Table 5.5. Because of periodically replacement of sand this percentage appears to be less, if sand was not replaced the percentage of potassium in bed ash should be more than this. Also from the literature survey it is clear that potassium is mainly responsible for agglomeration.

During combustion sulphur is converted to SO_2 which reacts with alkali to form sulphates. Sulphates have very low vapor pressure and condense readily on cooler surfaces, such as heat transfer tubes and bed particles. It is evident from elementary ash analysis that percentage of sulphur increases with reuse of sand continuously.

CFD Analysis

The hydrodynamic features of a bubbling bed with or without bed superheater tubes are explained with the help of solid volume fraction contour plots and velocity contour profiles. The velocity taken at the lower side of bed is 120 cm/s as this is available operating velocity in plant at JPP. The temperature of fluidized bed is assumed to be 800^{o}C, as taken from plant. The contours of temperatures are least significance in fluidized bed as it assumed to be constant i.e isothermal in all previous calculations that meant for exit gas and solid population balance. Fluidized bed acts as thermal reservoir with no change in temperature. The variation of temperature generally exists above the fluidized bed i.e the freeboard region. The main purpose is to strengthen the three phase mathematical modeling technique as used in exit gas model.

When gas is passed through a bed of solid particles above the minimum fluidization velocity, small bubbles form at the bottom of the fluidized bed. Result of the simulation for the bubbling bed without bed super heater tubes with inlet gas velocity of 120 cm/s in terms of solid volume fraction contour at a particular time is shown in Figure 7.25 - 7.26. These contours are at different time intervals starting from 0.2 s and ends at 4.0 s.

The bubble starts evolving from lower side of bed. The bubble is rising upwards in the bed. The bubble is shown with blue green patch and solid are shows with red patches. The diameter of bubble is clearly increasing with bed height. These bubbles formed and evolved at the bed surface. Clearly the bubble is surrounded by cloud phase. At the center of bubble blue

patch is present and at the surrounding green patch is there which clearly indicates the presence of cloud- phase even with particles size of 0.438 cm. Figure 7.27-7.28 show the contours of velocity of air passing through bed at different time. The velocity of air along the walls is zero. Velocity of air inside bubbles is high as comparable to initial velocity. Blue patches is inside the bed are showing zero velocity. Zero velocity indicates the velocity of solid rice husk particles. While air is passing through the bed the solid rice husk particles are also in small motion. During the initial few seconds the velocity of air is zero at the top of bed which is further increased as the time advances.

Figure 7.29 shows the velocity vectors of air at different times 0.4 s, 1.0 s, 2.0 s, 3.0 s and 4.0 s respectively. Clearly in this Figure velocity is greater when passing through bubbles.

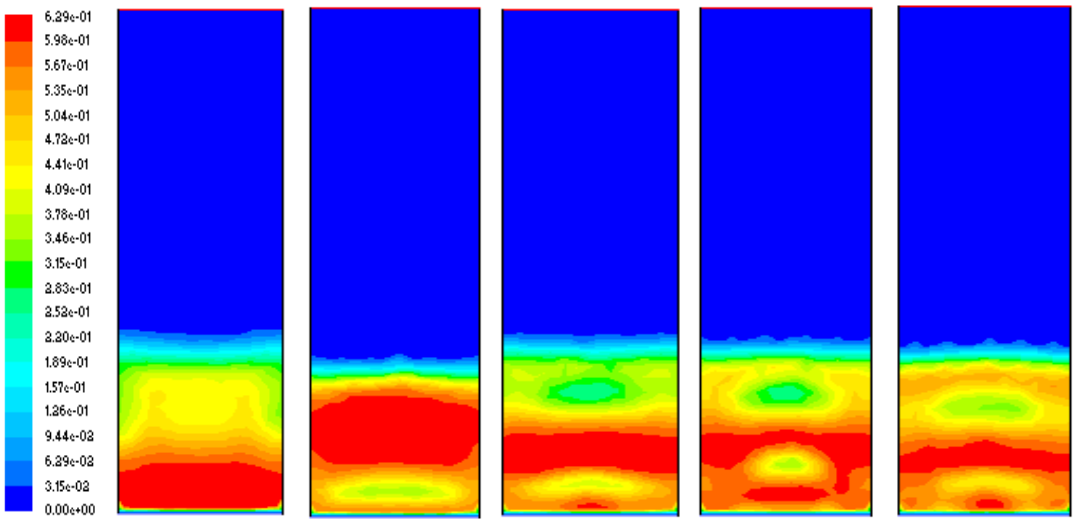

Figure 7.25 Solid volume fraction contours at 120 cm/s and rice husk diameter 0.438 cm

(a) 0.2 s (b) 0.4 s (c) 0.8 s (d) 1.0 s (e) 1.6 s

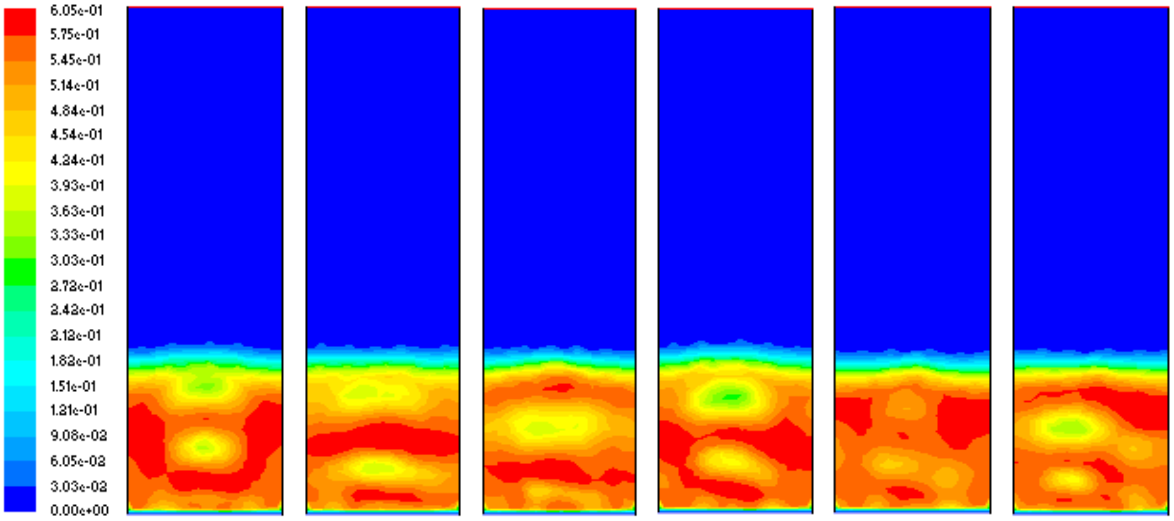

(a) (b) (c) (d) (e)

Figure 7.26 Solid volume fraction contours at 120 cm/s and rice husk diameter 0.438 cm (a) 2.0 s (b) 2.4 s (c) 3.0 sec (d) 3.4 s (e) 3.6 s (f) 4.0 s

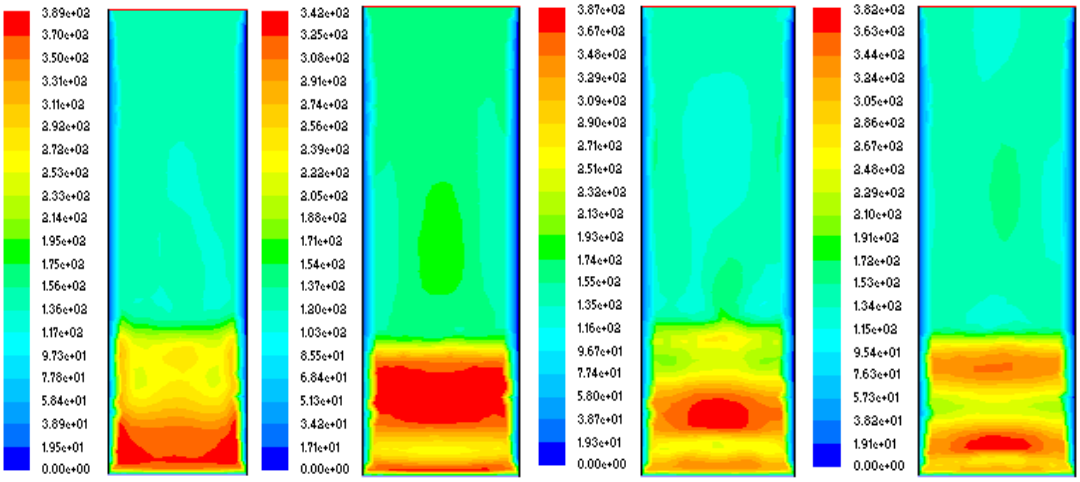

Figure 7.27 Contours of velocity (air) at (a) 0.2 s (b) 0.4 s (c) 0.8 s (d) 1.0 s

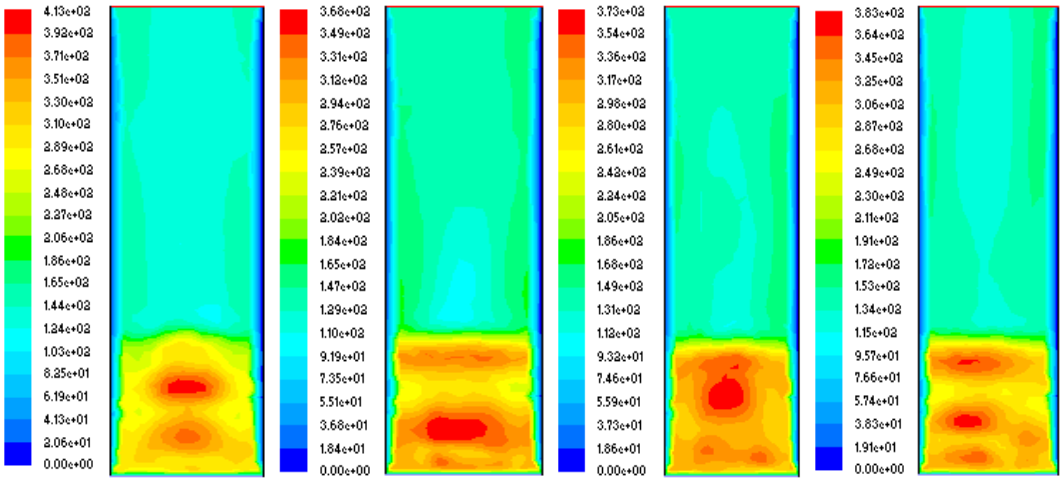

Figure 7.28 Contours of velocity (air) at (a) 2.0 s (b) 3.0 s (c) 3.6 (d) 4.0 s

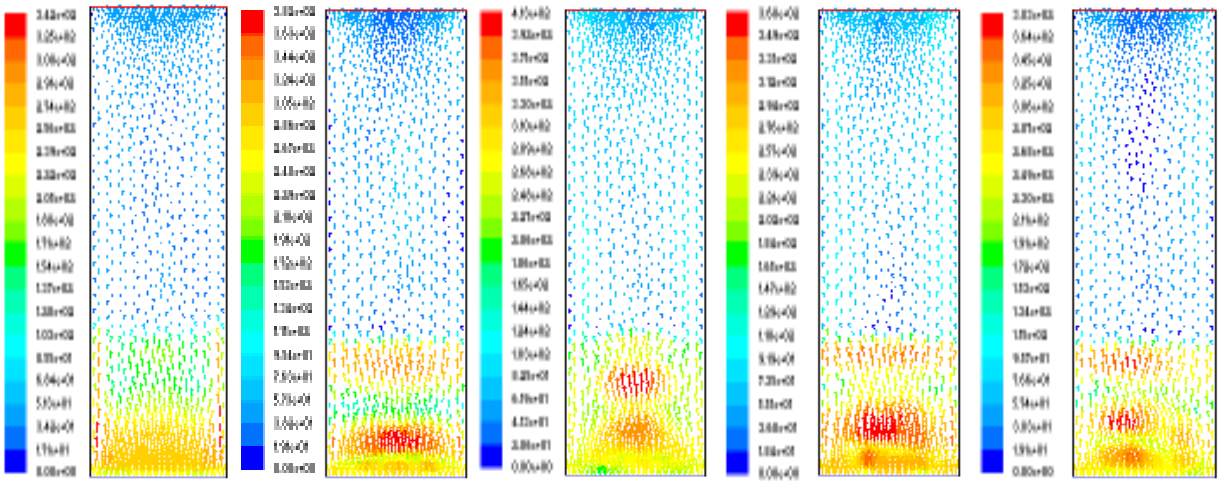

Figure 7.29 Velocity vectors (air) (a) 0.4 s (b) 1.0 s (c) 2.0 s (d) 3.0 s (e) 4.0 s

For bubbling bed with bed super heater tubes, bed flow structure at different times have been shown in Figures 7.30-7.32 in terms of solid volume fraction contours at particle size of 0.438 cm and velocity of 120 cm/s. The operating velocity of 120 cm/s is chosen here as this is velocity of air at JPP. The contours of velocity profiles for different time intervals have been shown in Figure 7.33. Initially due to the imposed symmetry in the bed, the gas is seen to rise in the form of a plug. However, this soon disappears, and bubbles start taking their shape.

The bubbles are defined as the regions inside the bed where the solid volume fraction is less than 20%. The bubbles increase in size as they rise. On striking the tubes they break up into smaller bubbles. This necessarily removes any symmetry that was there in the beginning. From this time onwards, the entire bed develops an unsymmetrical flow structure, giving rise to a typical bubbling fluidized bed. The bubbles coalesce, break and re-coalesce. Within the tubes, due to excessive breakage, the bubble sizes are smaller than in the regions outside the bed super heater tubes. Above the tube bank the bubbles behave as they should in a bubbling bed without tube banks, increasing in size with height. On reaching the bed surface, the

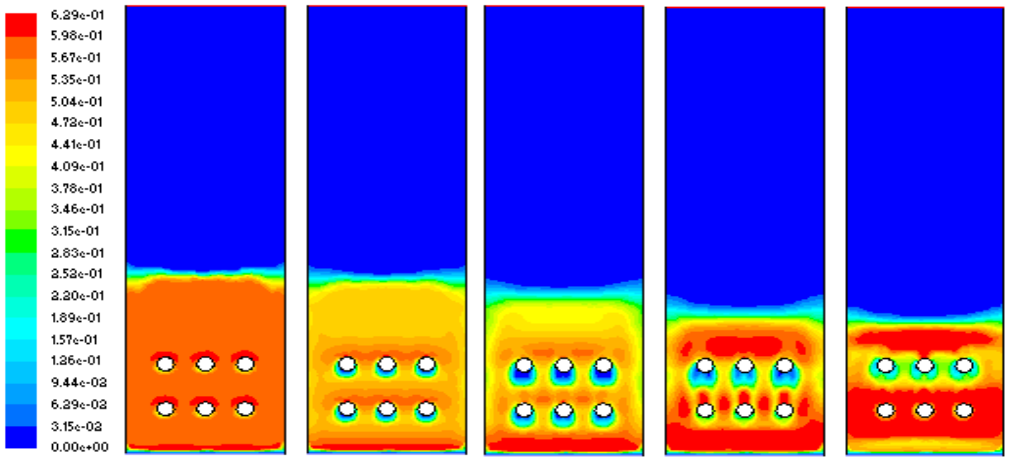

(a) (b) (c) (d) (e)

Figure 7.30 Contours of solid volume fraction (particle size 0.438 cm and velocity 120 cm/s) at (a) 0.02 s (b) 0.06 s (c) 0.12 s (d) 0.18 s (e) 0.26 s

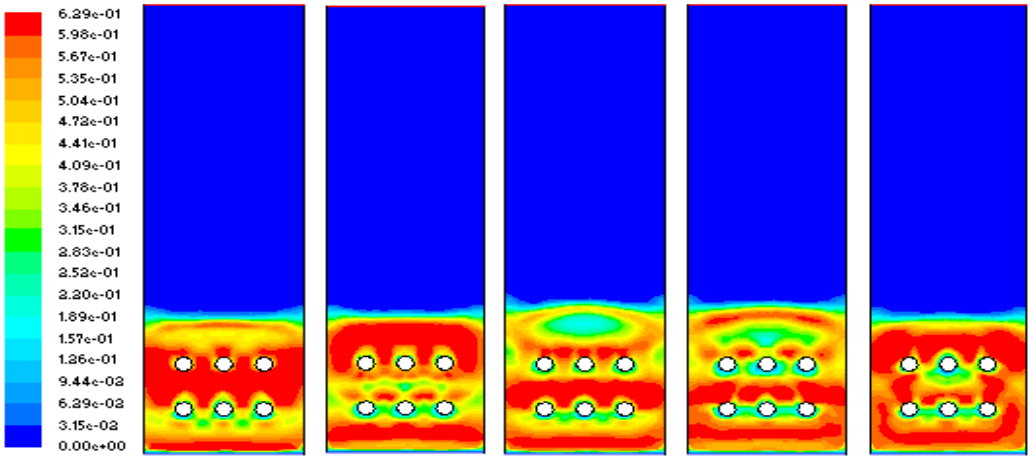

(a) (b) (c) (d) (e)

Figure 7.31 Contours of solid volume fraction (particle size 0.438 cm and velocity120 cm/s) at (a) 0.4 s (b) 0.5 s (c) 0.7s (d) 1 s (e) 1.2 s

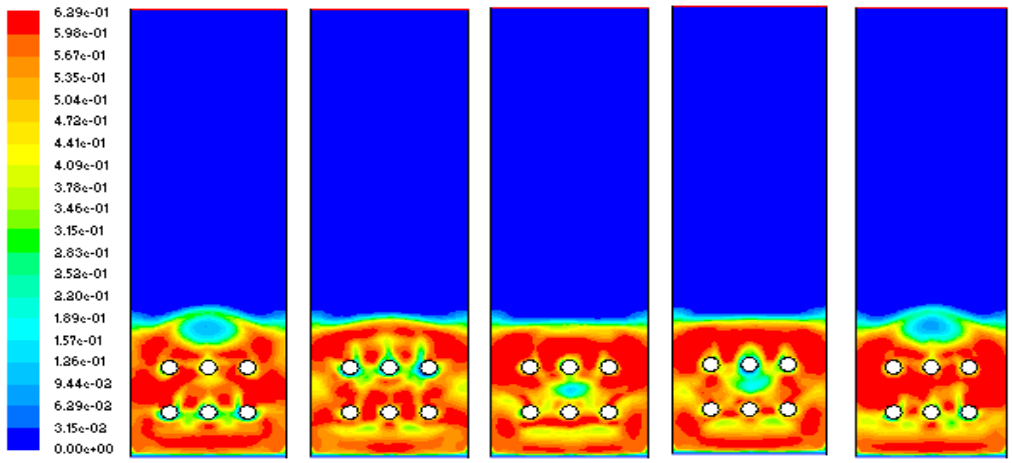

(a) (b) (c) (d) (e)

Figure 7.32 Contours of solid volume fraction (particle size 0.438 cm and velocity 120 cm/s) at (a) 1.4 s (b) 1.56 s (c) 1.76 s (d) 1.8 s (e) 2 s

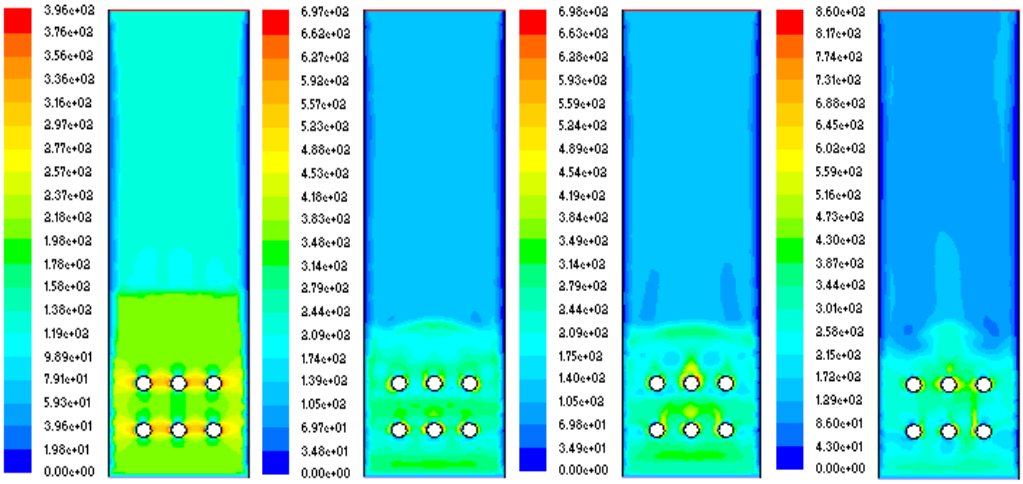

(a) (b) (c) (d)

Figure 7.33 Contours air velocity (particle size 0.438 cm and initial velocity 120 cm/s) at (a) 0.02 s (b) 0.7 s (c) 1 s (d) 2 s

bubbles burst resulting in a violently fluctuating top surface. Clearly here also blue-green patches represent bubbles and these are surrounded by light green-yellow patches which indicates the presence of cloud-wake phase even at large size i.e rice husk particles.

Qualitatively it may be seen that near the inlet the bubbles are small in size and they increase with height until they encounter the first row of tubes. When bubbles encounter a series of tubes, there are two possibilities of bubble breakage (i) smooth splitting of bubbles to

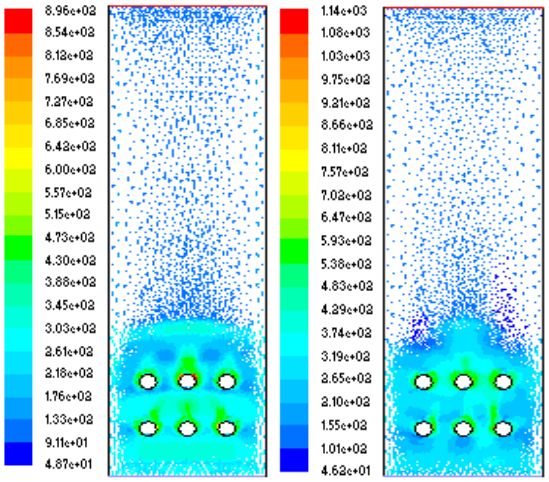

(a) 1.0 s (b) 2 s

Figure 7.34 Velocity vectors (air) (a) 1.0 s (c) 2.0 s

form smaller bubbles of roughly equal size (ii) the bubbles bridging the gaps between two consecutive horizontal tubes. These two mechanisms dictate the eventual size of the bubbles inside and just above the tube bank region. With increase in the gas velocity, the diameter of bubbles increases, although the effect is pronounced only below and above the bed super heater region. The bubbles which are passing between wall and bed super heater tubes without contacting these grow along with bed height as shown in Figures 7.30-7.32. These bubbles will erupt after reaching at the top of bed. Sometimes two small bubbles are going to coalesce.

Figure 7.33 shows the contour of velocity at different instants of time. The velocity at the top of tube and near the wall seems to be zero. The velocity of bubbles is higher as shown clearly in Figure 7.33. Figure 7.34 shows the velocity vectors of air at different times of 1.0 s and 2.0 s respectively. Clearly in this Figure velocity is greater when passing through bubbles.

- From the above results and discussions it can be emphasized that fuel composition, fuel properties, fluidization velocities, bubble size and causes of agglomeration will help immensely a practicing engineer for modification of design of existing plant and new design if any.

CHAPTER 8

CONCLUSION AND FUTURE SCOPE

8.1 Conclusions

Due to huge amount of rice waste generated in India, boiler manufactures are set increasing demand for rice waste based combustors. Rice husk and rice straw are only types of rice waste which could be incinerated in fluidized bed combustors. Due to higher collection cost, feeding problems and higher agglomeration problems rice straw in not much used for incineration in fluidized bed combustors of this region. The hydrodynamic parameters and performance of fluidized bed combustors are important, while designing fluidized bed combustors. The study done here with respect to rice waste in fluidized bed combustor leads us to following major conclusions.

- **The three phase model presented here predicts exit gas composition from the 10 MW FBC power plant using rice husk with reasonable accuracy. With increase in fraction of excess air from 0.1 to 0.5, the percentage of oxygen in flue gas increases from 6.1 to 9.8 and carbon dioxide decreases from 14.8 to 11.2.**
- The fractional oxygen conversion in the FBC plant decreases from 0.7 to 0.53 as the fraction of excess air increases from 0.1 to 0.5. Superficial velocity increases from 113.8 to 160.1 cm/s, minimum fluidization velocity decreases from 26.5 to 26.3 cm/s, bubble diameter increases from 19.2 to 22.8 cm, expanded bed height increases from 81.7 to 93.6 cm and overall reaction rate increases from 21 to 24.4 cm/s with increase in fraction of excess air from 0.1 to 0.5. Bed carbon load decreases from 861.2 to 742.6 g, carbon utilization efficiency decreases from 98.8 to 96.2 percent and shrinkage rate increases from 0.033 to 0.039 cm/s with increase in fraction of excess air from 0.1 to 0.5.
- With increase in moisture percentage in fuel from 6.5 to 12.5 there is decrease in percentage of oxygen from 7.3 to 6.2 in the flue gas and there is increase in the percentage of carbon dioxide from 13.4 to 14.8 in the flue gas. Superficial velocity decreases from 128.3 to

113.4 cm/s, minimum fluidization velocity increases from 26.4 to 26.8 cm/s, bubble diameter decreases from 20.6 to 19.2 cm, expanded bed height decreases from 86 to 81.5 cm and overall reaction rate decreases from 22.8 to 20 cm/s with increase in percentage of moisture in the fuel from 6.5 to 12.5. Bed carbon load increases from 795.3 to 892 g, carbon utilization efficiency increases from 98.2 to 98.8 and shrinkage rate decreases from 0.036 to 0.032 cm/s with increase in moisture percentage in fuel from 6.5 to 12.5.

- Cloud-wake ratio is also affecting the exit gas composition of the plant. As cloud wake ratio increases from 0.26 to 0.34, the fractional conversion of oxygen increases from 0.62 to 0.68. The most suitable value of cloud-wake ratio is 0.3. At cloud wake ratio of 0.3 the percentage of oxygen in flue gas decreases from 10.3 to 6.2 and percentage of carbon dioxide increases from 10.7 to 14.8 with increase in bed height from 20 to 60 cm. The gases emitted in flue gas from Jalkheri power plant are within permissible limits set by local pollution board at normal operating conditions.
- The agglomeration in Jalkheri power plant and cogeneration power plant using rice husk particles is caused by the inorganic content of rice husk. Agglomeration problem is mainly caused by high potassium content in the fuel. Na and Mg are also responsible towards agglomeration problem. Calcium and sulphur do not contribute towards agglomeration.
- A decrease in bed temperature can extend defluidization significantly and also result in increased CO. Fluidization velocities should be higher to avoid defluidization. Fuel should enter inside the furnace without debris and ferrous particles.
- The traditional way to reduce the negative effects of bed agglomeration lies in increasing the bed drain with the addition of the fresh inert material. Practically, it is important to evaluate the necessary flow rate to prevent agglomeration. 8 to 10 percent replacement of sand after each week will decrease defluidization at both plants.
- Simulation of the hydrodynamics of a bubbling fluidized bed considering rice husk with and with out bed super heater tubes were carried out using CFD. Three phase mathematical modeling has been established by CFD analysis based on rice husk.

- Bubbles vary in size along with bed height in fluidized bed combustor without bed superheater tubes based on rice husk. With the use of bed super heater tubes bubbles formed and erupted at the tubes. The bubble flow structure is affected due to the presence of tubes.

  .

8.2 Scope of Future Work

1. The model can be further extended to study the effect of bubble size variation on various parameters of the bubbling fluidized bed combustion.

2. The model presented here can be used to calculate hydrodynamic parameters and exit gas composition for other biomass fuel like cotton stalks, cotton seed husk, ground nut husk, maize stalks, maize husk, coffee husk etc. and can also be tested at any other plant based on rice husk.

3. In the solid population balance model in order to calculate bed carbon load, attrition rate of rice husk particles and overflow rate could be considered.

4. The method adopted for study of agglomeration can be used for other fuels like wheat straw, cotton stalks etc.

5. CFD analysis of free board has to be calculated using two-mixture fraction technique and commercial code.

REFERENCES

[1] www.monstersandcritics.com/news/business/news/article 1404829.php/UN_record_world _rice_production_but_prices_set_to_remain_high.
[2] Smil V, 1999, "Crop residues: Agriculture's largest harvest", *Bioscience*, 49, 4, 299 -308.
[3] Hall D O, Rosillo-Calle F, Williams R H, Woods J, 1993, "Biomass for energy: supply prospects", Chapter 14, *Renewables for Fuels and Electricity*, Washington D C, Island Press, 593 - 652.
[4] Andreae M O, 1991, "Biomass burning: its history, use, and distribution and its impacts on the environmental quality and global change", *Global Biomass Burning: Atmospheric, Climatic, and Biosphere Implications*, Cambridge, Levine J S (ed), M A, MIT Press, 3 - 21.
[5] Bhattacharya S C and Wu W, 1989, Fluidized-bed combustion of rice husk for disposal and energy recovery, *Proceeding Energy from Biomass and Wastes XII*, 591-601.
[6] Jenkins B M, 1989, "Physical properties of biomass", *Biomass-Handbook*, Kitani O and Hall C W(Ed.), Gorden and Breach Press, New York, 860-891.
[7] Mahin B, 1986, "Rice husk energy systems", *Report Bioenergy Systems*, Office of Energy-U.S Agency for International Development.
[8] Jain A , Rajeshwar Rao T, Sambi S S and Grover P D, 1995, "Energy and chemicals from rice husk", *Biomass and Bioenergy*, 7, 285-289.
[9] FAO Statistical Database, 2002, http://apps.fao.org.
[10] http:/Punjabgovt.nic.in/Punjabataglance/LeadingbyExample.htm.
[11] Singh Jagtar, Panesar B S and Sharma S K, 2008, **"**Energy potential through agricultural biomass using geographical information system-A case study of Punjab", *Biomass and Bioenergy*, 32, 4, 301-307
[12] Flanigan V J, Xu B Y and Huang E, 1987, "Fluidized bed gasification of rice hulls", *The Tenth Annual Energy-Sources Technology Conference and Exhibition*, Dallas, Texas, 19-34.
[13] Salour D, Jenkins B M, Vafei M and Kayhaian M, 1993, "Control of in-bed agglomeration by fuel blending in a pilot scale straw and wood fuelled AFBC", *Biomass and Bioenergy*, 4, 2, 117-133.
[14] Hupa M, 2005, "Current status and challenges within fluidized bed combustion", *Advanced Combustion and Aerothermal Technologies*, N. Syred and A. Khalatov (eds.), Springer Netherland, 87-101.
[15] Williams A, Pourkashanian M, Jones J M, 2001, *"*Combustion of pulverised coal and biomass", *Progress in Energy and Combustion Science*, 27, 587-610.
[16] Backreedy R I, Fletcher L M, Jones J M, Ma L, Pourkashanian M, Williams A, 2004," Co-firing pulverized coal and biomass: A Modeling Approach", *Proceedings of the Combustion Institute*, 30, 2955-2964.
[17] Demirbas A, 2003, "Combustion characteristics of different biomass fuels", *Progress in Energy and Combustion Science*, 30, 219-230.

[18] Walsh, A R, 2006, "*CFD* modeling of waste-fuel boiler combustion systems"*, Proceeding 7th European Conference on Industrial Furnaces and Boilers*, Porto, Portugal, April 18-21, 1-11.
[19] Bridgeman T G, Darvell L I, Jones J M, Williams P T, Fahmi R, Bridgewater A V, Barraclough T, Shield I, Yates N, Thain S C, Donnison I S, 2007, "Influence of particle size on the analytical and chemical properties of two energy crops", *Fuel*, 86, 60-72.
[20] Buligins L, Lacis S, Krauze A, 2001, "*Optimization of Wet Sawdust Burner*", *Proceeding International Scientific Colloqium- Modeling for Saving Resources*, Riga, May 17-18, 184-189.
[21] http://www.answers.com/topic/rice?cat=technology.
[22] http://www.thelaststraw.org/backissues/articles/Rice%20Hull%20House.pdf.
[23] Seibutukei Haikibutsu, Risaikuru Genjo, Kadai, 1999, "Status quo and problems for recycling biomass wastes", *Biomass Waste Recycle Research Group*, In Japanese.
[24] Pathak B S and Jain A K, 1984, "Characteristics of crop residues", *Report on Physicals, Chemical and Thermochemical Properties of Ten Selected Crop Residues*, Punjab Agricultural University, Ludhiana, Punjab, India.
[25] Osman, E A, 1982, "A study of the effects of ash chemical composition and additives on fusion temperature in relation to slag formation during gasification of biomass", *PhD Dissertation*, University of California, Davis.
[26] Simonov A D, Mishenko T I, Yazkov N A and Parmon V N, 2003, "Combustion and processing of rice husk in the vibrofluidized bed of catalyst or inert material", *Chemistry for Sustainable Development*, 11,277-283.
[27] F Osaka, 2007, Staged combustion of rice straw in a fluidized bed, *Experimental Thermal and Fluid sciences*, 32, 1, 52-59.
[28] Sen R and Gosh D N,1992, "Fluidization and combustion characteristics of rice husk", *Indian Chemical Engineer*, 34,4.
[29] Bingyan X and Zongnan L, 1987, "A study of fluidized bed gasification of rice hulls", *Proceeding Advances in Solar Energy Technology*, Biennial congress, Hamburg Germany, 2312-2316.
[30] Xu B Y, Huang W C, Flanigan V J and Sitton O C, 1985, "Design and operation of a 6 inch fluidized bed gasifier for rice hulls", *Symposium on Energy from Biomass and Waste IX,* IGT, Chicago, U.S.A, 595-613.
[31] Qiaoqun S, Huilin L, Wentie L, Yurong H, Lidan Y and Gidaspow D ,2005, "Simulation and experiment of segregating/mixing of rice husk-sand mixture in a bubbling fluidized bed", *Fuel*, 84, 14-15, 1739-1748.
[32] Nguyen X Q, 2006, "Study on fluidization phenomena related to gasification of biomass in fluidized beds", *Dissertation in Gedruckter Form*, Technische Universität Wien, Institut für Verfahrenstechnik, Umwelttechnik und Technische Biowissenschaften.
[33] Datta A B, Chatterjee P K, Karmakar M K, Sen K and Hussain S A, 2007, "Production of hydrogen rich syngas by thermo chemical gasification of biomass in a fluidized bed reactor", *Proceeding of First International Conference on Advances in Energy Research*,76-82.

[34] Mansaray K G, Ghaly A E, Al-Taweel A M, Hamdullapur F and Ugursal V I, 2000, "Mathematical modeling of a fluidized bed rice husk gasifier: Part-I-Model development", *Energy Sources*, 22, 83-98.
[35] Geldart D, 1986, Gas fludization theory, *Wiley-International Publisher*, 296.
[36] Smith I W, 1978, "The Intrinsic reactivity of carbons to Oxygen", *Fuel*, 57, 409.
[37] Spalding D B, 1955, "Some fundamentals of combustion", *Butterworths*.
[38] Field M A, 1969, "Rate of combustion of size graded fractions of char from a low rank coal between 1200-2000K", *Combustion and Flame*, 13, 3,237.
[39] Caram H S and Amundson N R, 1977, "Diffusion and reaction in a stagnant boundary layer about a carbon particle", *Ind. Eng. Chem. Fundam.*, 16, 171.
[40] Yates J G and Walker P R, 1978, "Particle temperatures in a fluidized bed combustor", *Fluidization (eds. Davidson and Keairns),* Cambridge University Press, 241-245.
[41] Bukur D B and Amundson N R, 1981, "Fluidized bed combustion diffusion limited models", *Chem. Eng. Sci.*, 36, 1239.
[42] Ross I B, Davidson J F, 1981, "The combustion of carbon particles in a fluidized bed", *Trans. I. chemE.*, 59, 108-114.
[43] Turnbull E, Kossakowski E R, Davidson J F, Hopes R B, Blackshaw H W and Goodyer P T Y, 1984, "Effect of pressure on combustion of char in fluidized beds", *Chem. Eng. Res. Des.,* 62, 223.
[44] Park D, 1989, "Estimation of temperature difference between char particles and the fluidized bed in char combustion", *Fuel*, 68, 1320.
[45] Yagi S and Kunii D, 1955, "Studies on combustion of carbon particles in flames and fluidized beds", *Proc of 5th Symp. (Int.) on Combust.*, The Combustion Institute, 231-244.
[46] Davidson J F and Harrison D, 1963, *Fluidized Particles*, Cambridge University Press.
[47] Toomey R, Johnstone H F, 1952, "Gas fluidization of solid particles", *Chem. Eng. Prog.*, 48, 220–226.
[48] Kunii, D and Levenspiel O, 1968, "Bubbling bed model for kinetic processes in fluidized beds", *Ind. Engng. Chem. Process Des.*, 7, 481-492.
[49] LaNauze R D, 1985, "Fundamentals of coal combustion in fluidized beds", *Chem. Eng. Res. Des.*, 63, 3.
[50] Adanez J and Abanades J C, 1992, "Modeling of lignite combustion in atmospheric fluidized bed combustion. 1. Selection of submodels and sensitivity analysis", *Ind. Eng. Chem. Res.*, 31, 2286.
[51] Chen T P and Saxena S C, "Mathematical modeling of coal combustion in fluidized beds with Sulphur Emission Control by Limestone or Dolomite", *Fuel*, 56, 401.
[52] Sriramulu S, Sane S, Agarwal P and Mathews T,1996, "Mathematical modeling of fluidized bed combustion. 1. Combustion of carbon in bubbling beds", *Fuel*, 75, 1351.
[53] Gordon A L, Caram H S and Amundson N R, 1978, "Modeling of fluidized bed reactors – V. Combustion of carbon particles – an Extension", *Chem. Eng. Sci.*, 33, 713.
[54] Bukur D B and Amundson N R, 1982, "Fluidized Bed Combustion Kinetic Models", *Chem. Eng. Sci.*, 37, 17.

[55] Horio M and Wen C Y, 1978, "Simulation of fluidized bed combustors Part-I and Part-II, combustion efficiency and temperature profile", *AIChE Symp. Series*, *Fluidization, Application to Coal Conversion Process*, 74, 176.
[56] Rajan R R, Krishnan R and Wen C Y,1978, "Simulation of fluidized bed combustors: Part II. coal devolatilization and sulfur oxides retention", *AIChE Symp. Ser. 176*, 1978, 74, 112.
[57] Rajan R R and Wen C Y, 1980, "A comprehensive model for fluidized bed coal combustors", *AIChE J*, 26, 642.
[58] Becker H A, Beer J M and Gibbs B M, "A model for fluidized-bed combustion of coal", *Inst. Fuel Symp. Ser., 1*, 1975, A1-1.
[59] Arena U, Chirone R, DAmore M, Miccio M and Salatino P, 1995, "Some Issues in Modeling Bubbling and Circulating Fluidized-Bed Combustors", *Powder Tech.*, 82, 301.
[60] Park D, Levenspiel O and Fitzgerald T J, 1980, "A plume model for large scale atmospheric fluidized bed combustors", *Proc. 6th Int. Conf. Fluidized Bed Combust.*, 791-802.
[61] Bellgardt D, Hembach F, Schoessler M and Werther J, 1987, "Modeling of Large Scale Atmospheric Fluidized Bed Combustors", *Proc. 9th Int. Conf. Fluidized Bed Combust.*, 713-722.
[62] Chakraborty R K and Howard J R, 1981, "Combustion of char in shallow fluidized bed combustors: Influence of some design and operating parameters", *J Inst. Energy*, 54, 48.
[63] Fan L T, Tojo K and Chang C E, 1979, "Modeling of shallow fluidized bed combustion of coal particles", *Ind. Engg. Chem. Process Des. Dev.*, 18, 2.
[64] Avedesian M M and Davidson J F, 1973, "Combustion of carbon particles in a fluidized Bed", *Trans I chem. E*, 51, 121.
[65] Saxena S C and Rehmat A, 1980, "A mathematical model for char combustion in a fluidized bed", *Proceeding 6th International Conference Fluidized Bed Combustion*, 1138-1149
[66] Lemcoff N O, 1988, "Fluidized bed combustion of high ash chars", *Combust Sci and Tech*, 62, 131.
[67] Li S H, Yang H R, Zhang H, Wu Y X, Lu J F, Yue G X, 2009, "Combustion model for a cfb boiler with consideration of post-combustion in the cyclone' *Proceeding of The 20th International Conference on Fluidized Bed Combustion*, Springer, 824-829.
[68] Reddy G V and Mohapatra S K, 1994, "A mathematical model for exit gas composition in a 10 MW fluidized bed coal combustion power plant", *Energy Conversion and Management*, 35, 12, 1049-1060
[69] Galgano A, Salatino P, Crescitellis S F and Maffettone P L, 2005, "A model of the dynamics of a fluidized bed combustor burning bio-mass", *Combustion and Flame*, 140, 311-384.
[70] Arena U, Chirone R and Salatino P, 1996, "The fate of fixed carbon during the fluidized-bed combustion of a coal and two waste-derived fuels", *Proc of 26nd Symp. (Int.) on Combust.*, The Combustion Institute, 3243-3251.
[71] Irusta R, Antolin G, Velasco E and Miguel D R, 1995, "Modeling of lignocellulose waste combustion in an atmospheric bubbling fluidized bed, using an internal devolatilization degree parameter", *Fluidization VIII*, Engineering Foundation, New York, 855-862.

[72] Borodulya V A, Didalenko V I, Palchonok G I and Stanchitis L K, 1995, "Fluidized bed combustion of solid organic wastes and low-grade coals: Research and Modeling", *Proc. 13th Int. Conference on Fluidized Bed Combustion,* 935-942.
[73] Mansaray K G, Ghaly A E, Al-Taweel A M, Hamdullapur F and Ugursal V I, 2000, "Mathematical modeling of a fluidized bed rice husk gasifier: Part-II-Model Sensitivity", *Energy Sources*, 22, 167-185.
[74] Mansaray K G, Ghaly A E, Al-Taweel A M, Hamdullapur F and Ugursal V I, 2000, "Mathematical modeling of a fluidized bed rice husk gasifier: Part-III-Model Verification", *Energy Sources*, 22, 281-296.
[75] Khan A A, Jong W D, Gort D R, and Spliethoff H, 2007 "A fluidized bed biomass combustion model with discretized population balance"**,** *Energy Fuels*, 21, 4, 2346-2356.
[76] Yoshida K and Wen CY, 1970, "Non catalytic soild-gas reaction in a fluidized bed reactor", *Chem. Eng. Sci.*, 25, 1395-1404.
[77] Avedesian M M and Davidson J F, 1973, "Combustion of carbon particles in a fluidized bed", *Trans. Inst. Chem. Eng.*, 51, 121.
[78] Campbell E K and Davidson J F, 1975, "The Combustion of coal in fluidized beds", *Inst Fuel Symp Ser 1*, A2-1.
[79] Becker H A, Beer J M and Gibbs B M, 1975, "A model for fluidized-bed combustion of coal", *Inst Fuel Symp Ser 1*, A1-1.
[80] Basu P, Broughten J and Elliot D E, 1975, "Combustion of single coal particle in fluidized beds", *Proc. Inst. Fuel Symp. Ser No. 1,* Fluidized Combustion, A 3-1.
[81] Gibbs B M, 1975, "A mechanistic model for predicting the performance of a fluidized bed combustor", *Inst. Fuel Symp. Ser. 1*, A5-1.
[82] Mori S and Wen C Y, 1976, "Simulation of fluidized bed reactor performance by modified bubble assemblage model", *Fluidisation Technology,* 1, Hemisphere, Washington, 179-203.
[83] Baron R E, Hodges J L and Sarofim A F, 1978, "Mathematical model for predicting efficiency of fluidized bed steam generators", *AICHE Sym. Ser.*, 74, 120-124.
[84] Bear J M, Sarofim A F and Lee Y Y, 1981, "NO formation and reduction in fluidized bed combustion of coal", *Journal of Institute of Energy*, 38, 38-47.
[85] Donsi G, Massimila L and Miccio M, 1990, "The elutriation of solid carbon from a fluidized bed coal combustor", *La Rivista Des Combustible*, 30, 4.
[86] Ross I B, Patel M S and Davidson J F, 1981, "The temperature of burning carbon particles in fluidized bed", *Trans I Chem.*, 59,83.
[89] Chang C C, Rong S X and Fans L T, 1982, "Modeling of shallow fluidized bed reactors", Can. J. Chem. Eng., 60, 781-790.
[90] Miccio M and Salatino P, 1985, "Computations of the performance of fluidized coal combustors", *Powder Tech.*, 43, 163.
[91] Sundback C A, Beer J M and Sarofim A F, 1984, "Fragmentation behavior of single coal particles in a fluidized bed", *Proc of 20th Symp. (Int.) on Combust.*, The Combustion Institute, 1495-1503

[92] Mahmoud M El-Halwagi', Mahmoud A El-Rifai, 1988, "Mathematical modeling of catalytic fluidized-bed reactors—I. The multistage three-phase model", *Chem. Eng. Sci.* 43, 9, 2477–86.
[93] De Souza-Santos M L, 1989 "Comprehensive modeling and simulation of fluidized bed boilers and gasifiers", *Fuel*, 68, 1507.
[94] Basu P and Sarkar P K, 1989, "Combustion of single carbon particles in a part fluidized bed of fine solids", *Fuel*, 68, 1056-1062.
[95] Westby T S, Dangtran K Y and Thomas F E, 1990, "Fluidized bed combustion of Texas lignite", *Fuel*, 69.
[96] Reddy G V and Prasad S, 1993, "Modeling and simulation of fluidized bed coal combustor", *Ind. Inst. of Chem. Engrs.*
[97] Hovmand S and Davidson J F, 1971, "Pliot plant and laboratory scale fluidized bed reactors at high gas velocities; the relevance of plug flow, *Chapter 5 in Fluidization (Eds. J F Davidson and D Harrison),* Academic Press, London, 193-259.
[98] Fang M, Yang L and Cheng S, 2004, "Experimental study on rice husk combustion in a circulating fluidized bed", *Fuel Processing Technology*, 85, 1273-1282.
[99] Natrajan E, Nordin A and Rao A N, 1998, "Overview of combustion and gasification of rice husk in fluidized bed reactors", *Biomass and Bioenergy,* 14, 533-546.
[100] Thipwimon C, Gheewala S H, and Patumsawad S, 2004, "Environmental profile of power generation from rice husk in thailand", 6-024 (O), *The Joint International Conference on Sustainable Energy and Environment (SEE)*, 1-3 Dec, Hua Hin, Thailand,739-742.
[101] Premchart W and Koupranov V I, 2004, "Emission performance and combustion efficiency of a conical fluidized combustor firing various bio-mass fuels", *Bio Resource Technology,* 92*,* 83-91.
[102] Kaewklum R, Kuprianov V I and Permchart W ,2006, "Effects of operating conditions and fuel properties on the combustion efficiency and environmental performance of a fluidized-bed combustor firing rice husk", *Proceedings of the International Conference on Energy for Sustainable Development (ESD-2006),*1-3 March, Phuket, Thailand. Paper No. TI-11, 7.
[103] Madhiyanon T, Lapirattanakun A , Sathitruangsak P. , Soponronnarit S., 2006, "A novel cyclonic fluidized-bed combustor (ψ-FBC): Combustion and thermal efficiency, temperature distributions, combustion intensity, and emission of pollutants". *Combustion and Flame*, 146, Issues 1-2, 232-245.
[104] Bhattacharya S C, Shah N and Alikhani Z, 1984, "Some aspects of fluidized bed combustion of paddy husk", *Applied Energy*, 16, 4, 307-316.
[105] Bhattacharya S C , Alikhani Z and Shah N, 1984, "Fluidized bed combustion of paddy husk", *Renewable Energy sources: International Progress*, ed. T.N Veziroglu. Part B. Elsevier Science, Amsterdam, 113-120.
[106] Preto F, Anthony E J, Desai D L and Friedrich F D, 1987, "Combustion trials of rice hulls in a pilot-scale fluidized bed", *Proceeding International Conference Fluidized Bed Combustor*, 2, 1123-1127.

[107] Ganesh A, Grover P D and Ramachandra P V I, 1992, "Combustion and gasification characteristics of rice husk", *Fuel*, 71, 889-894.
[108] Armestoa L, Bahilloa A, Veijonenb K, Cabanillasa A and Oteroa J, 2002, "Combustion behavior of rice husk in a bubbling fluidized bed", *Biomass and Bioenergy*, 23, 171 – 179.
[109] Swasdisevi T, Soponronnarit S, Wetchacama A S S and Thepent V, 1997, *"*Rice husk furnace for fluidized bed paddy dryer*", 2nd ASEAN Renewable Energy Conference*, Phuket, Thailand.
[110] Skrifvars B J , Yrjas P, Kinni J, Siefen P, and Hupa M, 2005," The fouling behavior of rice husk ash in fluidized-bed combustion.: Fuel characteristics", *Energy and Fuels*, 19, 1503-1511.
[111] Chungsangunsit T, Gheewala S H and Patumsawad S, 2004, " Environmental assessment from rice husk: a case study in Thailand", *Electricity Supply Industry in Transition: Issues and Prospect for Asia*.20,51-62.
[112] Rajaram S and Malliah K T U, 1987, "A 10 MW fluidized bed power plant for paddy straw", *Proceeding 9th International Conference Fluidized Bed Combustion,* ASME, N.Y. 10-17.
[113] Olanders B and Steenari B M, 1995, "Characterization pf ashes from wood and straw" , *Biomass and Bioenergy* , 8, 105-115.
[114] Jenkins B M, Baxter L L, Miles T R, Miles Jr T R, Oden L L, Beyer R W and Winther E, 1994, "Composition of ash deposits in biomass fueled boilers:Results of full-scale experiments and labortary simulations", *Proceeding of the International ASAE Summer Meeting*, Kansas City, Kansas, June, 19-24.
[115] Skrifvars B J, Ohman M, Nordin A, Hupa M, 1999, "Predicting bed agglomeration tendencies for biomass fuels fired in FBC boilers: a comparison of three different prediction methods", *Energy Fuels*, 13, 359-363.
[116] Ergudenler A and Ghaly A E, 1993, "Agglomeration of silica sand in a fluidized bed gasifier operating on wheat straw", *Biomass and Bioenergy*, 4*,* 135-147.
[117] Grubor B G, Oka S N, Ili M S, Daki D V, Arsi B T, 1995, "Biomass FBC combustion – bed agglomeration problems", *Proceedings 13th Conference on Fluidized Combustion*, May 7-10, Orlando, USA, 1, 515-522.
[118] Nordin A, Ohman M, Skrifvars B J, Hupa M, 1995, "Agglomeration and defluidization in FBC of Biomass fuels-Mechanisms and measures for prevention", *Proceedings of the Engineering Foundation Conference on the Application of Advanced Technology to Ash Related problems in Boilers,*Waterville Valley, NH, USA.
[119] Ryabov G A, Litoun D S, and Dik V P, 2003, "Agglomeration of Bed material: Influence on efficiency of biofuel fluidized bed boiler", *Thermal Science* ,7, 1, 5-16.
[120] Weiganag L, Dam-Johansen K and Flemming F, 2003, "Agglomeration in bio-fuel fired fluidized bed combustors", *Chemical Engineering Journal*, 96,171-185.
[121] Elisabet B, Marcus Ö and Nordin A, 2005, "Mechanisms of bed agglomeration during fluidized-bed combustion of biomass fuels", *Energy Fuels,* 19, 3, 825 -832.

[122] Korbee R, Van Ommen J.R, Lessellink J, Nijenhuis J, Keil J H A, Van den Bleek C M, 2006, "Early agglomeration recognition system(EARS)", *Journal of Energy Resource Technology*, ASME, 128, 143-149.

[123] Natarajan E, Ohman M, Gabra M, Nordin A, Liliedahl T and Rao A N, 1998, "Experimental determination of bed agglomeration tendencies of some common agricultural residues in fluidized bed combustion and gasification", *Biomass and Bioenergy*, 15, 2, 163-169.

[124] Mansaray K G and Ghaly A E, 1997, "Agglomeration characteristics of alumina sand-rice husk ash mixtures at elevated temperatures", *Energy Sources*, Part A: Recovery, Utilization, and Environmental Effects, 19, 9 ,1005-1025.

[125] Gera D, Gautam M, Tsuji Y, Kawaguchi T and Tanaka T, 1998, "Computer simulation of bubbles in large-particle fluidized beds", *Powder Technology,* 98, 38–47.

[126] Kobayashi N, Yamazaki R and Mori S, 2000, " A study on the behavior of bubbles and solids in bubbling fluidized beds", *Powder Technology,* 113, 327–344.

[127] Kaneko Y, Shiojima T and Horio M, 1999, "DEM simulation of fluidized beds for gas-phase olefin polymerization", *Chemical Engineering Science,* 54, 5809–5821.

[128] Pain C C, Mansoorzadeh S, De Oliveira C R E, 2001 "A study of bubbling andslugging fluidized bed using the two-fluid granular temperature model", *International Journal of Multiphase Flow,* 27, 527–551.

[129] Sharma S K D and Mohan R, "Numerical study of the influence of horizontal tube banks on the hydrodynamics of a dense gas-solid bubbling fluidized bed", *International Journal of Chemical Reactor Engineering*, 2003, Volume 1 , Article A26, 1-12.

[130] Taghipour F, Ellis N, Wong C, 2005, "Experimental and computational study of gas–solid fluidized bed hydrodynamics", *Chemical Engineering Science* , 60, 6857 – 6867.

[131] Behjat Y, Shahhosseini S, Hashemabadi S H, 2008, "CFD modeling of hydrodynamic and heat transfer in fluidized bed reactors" *International Communications in Heat and Mass Transfer,*35, 3, 357-368.

[132] Chiesa M, Mathiesen V, Melheim J A, Halvorsen B, 2005, "Numerical simulation of particulate flow by the Eulerian–Lagrangian and the Eulerian–Eulerian approach with application to a fluidized bed", *Computers and Chemical Engineering*, 29 , 291-304.

[133] Ranade V V, 2002, "Computational flow modeling for chemical reactor engineering", *First ed. Academic press*, New York.

[134] Dixon T, Mann A P, Plaza F, Gilfillan W N, 2005, "Development of advanced technology for biomass combustion-CFD as an essential tool", *Fuel*, 84, 1303–1311.

[135] Ravelli S, Perdichizzi A, Barigozzi G, 2008, "Description, applications and numerical Modeling of bubbling fluidized bed combustion in waste-to-energy plants", *Progress in Energy and Combustion Science,* 34 , 224–253.

[136] Stastny M, Ahnert F, Spliethoff H, 2002, "Three-dimensional combustion modeling of a biomass fired pulverized fuel boiler", *Advanced Computational Methods in Heat Transfer VII*, edited by B.Sundén, C.A. Brebbia, WIT Press, Boston, 439-448.

[137] Walsh A R, 2006, "CFD modeling of waste-fuel boiler combustion systems*", Proceeding 7th European Conference on Industrial Furnaces and Boilers*, Porto, Portugal, April 18-21, 1-11.

[138] Kaer S K, 2004, "Numerical modeling of a straw-fired grate boiler", *Fuel,* 83, 1183-1190.
[139] Ma L, Jones J M, Pourkashinian M and Williams A, 2007, "Modeling the combustion of pulverized biomass in an industrial combustion test furnace", *Fuel*, 86, 1959-1965.
[140] Backreedy R I, Fletcher L M, Jones J M, Ma L, Pourkashanian M, Williams A, 2005, "Co-firing pulverised coal and biomass:a modeling approach", *Proceedings of the Combustion Institute,* 30, 2955–2964.
[141] Skrifvars B J, Yrjas P, Laurén T, Kinni J, Tran H, and Hupa M, 2005 "The fouling behavior of rice husk ash in fluidized-bed combustion.: Pilot-scale and full-scale measurements", *Energy and Fuels*, 19, 1512-1519.
[142] Geldart D, Baeyens J, Pope D J, Van de Wijer P,1981, "Segregation in beds of large particles at high velocities", *Powder Technology*, 30, 2, 195-205.
[143] Wen C Y and Yu Y H, 1966, "A generalized method for predicting the minimum fluidization velocity", *AIChE*, 12, 610–612.
[144] Bird R B, Stewart W E and Lightfoot F N, 1960, *Transport Phenomenon*, Wiley, New York.
[145] Stubington J F, Barrt D, Lowry G, 1984, "Bubble size measurements and correlation in a fluidized bed at high temperature", *Chem. Eng. Res. Des.*, 62, 173-178.
[146] Rowe P N and Patridge B A, 1965, "An X ray study of bubbles in fluidized beds", *Trans. I. Chem. Engrs.*, 43.
[147] Kunii D and O Levenspiel, 1997, "Circulating fluidized reactors", *Chemical Engineering Science* 52,
[148] La Nauze R D, 1985,"Fundamentals of coal combustion in fluidized beds", *Chem. Eng. Res. Des.*, 63, 3.
[149] Zhang J Q, 1987, *Proc 9th Int. Conf. on FBC*, Boston.
[150] Bellgardt D and Werther J A, 1986, "A novel method for the investigation of particle mixing in gas solid systems", *Powder Technology*, 48.
[151] Paul J, Peeler K and Howard J P, 1992, "Devolatilisation of large coal particles under fluidized bed conditions", *Fuel*, 71, 425-430.
[152] Park D, 1989, "Estimation of temperature difference between char particles and the fluidized bed in char combustion", *Fuel*, 68, 1320.
[153] Parker Almon S and Hottel H C, 1936, "Combustion rate of carbon. Study of gas-film structure by micro sampling", *Ind. Eng. Chem.*, 28, 11, 1334-134.
[154] La Nauze R D, Jung K and Kastl J, 1984, "Mass transfer to large particles in fluidized beds of smaller particles", *Chem Eng Sci*, 39, 1623-1633.
[155] Wen C Y, Yu Y H, 1966, "A generalized method for predicting the minimum fluidization velocity", *IChE*, 12:610–2.
[156] Reddy G V, Prashad S, Mohapatra S K, 1995, "Mathematical model for coal combustion in a fluidized bed combustor: Particle size distribution effects", *Indian Journal of Engineering and Material Sciences*, 2, 224-230.

[157] Daizo Kunii and Octave Levenspiel, 1991, *Fluidization Engineering*, Butterworth-Heinemann, USA.
[158] Yagi S and Aochi T, 1958, "Elutriation of particles from a batch fluidized bed", *Soc. Chem. Engrs. (Japan)*, Spring Meeting.
[159] Zenz F A and Weil F A, 1958, "A theoretical-empirical approach to the mechanism of particle entrainment from fluidized beds", *AIChE J*, **4**, 472.
[160] Wen C Y and Harshinger R F, 1960, "Elutriation of solid particles from a dense-phase fluidized bed", *AICHE*, 6, 2, 220.
[161] Gedart D, Bayens J, Pope D J, Van de Wijer P, 1981, " Segregation in beds of large particles at high velocities", *Powder Technology*, 30, 2, 195-205.
[162] Wen C Y and Ishida M, 1968, "Comparison of kinetic and diffusional models for solid-gas reaction", *AICHE J*, 14, 311-317.
[163] Wen C Y and Wang S C, 1970, "Oxidation of carbon in porous solids", *National meeting of the American Chemical Society*, Fall, Chicago, 14, 5, 80-89.
[164] Skrifvars B J, Hupa M, Moilanen A and Lundqvist R, 1996, " Characterization of biomass ashes", *Application of Advanced Technology to Ash Related Problems in Boilers*, *Baxter L and Desollar R*, 383-398.
[165] Bryers R W, 1996, "Fireside slagging, fouling and high temperature corrosion of heat transfer due to impurities present in steam raising fuel", *Progress of Energy and Combustion Science*, 22, 29-120.
[166] Steenari B M, 1994, "A practical and theoretical study of sintering of coal ash and limestone in a fluidized bed combustor", *Staten Energiverk*, FBT-87/34.
[167] Misra M K, Ragland K W and Baker A J, 1993, "Wood ash composition as function of furnace temperature, *Biomass and Bioenergy*, 4, 2, 103-116.
[168] Linvingstone W R, 1991, "Straw ash characteristics", *Department of Energy*, DE92-519748.
[169] Padban N, Kiuru S and Hallgren A L, 1995, "Bed material agglomeration in PFB biomass gasification", *American Chemical Society*, Division of fuel chemistry, 40, 3, 743-747.
[170] Ahmaruzzaman M, Sharma D K, 2007, "Kinetic studies on cocracking of petroleum vacuum residue with thermoplastics and biomass (petrocrop)", *Petroleum Science and Technology,* 25, 7, 925 – 936.
[171] Gupta D K and Gadgil Kasturi, 2006, "Experimental studies related to pulverised thin layer coal combustion", *International Journal of Pure and Applied Chemistry*, 1, 2**.**
[172] Miles T R, Bryers R W, Baxter L L, Jenkins B M and Oden L L, 1996, "Alkali deposits found in biomass power plants: A preliminary investigation of their extent and nature", *NREL:NREL/TP*,433-8142.
[173] Delvinquer V, 1995, "Defluidzation at high temperature in fluidized bed of sand by addition of calcium carbonate", *Proceeding Fluidized Bed Combustion*, ASME, 2, 801-806.
[174] Atakul H and Ekinci E, 1989, "Agglomeration of turkish lignites in fluidized bed combustion", *Journal of the Institute of Energy*, March, 56-61.

[175] Vander Drift A and Olsen A, 1999, "Conversion of biomass{private} prediction and solution methods for ash agglomeration and related problems", *Contract JOR3-95*, March, ECN Holland, Riso Denmark.
[176] Zhang D Z and Rauenzahn R M, "A visco elastic model for dense granular flows", *J.Rheol.*, 41, 1275.
[177] Scahaeffer D G, 1987, "Instability in the evolution equations describing incompressible granular flows", *J. Diff. Eq.,* 66, 19.
[178] Syamlal M, Rogers W and O'Brien T J, 1993, "MFIX documentation: theory guide", U.S. Dept of Energy, Office of fossil energy, *DOE/METC*-94/1004(DE94000087).
[179] Gidaspow D, 1994, "Multiphase flow and fluidization: continuum and kinetic theory descriptions", *Academic Press*, London.
[180] Patankar S V, 1984, "Numerical heat transfer and fluid flow", *Hemisphere Publishing Corporation*.
[181] Mohapatra S K and Singh Ravi Inder, 2008, " Study of some performance parameters of an atmospheric bubbling fluidized bed boiler based on coal washery rejects considering bubble growth along bed height", *Journal of Solid Waste Technology and Management*, 34, 4, 213-223.
[182] Lin W, Dam-Johansen K, 1999, "Agglomeration in fluidized bed combustion, biomass mechanisms and co-firing with coal", *15th International Conference of Fluidized Bed Combustion*, May 16-19, Savannah, USA, CD – FBC99-0120.
[183] Fluent 6.2 User's Guide. Labenon, USA.
[184] Energy Efficiency in Thermal Utilities, 2005, *A Guide Book for Energy Managers and Auditors*, Bureau of Energy Efficiency, Ministry of Power, Government of India.
[185] http://en.wikipedia.org/wiki/Bran.

APPENDIX

A.1.0 Proximate Analysis of Rice Husk/Rice Straw/Fly Ash Sample

In this type of analysis the percentage of moisture content, volatile matter, ash and fixed carbon is determined. This was done in chemistry lab, Guru Nanak Dev Engineering College, Ludhiana. The instruments required for this analysis are muffle furnace, weighing machine, and silica crucible and air oven.

A.1.1.1 Air Oven

Ventilated drying oven in which constant and uniform temperature of 110°C can be maintained.

A.1.1.1 Silica Crucible

One silica crucible is required. A translucent silica crucible with lid having external diameter of 2.5 cm should be used. The total height of crucible should not exceed 3.8 cm and internal diameter should not be less than 2.2 cm.

A.1.1.1 Weighing Machine

Weighing machine is required for weighing sample.

A.1.1.1 Muffle Furnace

A muffle furnace capable of giving uniform temperature of 900°C with the necessary thermocouples and pyrometers is shown in Figure A.1.1.1.

Figure A.1.1.1 – Silica crucible carrying fuel (rice husk) inside the muffle furnace

A.1.2 Determination of Moisture

Moisture is defined as the difference in weight of sample rice husk or rice straw when the same is heated at 110 °C for one hour under specified conditions.

A.1.2.1 Procedure

Silica crucible was taken, cleaned and dried in an oven at 110°C for one hour. It was cooled for 15 minutes and then weighed accurately. Approximately one gram of sample rice husk or rice straw was weighed and put into the silica crucible. Then crucible was kept in an air-dried oven, which was maintained at 110°C for one hour. After one hour crucible was removed from the oven, cooled in a desicator and then weighed accurately.

A.1.2.1 Calculations

Weight of dried and empty crucible with lid = x gm

Weight of sample and crucible with lid = y gm

Weight of sample and crucible after heating = z gm

Therefore, weight of sample before heating = (y-x) gm

Weight of Moisture loss due to heating = (y-z) gm

Percentage of Moisture = $\{(y-z) / (y-x)\} \times 100$

A.1.3 Determination of Volatile Matter

Volatile matter is defined as the loss of weight of sample when the same is heated under specified conditions in the absence of air at 900°C for 9 minutes.

A.1.3.1 Procedure

For the determination of volatile matter, a crucible with lid was taken and then weighed accurately. Now one gram of sample rice husk or rice straw was weighed accurately into the crucible and spread evenly in the crucible by gentle tapping the crucible with the lid was

transferred in the furnace at 900°C for nine minutes. After nine minutes, the crucible was removed from the furnace and placed on a cooled iron plate to ensure rapid cooling. Then the crucible was placed in a desicator for 15 minutes for further cooling and then weighed accurately.

A.1.3.1 Calculations

Weight of dried and empty crucible with lid = x gm

Weight of sample and crucible with lid = y gm

Weight of sample and crucible after heating = z gm

Therefore, weight of sample before loss of weight = (y-x) gm

Loss of weight = (y-z) gm

Percentage of volatile matter = $\{(y-z) / (y-x)\} \times 100$

A.1.4 Determination of Ash

Ash is defined as the weight of residue left when a known weight of sample is burnt at 800°C for one hour under specified conditions.

A.1.4.1 Procedure

For the determination of ash, a silica dish was taken, heated at 800°C for one hour. Then the dish was cooled for 20 minutes and then weight of empty dish was taken. Now one gram of sample was weighed accurately into the crucible and spread evenly in the crucible by gentle tapping the crucible with the lid. The silica dish was transferred in the furnace at 450°C for half an hour. Then the temperature of the furnace was raised to 800°C. The dish was kept at this temperature for another one hour. The crucible was removed from the furnace, cooled and then weighed accurately.

A.1.4 Calculations

Weight of dried and empty crucible = x gm

Weight of sample and crucible = y gm

Weight of sample and crucible after heating = z gm

Therefore, weight of sample before heating = (y-x) gm

Weight of ash = (z-x) gm

Percentage of ash = $\{(z-x) / (y-x)\} \times 100$

A.1.5 Determination of fixed carbon

The percentage of the fixed carbon can be found by subtracting the percentage of moisture content, volatile matter and ash content from 100.

A.1.5.1 Calculations

Percentage of fixed carbon = 100 – (1-XW + XVM + XA)

XW = Moisture content of fuel

XVM = Volatile matter content of fuel

XA = Ash content of fuel

A.2.0 Ultimate Analysis of Rice Husk/Rice Straw Samples

The ultimate analysis of the rice husk/rice straw was carried out at Regional sophisticated instrumentation centre Panjab University, Chandigarh. The value of ultimate analysis is then directly used in the model.

A.3.0 Sieve Analysis Test

The sieve analysis test is generally used in classification of soils. The below mentioned test was done to look out the bed agglomeration characteristics of sand and size of fuel. Above test is done at Foundry shop, Central Workshop, Guru Nanak Dev Engineering College. The average

size of feed particles found to be 0.438 cm. The rice husk is uniformly of same size, so there is no variation in the size of rice husk particles.

Figure A.3.1 Sieves in stack

Figure A.3.2 Sieve shaker (Model-VGH, M/s. Versatile Equipments Pvt. Limited, Kohlapur, India)

For looking bed agglomeration the samples of ash were taken at different time intervals and undergone sieve analysis at GNDEC, Ludhiana. The following procedure was adopted and readings were obtained in below mentioned Table 3.1.

A.3.1 Test Procedure

1. Take a representative oven dried sample of bed ash.
2. Determine the mass of sample accurately. W(g)
3. Prepare a stack of sieves. Sieves having larger opening sizes are placed above the ones having smaller opening sizes. The very last sieve at bottom is 400 μm and a pan is placed under it to collect the portion of soil passing sieve.
4. Make sure sieves are clean; if many sand particles are stuck in the openings try to poke them out using brush.
5. Pour the sand along bed ash from step 2 into the stack of sieves from the top and place the cover, put the stack in the sieve shaker and fix the clamps, adjust the time on 2-3

minutes and get the shaker going. We can-not shake more than two minutes other wise agglomerates will be broken.

6. Stop the sieve shaker and measure the mass of retained sand. (fill in Table A.3.1)

Table A.3.1 Sieve analysis data sheet

ISO Nominal Aperture		Weight retained in gms.	Cumulative weight retained in gms.	Percent (%) weight retained
Principal sizes	Supplementary sizes			
R20/3	R20			
2000 μm				
	1800 μm			
	1600 μm			
1000 μm				
	800μm			
	630μm			
	400μm			

A.4.0 Measurement of Concentration of Various Gases

As plant is quite old and there was no measuring instrument except monitoring for carbon dioxide, oxygen and SPM at the plant site. We measured O_2, CO_2 and CO using IMR 1400 gas analyzer. SO_2, NOx(NO_2) and SPM were measured using the APM Envirotech 610. Even though IMR 1400 is capable of measuring CO and NO_2 but we used IMR 1400 only for measuring O_2, CO and CO_2. Both the instruments were taken from Environmental pollution lab, Guru Nanak Dev Engineering College, Ludhiana and subsequently used for measurement at the plant site.

A.4.1 Specifications of IMR 1400

IMR combustion gas analyzer can measure the flue gases of boiler, burners and engines. It is using the latest sensor technology. Figure A.4.1 shows the IMR 1400 gas analyzer. It has all important parameters to adjust and optimize the combustion process. It includes all needed features for a complete analysis. IMR 1400 gas analyzer is portable and very compact

combustion gas analyzer housed in a rugged aluminum case. It can measure O_2 Oxygen CO_2 Carbon dioxide, NO Nitric oxide, CO Carbon monoxide, TG Flue-gas temperature, AG Ambient air temperature simultaneously. It can calculate combustion efficiency, excess air and

Figure 4.1 IMR 1400 gas analyzer

losses as per ASME equations. It can be automatically calibrated and it has thermal printer. It is having memory for 200 measurements. The length of gas sampling probe having heated handle of length 0.9 ft and 11.5 ft diameter. It can measure O_2 with accuracy of ± 0.2% and CO_2 with accuracy of ± 5% and CO range from 0 to 2000 ppm, NO_x range from 0-2000 ppm.

A.4.2 Experimental Details of Stack Monitor Kit Envirotech APM 610

The flue gas velocity measurement is accomplished with the help of a double S type Pitot tube and a manometer. APM 610 provides a calibrated Pitot tube and an inclined cum vertical manometer to ensure accuracy in flow measurements. The manometer scales are directly calibrated in water gauge units. The temperature is measured with the help of a thermocouple probe with a digital temperature display and gives temperature values directly in °C. SPM concentration is worked out on the basis of weight of particles collected on a filtration thimble over a time at a preset isokinetic sampling rate. APM 610 provides separate rotameters for SPM

and gaseous sampling. To allow sampling under isokinetic conditions a set of nozzles are provided. The concentration of gaseous pollutants is calculated by analysis of absorbing reagents through which flue gases have been passed.

Figure A.4.2 Detailed unassembled picture of stack monitor Envirotech APM 610 Kit

A.4.2.1 Test Procedure for Determination of Gaseous Concentration

A.4.2.1.1 Sulphur Dioxide: Following procedure is adopted for measurement.

Let sampling rate be – 1.0 lpm

Sampling time -60 min

Volume of absorbing -50 ml

Solution [3 % H_2O at ph 5]

Now, volume of 0.02 N NAOH consumed for changing the color of 10 ml volume of absorbing solution from red to green = 4.5 ml.

Now by using equation $N_1 V_1 = N_2 V_2$

N_1 =0.02 * 4.5 /10 mg/ml

Or SO_2 = 0.02 * 4.5 * 32 /10 mg/ml

Total SO_2 absorbed in 50 ml solution =0.02 * 4.5 * 32 * 50 /10 = 14.44 mg SO_2

Volume of gas passed through the absorbent is = 1.0 * (273+25) * 60 / 273+28

{The pressure drop across the gaseous stream is zero while the temperature of gases at the metering point is 28^oC (from the example above) and gaseous sampling is done at 1.0 lpm for 60min}

59.4 litre ----- (a)

Conc. of SO_2 =14.4 * 1000/ 59.4 =237.6 mg/Nm^3

A.4.2.1.2 Nitrogen Dioxide

Using the spectrophotometer, the concentration of NO_X after plotting the calibration curve between optical density and NOx concentration curve between optical density and NOx concentration comes out to be - 1.2 µg/ml

Hence , NOx absorbed solution was taken

NOx concentration = 60 * 10-3 / 0.0606 * 0.35 = 2.82 mg/Nm^{-3}

(Where 0.0606 m is the volume of gas (emission) passed through the absorbing solution from (a) of 3.9.1, and 0.35 is the overall absorbing efficiency factor).

A.4.2.1.3 Detailed Procedure for Determination of Dust Concentration

i) Weight of the thimble before sampling - "W_1" gm

ii) Temperature of stack gases taken with the help of thermocouple -"T_1" ^oC

iii) Displacement of manometer fluid due to placement of pitot tube inside the stack -"H" cm

iv) Therefore the velocity, from relation $V= C (H (273+ T_1))^{1/2}$

Here C is variable can be determined using a known value of D_m(Density of manometric fluid) and K (Pitot calibration constant)

v) Isokinectic sampling flow rate is calculated using relation (5) of section 1.3.5

$Q^{'}s = Q_s \times (273+ 25)/Ts$

Where $Q_s= V \times A_n \times 60 \times 1000$

The nozzle is to be selected in such a way so that 'Qs' falls within the range of 60 LPM rotameter. If two or more nozzles are giving that much of flow, then one (flow) falling in the centre of the range should be selected.

vi) Sample is taken by adjusting a flow rate of "Q_s" – Q_g { Q_g-flow rate which is to be set on gaseous rotameter} on 60 LPM rotameter for "t" minutes

vii) Weight of thimble after sampling –" W_2" gm

viii) Weight of dust collected –"W_2"-W_1" gm

Volume of flue gas – $Q_m \times$ t sampled in litres

Here $Q_m = Q'_s \times (P'_m – P_m)/P_s \times (273+25) / T'_a$

Here Q_m = Actual flow rate in LPM

Q'_s = Sampling rate from stack given by relation $Q'_s = Q_s \times (273 +25)/T_s$

$Q_s = V \times A_n \times 60 \times 1000$ LPM

A_n = Area of nozzle in m^2

V = Stack gas velocity m/sec

P_s = Static pressure in the stack

P_m = Average mean pressure at metering point

P'_m =Barometric pressure at the sampling point

T_s = Stack gas temperature in (K)

T'_a = Temperature at metering point (K)

Therefore

SPM=Weight of dust collected / Volume of gas sampled mg/Nm^3

$= (W_2 - W_1) \times 10^6 / Q_m \times t$ mg/Nm^3

A.5.0 Perkin Elmer TGA 6

Perkin Elmer is high-sensitivity thermal analysis instrumentation to achieve fast, accurate, reproducible results. Perkin Elmer TGA 6 is recently installed in mechanical engineering department under the AICTE grant. It used mainly for thermal analysis of polymers and biomass etc. Proximate analysis can also be done at Perkin Elmer TGA 6. It is automatically controlled

Figure A.5.1 Furnace of TGA

Figure A.5.2 Perkin Elmer TGA

through a software Thermal Analysis Pyris. First of all powdered samples were placed in small crucible. Then continuous water supply is maintained through out the experiment. Supply of nitrogen and oxygen were supplied at regularly as per requirement. Then crucible with rice husk

(As shown in Figure A.5.1) is placed in instrument) and lid is closed. Then uniform temperature is maintained from 30^{o}C to 750^{o}C. Thermal analysis of rice husk is done and results can visualized from the software, which later could be printed.

A.6.0 SEM Test

To look the structure of agglomerates samples were tested using Scanning Electron Microscope (SEM) facility of RSIC, Panjab University, Chandigarh. SEM is an essential component for scientific analysis of a variety of materials. SEM is a powerful tool in studying (cell and molecular biology, anatomy, microbiology, pathology and forensic science) biological specimens, food stuffs and several other areas of material sciences (electronics, metallurgy, polymer and surface science).

Figure A.6.1 Front view of scanning electron microscope installed at RSIC, Panjab University Chandigarh

SEM is becoming a valuable new tool for the nondestructive inspection, examination and evaluation of materials, both metallic and non-metallic, as well as assemblies and surfaces. The item to be examined and evaluated is placed on a specimen stage inside a vacuum enclosure of the SEM station and is irradiated with a finely focused electron beam that can be static or swept in a cyclic fashion over the specimen's surface. The resulting signals that are produced when the

scanning electron beam impinges on the surface of the specimen include both secondary emission electrons as well as backscattered electrons. These signals vary as the result of differences in the surface topography as the scanning electron beam is swept across the specimen surface. The secondary emission of electrons from the specimen surface is usually confined to an area near the beam impact zone that permits images to be obtained at a relatively high resolution. These images as seen on a cathode ray tube provide a three dimensional appearance due to the large depth of field of the SEM as well as the shadow relief effect of the secondary electrons contrast.

Figure A.6.1 show 120 kV scanning electron microscope, Hitachi (H-750) installed at Panjab University, Chandigarh. It is equipped with CCD camera This instrument has the resolution of 0.36 nm (point to point) with 40-120 kV operating voltage and can magnify object up to 6 lakh times in high resolution mode. It has electron diffraction, tungsten filament, low dose function, high contrast mode with ergodynamic look. The specific features of the instrument are: maximum field of views at x700 with dual picture modes, auto-navigation, largest possible field with mose contrast, auto pre-irradiation mode (APIS).

A.7.0 Quantitative Analysis of Bed Ash

Quantitative analysis of bed ash was done at Delhi test house, Delhi. Approximately 2 kg of samples at different time interval after week and one month were taken and sent to Delhi test house and subsequently the results were taken which are provided in dissertation.

A.8.0 Input Data for Computer Program

The computer program was generated in Matlab 7, which is available in Electrical Engineering Department, Guru Nanak Dev Engineering College, Ludhiana. Following table shows the main input the model.

Program	
Exit gas model and solid population balance model	
Input Data	
Ultimate analysis of Rice Husk	
Enter the value of Carbon	0.389
Enter the value of Hydrogen	0.051
Enter the value of Sulphur	0.0012
Enter the value of Oxygen	0.379
Enter the value of Nitrogen	0.0217
Proximate analysis of Rice Husk	
Enter the value of moisture	0.025
Enter the value of ash	0.1782
Enter the value of volatile matter	0.6303
Enter the value of fixed carbon	0.1665
Physico chemical parameters	
Enter the fuel feed rate (g/s)	3200
Enter the excess air	0.2
Enter the area of bed in cm^2	391000
Enter the value of bed temperature (K)	1073
Enter the value of rice husk density (g/cm^3)	0.12
Enter the value of minimum fluidization height (cm)	48
Enter the value of number of holes	22500
Enter the value of minimum voidage	0.48
Enter the char particle surface temperature (K)	1273

A.9.0 Output Results of Computer Program

The program generates the following output results. The main output is O_2, CO_2 N_2, bed carbon load and carbon utilization efficiency along with many other parameters. The gaseous concentration is g-mol/cm^3 which will be later converted into percentage by volume.

The superficial velocity	119.9483
The inlet concentration of oxygen	$2.5018e-^{006}$
The viscosity of gas at bed temperature	$4.4778e-^{004}$
The density of gas at bed temperature	$3.4526e-^{004}$
The minimum fluidization velocity	26.8100
The diameter of bubble	19.7573
The expanded bed height	83.3151
The diffusivity of gas at bed temperature	1.6818
The gas interchange co-efficient from bubble to cloud wake phase	7.1254
The gas interchange co-efficient from cloud wake to emulsion phase	0.9613
The density of char	0.0414
The intrinsic chemical reaction rate constant	167.6369
The Sherwood number	5.6342
The Mass transfer coefficient	21.6340
The overall reaction rate	19.1612
The number of stages in bed	$4.2169 \approx 4$
The average concentration of oxygen leaving the bed	$8.4487e-^{007}$
The average concentration of carbon dioxide leaving the bed	$1.6570e-^{006}$
The fractional conversion of oxygen	0.6623
The average concentration of nitrogen leaving the bed	0.7941
The shrinkage rate of rice husk particles at bed temperature	0.0308
The elutriation rate constant	$2.1726e-^{004}$
The carbon feed rate of fuel	532.8000
The carry over rate	84.9500
The carbon carry over rate	7.2208
The bed carbon load	946.2084
The carbon utilization efficiency	98.6448

ABOUT THE AUTHOR

Author is born on 18th Oct 1979 in Ludhiana in State Punjab, India. He did his Bachelors in Technology (Mechanical Engineering) from Guru Nanak Dev Engineering College in 2001. He did his Masters in Engineering (Mechanical) from Punjab Engineering College Chandigarh in 2003. While working in private institution near Chandigarh he started doing his PhD in Thermal Engineering. He worked here for three years. During his three years tenure he taught B.Tech and M.Tech (Thermal Engineering). He taught mainly thermal and fluid related subjects.

In 2006 he joined as lecturer in his alma mater Guru Nanak Dev Engineering College (Which ranked 19th during 2006, India Today survey in all India ranking). In Sep 18, 2006 he was blessed with a sweet daughter. He served his alma mater in various social posts apart from others like as a student, teacher, son, husband and father. He is also faculty advisor of Sae India-Gndec. He visited Xian, China and attended 20th International Conference on fluidized bed combustion in May 2009. He also attended 52nd IEA meeting in connection with FBC systems at Xian, China.

ABOUT THE AUTHOR

Author is born on 18th Oct 1979 in Ludhiana in State Punjab, India. He did his Bachelors in Technology (Mechanical Engineering) from Guru Nanak Dev Engineering College in 2001. He did his Masters in Engineering (Mechanical) from Punjab Engineering College Chandigarh in 2003. While working in private institution near Chandigarh he started doing his PhD in Thermal Engineering. He worked here for three years. During his three years tenure he taught B.Tech and M.Tech (Thermal Engineering). He taught mainly thermal and fluid related subjects.

In 2006 he joined as lecturer in his alma mater Guru Nanak Dev Engineering College (Which ranked 19th during 2006, India Today survey in all India ranking). In Sep 18, 2006 he was blessed with a sweet daughter. He served his alma mater in various social posts apart from others like as a student, teacher, son, husband and father. He is also faculty advisor of Sae India-Gndec. He visited Xian, China and attended 20th International Conference on fluidized bed combustion in May 2009. He also attended 52nd IEA meeting in connection with FBC systems at Xian, China.